THE UNIVERSITY *of* EDINBURGH

Understanding kinetochore dependency pathways using vertebrate conditional knockout cell lines and quantitative proteomics

Laura Wood

Thesis submitted for the Degree of Doctor of Philosophy
The University of Edinburgh

2014

Declaration

I declare that this thesis is composed entirely by myself and that the work presented is my own, except where contributions by others are clearly stated. The work has not been submitted for any other degree or professional qualification.

Laura Wood
Edinburgh
April 2014

Acknowledgments

I would like to thank:

The BBSRC for four years of funding and allowing me to enjoy the beautiful city of Edinburgh!!

Thank you to my supervisor, Bill Earnshaw, for giving me the opportunity to work in your lab, for all of the support and encouragement over the last four years, and for helping me to build confidence in my capabilities as a researcher. Wishing you and your family all the best.

All Earnshaw lab members past and present: Jan, Shinya, Diana, Melpi, Dan, Oscar, Giulia, Florence, Mar, Kumiko, Itaru, Hiromi, Helena, Alisa, Paola and Nuno.
Shinya, thank you for taking the time to teach me the chromosome preps and for being such a kind, generous person.
Jan- one of the first friends I made in Edinburgh. You really helped in those first few months and thank you for letting me live in your flat for 3 years!
Diana- for being such a positive person and dealing with my bad moods.
Thank you to Melpi, Dan, Kumiko and Florence for reading parts of my thesis.
Good luck everyone!!

Juri for being my second supervisor and giving me the freedom to run the mass spectrometry samples myself. My gratitude goes out to every single Rappsilber lab member, you have all helped me at some point over the last couple of years- Angel, Lutz, Colin, Adam, Lauri, Cristina, Flavia, Juan, Salman, Jimi, Karen and Georg. For all the times anyone ever stayed late to help me out, answered a panicked phone call at the weekend because something had gone wrong, or just took the time to answer my numerous questions- thank you, you are all amazing!!

Stefan, for feeding me during those last few weeks of writing and having to deal with my very messy flat. On that note….I would NOT like to thank the man that broke into my flat and stole my laptop 3 weeks before hand in, but thank you to the computer virus that prompted me to back-up everything a few days prior to this event!

All Edinburgh and non-Edinburgh friends! Sarah and Louise for being my holiday-buddies during those brief moments of relaxation. Mike, thank you for being there, and talking sense during those moments of project/thesis/life freak-outs.

Finally, thank you to my parents for being so supportive and patient, I appreciate everything you have done for me.

Lay Summary

When a single cell divides it is very important that the same amount of DNA is distributed equally into the two cells. To do this, DNA must first make two copies of itself through a process called replication. There is a slight problem however, unravelled DNA is very long (two metres) and it would be impossible to tease apart these strands successfully. Instead, the two sets of DNA are folded up into very distinct units, which in turn form the two identical arms of the classical X-shaped chromosome. Chromosomes must then line up along the centre of the cell and a 'tug of war' can commence. In this case, the rope represents an assembly called spindle microtubules and chromosomes must grab these ropes, one on either side, so that enough force can be generated to pull the two arms apart. The sites of these contacts are what my PhD is focused on and is mediated by a structure called the kinetochore. The kinetochore is made up of many different parts called proteins, over 100 infact, and can be thought of as the 'nuts and bolts' and 'cogs and springs' that keep the kinetochore machinery running. If we were to dismantle the kinetochore and lay all the pieces out, current research would be able to tell us, in many cases, what each part does and instructions on how to re-assemble some of the smaller internal mechanisms. However, putting it all back together correctly would be near on impossible. To try and fill in some of these blanks I have been looking at which parts depend on each other for their assembly into kinetochores. I am doing this by isolating chromosomes from cells missing the particular piece of interest and using a method called mass spectrometry to estimate how much of all the other kinetochore proteins still remain intact. This is important as malfunctions in the kinetochore have been directly linked to cancer progression and some developmental diseases, and to know not only the 'target' but how this change impacts downstream may lead to more tailored therapies.

Abstract

When cells divide, a series of events must proceed in a timely and co-ordinated manner to ensure that all DNA is replicated and partitioned equally between the two daughter cells. A central component of this process is the kinetochore, a large proteinaceous complex (>100 proteins) found within the centromere of all chromosomes. During the dynamic process of cell division, this machinery must be able to capture microtubules, promote chromosome movements towards the spindle midzone and ensure that segregration only occurs once this alignment has been successfully completed. This requires intricate mechanical and regulatory co-ordination between components and it is therefore no surprise that the structures responsible are structurally and functionally varied. It has, however, become clear that many kinetochore proteins assemble into distinct sub-complexes and despite the fact that their specific contributions are well studied, the way the many unique sub-assemblies come together to form a fully operational kinetochore is still poorly understood.

Here, chromosome isolation techniques from chicken DT40 cells combined with mass spectrometry employing Stable Isotope Labeling by Amino acids in Cell culture (SILAC), is used to compare the proteome of mitotic chromosomes from different conditional kinetochore knockout (KO) cell lines. This includes components of the inner kinetochore; CENP-C, CENP-T and CENP-W, and a sub-unit of the Ndc80 complex that is important for microtubule attachment. With these large data sets I have focused on the impact these depletions have on the architecture of the holo-kinetochore by measuring the SILAC ratios of individual proteins. From these measurements I can define whether specific components are decreased, increased or unchanged in terms of their abundance on chromosomes in response to the various deletions. I have found that proteins within the same complex typically behave in a similar manner across the different KO conditions. By integrating all of the data sets, dependency networks are revealed, as well as highlighting potential novel kinetochore proteins worthy of further study.

The KO cell lines listed above all exploit the doxycycline inducible shut-down of gene expression. This has proven to be a highly valued system in the study of many cellular processes; however, although gene expression is abolished immediately, full loss of function requires that proteins translated before drug addition are degraded. Depending on protein stability, this can take hours, or even days, and lead to the accumulation of unwanted secondary effects. To address this problem, an auxin-inducible degron (AID) system has been used to rapidly reduce the expression of kinetochore sub-units at the protein level. I find that AID-tagged CENP-T in DT40 cells is rapidly depleted within 1 hour of auxin addition, immediately preventing further proliferation. Importantly, this gives us a unique opportunity to study the effects and phenotypes of CENP-T depletion in a highly regulated way at different phases of the cell cycle.

Table of Contents

List of Figures

List of Tables

Abbreviations

ACA	anti-centromere antibodies
ACN	acetonitrile
AID	auxin-inducible degron
APC/C	anaphase promoting complex/cyclosome
bp	base pair(s)
BSA	bovine serum albumin
CATD	CENP-A targeting domain
CCAN	constitutive centromere associated network
CDKs	cyclin-dependent-kinases
cDNA	complementary DNA
C. *elegans*	*Caenorhabditis elegans*
CENP	centromere protein
CH	calponin homology
CLEM	correlative light and electron microscopy
CPC	chromosomal passenger complex
C-terminus	carboxyl-terminus
DAPI	4',6'-diamidino-2-phenylindole
ddH_20	double-distilled water
DNA	deoxyribonucleic acid
dNTPs	deoxynucleotidetriphosphate
Drosophila	*Drosophila Melanogaster*
DTT	dithiothreitol
E. *coli*	*Escherichia coli*
ECL	enhanced chemiluminescence
EDTA	ethylenediaminetetraacetic acid
EM	electron microscopy
EtOH	ethanol
EGFP	enhanced green fluorescent protein

H/L	heavy/light
IAA	iodoacetamide
IAA/Auxin	indole-3-acetic acid/Auxin
kDa	kilodalton
K-fibres	kinetochore-fibres
KI motif	Lysine-Isoleucine motif
KMN	KNL-1-Mis12-Ndc80
K-MTs	kinetochore-microtubules
KO	knockout
LacO	lac operator
LB	Luria-Bertani
LC-MS/MS	liquid chromatography-tandem mass spectrometry
MAD	median absolute deviation
MCC	mitotic checkpoint complex
MeOH	methanol
mg	milligram
ml	millilitre
mM	millimolar
µM	micromolar
µm	microns
µg	microgram
NAC/NAD	CENP-A-nucleosome-associated/CENP-A-nucleosome distal
NEB	nuclear envelope breakdown
N-terminus	amino-terminus
PBS	phosphate buffered saline
PCR	polymerase chain reaction
ppm	parts per million
RNAi	RNA interference
RZZ	Rod-Zwilch-Zw10
SAC	spindle assembly checkpoint

SCF	Skp1-Cullin-1-Fbox protein
SCX	strong cation exchange
SDS-PAGE	sodium dodecyl sulphate-polyacrylamide gel electrophoresis
SILAC	Stable Isotope Labelling with Amino acids in Cell culture
siRNA	small interfering RNA
TCA	trichloroacetic acid
tTA	tetracycline transactivator
WT	wild type
Xenopus	*Xenopus laevis*

1 Introduction

1.1 The Cell Cycle

For a cell to divide and successfully pass on its genetic information into two daughter cells four main events must proceed in a highly co-ordinated fashion: cell growth, DNA replication, chromosome segregation and cell division. In eukaryotes these events do not overlap and can be split up into distinct phases. S phase is when DNA synthesis takes place and extra gap phases are inserted before (G1) and after (G2) to allow for growth and increases in cell mass (Norbury and Nurse, 1992) (Figure 1). These three phases define interphase (Figure 1; inner grey arrows) and make up the majority of the cell cycle. M phase, or mitosis, can then proceed; this is the time when duplicated DNA can be separated into two daughter cells. There is also a phase called G0, which represents cells that have exited the cell cycle from G1. These cells cease to proliferate and can, for example, differentiate or become senescent. Senescent cells are unable to re-enter the cell cycle, but other 'dormant' cell types are recruited to return to G1 if the appropriate environmental stimuli are present.

An important aspect of the cell cycle is that it must maintain uni-directionality. This requires a careful balance between mechanisms that drive forward progression and those that sense and halt processes if abnormalities are detected. The key regulators involved in these roles are the cyclin-dependent-kinases (CDKs)/cyclins and the associated inhibitory checkpoint pathways. CDKs are only active when they are bound by cyclins and drive forward the cell cycle by phosphorylating a variety of target substrates (Evans et al., 1983; Hadwiger et al., 1989; Lohka et al., 1988; Nash et al., 1988). While CDKs are constitutively expressed, cyclins are destroyed periodically by ubiquitin mediated proteolysis and display oscillations in their cellular abundance (Glotzer et al., 1991; Hershko et al., 1991). There are cyclins associated with G1 (cyclin D), S phase (cyclins E and A) and mitosis (cyclins B and A) and temporal activation at these points can be

quickly reversed by proteolysis; this feature allows progression in an irreversible manner.

Checkpoints function to counteract cell cycle progression and can delay transition from one cell cycle phase to the next until each phase has been accurately completed (Figure 1). In interphase, the DNA damage and DNA replication checkpoints ensure that mitosis cannot occur until damaged DNA (for example through irradiation) is repaired, and all of the genome has been duplicated without significant errors (Painter and Young, 1980; Weinert and Hartwell, 1988). In mitosis, the spindle assembly checkpoint prevents anaphase onset until all chromosomes are correctly attached to spindle microtubules (Rieder et al., 1995; Sluder, 1979, 1989). If this signal was perturbed, genetic material might not be segregated equally and would give rise to aneuploidy, a genetic imbalance characteristic of cancer cells and some developmental diseases (Gordon et al., 2012).

1.2 Stages of Mitosis

Mitosis is a short (~1 hour in human cells), but highly dynamic process characterised by dramatic changes in cell morphology, concluding with the generation of two identical daughter cells. Mitosis consists of six stages: prophase, prometaphase, metaphase, anaphase and telophase/cytokinesis (Figure 2).

During prophase, chromatin starts to condense and the nucleoli and nuclear envelope begin to disassemble. The replicated DNA molecules become highly-compacted and assemble into chromatids; the distinct structures making up the two arms of the classical 'X shaped' chromosomes (Figure 2). At this point in time the sister chromatids are held together along the arms and central regions by a protein complex called Cohesin (Nasmyth et al., 2000). The centrosomes, which were duplicated starting in S phase, show an increase in microtubule nucleation and re-organise the cytoskeleton into radial arrays (asters), and begin to move apart across the nuclear surface.

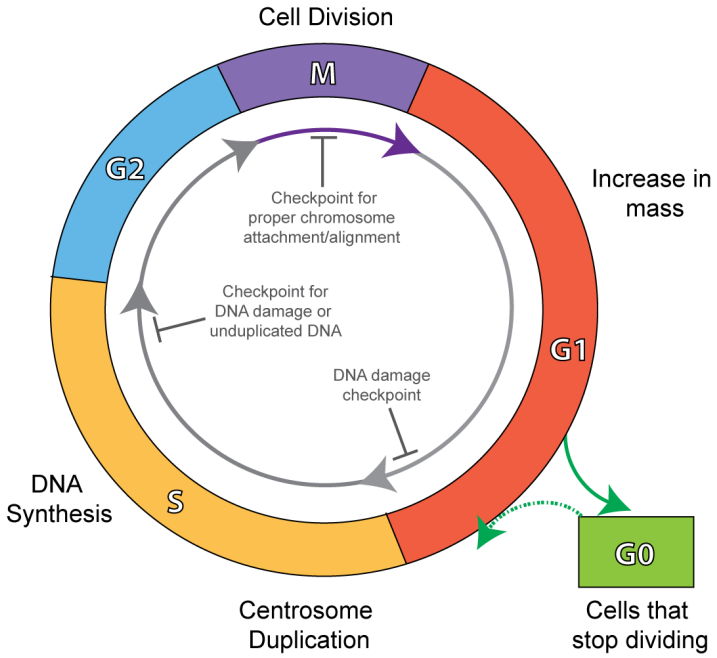

Figure 1. Schematic representation of the eukaryotic cell cycle. The consecutive events of the cell cycle, represented by various colours, are proportional to the relative duration of that cell cycle phase. The inner arrows indicate the direction of the cell cycle: grey arrows within the G1, S and G2 phases reflect interphase, while purple depicts mitosis. Checkpoints operating at different cell cycle stages are also indicated.

The transition into prometaphase is defined by nuclear envelope breakdown (NEB). The contents of the nucleus are no longer compartmentalised from the cytoplasm and this allows microtubules emanating from the two centrosomes to make contacts with chromosomes. The dynamic spindle microtubules are rapidly polymerising and de-polymerising and are only stabilised once end-on attachments (microtubule plus ends) are formed with protein assemblies called kinetochores (Cheeseman and Desai, 2008) (Figure 2). These structures are found on either side of chromosomes and connect with microtubules extending from each of the two poles. Biorientation of the chromosomes (each kinetochore is stably bound by microtubules from opposite poles) does not happen straightaway and intermediate associations such as lateral (kinetochores bind to the sides of microtubules), syntelic (sister kinetochores attach to the same pole) and merotelic (single kinetochore bound by microtubules from both poles) attachments must be

corrected (Tanaka, 2013). During this time inter-polar microtubules from the two poles also take part in anti-parallel interactions aiding bipolar spindle formation.

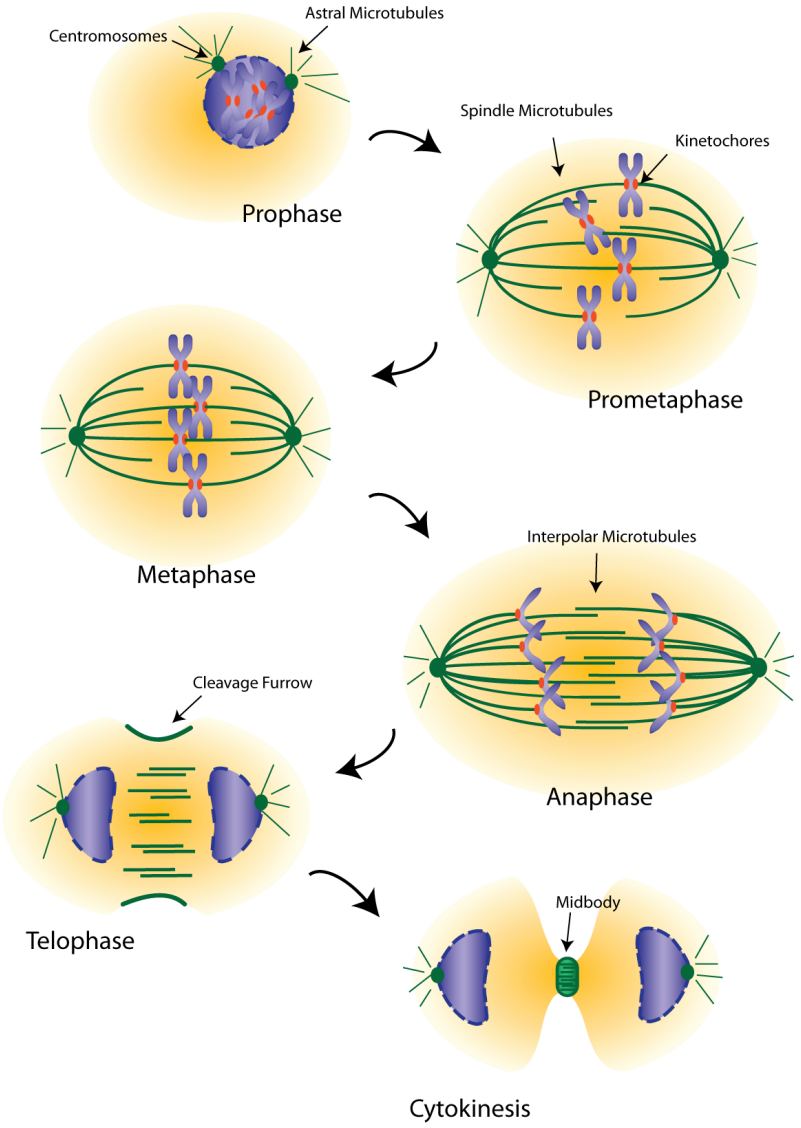

Figure 2. The different stages of mitosis. The main morphological changes the cell must go through to complete mitosis successfully are shown through the changing dynamics of DNA (blue) and microtubules (green). The dashed blue lines surrounding the DNA in prophase and cytokinesis represent nuclear envelope breakdown (NEB) and reformation, respectively. Red dots on either side of the chromosomes depict kinetochores. Green dots connected to microtubules represent centrosomes.

When kinetochores are bound by multiple microtubules they form stable bundles called kinetochore-fibres (K-fibres). These structures generate co-ordinated forces to align chromosomes along the plane equidistant between the cell poles (Tanaka, 2013). The resulting configuration is called the metaphase plate (Figure 2). The spindle assembly checkpoint (SAC) monitors the state of this transition, and only once all chromosomes are bi-orientated can anaphase onset commence. The consequence of satisfying the checkpoint is that the anaphase promoting complex/cyclosome (APC/C), a multi-subunit E3 ubiquitin ligase, is activated and can target substrates for degradation (Peters, 2002). A primary target is securin, a protein that binds separase and keeps the enzyme in an inactive state. When securin is destroyed by ubiquitin-mediated degradation, separase is able to cleave cohesin allowing segregation of sister chromatids (Nasmyth et al., 2000).

The pulling action generated by depolymerising kinetochore-microtubules (K-MTs) allows sister chromatids to move towards their respective poles (Scholey et al., 2003). This movement is co-ordinated by both microtubule depolymerisation at kinetochores and poleward microtubule flux (Ganem and Compton, 2006). While these populations of microtubules shorten, non-K-MTs (inter-polar) push-apart centrosomes in the later stages of anaphase (Scholey et al., 2003), further increasing the distance between the two sets of genetic material (Figure 2). The anti-parallel attachments localised in the midzone become more concentrated in telophase and the nuclear envelope also reforms around chromosomes that have begun to de-condense. In cytokinesis, ingression of the cleavage furrow is mediated by actin and myosin re-organisation and formation of the contractile ring (Salmon, 1989). Invagination of the plasma membrane at this site eventually leads to the creation of an intracellular bridge of compressed microtubules called the mid-body (Salmon and Wolniak, 1990). This is followed by abscission (Carlton et al., 2012), with the creation of two identical daughter cells.

1.3 The Kinetochore

1.3.1 Ultrastructure of the Kinetochore

The kinetochore is a protein-based structure that is found at the constriction site and on either side of all mitotic chromosomes. These structures do not just simply act as a docking site for K-MTs. A kinetochore must (a) detect and correct all improper attachments, (b) support and generate enough force for chromosome movements, (c) ensure sister chromatids are only separated once all chromosomes are bi-orientated along the metaphase plate (Cheeseman and Desai, 2008; Santaguida and Musacchio, 2009).

The complexity of the kinetochore varies significantly between different organisms. In budding yeast the base of this structure takes shape as a 'point' centromere and is defined by a 125 bp sequence consisting of three distinct DNA elements: centromere DNA element I (CDEI), II and III (McAinsh et al., 2003). Importantly, this sequence is sufficient to support kinetochore assembly in a sequence-dependent manner. Some organisms, such as *C. elegans*, assemble holocentric kinetochores, which are defined by centromeres that extend along the whole of the chromosome (De Rop et al., 2012). Higher eukaryotic cells possess 'regional' centromeres, formed by repeating domains several megabases in length. For example, human centromeres consist of higher order alphoid DNA arrays consisting of head-to-tail arrangements of a 171 bp alpha satellite repeat (1-5 Megabases in total) (De Rop et al., 2012; Willard, 1990). However, these repeats do not themselves define centromere assembly, as neocentromeres that lack alphoid sequences can still assemble a functional kinetochore (Alonso et al., 2007; Warburton et al., 1997).

At the ultrastructural level, regional centromeres are characterised by the formation of trilaminar plates. These vary in size in different eukaryotes with larger structures in general correlating with an increase in microtubule attachments, which remain singular

in *S. cerevisiae* and comprise up to 15-20 in human cells (Cheeseman and Desai, 2008; Santaguida and Musacchio, 2009).

This trilaminar morphology of vertebrate kinetochores is formed from two blocks of electron dense material, the inner and outer plate, and a 15-35 nm electron-translucent middle region that separates these disks (Figure 3A) (Cheeseman and Desai, 2008; Comings and Okada, 1971; Jokelainen, 1967; Maiato et al., 2004). The inner plate acts as a stabilizer through contacts with centromeric chromatin and the outer plate provides a surface for microtubule attachment. Although not depicted in Figure 3A, electron microscopy (EM) has also distinguished a 'fibrous corona' in kinetochores free of microtubules. These fibril-like structures are found on the surface of the outer plate and extend out towards the cytoplasm (Cheeseman and Desai, 2008; Ris and Witt, 1981). This tri-laminar structure has come under scrutiny recently with freeze-substitution fixation and electron tomography studies used to visualise kinetochores at high resolution (Dong et al., 2007; McIntosh et al., 2013). In mammalian PtK_1 cells these distinct plates are composed of a meshwork of fibres, some of which re-orientate outwards upon microtubule attachment and specifically associate with microtubule walls (Dong et al., 2007). The three-tiered structure is also absent or faint in other eukaryotic species (McIntosh et al., 2013).

Whether this trilaminar conformation holds true *in vivo* does not over-shadow the fact that numerous studies employing genetic and biochemical approaches have dramatically expanded the list of known kinetochore proteins across species (Figure 3B) (Welburn and Cheeseman, 2008; Westermann et al., 2007). These can be classified into different subgroups, localise to different regions across the kinetochore and perform a diverse array of functions.

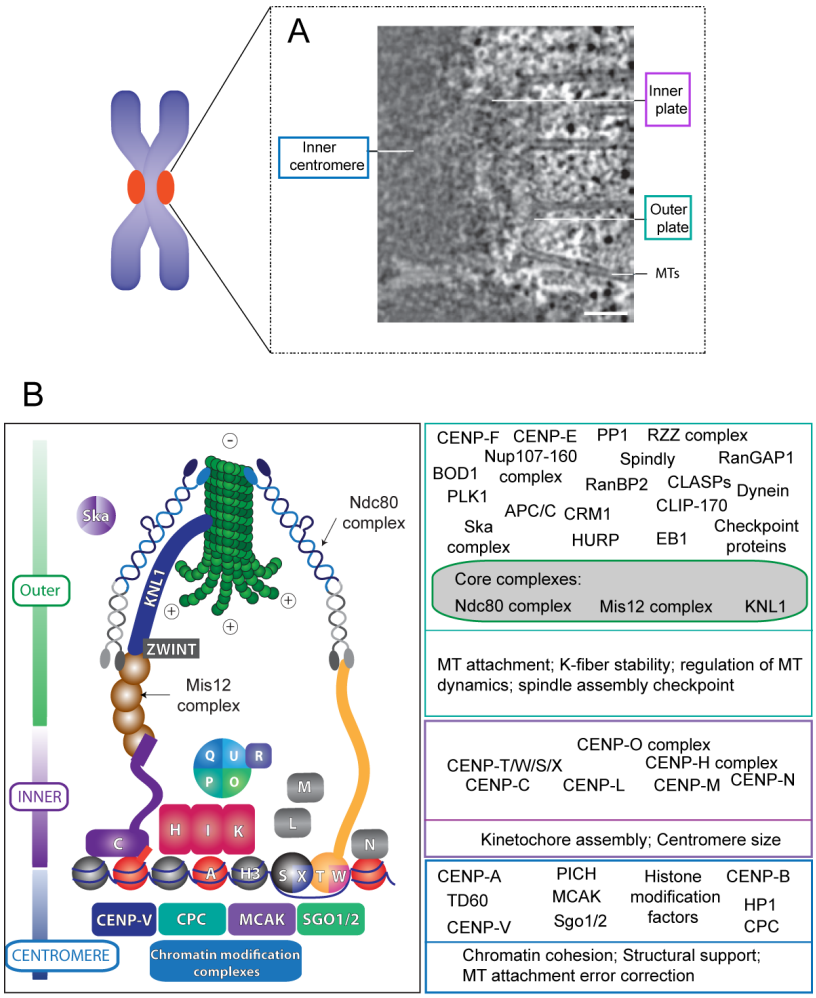

Figure 3. The architecture of vertebrate kinetochores at the ultrastructural and molecular level of assembly. A. An electron tomographic slice through human kinetochores depicts an inner centromeric region formed from highly condensed DNA, an inner plate, and a number of spindle microtubules simultaneously contacting the outer plate. Assembly of this trilaminar structure is transient, forming from a condensed ball of chromatin at the beginning of prophase and disassembling at the end of mitosis. Scale bar: 100 nm (Adapted from (Cheeseman and Desai, 2008)). **B.** A schematic representation and list of core kinetochore components found within the inner centromere (Centromere), inner plate (Inner) and the outer plate (Outer). The main functions associated with these groupings are also listed. CENPs are labelled with their respective letter (e.g. 'C' is CENP-C). A and H3 depict a CENP-A or histone H3 containing nucleosome. Chromosomal Passenger Complex (CPC), Shugoshin 1/2 (Sgo1/2), Mitotic centromere-associated kinesin (MCAK), ZW10-interacting protein 1 (ZWINT), Spindle and kinetochore-associated protein (Ska) complex, Nuclear division cycle 80 (Ndc80) complex, Missegregation 12 (Mis12) complex and Kinetochore null protein 1 (KNL-1). Schematic based on Figure from (Maiato et al., 2004)

The heterochromatin of the inner centromere is where the chromosomal passenger complex (CPC) is located. The CPC plays a role in correcting improper microtubule attachments in a tension dependent fashion (Figure 3B) (Carmena et al., 2012). The Aurora B kinase is at the centre of this activity and combines with inner centromere protein (INCENP), Borealin and Survivin to localise to inner centromeric regions during early mitosis. The CPC redistributes to the spindle mid-zone during late mitosis (Carmena et al., 2012). Recently, two important histone phosphorylation sites have been shown to be important for CPC localisation to the inner centromere. First, phosphorylation of histone H3 at Threonine 3 (H3T3) by Haspin kinase promotes contacts with Surivivin via its Baculovirus IAP Repeat (BIR) domain. Second, Borealin that has been phosphorylated by Cyclin-dependent kinase 1 (Cdk1) binds Shugoshin 1 (Sgo1), which in turn interacts with phosphorylated histone H2A at Threonine 120 (H2AT120) (reviewed in (Carmena et al., 2012)). Once at this site, phosphorylation of target substrates by Aurora B is counteracted by Protein Phosphatase 1 (PP1) activity; this gradient promotes bi-orientation by destabilising K-MT attachments that do not generate tension (i.e. syntelic and merotelic attachments) (Liu et al., 2009; Liu et al., 2010; Tanaka et al., 2002). Additional chromatin modification factors are also associated with the underlying chromatin and must create an epigenetic environment suitable for kinetochore assembly (Bergmann et al., 2012).

The constitutive centromere associated network (CCAN) localises to the inner plate, with some of these components interacting directly with the underlying DNA, while outer components, such as the KNL-1-Mis12-Ndc80 (KMN) network, are directly involved in mediating spindle microtubule attachments (Cheeseman et al., 2006). Ultimately, all components must work together to co-ordinate microtubule capture and the successful segregation of chromatids during mitosis. I will first discuss the role of CENP-A in kinetochore assembly, followed by a description of the molecular composition of inner and outer kinetochore compartments. Finally, I will discuss current models of dependency pathways defining kinetochore architecture.

1.3.2 CENP-A

Centromere assembly in many species appears to be independent of the underlying DNA sequence. Instead, it is thought that the epigenetic make-up of the centromere is crucial and is based is on the composition/organisation of the chromatin (Allshire and Karpen, 2008). CENP-A is a histone H3 variant that plays a prominent role in determining centromere identity. In budding yeast, a single CENP-A containing nucleosome defines the point centromere, while higher eukaryotic cells contain domains of CENP-A and H3 containing nucleosomes interspersed over several megabases of DNA. CENP-A was originally identified using antibodies from autoimmune patient sera (Earnshaw and Rothfield, 1985). But now homologues have been described across many species, including budding yeast (Cse4) (Meluh et al., 1998), fission yeast (Cnp1) (Takahashi et al., 2000), *C. elegans* (HCP3) (Buchwitz et al., 1999) and *Drosophila* (CID) (Henikoff et al., 2000). When CENP-A is over-expressed in *Drosophila*, ectopic kinetochores can assemble on chromosome arms, indicating that it can function alone as an initial platform for assembly (Heun et al., 2006). Also, synthetic CENP-A chromatin arrays when exposed to *Xenopus* egg extracts can selectively recruit a number of core kinetochore proteins (Guse et al., 2011). These kinetochores are partially functional, as an increase in spindle checkpoint protein recruitment is observed in the absence of microtubules. CENP-A is required for the localisation of all other constitutive centromere proteins, placing it at the top of the hierarchy in terms of kinetochore assembly (Cheeseman and Desai, 2008). However, in human cells CENP-A over-expression is not sufficient to nucleate kinetochore formation and additional factors are thought to be involved (Gascoigne et al., 2011).

1.3.3 The interface with centromeric chromatin: CCAN

The CCAN is a group of 16 proteins that remain constitutively bound to centromeric chromatin throughout cell division (Westhorpe and Straight, 2013). They act as the direct platform connecting the underlying DNA with outer kinetochore proteins required for spindle microtubule attachment during mitosis. Several members were first enriched, along with ~40 other proteins, in CENP-A chromatin isolated from human interphase nuclei and in a fraction called the interphase centromere (ICEN) complex (Izuta et al., 2006; Obuse et al., 2004). Other subsets of the CCAN were subsequently described using affinity-purification combined with proteomics approaches. These included the CENP-A-nucleosome-associated (NAC)/ CENP-A-nucleosome distal (NAD) complex and the CENP-H/I complex (Foltz et al., 2006; Okada et al., 2006a). When taken together, the complete list contained CENP-C, H, I, K-U and was later expanded to include two additional core components, CENP-W (Hori et al., 2008a) and CENP-X (Amano et al., 2009).

At the ultrastructural level CENP-A, CENP-C, CENP-R and CENP-T map to the inner kinetochore plate by immuno-EM (Saitoh et al., 1992; Suzuki et al., 2011) and super-resolution microscopy has placed CENP-C, CENP-H, CENP-I and CENP-T in close proximity to CENP-A nucleosomes (Ribeiro et al., 2010). Although these proteins are closely associated and localise together within the inner kinetochore, biochemical and phenotypic analysis has begun to unravel distinct complexes within the internal sub-structure of the CCAN. Several groups have been reported; a discrete CENP-O complex consisting of CENP-O, P, Q, R, U, a CENP-H complex formed from CENP-H/I/K, and complexes containing CENP-L/M/N, CENP-T/W/S/X and CENP-C (Figure 4A). CCAN subunits and their respective homologs in S. *pombe* and S. *cerevisiae* are listed in Table 1. Despite these groupings, the literature remains very confusing and there are many contradictory findings in terms of direct contacts, interdependencies and functional inputs across different model organisms. Some of these will be discussed below.

Table 1- Inner kinetochore proteins across humans, S. *pombe* and S. *cerevisiae*. Adapted from (Schleiffer et al., 2012).

Humans	S. pombe	S. cerevisiae	Sub-complex
CENP-A	Cnp1	Cse4	CENPA Nucleosome
CCAN			
CENP-C	Cnp3	Mif2	CENP-C
CENP-O	Mal2	Mcm21	CENP-O complex
CENP-P	Fta2	Ctf19	
CENP-Q	Fta7	Okp1	
CENP-U	Mis17	Ame1	
CENP-R			
CENP-H	Fta3	Mcm16	CENP-H complex
CENP-I	Mis6	Ctf3	
CENP-K	Sim4	Mcm22	
CENP-T	SBPC800/Cnp20	Cnn1	CENP-T/W/S/X complex
CENP-W	SPAC17G8.15	Wip1	
CENP-S	SPBC2D10.16	Mhf1	
CENP-X	SPCC576.12c	Mhf2	
CENP-M			CENP-L/M/N
CENP-N	Mis15	Chl4	
CENP-L	Fta1	Iml3 (Mcm19)	

1.3.3.1 Direct link with underlying chromatin

Some CCAN components have been shown to exhibit DNA binding activity. To date, there are 3 paths directly linked to centromeric chromatin: CENP-N, CENP-C and the CENP-T/W/S/X complexes.

CENP-N has been shown to bind directly to CENP-A nucleosomes in vitro (Carroll et al., 2009). If CENP-A is exchanged for histone H3 in reconstituted nucleosomes, contacts with CENP-N are abolished, while CENP-A/H3 chimeras containing only the CENP-A targeting domain (CATD) still possess CENP-N binding activity. In human cells, incorporation of overexpressed GFP-CENP-A into chromosome arms leads to ectopic CENP-N recruitment (Gascoigne et al., 2011). However, CENP-N can also be assembled into kinetochore-like structures formed on Lac operator (Lac-O) arrays in the

absence of CENP-A after the targeting of amino (N)-terminal portions of CENP-C or CENP-T (Gascoigne et al., 2011). Therefore, contacts with CENP-A nucleosomes and additional CCAN components may co-ordinate CENP-N centromere recruitment.

CENP-C can be affinity purified with CENP-A containing nucleosomes/chromatin (Foltz et al., 2006; Obuse et al., 2004). The exact region for this interaction has been attributed to a short six amino acid sequence in the carboxyl (C)-terminal tail of CENP-A, which is independent of the CATD/CENP-N binding interface (Figure 4B) (Carroll et al., 2010; Guse et al., 2011). Conflicting reports in chicken DT40 cells show that extensive digestion of DNA allows CENP-C to preferentially bind histone H3 nucleosomes (Hori et al., 2008a), while super-resolution microscopy demonstrates co-localisation with CENP-A sub-domains in unfolded centromeres (Ribeiro et al., 2010). In higher eukaryotes, interspersed domains of CENP-A and H3-containing nucleosomes define centromeres. This close proximity would allow CENP-C to contact both nucleosome variants, but this would depend heavily on how the chromatin is packaged. Certainly, the C-terminal portion of CENP-C has been reciprocally pulled down with both CENP-A and histone H3 in human Hek-293 cells (Trazzi et al., 2009).

Although CENP-T and CENP-W are required for viability of chicken cells (Hori et al., 2008a), CENP-S and CENP-X are not (Amano et al., 2009). CENP-T/W and CENP-S/X form separate dimers through their histone fold domains and come together to generate a heterotetrameric complex capable of binding and supercoiling DNA (Nishino et al., 2012). This complex displays structural similarities with canonical histones (Nishino et al., 2012). Interactions with surrounding nucleosomes are still important however as CENP-T is reduced at centromeres in CENP-A deficient chicken cells despite being preferentially bound to H3 nucleosomes in micrococcal nuclease (MNase) digested chromatin fractions (Hori et al., 2008a). In contrast to the 146 bp sequences wrapped around canonical nucleosome cores, the CENP-T/W/S/X complex can only protect 100 bp DNA segments from digestion (Nishino et al., 2012). How this partial DNA bending functions collaboratively with CENP-A and H3 subdomains requires further study.

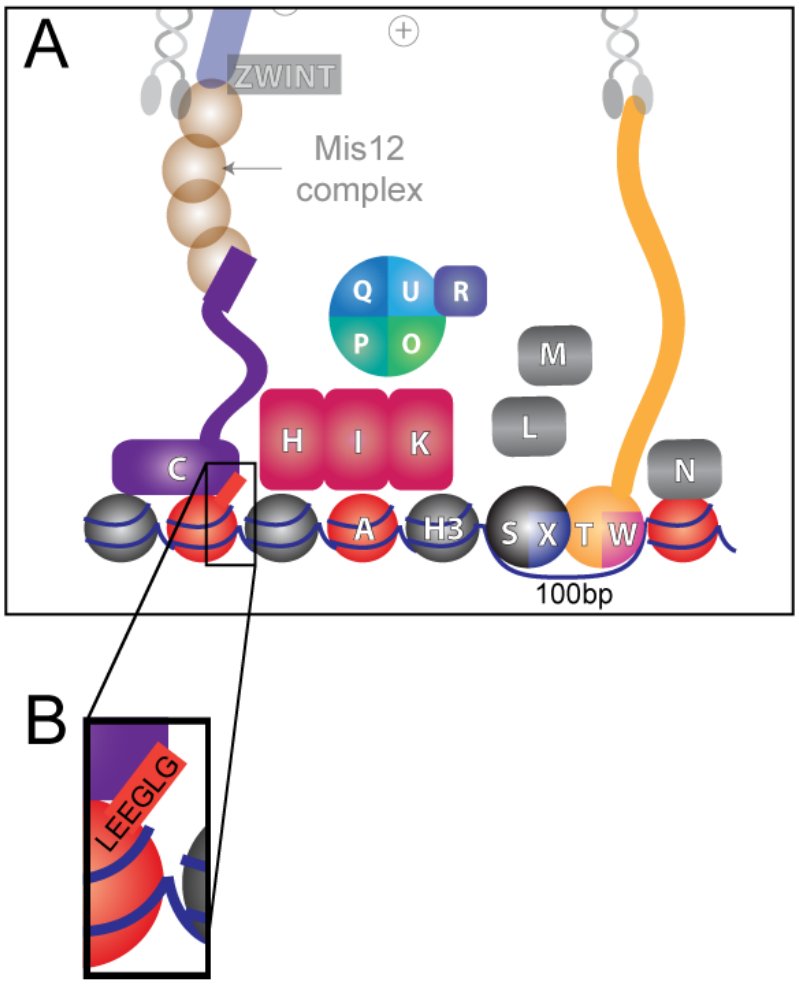

Figure 4. The constitutive centromere associated complex (CCAN). A. Schematic representation of histone H3 and CENP-A containing nucleosomes with 16 components of the CCAN. These can be split into different sub-complexes: CENP-C, CENP-H/I/K, CENP-L/M/N, CENP-O/P/Q/R/U and CENP-T/W/S/X. CENP-T/W/S/X can protect 100bp lengths of DNA from digestion. **B.** CENP-C can make direct contacts with the LEEGLG amino acid sequence at the C-terminus of CENP-A.

1.3.3.2 Dependencies within the CCAN

CENP-H, I and K exhibit strong G2/M arrest phenotypes leading to subsequent cell death in mitosis after depletion (Fukagawa et al., 2001; Nishihashi et al., 2002; Okada et al., 2006a). More recently, components of the CENP-H complex have been linked to regulating microtubule dynamics (Amaro et al., 2010) and targeting CENP-A deposition at centromeres (Hori et al., 2013; Okada et al., 2006a) (the latter will be described in more detail later).

CENP-H/I levels on kinetochores change during chromosome oscillations, accumulating on the sister kinetochores associated with growing microtubules (Amaro et al., 2010). It has been proposed that this preferential distribution promotes regular chromosome movements required for alignment on the metaphase plate by reducing the rate of growth and shrinkage of microtubules. Congression defects associated with CENP-H depletion have also been reported elsewhere (Fukagawa et al., 2001; McClelland et al., 2007). In chicken cells, the CENP-H complex is upstream of CENP-M and the CENP-O subgroup (Okada et al., 2006a), but is downstream of CENP-A and CENP-T/W (Hori et al., 2008a). In HeLa cells, as well as relying on CENP-T for centromere localisation, CENP-H is also dependent on CENP-C (Gascoigne et al., 2011). Therefore two paths, instead of one, must work together to maintain full CENP-H signals in humans.

Differences between model systems are also seen for CENP-C dependency networks. As well as trying to clarify the exact chromatin interface there is also some controversy as to whether CENP-C is required for the recruitment of additional CCAN components. In one study, small interfering RNA (siRNA) depletion of CENP-C in human culture cells mislocalised CENP-H, I, K and T signals at centromeres (Carroll et al., 2010), while another group reported no effect on CENP-T levels (Gascoigne et al., 2011). In contrast, CENP-C deficient chicken cells still maintain some CENP-H, CENP-O, CENP-T, CENP-K, CENP-U and CENP-S localisation to centromeric regions (Hori et al., 2008a; Kwon et al., 2007). But in fission yeast the CENP-C homolog (Cnp3) can directly

interact with CENP-L (Fta1), a Sim4-complex subunit (vertebrate CENP-H-I complex) (Tanaka et al., 2009). For budding yeast proteins, CENP-L (Iml3) binds and stabilises the C-terminal of CENP-N (Chl4) and this in turn allows the N terminal of CENP-N to make contacts with CENP-C (Mif2) (Hinshaw and Harrison, 2013). Establishing the correct order of CCAN relationships in different organisms is therefore a crucial goal in understanding CENP-C directed assembly.

Although a protein might be defined as functioning in a specific subcomplex, the contributions of these proteins to kinetochore assembly may vary. In chicken DT40 cells removal of CENP-T/W affects the recruitment of most other CCAN components (including S/X complex) (Hori et al., 2008a), while CENP-S/X loss does not (Amano et al., 2009). Differences are also reflected in the resulting phenotypes, where a strong mitotic block and milder chromosome segregation defects are associated with CENP-T/W and CENP-S/X knock out (KO) cells, respectively (Amano et al., 2009; Hori et al., 2008a).

Members of the CENP-O complex co-localise with CENP-K and CENP-L at ectopic chromatin arrays (Eskat et al., 2012), but are downstream of CENP-H/I/K in the hierarchy of CCAN assembly pathways (Hori et al., 2008b; McClelland et al., 2007; Okada et al., 2006a). Within the subgroup they form highly inter-dependent interactions (Amaro et al., 2010; Foltz et al., 2006; Hori et al., 2008b). These proteins are non-essential in chicken cells. Their loss results in general chromosome segregation defects and an inability to recover from nocodazole-induced spindle damage (apart from CENP-R) (Hori et al., 2008b; Minoshima et al., 2005). CENP-L is classed with CENP-M and N as loss of these proteins results in a severe phenotype characterised by a strong mitotic arrest/cell death (Okada et al., 2006a; Takeuchi and Fukagawa, 2012).

In some instances similar depletion phenotypes may not be a good read-out of subcomplex composition. For example, CENP-L and CENP-O, which are typically thought to associate within different subgroups, have a similar siRNA depletion

phenotype in human cells. This is characterised by an increase in the rates of monopolar spindle formation (McAinsh et al., 2006; McClelland et al., 2007). It has been proposed that reduced K-fibre stability affects kinetochore-generated pushing forces on centrosomes and centrosomal separation is therefore affected (Toso et al., 2009). Similar phenotypes do not necessarily mean that the loss and recruitment of other kinetochore proteins is the same. For instance, CENP-H levels are increased upon CENP-O loss, but decreased in CENP-L deficient cells, and might support the fact that they are part of different subcomplexes (McClelland et al., 2007).

1.3.4 CCAN dynamics

Although CCAN proteins are present constitutively throughout the cell cycle, it has been shown that many of the proteins display variations in turnover rates at centromeres and overall levels during the different phases of cell division.

For many of the CCAN components the rate of turnover has been measured at different cell cycle stages using Fluorescence Recovery After Photobleaching (FRAP). Both CENP-C and CENP-H have higher rates of exchange in G1 and G2, but become more stable in S-phase (Hemmerich et al., 2008). In comparison, CENP-I only exchanges during S phase (Hemmerich et al., 2008) and both CENP-T and CENP-W are more stable during the G1/early stages of replication, but exchange in late S phase (Prendergast et al., 2011). To support these findings CLIP-tagged CENP-T and CENP-W, which is a method that can 'pulse-label' a population of the given protein, loads onto centromeres in late S phase and G2 (Prendergast et al., 2011). CENP-O complex components display varying extents of recovery in G1, S and G2 phases and it has been suggested that these differences argue against a pre-formed complex that is recruited onto kinetochores (Eskat et al., 2012).

CENP-C, CENP-T and CENP-I levels peak in late G2/mitosis (Eskat et al., 2012; Gascoigne and Cheeseman, 2013; McClelland et al., 2007). Recently, live-cell imaging

has been used to quantitate the levels of kinetochore proteins during mitosis, with the amount of CENP-C, CENP-T and CENP-H increasing dramatically after NEBD and dropping to pre-mitotic levels following anaphase onset (Gascoigne and Cheeseman, 2013). The opposite has been observed for CENP-N where signals increase during S-phase and decrease at mitosis (Gascoigne and Cheeseman, 2013; Hellwig et al., 2011; McClelland et al., 2007). Similarly, CENP-O is loaded in S-phase and is found at lower levels on centromeric regions in mitosis (Eskat et al., 2012; McAinsh et al., 2006).

It is still unclear how many of these subtle temporal changes in protein levels affect the structure and function of the kinetochore. However, the differences in CCAN dynamics are likely to have an impact on dependency pathways that define the kinetochore at different stages of the cell cycle. For example, re-organisation of the kinetochore has been implicated in chicken cells where removal of CENP-H and CENP-K reduces CENP-C levels in interphase, but not in mitosis (Fukagawa et al., 2001; Kwon et al., 2007). Another example involves CENP-U and CENP-Q, where a sub-population has been shown to form a stable complex in G1/S phase. This complex recruits Plk1 in late G2/early mitosis via Plk1 phosphorylation of CENP-U (Kang et al., 2011). As Plk1 becomes active in early mitosis, it in turn phosphorylates CENP-Q, promoting the release of the complex from kinetochores. Therefore establishing dependency pathways downstream of CENP-U or CENPQ would depend on the cell cycle stage being studied. It would therefore be very interesting to be able to compare kinetochore assembly pathways in G1, S, G2 and mitosis.

1.3.5 Bridging the gap- linking the CCAN to the outer kinetochore

The CCAN acts as a platform anchoring constituents of the outer kinetochore plate. The latter proteins are more dynamic and predominantly associate with the structure only upon progression into mitosis. The KMN is a highly conserved network of proteins in eukaryotes and contains kinetochore null protein 1 (KNL1) plus the nuclear division cycle 80 (Ndc80) and missegregation 12 (Mis12) complexes. These proteins associate

with kinetochores in prophase and persist at these regions until telophase. The KMN network forms a crucial part of the microtubule binding apparatus and is required for end on attachments of spindle microtubules. Defective assembly of the KMN leads to problems with biorientation and faithful segregation (Cheeseman et al., 2006; Cheeseman and Desai, 2008).

The Ndc80 complex contains four subunits that come together to form a ~57 nm rod-like structure with two globular heads at either end. While the spindle pole Spc24 and Spc25 subunits face inwards and make contacts with kinetochores, the N-terminal Ndc80 (also called Hec1 in humans) and Nuf2 subunits bind directly to microtubules. These two dimers are held together by alpha-helical colied-coil domains (Cheeseman and Desai, 2008; Santaguida and Musacchio, 2009). The globular domains of the Ndc80-Nuf2 dimer fold into a calponin homology (CH) domain, which can mediate interactions with microtubules. This CH domain contains a site termed the 'toe print' that acts like a conformation sensor by distinguishing between straight and curled microtubule protofilaments (Alushin et al., 2010). The latter represent populations of depolymerising microtubules to which Ndc80 binds with less affinity. In addition, the positively charged N-terminal tail of the Ndc80 subunit makes electrostatic interactions with the acidic E-hook of tubulin (Alushin et al., 2010; Ciferri et al., 2008; Wei et al., 2007). This aids in co-operative binding of the Ndc80 complex to microtubules (Alushin et al., 2010). If the 'toe print' of Ndc80 is displaced upon depolymerisation of microtubules, it has been hypothesised that biased diffusion of the Ndc80 complex helps co-ordinate contacts that shift towards the more stable ends of microtubules (minus ends), although other models have also been proposed (Asbury et al., 2011; Foley and Kapoor, 2013). This would explain how end-on microtubule binding is maintained during anaphase.

KNL-1 (Blinkin, Spc105) was first discovered in *C. elegans* using an RNA interference (RNAi) based screen to look for genes involved in chromosome segregation (Desai et al., 2003; Gonczy et al., 2000). The KNL-1 human homolog is large (300 kDa) and forms a heterodimer (Varma and Salmon, 2012). KNL-1 depletion leads to a

misalignment of chromosomes at metaphase and in conditional KO chicken DT40 cells viability is lost (Cheeseman et al., 2008). In *C. elegans* and *Drosophila* KNL-1 is absolutely required for Ndc80 localisation to centromeres (Desai et al., 2003; Przewloka et al., 2007), but in human cells CENP-H/I/K has also been shown to play a prominent role (Cheeseman et al., 2008). S. *cerevisiae* and humans orientate KNL-1 (yeast Spc105) along the K-MT axis, with the N-terminus closer to microtubules (Joglekar et al., 2009; Wan et al., 2009). This agrees with findings showing that KNL-1 can support an additional microtubule-binding site *in vitro* and act synergistically to increase overall binding affinity of the KMN (Cheeseman et al., 2006).

The human Mis12 complex is a 22 nm rod-like structure that forms consecutive links of Nnf1, Mis12, Dsn1 and Nsl1 that are directed along the inner-to-outer axis of the kinetochore (Petrovic et al., 2010; Wan et al., 2009). *In vitro* reconstitutions of the yeast functional homolog (Mtw1/MIND complex) form a similar extended structure that is bilobed in appearance. This complex is able to make contacts with Spc24/25 subunits of the Ndc80 complex (Hornung et al., 2011; Maskell et al., 2010). Direct associations with the vertebrate KMN network have also been highlighted in crosslinking studies. Interestingly, the C-terminal tail of Nsl1 makes contacts with Ndc80 and KNL-1 complexes, but the two latter subgroups do not interact themselves (Figure 5A) (Petrovic et al., 2010). The Mis12 complex can therefore be thought of as a ‘hub’ of KMN assembly (Petrovic et al., 2010).

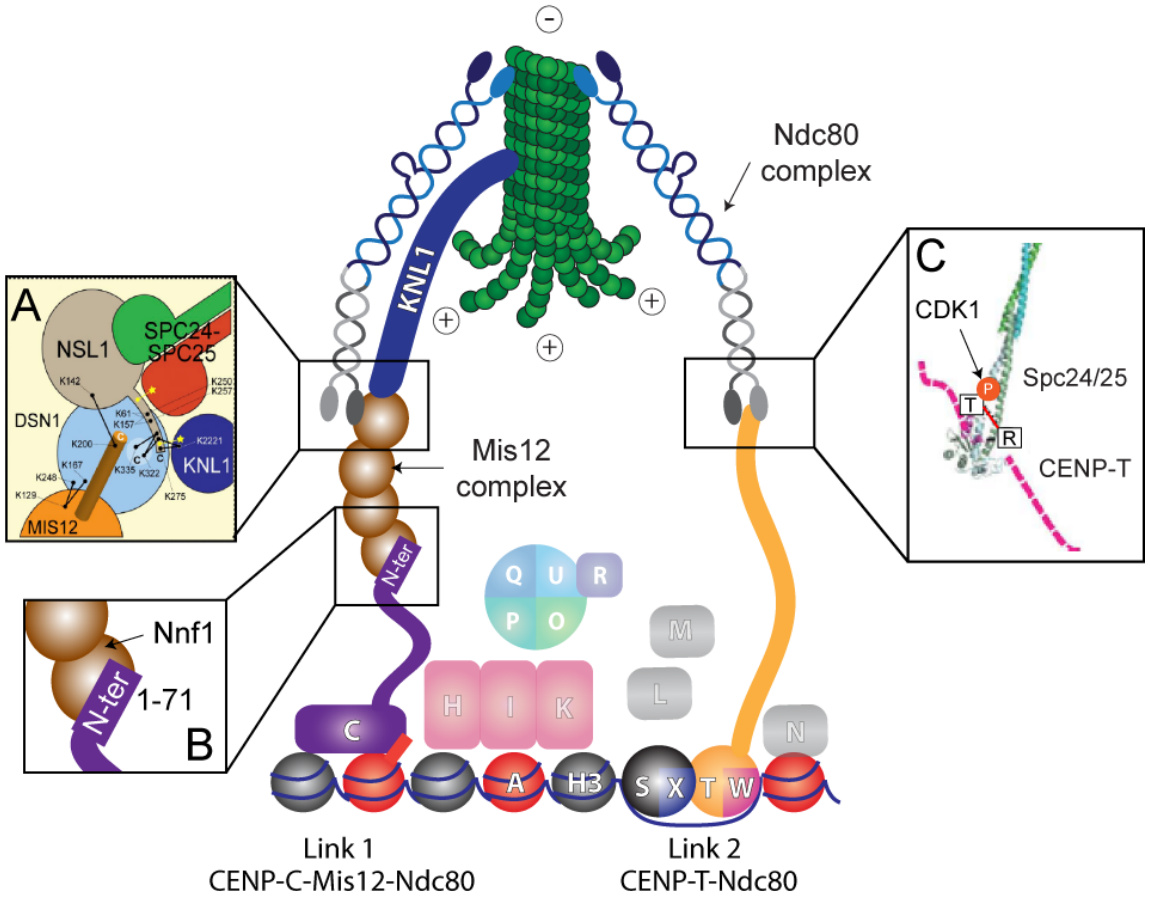

Figure 5. Connections linking inner and outer kinetochores. A. The Nsl1 C- terminal tail (Mis12 complex component) makes contacts with KNL-1 and Spc24/Spc25 subunits of the Ndc80 complex. Taken from (Petrovic et al., 2010). For more details on the exact crosslinks please refer to the original paper. Two paths linking inner and outer kinetochores have been studied in depth. **B.** CENP-C is able to bind directly to the Nnf1 subunit of the Mis12 complex. In humans, residues 1-71 have been shown to be important for this interaction (Screpanti et al., 2011). **C.** Cdk1 phosphorylation of CENP-T Threonine 72 (chicken T72) causes it to form a salt bridge with Arginine 74 (R74), which allows downstream hydrophobic residues to interact with Spc24/25 of the Ndc80 complex (image adapted from (Nishino et al., 2013)).

CENP-C and CENP-T have been proposed to directly mediate inner and outer kinetochore interactions. While middle and C-terminal sequences of CENP-C have been linked to CENP-A interactions (Carroll et al., 2010; Trazzi et al., 2009), the N-terminus is critical for kinetochore assembly (Figure 5B) (Milks et al., 2009; Przewloka et al., 2011; Screpanti et al., 2011; Tanaka et al., 2009). In *Drosophila* cells, ectopic redirection of all KMN components from centromeres to centrosomes was achieved by

expressing an N-terminal fragment of CENP-C linked to a targeting domain of Plk4. This is possibly mediated by direct interactions with Nnf1, a subunit of the Mis12 complex (Przewloka et al., 2011). Interestingly, EM analysis shows that human CENP-C N-terminal regions can bind and promote rigid, rather than bent, structures of the Mis12 complex (Screpanti et al., 2011) and CENP-C loss leads to a reduction in Mis12 complex signals at centromeres (Gascoigne et al., 2011; Kwon et al., 2007).

CENP-T contains a long flexible arm that spans the inner and outer kinetochore and makes direct contacts with Spc24/Spc25 subunits of the Ndc80 complex in a Cdk1 phosphorylation dependent manner (Figure 5C) (Gascoigne et al., 2011; Nishino et al., 2013; Suzuki et al., 2011). CENP-T phosphorylation by Cdk1 enhances the CENP-T-Ndc80 interaction and functions with MIS12-Ndc80 pathways throughout the early stages of mitosis (Gascoigne and Cheeseman, 2013; Gascoigne et al., 2011; Nishino et al., 2013). In yeast, Cnn1 (CENP-T homolog) also binds Ndc80, but this interaction must compete directly with the Mtw1 complex (Mis12 components) and predominates in anaphase when Cdk1 and Mps1 activity is reduced (i.e. CENP-T is unphosphoryated at Cdk1/Mps1 specific sites when bound to Ndc80 components) (Bock et al., 2012; Malvezzi et al., 2013; Schleiffer et al., 2012).

The importance of these two direct links to the outer kinetochore has been emphasised by ectopic localisation studies. Kinetochore-like structures that are able to form robust interactions with microtubules can be built on Lac-O arrays simply by tethering the KMN interacting fragments of CENP-C and CENP-T proteins. More importantly, this system bypasses the requirement for CENP-A nucleosomes and other CCAN components (Gascoigne et al., 2011). In *Drosophila* and *C. elegans*, a single CENP-C bridge may link the inner and outer kinetochore, as other CCAN homologs have not yet been found (Screpanti et al., 2011).

Future work must also focus on fully understanding how other CCAN components, that do not themselves physically bind to the KMN, fine-tune kinetochore assembly/function.

1.3.6 KMN: a platform for the assembly of outer kinetochore components

The KMN, as well as serving as a direct link with microtubules, also functions as a platform for recruiting additional outer kinetochore components (Cheeseman and Desai, 2008; Varma and Salmon, 2012). Included in this group are the spindle assembly checkpoint (SAC) proteins. The SAC signalling pathway is activated on unattached kinetochores and prevents progression from metaphase to anaphase by inactivating Cdc20, a cofactor of the APC/C. This is achieved via kinetochore localised Mad1-Mad2 which acts as a template for the formation of an anaphase inhibitory complex. This assembly is called the mitotic checkpoint complex (MCC) and is composed of Cdc20, Mad2, BubR1/Mad3 and Bub3 (Figure 6) (Foley and Kapoor, 2013; Musacchio and Salmon, 2007). Timing is critical, and silencing of the checkpoint must only be triggered once all chromosomes have formed bi-orientated attachments. The APC/C can then target Cyclin-B and Securin for proteosomal degradation, promoting cell cycle progression and sister chromatid separation (Musacchio and Salmon, 2007).

A recent model implicates KNL-1 phosphorylation by Mps1 at conserved MELT (M[D/E][I/L/V/M][S/T]) repeats in the targeting of Bub1 and Bub3 to kinetochores (Figure 6) (London et al., 2012; Shepperd et al., 2012; Yamagishi et al., 2012). In turn, Bub1 is implicated in Mad1 recruitment (Foley and Kapoor, 2013; London and Biggins, 2014; Yamagishi et al., 2012). Immunoprecipitations against Nuf2-3Flag or KNL-1-3Flag (Spc105) in budding yeast have shown an association between KNL-1 and Mad1 (London and Biggins, 2014). This association was mediated by Mps1 phosphorylation of the mid-region of Bub1, which acts as a platform for Mad1 binding (Figure 6) (London and Biggins, 2014). In C.*elegans*, an interaction between Mad1 and Bub1 has also been shown and this is important for the targeting of the Mad1-Mad2 complex to kinetochores (Moyle et al., 2014). However, Bub1 has also been shown to be sufficient for the ectopic targeting of BubR1 to telomeric regions in fission yeast, suggesting that BubR1 might also play a role with the Bub1-Bub3 SAC subgroup (Rischitor et al., 2007). Alternatively, two KI (Lysine-Isoleucine) motifs in the N-terminus of KNL-1 have been

shown to act as interfaces for Bub1 and BubR1 interactions (Figure 6) (Bolanos-Garcia et al., 2011; Kiyomitsu et al., 2011; Krenn et al., 2012).

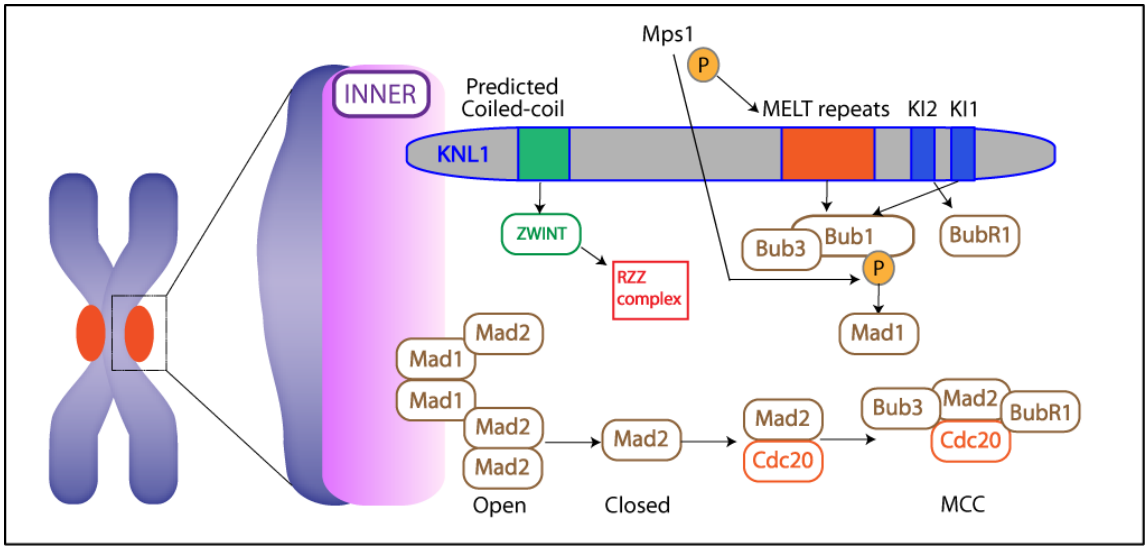

Figure 6. Spindle assembly checkpoint proteins. The "wait anaphase" signal is generated at unattached kinetochores. KNL-1 is an important scaffold protein for the recruitment of spindle assembly checkpoint (SAC) proteins. One path is defined by Mps1 phosphorylation of KNL-1, which functions to bring in Bub1-Bub3. Direct phosphorylation of Bub1 by Mps1 has also been shown to be important for the recruitment of Mad1. The second path uses two KI motifs that are found at the N-terminus of KNL-1; the KI1 motif is important for Bub1 interactions, while KI2 motif has been linked with BubR1 recruitment. In metazoans, KNL-1 can also recruit the RZZ complex via Zwint-1 and both of these paths have been linked to Mad1-Mad2 recruitment. In the Mad2 template model, Mad1 dimers associate with Closed (C)-MAD2 (the template) and recruit Open (O)-MAD2 to kinetochores and promote its conversion to the active/closed state. In the cytoplasm only (C)-Mad2 can bind Cdc20. These proteins are then bound by BubR1 and Bub3 to produce the MCC. In this form Cdc20 cannot active the E3 ligase APC/C. Adapted from (Foley and Kapoor, 2013) and (Caldas and Deluca, 2013).

In higher eukaryotes, KNL-1 supports a second SAC pathway via interactions with Zwint and the recruitment of the Rod-Zwilch-ZW10 (RZZ) complex (Figure 6) (Caldas and Deluca, 2013; Kops et al., 2005; Varma and Salmon, 2012; Wang et al., 2004). The RZZ complex binds the adaptor protein Spindly, which is required for the targeting of Dynein/Dynactin (Stukenberg and Foltz, 2010). 'Stripping' of Mad1-Mad2 from kinetochores by Dynein-mediated transport occurs upon the transition from lateral to end-on microtubule attachment and silences the "wait anaphase" checkpoint (Howell et al., 2001; Wojcik et al., 2001).

Downstream components of the KMN can directly bind microtubules. For example, CENP-E is a mitotic kinesin that transports chromosomes towards the metaphase plate (congression) to promote biorientation (Kapoor et al., 2006). Both BubR1 and the Ndc80 complex have been associated with CENP-E kinetochore localisation (Chen, 2002; Liu et al., 2007; Mao et al., 2003; Tooley et al., 2011). The Ndc80 complex is also responsible for targeting of the Ska complex via a conserved loop region found within the extended coiled-coil of Ndc80 (Zhang et al., 2012).

The full composition of the Ska complex was elucidated by a number of groups and consists of three proteins: Ska1, Ska2 and Ska3 (Rama1) (Daum et al., 2009; Gaitanos et al., 2009; Hanisch et al., 2006; Ohta et al., 2010; Raaijmakers et al., 2009; Theis et al., 2009; Welburn et al., 2009). *In vitro*, the Ska complex can oligomerise, track depolymerising microtubules, and bind both straight and curled microtubule structures (Schmidt et al., 2012; Welburn et al., 2009). Although the Ska complex does not appear to form a ring-like structure in crystallography studies (instead it forms a 'W' shape) (Jeyaprakash et al., 2012), in vertebrates it is the proposed functional homolog of the yeast Dam/Dash complex (Gaitanos et al., 2009; Hanisch et al., 2006; Schmidt et al., 2012; Welburn et al., 2009).

Although I have focused on the structural aspects of the KMN and CCAN there are many more proteins required for co-ordinating K-MT attachments (>100 to date). Some have been shown to bind directly to microtubules. For example, CENP-E that facilitates chromosome congression during metaphase plate formation. The Ska complex mediates attachments on depolymerising microtubules. This has been shown to be important in mediating chromosome oscillations at the metaphase plate (Schmidt et al., 2012). This type of microtubule binding activity might also be relevant in anaphase. In contrast, the SAC monitors chromosome bi-orientation and the timing of the metaphase-to-anaphase transition. Therefore, kinetochore proteins function at specific times in mitosis. This means there is also a temporal aspect to consider in assembly, where complexes can hop

on and off kinetochores, or change configurations at different phases of the cell cycle and this would give rise to a dynamic kinetochore conformation.

1.4 Putting everything together: The kinetochore as a whole unit

While the functions of many of the individual kinetochore components are beginning to be characterized, how they assemble onto centromeric regions is still under study. Although the literature has many agreements, there are also many contradictory findings in respect to dependency networks within the kinetochore and the structure as a whole requires further detailed and systematic analysis.

1.4.1 Super resolution structure: Localisation and Copy Number

As an additional indicator of structure and potential assembly patterns, super-resolution microscopy has uncovered the precise location of pairs of fluorescently tagged kinetochore proteins with respect to one another. The kinetochores of chromosomes aligned along the metaphase plate exhibit a distinct protein pattern along the spindle axis, which remains relatively consistent for constituents common to budding yeast (Joglekar et al., 2009), *Drosophila* (Schittenhelm et al., 2007) and human cells (Wan et al., 2009).

On metaphase chromosomes of *S. cerevisiae* the kinetochore is built with inner components of the Ctf19 complex (equivalent to CCAN) closest to the CENP-A nucleosome, while the N-terminal portion of Ndc80, along with Dam complex components, define the most outer positions (Figure 7) (Joglekar et al., 2009). In both budding yeast and human metaphase cells the C-termini of KNL-1, Mis12 components and Spc24/25 are in close proximity to each other (Joglekar et al., 2009; Wan et al., 2009). Importantly, this analysis allows for changing configurations to be monitored. During anaphase the measured distance between opposite ends of the Ndc80 sub-units decreases and could represent bending within the complex (Joglekar et al., 2009). This

flexibility is not observed in human cells in the presence of taxol (microtubule binding; no tension) (Wan et al., 2009), suggesting this change is specific to the latter stages of mitosis.

Interphase prekinetochores have also been subject to high-resolution fluorescence imaging. Once unfolded, single molecule tracking co-localises CENP-H and CENP-C with CENP-A sub-domains, while CENP-T is interspersed along adjacent H3 rich regions (Ribeiro et al., 2010). The chromatin must therefore fold in a way that will accommodate these interactions. How this occurs will directly impact the way basal proteins assemble across the chromatin/kinetochore interface. From this recent work, Ribeiro et. al., (2010) propose a layered boustrophedon arrangement of chromatin, giving rise to inter-linked regions of CENP-A that still remain in close proximity to H3 nucleosomes (Ribeiro et al., 2010).

Another interesting outcome of these studies has been the ability to determine the copy number of proteins incorporated into a single kinetochore. Budding yeast chromosomes contain point centromeres with a single microtubule attachment (Westermann et al., 2007). By tagging inner and outer kinetochore proteins with GFP, conversion of fluorescence intensities into precise copy numbers found that *S. cerevisae* contain set values for every kinetochore studied (1-2 copies for conserved inner kinetochore components and 5-8 copies for conserved outer kinetochore components) (Joglekar et al., 2006). However, the accuracy of these values is highly dependent on the reference standard used for quantitation (Coffman et al., 2011; Lawrimore et al., 2011) and remains a subject of considerable controversy.

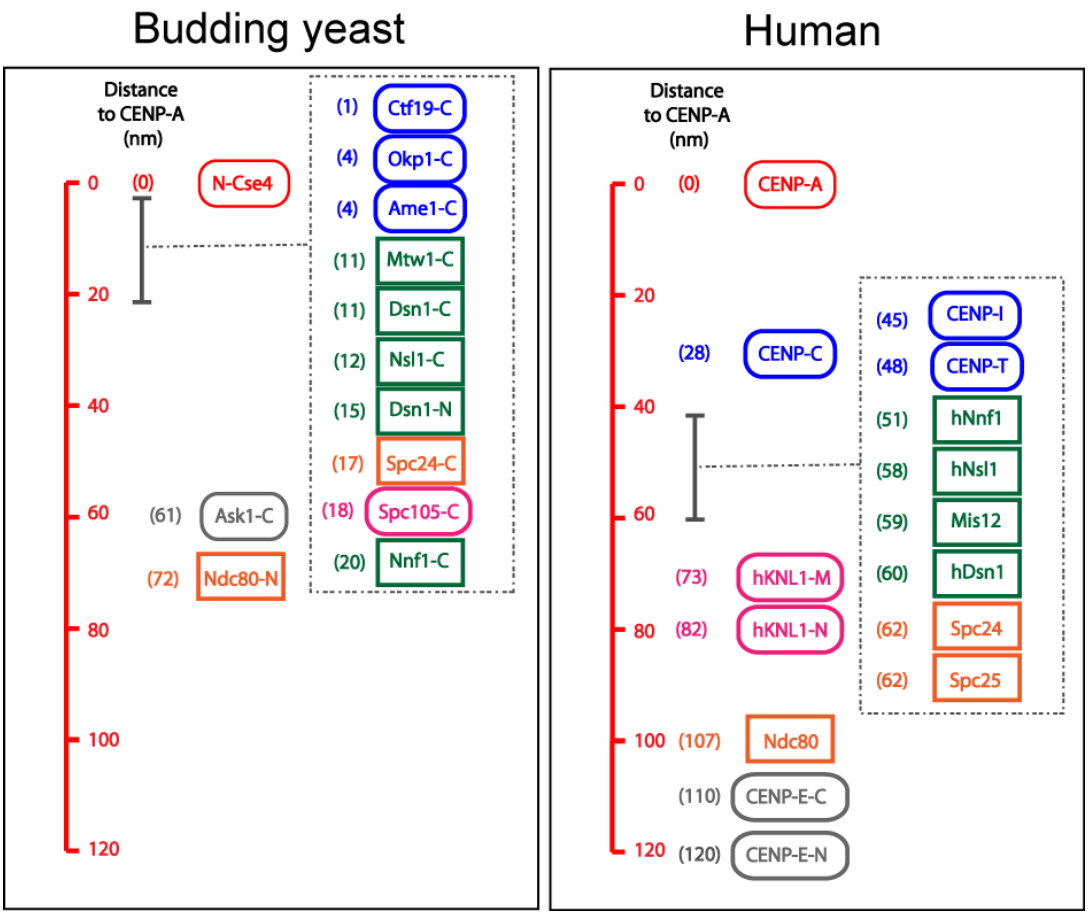

Figure 7. A summary of the relative localisations of key kinetochore proteins. A schematic representation of the calculated distances (nm) of various kinetochore proteins from CENP-A in budding yeast (Joglekar et al., 2009) and human cells (Wan et al., 2009). The average separation (Delta) of two kinetochore components labelled with different fluorophores can be calculated within a 5 nm range of accuracy. Measurements defining the N or C-terminus, or a midregion of a protein, are annotated with N, C and M, respectively. Budding yeast homologs: Cse4 (CENP-A), Okp1 (CENP-Q), Ame1 (CENP-U), Mtw1 (Mis12), Spc105 (KNL1). Ask1 is a Dam complex sub-unit. CENP-E is a kinesin motor that makes contacts with microtubules.

If the original published copy numbers hold true, fission yeast repeat this basic unit in a pattern that directly correlates with the number of additional microtubule attachments per kinetochore (Joglekar et al., 2008). The mean copy number for core CCAN components per K-MT attachment is higher in vertebrate cells, but is stoichiometric to KMN components which form ~8 module units (Johnston et al., 2010). This is consistent with values reported for outer kinetochore components in budding yeast. Together these studies argue towards a 'repeat unit' model, indicating that the human

kinetochore, which binds 15-20 microtubules, may consist of a corresponding number of basic units (6-9 modules per microtubule) which function together to link the underlying chromatin to spindles.

This basic repeat model is supported by recent EM and electron tomography studies which have been used to visualise high resolution structures of isolated yeast kinetochores (Gonen et al., 2012). The general architecture is characterised by a central hub surrounded by globular domains. Interestingly, the number (5-7) of these outer electron-dense regions is close to the copy numbers of KMN components (Spc105, Mtw1 complex, Ndc80 complex) found for a single kinetochore in budding yeast (Joglekar et al., 2006). The regularity of these structures around the central hub would support a unit-based model of KMN component assembly. These globular extensions, along with additional ring-like structures, have the capability to make contacts with taxol-stabilised microtubules *in vitro* (Gonen et al., 2012). In contrast, an indepth electron tomography study has depicted the outer plate as a meshwork of fibres, rather than arranging into a modular configuration, and therefore argues against the basic repeat model (Dong et al., 2007).

1.4.2 Dependency pathways for kinetochore assembly

Much of the information concerning the relative protein dependencies within the kinetochore has been obtained through proteomic based interaction studies and reciprocal localisation studies of proteins following depletion of various components from the kinetochore (Cheeseman et al., 2008; De Wulf et al., 2003; Hori et al., 2008b; Liu et al., 2006; Welburn and Cheeseman, 2008). If we were to take into account an inside-to-outside model of kinetochore structure, those proteins found on the outskirts would depend on more interior complexes. This has certainly been shown to be the case in many instances. However, cumulative dependencies and divergent assembly pathways also come into play, indicative of an intricate assembly network. Figure 8 depicts some of the assembly networks reported for a number of kinetochore components. The focus

of that Figure is on vertebrate cells, but it should be noted that many studies have also focused on the hierarchical assembly of budding yeast kinetochores (De Wulf et al., 2003; Roy et al., 2013; Westermann et al., 2003). This is not the definitive map of all the dependencies associated with these components (as described above there are many contradictory findings), though it does highlight a number of key themes that continue to arise in kinetochore assembly: strongly associated sub-complexes, parallel branches and reciprocal assembly pathways.

As described earlier many components of the kinetochore do not function alone, but instead associate strongly within complexes. An important feature is that members of the subcomplexes are stoichiometrically dependent on each other and depletion of one protein will result in the complete loss of others within the same complex. This is clearly seen with the 16 CCAN components that can be classed into distinct complexes based on biochemical interactions and phenotypic analysis (Westhorpe and Straight, 2013). One example is the CENP-O containing sub-class, where CENP-O, P, Q, U and R form a tight complex and dependent on each other for their localization to centromeric regions (Eskat et al., 2012; Hori et al., 2008b).

Multiple branches diverge and form independent networks within the assembly pathway of the kinetochore. One model suggests that CENP-C and CENP-T do not depend on each other for their centromeric localisation and can individually support links to the outer kinetochore; CENP-C-Mis12 and CENP-T-Ndc80 complex coupling has recently been extensively studied (Bock et al., 2012; Gascoigne et al., 2011; Hori et al., 2008a; Malvezzi et al., 2013; Nishino et al., 2013; Przewloka et al., 2011; Schleiffer et al., 2012; Screpanti et al., 2011). Another branch point appears to exist within the KMN, with the Mis12 complex acting as a bridge between KNL-1 and the Ndc80 complex (Petrovic et al., 2010). Although the loop region found within the coiled-coil region of Ndc80 has recently been implicated in protein-protein interactions, the complex as a whole is not typically thought of as a scaffold (Schmidt and Cheeseman, 2011; Zhang et al., 2012). In contrast, KNL-1 functions as an interface for a number of proteins

including Zwint, Spindly, the RZZ complex, Dynein, Bub1-Bub3 and BubR1 (see section 1.3.6). However, there do appear to be points of inter-connectivity as Ndc80 has been shown to bind Zwint, which is in turn required for RZZ recruitment, and highlights the complex interplay between subgroups (Lin et al., 2006).

Reciprocal pathways have become an important factor to consider in the maintenance of kinetochore structure. For example, Ndc80 kinetochore targeting is dependent on CENP-I (Hori et al., 2003; Liu et al., 2006). At the same time CENP-I signals are reduced by ~40% upon Ndc80 loss in human cells (Liu et al., 2006). A surprising feedback loop has come to light more recently and is centred on the complicated matter of CENP-A deposition at centromeric regions. CENP-A is classically thought of as the definitive upstream marker, both specifying centromere identity, and acting as a pre-requisite for the propagation of assembly pathways traversing inner and outer kinetochore compartments (Figure 8) (De Rop et al., 2012). In support of this, most CCAN components are dependent on CENP-A for their localisation at centromeric regions (Cheeseman and Desai, 2008). At the same time both CENP-C and CENP-I have been shown to be important in assembling CENP-A at endogenous kinetochores (Carroll et al., 2010; Erhardt et al., 2008; Okada et al., 2006a). It has been proposed that this 'CCAN mark' pinpoints sites for incorporation of newly synthesised CENP-A directly after mitosis (Hori et al., 2013). This propagating element is certainly true in multi-array (LacO) tethering assays; LacI-tagged CENP-C, CENP-I (CENP-H complex), or HJURP can assemble CENP-A into chromatin and form a functional ectopic centromere capable of replacing the endogenous counterpart, even after multiple generations (Hori et al., 2013). Similarly, *Xenopus* egg extracts containing CENP-C can assemble CENP-A onto sperm chromatin, but only upon exit from mitosis, and probably through KNL2/HJURP interactions (Moree et al., 2011).

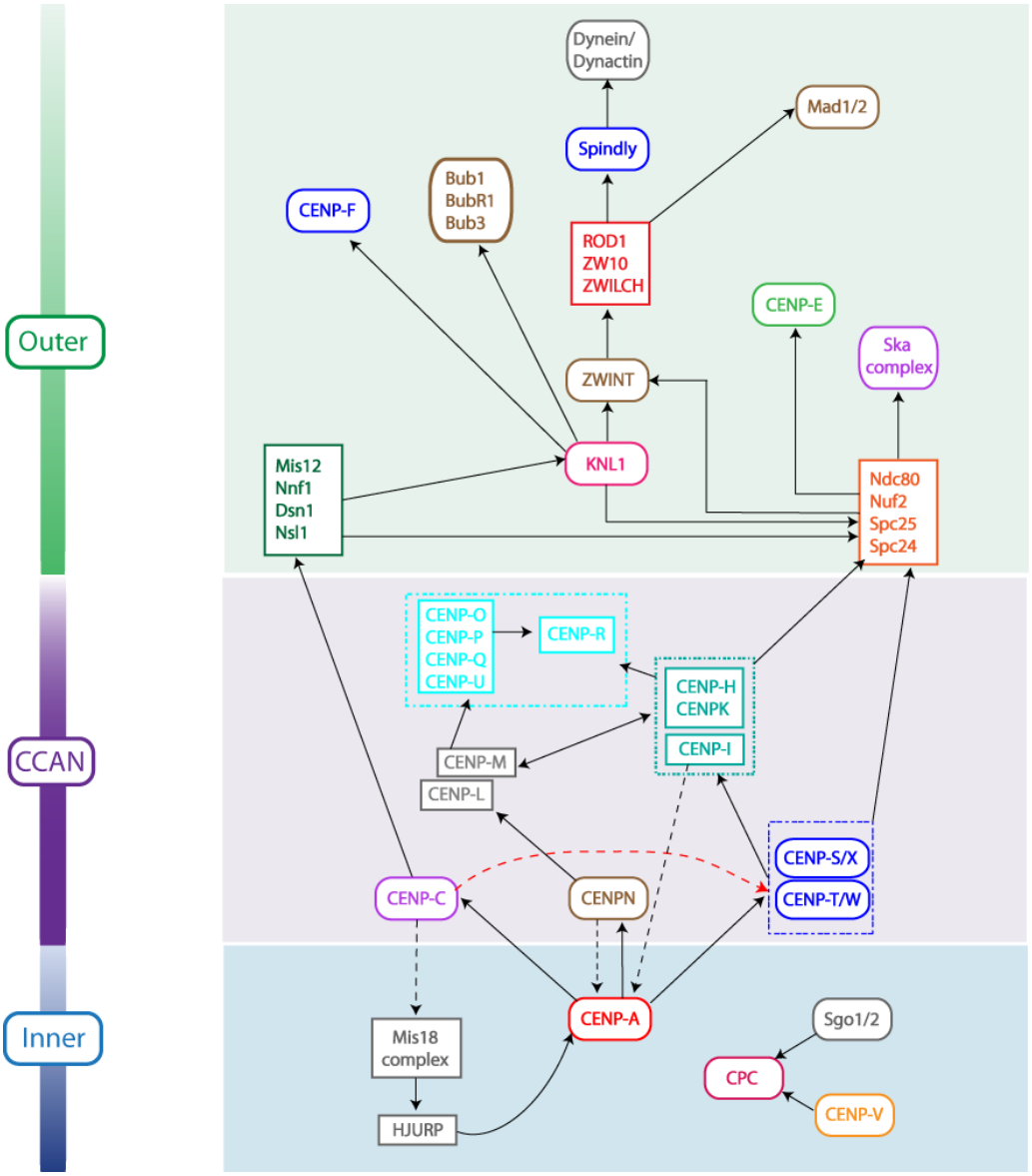

Figure 8. A summary of kinetochore dependency networks. The assembly network of key inner and outer kinetochore components. Note that CENP-A is upstream of all other constituents, but its levels at centromeric regions have been shown to be affected by additional CCAN components (Carroll et al., 2009; Hori et al., 2013; Moree et al., 2011; Okada et al., 2006a). There is some evidence that CENP-C loss reduces CENP-T levels at kinetochores (red arrows) (Carroll et al., 2009), but other studies show that they are independent (Gascoigne et al., 2011; Hori et al., 2008a). Although recent studies have focused on the direct link of CENP-C and CENP-T with outer kinetochore proteins, CENP-H may also play a role in Ndc80 recruitment (Cheeseman et al., 2008). A summary of KMN dependencies for the RZZ and checkpoint proteins is reviewed elsewhere (Foley and Kapoor, 2013; Varma and Salmon, 2012).

Across organisms and within the same system there are many contradictory findings when it comes to defining an overall map of kinetochore assembly. What is clear is that these relationships are not linear and there are many diverging branches and interconnections. Although direct interaction and localisation studies are important for defining the overall structure of the kinetochore, this is not enough to predict the dependency pathways connecting sub-units of the inner centromere, CCAN components and outer kinetochore compartments.

1.5 Thesis plan

In many of the studies mentioned above, immunofluorescence signals are used to determine how loss of one kinetochore protein affects the recruitment of other kinetochore proteins. There are two main limitations to these experiments. First, many of these antibodies are made 'in house' and are in short supply. Second, a limited number of colour channels means that only 2 to 3 proteins can be analysed in any given experiment. Therefore, the global effects on kinetochore assembly cannot be assessed. To overcome this problem mass spectrometry is going to be used to examine the assembly pathways required to build a functional kinetochore. This will be achieved using a number of conditional knock-out (KO) cell lines, where the expression of a particular kinetochore protein can be turned off within minutes of doxycycline treatment. By removing members of the inner or outer kinetochore and combining this with SILAC technology, a quantitative read-out of all proteins that assemble on chromosomes can be compared between wild type and kinetochore depleted cell lines. Our hypothesis is that purified mitotic chromosomes from cells lacking an essential kinetochore component will be depleted of close interactors within the same sub-complex and specific components downstream in the assembly pathway. With this data our aim is to beable to build dependency networks across the inner and outer kinetochore. We also hope that novel components of the kinetochore complex will be revealed through their dependency for known kinetochore components.

To expand upon this method the final section focuses on the generation and characterisation of a cell line that promotes rapid degradation of the kinetochore protein, CENP-T. This was achieved using the auxin-inducible degron (AID) system. The aim was to beable to assess the immediate changes on vertebrate kinetochore composition in the absence of CENP-T and compare these findings with the tet-regulated conditional KO system.

2 Materials and Methods

2.1 Buffers, Solutions and Reagents

All buffers and solutions were prepared using ddH_20 and chemicals purchased from Sigma-Aldrich unless otherwise indicated.

Table 2- General solutions

Name	Composition
General	
Electrophoresis buffer SDS (Severn Biotech Ltd)	25 mM Tris pH 8.8; 192 mM glycine; 0.1% SDS
Transfer Buffer	25 mM Tris-HCl pH 8.8; 192 mM glycine; 20% methanol
TAE	40 mM Tris-acetate; 1 mM EDTA; pH 8.0
3x Sample buffer (SB)	50 mM Tris-HCl pH 6.8; 15% sucrose; 2 mM EDTA; 3% SDS 1x SB: 300 μl 3xSB; 510 μl ddH_20; 90 μl Beta-mercaptoEtOH
PBS	0.01 M phosphate buffer; 137 mM NaCl; 2.7 mM KCl; pH 7.4
PBS/Tween (PBS-Tween) Tween-20 (Biorad)	PBS; between 0.1% and 0.05% Tween-20
LB	1% tryptone; 0.5% yeast extract; 10 mM NaCl; pH 7.4
Lower gel buffer	1.5 M Tris-HCl pH 8.8
Upper gel buffer	0.5 M Tris-HCl pH 6.8
Drugs	
Doxycycline (BD Biosciences)	1 mg/ml in ddH_20 and filtered with a 0.2 μm pore size filter (1:5000; 0.2 μg/ml) or (1:2000; 0.5 μg/ml)
Nocodazole	1 mg/ml diluted in DMSO (1:2000; 0.5 μg/ml)
3-Indolylacetic acid (IAA/Auxin) (Fluka analytical)	0.087 g diluted in 10 ml chemical grade EtOH (1:400; 125 μM)

2.2 Molecular Biology Techniques

2.2.1 cDNA generation, PCR and Electrophoresis of DNA

RNA was isolated from HeLa-Kyoto cells using TRIzol® (Invitrogen) RNA extraction protocols. Reverse transcription using either anchored-oligo $(dT)_{18}$ or random hexamer priming was performed on 2.5 μg of RNA according to the manufacture's guidelines (Roche; Transcriptor High Fidelity cDNA Synthesis Kit). RNA concentration/quality was determined using a Nanodrop2000 system (Thermo Scientific).

Lyophilized oligonucleotides (purchased from Sigma-Aldrich) were resuspended in ddH_20 (RNase free) to 100 μM and stored at -20 °C. Oligonucleotide primers were used with the peqGold Taq kit (Peqlab Ltd) to amplify genes of interest from freshly prepared cDNA by PCR. For generation of a full length C7orf50 insert 50 μl PCR reactions prepared with ddH_20 contained: 10x buffer Y, 5x Enhancer solution, 200 μM of each dNTP, 1.25 U Taq polymerase, 2 μl hexamer-primed cDNA and 400nM of each primer (Table 3). Reactions were run on a Biometra T3000 thermocycler. A denaturation step at 94 °C for 5 minutes was first performed. This was followed by 30 cycles of a 40 second 94 °C denaturation step, a 40 second 60 °C primer annealing step, and a subsequent elongation reaction at 72 °C for 50 seconds.

A 1.5% agarose gel solution was prepared with TAE buffer and 0.3 μg/ml ethidium bromide. The 50 μl PCR reaction was mixed with ~9 μl 6x gel loading dye (New England Biolabs) and gel electrophoresis of the PCR product was performed in TAE buffer at a constant voltage of 100V. The DNA fragment was visualised with a low-intensity UV light, excised with a scalpel, and purified using the QIAquick gel extraction kit (Qiagen). The DNA was diluted in RNase free ddH_20.

Table 3- Primers used for cloning and sequencing

Description	Sequence (5'-3')	Comments
Cloning		
C7orf50_FW	CACCATGGCAAAACAGAAGAGAAAAGT	Contains CACC at 5' end for gateway cloning
C7orf50_RV	CTACTAGGAGAGCAGCTGCAG	
Sequencing		
M13_FW	GTAAAACGACGGCCAG	Sequencing pENTR vector insert
M13_RV	CAGGAAACAGCTATGAC	Sequencing pENTR vector insert
pEGFP-C	CATGGTCCTGCTGGAGTTCGTG	Sequencing pDEST vector insert
pBGH/RV	TAGAAGGCACAGTCGAGG	Sequencing pDEST vector insert

2.2.2 Cloning

2.2.2.1 Recombination using the Gateway system

For the TOPO cloning reaction (Invitrogen; pENTR/D-TOPO cloning kit) 4 μl of fresh C7orf50 cDNA, 1 μl salt solution and 1 μl pENTR/D-TOPO vector was incubated at 22 °C for 20 minutes. This was followed by transformation into chemically competent TOP10 bacteria. A positive transformant was selected by sequencing the plasmid/cDNA insert isolated from 5-10 different kanamycin resistant colonies (Table 3). Once the entry clone had been obtained, a LR recombination reaction (Invitrogen; Gateway LR clonase II enzyme mix) was performed: 0.75 μl of the entry clone (DNA from mini prep), ~120 μg destination vector (pDEST3.2NGFP; N-terminal GFP tagging of the insert), 0.5 μl LR clonase II enzyme and 0.75 μl ddH_20. The reaction was incubated for 2 hours at 25 °C. Following this, 2 μg of proteinase K was added and incubated at 37 °C for 20 minutes. The reaction was transformed into TOP10 bacteria and spread onto LB agar plates containing 100 μg/ml ampicillin. 10 colonies were screened by sequencing the cDNA insert in the destination vector (Table 3) and a positive tranformant containing the destination vector with the correct C7orf50 sequence was selected for further experiments.

2.2.2.2 Other constructs

Human cDNA for 32 uncharacterised genes already cloned into the pDONR201 vector (Human Gateway entry clones) were purchased from the National Institute of Technology and Evaluation (NITE, Kisarazu Japan). Using the Gateway system the cDNA was recombined into a pDEST3.2NGFP plasmid to N-terminally tag the expressed proteins with GFP (Table 9). Full length human DDX27 (cPERP-F) was cloned into the pDEST3.2NGFP plasmid by Dr Shinya Ohta using the same gateway cloning method described above (Ohta et al., 2010). The GFP-GgCENPA construct was generated by cloning GgCENP-A into the pEGFPC1 vector (Clontech) with a 17-amino acid linker (Ribeiro et al., 2009). The OsTIR1-T2A-AID-GgCENP-T vector was generated by Dr Kumiko Samejima. The OsTIR1-T2A-AID sequence was digested from a pUC57 vector and inserted N-terminal to the Gg CENP-T ORF sequence within a pN1 plasmid (vector from the Fukagawa laboratory, missing N-terminal GFP tag).

2.2.3 Preparation and transformation of competent E. *coli* cells

Chemically competent E. *coli* TOP10 cells were made in house and all steps carried out at 4 °C. TOP10 cells were cultured in 100 mls of LB supplemented with 1M $MgSO_4$ at 37 °C to an OD600 of 0.5, cooled on ice for 5 minutes, and then pelleted at 3300 x g for 15 minutes at 4 °C. The cells were resuspended in 40 ml TfbI (AcOH pH 5.8. 30 mM KAc,100 mM RbCl2, 10 mM CaCl2, 50 mM MnCl2, 15% (v/v) glycerol), pelleted and resuspended for a second time in 4 ml TbfII (KOH pH 6.5, 10 mM MOPS,10 mM RbCl2, 75 mM CaCl2, 50 mM MnCl2, 15% (v/v) glycerol). Chemically competent cells were aliquoted, snap frozen and stored at -80 °C.

For transformation of TOP10 E. *coli* cells, 60 µl aliquots of competent cells were thawed on ice and mixed with the gateway cloning reactions and incubated on ice for 30 minutes. This was followed by a heat shock treatment at 42 °C for 90 seconds and placed back on ice to recover for 1 minute. The cells were then incubated in 1 ml LB and gently agitated

at 37 °C for 1 hour before plating on agar plates containing either 50 μg/ml kanamycin sulfate or 100 μg/ml ampicillin. Plates were incubated overnight at 37 °C.

2.2.4 Recovery of DNA from bacterial cultures

A single colony picked from an LB-Agar plate was used to inoculate LB medium supplemented with the appropriate antibiotic (concentrations described above). Depending on the size of the bacterial culture either a Qiagen mini-prep kit (2ml culture; small scale) or Qiagen midi-prep kit (50ml; large scale) was used to isolate plasmid DNA according to the manufacturer's instructions. Miniprep kits were used when DNA was required for cloning and midi-kits were used when the DNA was required for transfection. Bacterial stocks were stored at -80 °C by mixing 300 μl of bacterial culture with 300 μl of 100% glycerol (autoclaved).

2.2.5 Sequencing reactions

Sequencing reactions were performed based on the di-deoxynucleotide method, using the BigDye v3.1 Cycle Sequencing kit provided by Applied Biosystems. A 10 μl reaction contained: 2 μl Big Dye mix, 2 μl mini prep DNA, 2 μl sequencing primer (5 μM) and 4 μl ddH_20. The initial denaturation step was performed for two minutes at 96 °C, followed by 25 cycles of a 30 second denaturation at 96 °C, a 15 second annealing step at 50 °C and a four minute extension step at 60 °C. Sequencing reactions were analysed on an ABI 3730 DNA Analyzer (Applied Biosystems) by the GenePool Sequencing Facility (The University of Edinburgh) and the resulting files were processed using Lasergene software.

2.3 SDS PAGE, Western blot analysis and Gel staining

2.3.1 Western blot analysis

Denaturing protein gel electrophoresis was carried out using the Tris-glycine buffer system described previously (Laemmli et al., 1978). Polyacrylamide gels were prepared from a 30% (v/v) acrylamide/bisacrylamide mixture (Severn Biotech) and the upper and lower gel Tris solutions in Table 2. The stacking gel contained 8M Urea for better resolution of chromosomal banding patterns. Proteins were dissolved in sample buffer (Table 2) by sonication and boiling, resolved using SDS-PAGE (electrophoresis apparatus; BioRad), and transferred to nitrocellulose (Amersham Pharmacia) in transfer buffer (Table 2). The membrane was blocked with 5% nonfat milk in PBS-Tween for 1-2 hours and probed with appropriate primary antibodies (Table 4). After three washes for 5 minutes with PBS-Tween the membrane was incubated with the relevant secondary antibodies (Table 4) for 30-45 minutes. When using secondary antibodies conjugated to horseradish peroxidase three PBS-Tween washes were performed for 5 minutes each and protein bands detected using ECL Western blot detection (GE healthcare). When using the Licor Odyssey system, membranes probed with secondary antibodies were washed for at least 45 minutes (PBS-Tween was changed every 5-10 minutes). The final wash was in PBS for 5 minutes. The blots were scanned using the Licor system. For individual protein bands quantitation was performed based on median fluorescence intensity values (minus local background signals).

Table 4- Antibodies used for immunoblotting

Antibodies	Source	Species	Dilutions	Comments
Primary				
GgINCENP	**3D3**	Mouse	1:3	1 -2 hours
Histone H3	Abcam	Mouse	1:500	Overnight incubation is best
Topo II	**Rabbit G, bleed 6**	Rabbit	1:500	At least 2 hours
ATP-synthase subunit alpha	MitoSciences	Mouse	1:500	1-2 hours
GgCENP-T	Fukagawa*	Rabbit	1:2000	1-2 hours
GgNdc80	Fukagawa*	Rabbit	1:2000	1-2 hours
GgCENP-C	**WCE30b**	Rabbit	1:500	Overnight incubation is best
Secondary				
HRP-conjugated	Jackson ImmunoResearch Laboratories, Inc.	Donkey anti-Mouse	1:5000	ECL
HRP-conjugated		Donkey anti-Rabbit	1:10,000	ECL
IRDye 800CW (green)	Licor Biosciences	Donkey anti-Rabbit	1:10,000	Licor analysis
IRDye 680LT (red)		Donkey anti-Rabbit	1:10,000	Licor analysis
IRDye 680 (red)		Donkey anti-Mouse	1:10,000	Licor analysis

* Tatsuo Fukagawa, National Institute of Genetics, Japan
antibodies from the Earnshaw laboratory are indicated in **bold**.

2.3.2 Gel staining

Chromosome samples were loaded onto 12.5% or 15% SDS-PAGE gels and resolved using gel electrophoresis (as described above). A kit was used to silver stain the gel according to the manufacturer's instructions (Thermo Scientific). Protein bands were also visualised by gel code blue stain reagent (Thermo Scientific) and InstantBlue (Expedeon), followed by destaining with ddH_20.

2.4 Cell Culture

Hela-Kyoto and U2OS cell lines were grown in Dulbecco's modified essential media (DMEM, Invitrogen) supplemented with 10% (v/v) heat-inactivated fetal bovine serum

(H-I FBS; Biosera) and 1% Penicillin/Streptomycin (P/S, Invitrogen) in a humidified atmosphere of 37 ºC/5% CO_2. Adherent cells were washed with Dulbecco's phosphate buffered saline (DPBS; Gibco) and incubated with 1-2 ml TrypLE (Gibco) at 37 ºC for two minutes. Cells were diluted with media as appropriate and changed every other day to prevent nutrient depletion. DT40 cell lines were cultured in RPMI media (Invitrogen) with 10% (v/v) H-I FBS, 1% Chicken Serum (Gibco) and 1% P/S at 39 ºC.

2.5 Transient transfection and generation of DT40 stable cell lines

2.5.1 Transient transfection in human cell lines

HeLa-Kyoto cells were seeded onto a 10cm dish to achieve 30-40% confluency. The cells were left to adhere before transfection. 500 µl Optimem (Invitrogen) containing 15 µl Xtreme Gene 9 DNA transfection reagent (Roche) was mixed and incubated for five minutes at room temperature. Following this, 2.5 µg of DNA was added, left for a further 15 minutes, and introduced to the cells in a drop-wise manner. This was up- or downscaled in relation to the surface area of the culture dish. U2OS cells were seeded onto 12 well dishes and 1 µg of GFP-cPERP-F transfected into cells using Fugene 6 (Roche) in a similar manner as described above.

2.5.2 DT40 transient transfections

The Neon transfection system (Invitrogen) was used to transiently transfect DT40 cells. In brief, $2x10^7$ DT40 cells were mixed with 100 µl resuspension buffer (R buffer). 8-10 µg of plasmid DNA was added and the electroporation protocol was set to a voltage of 1700V, width 20ms and pulse 1. After electroporation, cells were resuspended in a 10 cm dish containing pre-warmed medium (without antibiotics). For experiments with the AID-CENP-T cell line, doxycycline was added 2-3 hours after electroporation.

2.5.3 Generation of DT40 stable cell lines

The AID-CENP-T stable cell line was generated using electroporation. DT40 cells at a concentration of $1x10^6$ cells/ml (30-40 ml total) were centrifuged (1300 x g, 5 minutes) and resuspended in 30 ml ice-cold Optimem. Cells were centrifuged for a second time under the same conditions and diluted to 1-2 $x10^7$ cells/ml in Optimem. 0.5 ml of the cell suspension was distributed into a cuvette (BioRad; 0.4 cm) with 8-10 μg of plasmid DNA and placed on ice for 5-10 minutes. Cells were electroporated at 300 mA and 950 μF (Gene Pulser Xcell Electroporation System, BioRad) and maintained on ice for a further 5 minutes. The cell suspension was added to 10 ml pre-warmed medium and incubated overnight. The next day, 50 ml of media was added to the culture along with Geneticin (1.5 mg/mL; Gibco) and Zeocin (400 μg/mL; Invitrogen) to select for antibiotic resistant cells. With a multichannel pipette cells were plated in four 96 well plates using 150 μl of media per well. Two weeks later colonies were transferred to a 12 well dish with 500 μl of media (without antibiotic selection). Positive clones were screened by Western blot analysis.

2.6 Immunofluorescence microscopy

U2OS cells expressing the fluorescently tagged construct and plated on sterile 16 mm glass coverslips (VWR) were washed with 0.01% Triton X-100 (BioRad) in PBS and subsequently fixed with 4% paraformaldehyde (Electron Microscopy Services) in PBS for 7 minutes at 37 °C. Cells were then washed with PBS, permiabilised in 0.15% Triton X-100/PBS for 2 minutes at room temperature and washed for a second time. A block using 1% Bovine Serum Albumin (BSA) diluted in PBS for 30 minutes at 37 °C was performed. Primary antibodies (Table 5) diluted in blocking solution were incubated on coverslips for 30 minutes and then washed three times with PBS for 5 minutes each. Incubation for 30 minutes with fluorophore-conjugated secondary antibodies (Table 5) was followed by three consecutive washes. Coverslips were mounted on slides using VectorShield containing DAPI (Vector Labs) and sealed.

DT40 cells were adhered to coverslips using 0.1% poly-L-lysine (PLL; Sigma) solution diluted 1:10 in ddH_20. After incubation for 2 hours in the PLL solution, coverslips were washed five times with ddH_20 and DT40 cells given 30 minutes to attach before fixation. Cells were washed for 2 minutes with pre-warmed PBS and either fixed for 10 minutes with 100% Methanol (-20 °C) or 5 minutes with 4% paraformaldehyde at room temperature. This was followed by two washes with PBS and incubation with 0.15% Triton X-100/PBS for 2 minutes at room temperature. An additional wash with PBS was followed by primary and secondary antibody incubations as described above (Table 5), apart from washes were performed with 0.15% PBS-Tween. Coverslips were mounted on slides using VectorShield containing DAPI (Vector Labs) and sealed with nail polish.

Images were taken with a Brightfield Deconvolution Microscope (DeltaVision Core system, Applied Precision), based on an Inverted Olympus IX-71 microscope stand with Olympus UPlanSApo 100x oil immersion objective (NA 1.4), a 250 W Xenon light source and Camera (CoolSnap HQ, Photometrix). Filters for DAPI, FITC and TexasRed were purchased from Chroma. Shutter and stage were controlled through SoftWorx (Applied Precision). Z sections were collected for the entire depth of a cell with a spacing of 0.2 um (DT40 cells are typically 10 um in diameter) and deconvolved using the constrained iterative algorithm on SoftWorx (Swedlow et al., 1997; Wallace et al., 2001). Max intensity projections were created either using SoftWorx or ImageJ. Images were adjusted using the microscope software (Leica application suite), ImageJ and photoshop (adobe CS2) for final presentation.

To make comparisons and quantitative measurements images were processed in imageJ. 3D projections to be compared were thresholded at the same maximum and minimum intensities. The default setting for CraQcode v1.06 was used to generate quantifiable measurements (Bodor et al., 2012) (This macro was modified by Nuno Martins; Earnshaw lab).

Table 5- Antibodies for immunofluorescence

Antibodies	Source	Species	Dilutions	Comments
Primary				
Tubulin B512	Sigma	Mouse	1:3000	4% PF
ACA	**ACA**	Human	1:300	4% PF
CENP-T	Fukagawa*	Rabbit	1:1000	4% PF
Ndc80	Fukagawa*	Rabbit	1:100	100% MeOH
CENP-O	Fukagawa*	Rabbit	1:250	4% PF
CENP-H	Fukagawa*	Rabbit	1:250	4% PF
Secondary				
Cy5	Jackson ImmunoResearch Laboratories	Goat anti-human	1:400	
Texas Red		Donkey anti-mouse	1:200	
Alexa Fluor 594		Donkey anti-rabbit	1:500	

* Tatsuo Fukagawa, National Institute of Genetics, Japan
antibodies from the Earnshaw laboratory are indicated in **bold**.

2.7 Fixation of mitotic chromosomes

HeLa-Kyoto cells at a 50-60% confluency were incubated in 0.5 μg/ml nocodazole for 3 hours at 37 °C. Mitotic cells were collected by shake-off, centrifuged at 800 x g for 5 minutes at room temperature, and washed with pre-warmed PBS. Cells were spun for a second time (same conditions) and resuspended in 75 mM KCl at a concentration of $30x10^4$ cells/ml for 5 minutes at room temperature. 100 μl of cell suspension was cytospun for 5 minutes at 1800 rpm onto Superfrost glass slides previously cleaned with ethanol. The area of interest was marked with a diamond knife and the slide immediately placed in a coplin jar containing pre-warmed 0.1% Triton-X/PBS for 1 minute, followed by a wash with PBS and fixation for 8 minutes with 4% paraformaldehyde (room temperature). The slides were washed with PBS two more times and mounted with vectorshield containing DAPI (Vector Labs).

2.8 Cell assays

2.8.1 Trypan Blue and Annexin V assay

During cell counting experiments cells were maintained between a confluency of 25-100x10^4 cells/ml. This assay involved mixing 1 part 0.4% trypan blue (Sigma) with 1 part cell suspension (40 μl each) for 3-5 minutes at room temperature. 15 μl of the cell suspension was used to count unstained cells (viable) with a haemocytometer.

Annexin V-PE-Cy5 Apoptosis detection kit (Biovision) was used according to the manufacturer's instructions. Cells were counted and 1x10^5 cells and centrifuged at 1300 x g in 1.5 ml tubes. 500 μl of Annexin V binding buffer and 1μl of Annexin V-PE-Cy5 was mixed with the cell pellet and incubated at room temp in the dark for 5 minutes. Flow cytometry was used to detect positive cells using a FACsCalibur flow cytometer and CellQuest Software (BD Biosciences).

2.9 Electron microscopy

2.9.1 Sample preparation

AID-CENP-T cells (maintained in 0.5 μg/ml doxycycline) were treated with auxin (Table 2; 125 μM final) for 6 hours. 400 μL of cell suspension (40x10^4 cells/ml) was seeded onto PLL coated, glass bottomed, gridded dishes (MatTek Corporation, USA). Cells were left to adhere for 30 minutes before fixation.

2.9.2 CLEM processing

This CLEM processing method was adapted from a previously established protocol (Booth et al., 2013). Briefly, cells were fixed for 1 hour with 3% glutaraldehyde and 0.5% paraformaldehyde in 0.2 M cacodylate buffer containing 5 μg/ml Hoechst. Cells

were washed with PBS (3 x 5 minutes) and the last PBS wash was left on. Mitotic cells of interest were identified with a Brightfield Deconvolution Microscope (DeltaVision Core system, Applied Precision) using DAPI to visualise DNA, and transmitted light to map cell positions via etched coordinates. The reference images allowed for the correlative re-identification of cells of interest by EM. DeltaVision aquisition was followed by treatment with tannic acid (0.1% in water) for 20 minutes, followed by osmication (1% osmium tetroxide in PBS) for 1 hour. Samples were then washed with PBS (3 x 5 minutes), ddH_2O (2 x 20 minutes) and 30% ethanol (1 x 10 minutes) before incubation in uranyl acetate (0.5% in 30% ethanol) for 1 hour. Next, cells were dehydrated using a graded series of ethanol washes followed by 2 x 10 minute washes with 100% ethanol. Following dehydration, cells were infiltrated with ethonal:resin mixtures (2:1 and 1:1) for 20 minutes each. Finally, cells were embedded in 100% resin, with a gelatin capsule of resin covering the cells of interest, before curing at 60 °C for 3 days. Polymerised resin blocks were sectioned and post stained as routine. Micrographs were acquired using a Philips CM120 transmission electron microscope (FEI) and Gatan Orius CCD camera (Gatan).

2.10 Chromosome isolation

The isolation of human chromosomes using the Polyamine-EDTA buffer system (Lewis and Laemmli, 1982) has been adapted to isolate chicken mitotic chromosomes (Ohta et al., 2010; Samejima et al., 2012). For solutions please refer to Table 6. DT40 cells were blocked in nocodazole (0.5 μg/ml) for 12-13 hours generating a mitotic index of >80%. A 500 ml culture was split into two equal volumes and centrifuged at 1800 x g for 10 minutes in a Beckman F500 rotor at 4 °C. Cells were resuspended in solution 1 and after hypotonic swelling for 5 minutes at room temperature they were centrifuged in a Haraeus Megafuge 1.0R centrifuge for 3 minutes at 2100 rpm. All steps from here were performed on ice or at 4 °C. After removing the liquid, 50 μl of RNase solution was added to each pellet and 10 ml of solution 2 used to resuspend the cells. Immediately the liquid was redistributed to a 15 ml dounce (B type pestle; tight) and cells lysed with 10

moderate strokes. Cell debris and nuclei were pelleted by two sequential centrifugation steps (Hareus centrifuge), one at 1300 rpm for 5 minutes, followed by a second 5 minute spin at 1400 rpm. The remaining supernatant was layered over two 3-step sucrose gradients (80%, 60%, 15%; w/v) and centrifuged at 1400 rpm for 10 minutes and then increased to 2800 rpm for a further 30 minutes. The 15/60% interphase, the 60% phase, and the 60/80% interphase were maintained; these should contain the crude chromosomes. This was supplemented with 37.5 μl 1M spermidine and 17.75 μl 0.8M spermine and transferred to a 40 ml dounce (type-B pestle). The total volume remaining from each sucrose gradient should be ~10 ml per tube. 20 ml of percoll solution was added and dounced with 10 medium strokes to mix the percoll and sucrose solutions. After equal distribution into two tubes a further 14 ml of the percoll solution was added, mixed and spun at 19000 rpm for 45 minutes in a JA25.5 Beckman rotor. This created a percoll gradient *in situ* and a layer of material is observed near the bottom of the tube. This region was removed and re-distributed along with 40ml of solution 4 into the 40 ml dounce. 4 strokes were required to mix the two solutions. The mixture was split equally into 4 tubes and additional solution 3 was added to a final volume of 40 ml (per tube). A final spin on the Hareus top centrifuge was performed at 3700 rpm for 15 minutes at 4 °C. The pelleted chromosomes (form a ring on the bottom of the tube) were carefully resuspended in 1.5 ml solution 4 and immediately stored at -20 °C.

Table 6- Chromosome isolation buffers

Name	Composition
Chromosome Isolation	
Solution 1	7.5 mM Tris-HCl pH 7.4; 40 mM KCl; 1 mM K-EDTA pH 7.4; 0.375 mM spermidine; 0.15 mM spermine; 0.3-0.7 TIU/μg aprotinin; 10 μM PMSF; 0.1 μg/ml CLAP
Solution 2	15 mM Tris-HCl pH 7.4; 80 mM KCl; 2 mM K-EDTA pH 7.4; 0.75 mM spermidine; 0.3 mM spermine; 0.1% (w/v) digitonin; 0.6-1.4 TIU/μg aprotinin; 20 μM PMSF; 0.2 μg/ml CLAP
Sucrose gradients (15, 60 and 80%)	5 mM Tris-HCl pH 7.4; 2 mM KCl; 2 mM K-EDTA pH 7.4; Sucrose w/v (15, 60 or 80%); 0.375 mM spermidine; 0.1% n-Dodecyl Beta-D-maltoside; 3-7 TIU/μg aprotinin; 0.1 mM PMSF; 1 μg/ml CLAP
Solution 3	5 mM Tris-HCl pH7.4; 2 mM KCl; 2 mM K-EDTA pH 7.4; 0.375 mM spermidine; 0.05% (v/v) Ammonyx Lo; 3-7 TIU/μg aprotinin; 0.1 mM PMSF; 1 μg/ml CLAP
Percoll solution	5 mM Tris-HCl pH 7.4; 2 mM KCl; 2 mM K-EDTA pH 7.4; 1.875 mM spermidine; 0.752 mM spermine; 0.1% (w/v) digitonin; 3-7 TIU/μg aprotinin; 0.1 mM PMSF; 1 μg/ml CLAP; Percoll (GE healthcare; 17-0891-01)
Solution 4	5 mM Tris-HCl pH 7.4; 2 mM KCl; 0.375 mM spermidine; 1.5-3.5 TIU/μg aprotinin
Protease Inhibitor Cocktail (CLAP)	1 mg/ml each chymostatin, leupeptin, antipain, pepstatin diluted in DMSO
PMSF	100 mM PMSF diluted in isopropanol
10% Digitonin (Biosynth; D-3200)	Boil 1g Digitonin in 10 ml ddH_20 until dissolved
Ribonuclease A	Mix 10 mg in 1ml of 10 mM Na Acetate pH 4. Boil 7 mins.

2.10.1 Sample concentration

Original attempts to concentrate chromosome samples used TCA precipitation. This was applied to CENP-C SILAC experiment repeat 1 and CENP-T SILAC experiment repeat 1. 100% TCA was added to a final percentage of 16.5% and placed on ice for 30 minutes. The samples were centrifuged at 14,000 rpm for 15 minutes at 4 °C and after removing the supernatant 900 μl of acetone (-20 °C) and 100 μl of 0.1N HCl was used to wash the protein precipitate. Vortexing was performed to dislodge the pellet from the side of the tube and spun at 14,000 rpm for 15 minutes at 4 °C. The acetone was then removed and the wash step repeated. The pellet was dried at 37°C for 5-10 minutes and

re-solubilised in a small volume of sample buffer (~50 μl). The chromosome samples were combined for final mass spectrometry analysis.

It became apparent that the TCA precipitate was not easy to re-solubilise and this affected the amount of protein that could be retrieved from each preparation. For all other chromosome isolations, samples were concentrated using lyophilization. Samples were thawed on ice and tip sonicated for 30 seconds to break up the DNA (10 amplitude microns). This was performed three times with a 30 second break between each cycle and always kept on ice. Tubes were then transferred to dry ice for 20 minutes to re-freeze the samples. The lids were removed and parafilm with small puncture holes tightly wrapped across the opening. Tubes were placed in a pre-cooled speedvac (Maxi Dry Lyo; <1mbar; -110°C) for approximately 8 hours; this was enough time to remove 1.5 ml of frozen solution. A white powder remained and 70 μl of sample buffer was added to each tube. Samples were then boiled for 3 minutes, vortexed for 20 seconds and finally centrifuged for 10-20 seconds to recover the pellet. These steps were repeated for a second time and the supernatant removed (Supernatant 1; S1). Pellets from 3 or 4 chromosome preparations were combined in 70 μl of sample buffer, boiled for 1 minute and vortexed for 15 minutes at room temperature. The pellet was separated from the supernatant (Supernatant 2; S2) by a short spin and the pellet resuspended in 70 μl of sample buffer. Note these volumes change depending on the size of the pellet and may require more sample buffer at each step. S1 and S2 were combined and should be ~150 μl for loading and processing by in-gel digestion for final mass spectrometry analysis (described later).

2.11 Mass Spectrometry

2.11.1 In Gel Digestion

Denaturing protein gel electrophoresis was carried out using NuPAGE Bis-Tris 3-12% gels and MOPS SDS running buffer (Invitrogen). The run voltage was set to 200V and lasted 3-4 minutes to allow for the sample to run into the gel for about 0.5 cm. The gel was stained with Imperial protein stain (Thermo scientific) for two hours before destaining with ddH_20 overnight. The section of the gel containing the proteins was cut into approximately 2x2 mm pieces. In-del digestion with Trypsin has been described previously (Schevchenko et al., 2006). Briefly, gel pieces were destained through multiple washes with 50 mM ammonium bicarbonate (Sigma-Aldrich) and 100% ACN (Fisher Scientific). This was followed by a reducing step with 10 mM DTT solution for 30 minutes at 37°C and alkylation with 55 mM IAA for 20 minutes at room temperature in the dark. Washes with 50 mM ammonium bicarbonate and 100% ACN were then performed. Enough Trypsin buffer (10 mM ammonium bicarbonate, 10% ACN) was added to cover the gel pieces and contained 1 µg of Trypsin per 50 µg of protein. Digestion was performed overnight at 37°C.

For SCX fractionation the peptide solution was collected and peptides extracted from the gel pieces with 100% ACN for 20 minutes, shaking gently. Extracted peptide solution volume was reduced to ~100 µl to remove acetonitrile by evaporation using a Concentrator 5301 (Eppendorf). The peptide solution was mixed 1:1 with Buffer A (5 mM Dipotassium hydrogen phosphate, 10% ACN adjusted to pH 3 using phosphoric acid) and acidified to pH 3 with a couple of microliters of concentrated ortho phosphoric acid (Fluka) ready for SCX fractionation.

2.11.2 SCX fractionation

The SCX separation protocol was performed on an Ultimate 3000 HPLC system (Dionex) using a PolySULFOETHYL A^{TM} column (200 x 2.1 mm, 5 μm particles, 200 A pores, PolyLC Inc). Salt gradients of Buffer A (5 mM Dipotassium hydrogen phosphate, 10% ACN adjusted to pH 3 using phosphoric acid) and Buffer B (5 mM Dipotassium hydrogen phosphate, 10% ACN, 1 M Potassium chloride adjusted to pH 3 using phosphoric acid) were used to separate peptides at a flow rate of 200 μl/minute. The amount of peptides was measured by a UV detector at a wavelength of 214 nm. LC was operated via the Chromeleon 6.80 software (Dionex), three different gradients were used depending on the amount/complexity of the starting material.

Gradient I: **peptidetest_200μl_1min_50%c8_70%c5_26min_110616**
0%-50% Buffer B over 17 minutes using a concave upward slope (curve 8)
50%-70% Buffer B over 1 minute using a linear slope (curve 5)
Stays at 70% Buffer B for 1 minute before re-equilibrating the column

Gradient II: **peptidetest_60%B_200μl_1min_Shynia_50min_100211**
0%-1.2% Buffer B over 13 minutes using a linear slope (curve 5)
1.2%-60% Buffer B over 27 minutes using a concave upward slope (curve 7)
60%-70% Buffer B over 1 minute using a linear slope (curve 5)
Stays at 70% Buffer B for 1 minute before re-equilibrating the column

Gradient III: **peptidetest_200μl_1min_70%_c6_2step_35minGradient_41min**
0%-60% Buffer B over 33 minutes using a concave upward slope (curve 6)
60%-70% Buffer B over 1 minute using a linear slope (curve 5)
Stays at 70% Buffer B for 1 minute before re-equilibrating the column

Table 7. SCX gradients used for SILAC experiments

Sample	Gradient Name
CENP-C	
Repeat 1	Gradient I: **peptidetest_200µl_1min_50%c8_70%c5_26min_110616**
Repeat 2	Gradient II: **peptidetest_60%B_200µl_1min_Shynia_50min_100211**
CENP-T	
Repeat 1	Gradient II: **peptidetest_60%B_200µl_1min_Shynia_50min_100211**
Repeat 2	Gradient II: **peptidetest_60%B_200µl_1min_Shynia_50min_100211**
CENP-W	
Repeat 1	Gradient II: **peptidetest_60%B_200µl_1min_Shynia_50min_100211**
Repeat 2	Gradient I: **peptidetest_200µl_1min_50%c8_70%c5_26min_110616**
Ndc80	
Repeat 1	Gradient I: **peptidetest_200µl_1min_50%c8_70%c5_26min_110616**
Repeat 2	Gradient III: **peptidetest_200µl_1min_70%_c6_2step_35minGradient_41min**

2.11.3 C18-StageTips

After SCX fractionation the peptide solutions were mixed 1:1 with 0.1% Trifluoroacetic acid (TFA). Desalting was performed using C18-StageTips (Ishihama et al., 2006; Rappsilber et al., 2003). In brief, C18-StageTips were activated with 20 µl methanol, equilibrated with 2x 40 µl 0.1% TFA and the samples subsequently passed through to allow binding of the peptides. This was followed by washes with 0.1% TFA (2x 20 µl) and the StageTips stored at -20 °C. On the day of LC-MS/MS analysis samples were eluted with 3x 20 µl 80% ACN/0.1% TFA, concentrated in the Concentrator 5301 to remove acetonitrile, and finally adjusted to a final volume of 5 µl with 0.1% TFA.

2.11.4 LC-MS/MS

The LC-MS/MS analysis was performed on an LTQ-Orbitrap Velos (Thermo Fisher Scientific) utilising a Waters nano Acuity HPLC system (Table 8). For the HPLC

system, analytical columns (PicoTip emitters, 300 mm x 360 um, ID 75 um, New Objective) were packed with C18 material (ReproSil-Pur C18-AQ, 3 um particles, 120 A pores, Dr. Maisch GmbH, Germany) in a spray emitter connected to an air-pressure pump (Proxeon). Depending on the amount of peptides, gradients between 2-5 hours were used for analysis. The two most frequently used gradients are defined in Table 8.

The instrument parameters and acquisition method:

The LTQ Orbitrap Velos was operated in the data dependent mode with up to 20 MS/MS scans recorded for each precursor ion scan. Precursor ion spectra were recorded in profile in the Orbitrap (m/z 300-1800, R = 60 000, max injection time 500 ms, max 500000 charges); data-dependent MS/MS spectra were acquired in centroid in the LTQ (max injection time 100 ms, max 1 0000 charges, normalized Collision Energy (CE) 35%, wideband activation enabled). Mono-isotopic precursor selection was enabled, singly charged ions and ions with an unassigned charge state were rejected, each fragmented ion was dynamically excluded for 60 s. All measurements in the Orbitrap mass analyser were performed with lock-mass option enabled (lockmass m/z 445.120025).

Table 8- HPLC instrument set up and specification

HPLC system	Emitter	Buffer A	Buffer B	Loading and running flow rate
ACQUITY UPLC™ system (Waters)	360μm OD 75μm ID 8± 1μm opening (New Objectives, Inc.) 300mm column	0.1% formic acid in H_20	0.1% formic acid ACN	500nl/min 300nl/min
Gradients				
Velos 180minGra-225min (Buffer B %)	1.6% to 32% within 168.9 minutes 32% to 76% within 11 minutes 76% to 85% within 1 minute and maintained for 4 minutes before equilibration			
Velos 240minGra-285mi (Buffer B %)	1.6% to 32% within 188.9 minutes 32% to 76% within 51 minutes 76% to 85% within 1 minute and maintained for 4 minutes before equilibration			

2.11.5 Data analysis

Quantitation was performed using the program MaxQuant version 1.3.0.5 (Cox and Mann, 2008) and the peptide search engine Andromeda (Cox et al., 2011) using a Chicken UniProtKB database with reviewed and unreviewed sequences (downloaded February 2013). The enzyme was set to Trypsin/P with a maximum of 2 missed cleavages. The mass tolerance for the first search and main search were set to 20 and 6 ppm, respectively. Carbamidomethylation of cysteine was set as a fixed modification, while oxidation of methionine and protein N-acetylation were defined as variable modifications. A minimum of 1 razor or unique peptide and a false discovery rate (FDR) of 1% were required for protein identification. For quantitation, 1 unique peptide (1 ratio count) was used as a cut-off. The statistical tool Perseus was used for further calculations (hhtp://perseus-framework.org/). R (www.r-project.org) and RStudio (www.rstudio.com) were applied for analysis and the generation of graphical figures.

3 Results chapter 1: Kinetochore dependencies

3.1 Introduction: A new approach to study kinetochore assembly

When taking into account all of the literature surrounding dependency networks and the structural integrity of kinetochore subcomplexes, a number of internal pathways are beginning to be teased apart. On the other hand, the nature of many of these studies means that only a subset of 'core' proteins is monitored in any given experiment. To address this limitation, one goal might be to design an experiment in which a specific aspect of behaviour can be accurately measured across all kinetochore proteins in a single study. We have chosen to use mass spectrometry, combined with Stable Isotope Labelling with Amino acids in Cell culture (SILAC) technology, as a way to measure changes in abundance across all proteins bound to chromosomes after the removal of an integral component of the kinetochore. The success of this method depends not only on the removal of the kinetochore subunit of interest, but also on the quantifiable identification of all other parts of the machinery, which are in low abundance relative to other chromosomally bound proteins. Key features of the experimental design will be discussed below.

3.1.1 Why use DT40 chicken cells?

DT40 chicken B cells originate from a bursal lymphoma induced by the avian leukosis virus (ALV) (Winding and Berchtold, 2001). Further to having a fast generation time, one of the most useful features of this cell line is its higher rate of homologous recombination relative to other vertebrate systems – this facilitates the generation of targeted gene knockouts (Winding and Berchtold, 2001). The exact reason for this enhanced recombination is still unclear. This could be due to rapid growth rate and DNA replication activity – S phase forms a significantly higher proportion of the DT40 cell cycle than it does in most vertebrate systems.

As many proteins are essential for cell survival, conditional DT40 clones have become a powerful tool. In such cell lines, the expression of a gene can be conditionally suppressed by the addition of tetracycline or its analogue, doxycycline. The Fukagawa laboratory has used this technology to create many conditional kinetochore KO clones and have kindly allowed us to use several of these in our study (Hori et al., 2008a; Hori et al., 2003; Kwon et al., 2007).

To report on the kinetochore as a whole we must ensure that the structure remains intact during purification procedures. Although a variety of large multimeric assemblies have been analysed in isolation by mass spectrometry, including the nuclear pore complex (NPC) (Cronshaw et al., 2002; Rout et al., 2000), midbodies (Skop et al., 2004), telomeres (Dejardin and Kingston, 2009) and centrosomes (Andersen et al., 2003), structurally intact forms of the endogenous kinetochore have been obtained through their associations with whole chromosomes (Ohta et al., 2010), circular minichromosomes containing the budding yeast centromere (Akiyoshi et al., 2009) or isolated via FLAG-tagged Dsn1 (Mis12 complex) also in S. *cerevisiae* (Akiyoshi et al., 2010).

The proteome of mitotic chromosomes has been well characterised (reviewed in (Ohta et al., 2011)). Although the original mitotic chromosomal isolation protocols were optimised for human cells (Lewis and Laemmli, 1982), these have more recently been optimised for use in DT40 systems (Ohta et al., 2010; Samejima et al., 2012). DT40 cells contain many chromosomes, 78 all together: 10 pairs of macro-chromosomes, 28 pairs of micro-chromosomes and Z/X sex chromosomes (Masabanda et al., 2004; Shang et al., 2010). For our study, the micro-chromosomes may be of particular interest as their small arms are thought to act as a natural enrichment of centromeric regions. In isolated DT40 chromosomes, out of a pool of over ~4000 chromosomal constituents 101 kinetochore proteins can be consistently identified by mass spectrometry (Ohta et al., 2010).

3.1.2 Why use SILAC technology?

Mass spectrometry based proteomics has evolved into a discipline that is highly applicable to, and popular within, many scientific fields. Advances in mass spectrometry sensitivity, sample preparation and computational analysis mean that fundamental biological questions can, with the correct experimental design, can be answered on a system-wide scale. However, increased proteome resolution has led to issues with data interpretation. Notably, without an additional discernable feature to rank identifications, there is no quick/easy way to access the validity of outputs consisting of long lists of proteins. This can give rise to subjective reasoning or 'cherry picking' a protein of interest. This need for a more rigorous quantitation has been the driving force behind the rise of quantitative proteomics, with the most popular methods using the mass of a peptide or protein as a modifiable variable that can distinguish between different states. These 'mass-labels' can be introduced via chemical or enzymatic methods, as a spiked peptide standard, or in vivo through metabolic incorporation (Mann, 2006).

SILAC has emerged at the forefront of these quantitative methods. SILAC utilises metabolic labelling to highlight differences in protein levels between experimental cell populations (Ong et al., 2002). The technique relies on the incorporation of either 'light' (State A) or stable-isotope containing 'heavy' amino acids (State B) into proteins during their synthesis in dividing cells (Figure 9). Commonly used heavy amino acids include arginine and lysine that substitute ^{12}C with ^{13}C, or ^{14}N with ^{15}N. To reduce technical error, metabolically labelled 'heavy' and 'light' samples are then mixed, usually before cell lysis, prior to subsequent purification and fractionation steps. The defining feature of this technology is that after protein digestion the mass spectrometer can detect the mass difference between otherwise identical isotopically labelled and unlabelled peptide pairs. For example, Lysine [$^{13}C_6$, $^{15}N_2$] and Arginine [$^{13}C_6$, $^{15}N_4$] incorporation leads to a mass shift of 8 and 10Da, respectively (Figure 9). By distinguishing between these peptide pairs, relative abundance can be inferred by comparing peak intensities (Mann,

2006). In the example illustrated in Figure 9, the protein matched to this particular peptide pair should be more abundant in state B.

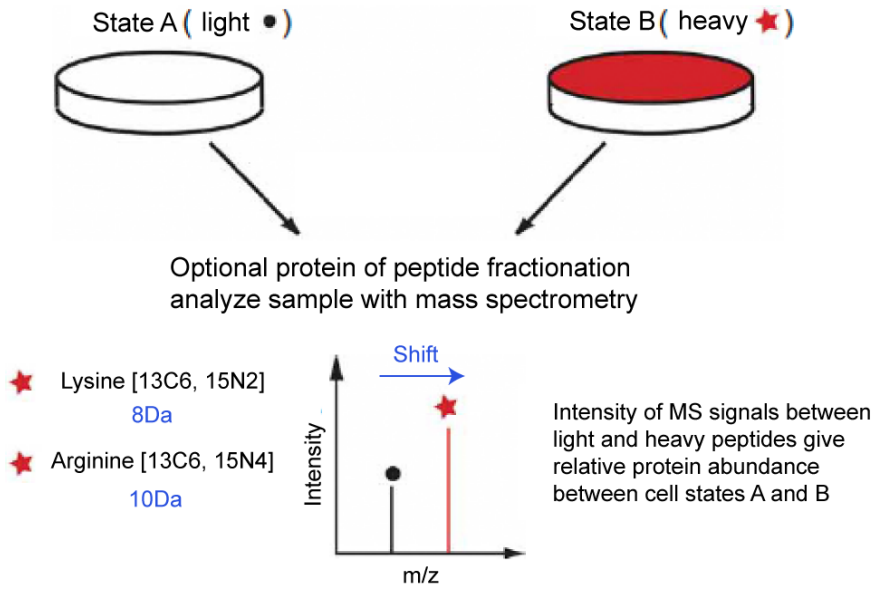

Figure 9. Quantitative mass spectrometry: SILAC. Cells are grown in either light (State A) or heavy (State B) medium. Natural amino acids are used under 'light' conditions, while stable-isotope containing amino acids are found in the 'heavy' state. Examples of stable isotope-labelled amino acids include lysine and arginine incorporating ^{13}C and ^{15}N. These are metabolically incorporated into the proteome during protein synthesis. Dialyzed serum, that has had naturally occurring amino acids removed, must be used under these heavy conditions for accurate quantitation. After mixing the two cell populations and processing for mass spectrometry the same peptide can be distinguished in light (black dot) and heavy (red star) states through a mass shift. For example, a peptide containing lysine with $6x^{13}Cs$ and $2x^{15}Ns$ will present a mass shift of 8Da relative to the light sequence. It is important to note that most peptides will contain only one heavy amino acid based on the method used for protein cleavage (e.g. Trypsin digestion cutting C-terminal to arginine and lysine). Figure modified from (Ong and Mann, 2006).

SILAC technology has already been utilised in the DT40 system to study different aspects of chromosome biology. Metabolic labelling experiments were used to separate 'hitchhiker' proteins, which bind chromosomes indiscriminately upon NEB, from the functionally significant portion of the mitotic chromosomal proteome. To do this, quantitative measures of abundance, enrichment, exchangeability on chromosomes, and

their dependency on condensins and the outer kinetochore Ska sub-complex were integrated using machine-learning procedures (for more details refer to section 4.1) (Ohta et al., 2010). Samejima and colleagues have taken the 'dependency' aspect of this experimental design to reveal the inter-dependent relationship of KIF4 and condensin subunits in regards to their ability to localise on chromosomes (Samejima et al., 2012).

I performed similar dependency studies based on the removal of key kinetochore proteins. SILAC was used to quantitatively compare the proteome of chromosomes with intact kinetochores against those missing individual integral kinetochore components. The cell lines I have chosen to use include conditional KO cells of the inner kinetochore plate: CENP-C, CENP-T and CENP-W; the Ndc80 conditional KO cell line has been chosen as a representative of the outer kinetochore compartment.

3.2 Results

3.2.1 A strategy for the prediction of kinetochore dependency pathways

In recent reports, the isolation of mitotic chromosomes from DT40 cells under SILAC conditions has elucidated the dependency networks associated with the removal of the condensin complex (Ohta et al., 2010; Samejima et al., 2012), the K-MT binding subunit Ska3 (Ohta et al., 2010), and the chromosomal scaffold protein, KIF4 (Samejima et al., 2012). We employ the same procedure to show how members of the inner compartment (CENP-C, CENP-T and CENP-W) and outer (Ndc80) kinetochore, contribute to sub-structure interactions within the kinetochore. In Figure 10A, a schematic of the general experimental strategy is illustrated using CENP-C conditional KO conditions, where gene expression of the protein of interest can be 'switched off' within hours of doxycycline treatment. The conditional KO cells are grown in medium containing natural amino acids (light), while wild-type (WT) cells are maintained under 'heavy' conditions (e.g. growth in dialyzed serum and heavy amino acids). For consistency I have chosen to use WT cells (Clone18) as a substitute for matched DT40 inducible KO

clones still expressing from the transgene (e.g. CENP-C 'ON') as heavy SILAC conditions, in many cases, dramatically slowed or inhibited cell growth. It is still unclear why this is the case, but loss of important growth factors during serum dialysis (used to remove natural amino acids) may play an important role.

As cells approach 5-6 cell divisions under SILAC growth conditions, doxycycline is added to the conditional KO cultures to suppress expression of the protein of interest. The length of drug treatment varies between different cell lines (optimisation procedures are described in section 3.2.2). Both heavy and light cell populations are blocked in mitosis using the microtubule-depolymerising drug nocodazole and mixed in equal quantities based on their respective mitotic indexes (Figure 10A). This is followed by chromosome isolation (Figure 10B) and preparation for mass spectrometry analysis (Figure 10C), resulting in a quantitative read-out of relative protein abundance based on SILAC ratios. A representative silver-stained gel of a chromosome preparation is shown in Figure 10B. From previous studies, it is known that a number of the higher molecular weight bands correspond to members of the chromosomal scaffold fraction (Gassmann et al., 2005; Morrison et al., 2002). For example, Topoisomerase II (Topo II), KIF4 and the condensin subunits are highly abundant proteins in this region. Histone H1, H3, H2A and H2B are also visible on the gel, as indicated by the high intensity low molecular weight banding pattern. Sequencing of the chicken genome, combined with a more complete manual annotation of chicken databases, means that >4000 proteins have been successfully identified on mitotic chicken chromosomes (Ohta et al., 2010).

Figure 10. Outline of experimental workflow. A. WT cells are grown in heavy SILAC medium, while the kinetochore KO cell line (e.g. CENP-C conditional KO- system) is cultured in the presence of light amino acids. Doxycycline (+Dox) is added for sufficiently long to 'turn off' the expression of the inducible transgene and ensure that the previously synthesised target protein has been degraded. While still maintained in doxycycline, both WT and KO cell lines are blocked in mitosis with nocodazole (12-13 hours). Equal numbers of mitotic cells from the two populations are mixed and the chromosomes isolated. After chromosome isolation, mass spectrometry is used to determine SILAC ratios for individual proteins. Deviation from a ratio of 1 is indicative of either an increase (red) or decrease (blue) in the recruitment of specific proteins onto chromosomes. **B.** The chromosome isolation technique involves: swelling the cells in hypotonic buffer, separating the chromosomes from interphase nuclei, and purifying using consecutive density centrifugation gradients (sucrose and percoll) in polyamine-EDTA buffers. The silver-stained gel shows the total complement of protein successfully isolated from chicken chromosomes. Components of the chromosomal scaffold and histone proteins are labelled (gel adapted from (Ohta et al., 2010)). **C.** For mass spectrometry analysis chromosomal samples are run onto an SDS-PAGE gel and the proteins digested with trypsin. The complex peptide mixture is then separated using a strong cation exchange (SCX) column and the fractions concentrated onto C18 StageTips (Ishihama et al., 2006; Rappsilber et al., 2003). Eluted peptides are analysed online by liquid chromatography (LC) coupled to electrospray ionization and tandem mass spectrometry (MS/MS). Maxquant software converts the resulting mass spectra into quantitative read-outs of abundance (H/L SILAC ratio) for large numbers of chromosomal proteins (Cox and Mann, 2008; Cox et al., 2011). Figure 10C modified from (Steen and Mann, 2004).

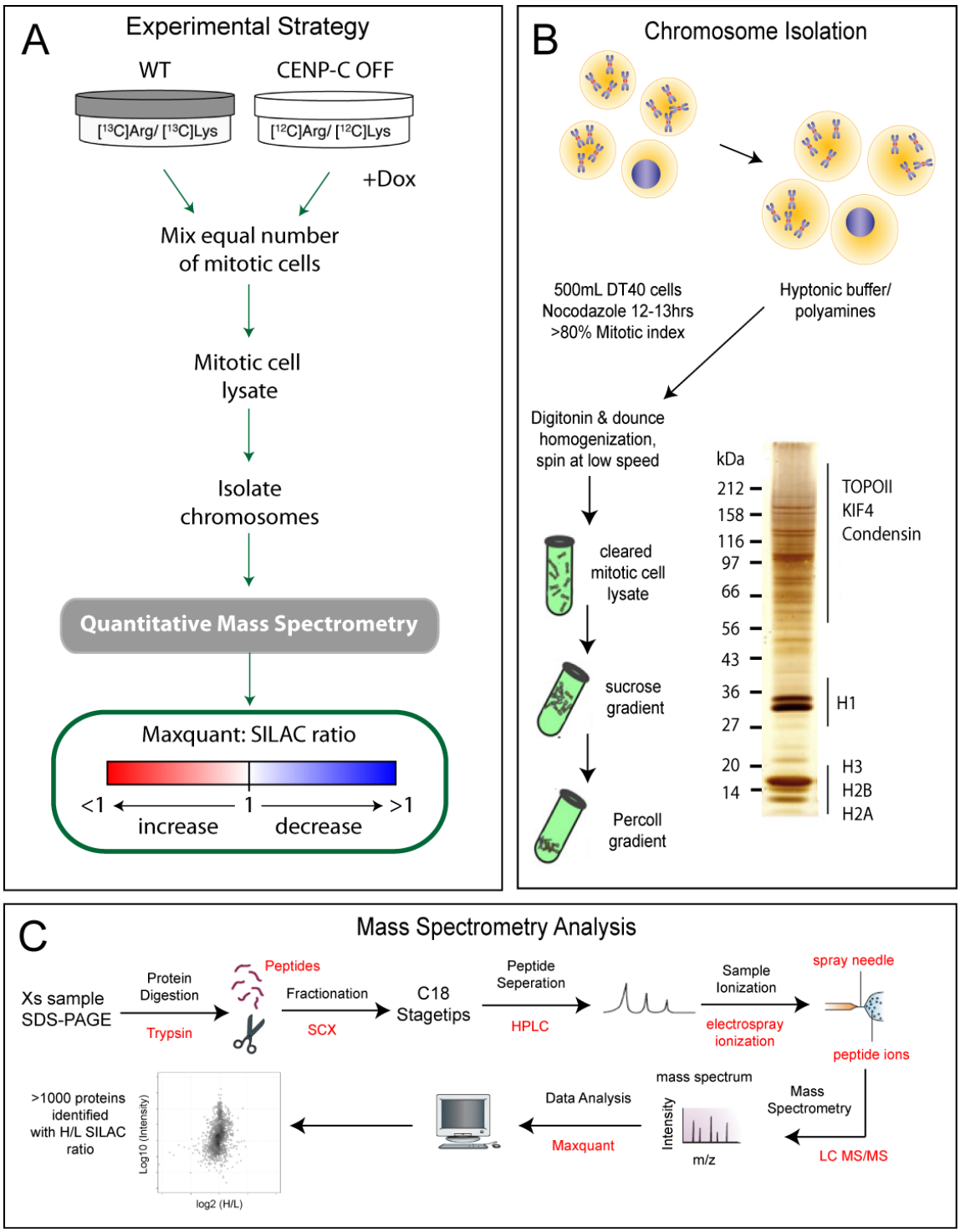
A
Experimental Strategy
WT
CENP-C OFF
[13C]Arg/ [13C]Lys
[12C]Arg/ [12C]Lys
+Dox
Mix equal number of mitotic cells
Mitotic cell lysate
Isolate chromosomes
Quantitative Mass Spectrometry
Maxquant: SILAC ratio
<1
1
>1
increase
decrease
B
Chromosome Isolation
500mL DT40 cells
Nocodazole 12-13hrs
>80% Mitotic index
Hyptonic buffer/ polyamines
Digitonin & dounce homogenization, spin at low speed
cleared mitotic cell lysate
sucrose gradient
Percoll gradient
kDa
212
158
116
97
66
56
43
36
27
20
14
TOPOII
KIF4
Condensin
H1
H3
H2B
H2A
C
Mass Spectrometry Analysis
Xs sample SDS-PAGE
Protein Digestion
Trypsin
Peptides
Fractionation
SCX
C18 Stagetips
Peptide Seperation
HPLC
Sample Ionization
electrospray ionization
spray needle
peptide ions
Mass Spectrometry
LC MS/MS
mass spectrum
Intensity
m/z
Data Analysis
Maxquant
>1000 proteins identified with H/L SILAC ratio
Log10 (Intensity)
log2 (H/L)

3.2.2 Isolation of chromosomes from kinetochore KO cell lines

Upon the commencement of chromosome isolation for a given mutant, the kinetochore protein of interest must be sufficiently depleted, whilst still maintaining cell viability, as characterised by the ability to generate both a high mitotic index (>80% mitotic index; Figure 10B) and a low apoptotic count. This is a careful balance, as unhealthy cells that have begun the process of cell death are less compatible with the multi-step chromosome isolation method and will lead to a low yield of material and increased identification of contaminants. Therefore, the response of each cell line to doxycycline must be thoroughly analysed to optimise drug treatments.

3.2.2.1 CENP-C conditional KO cell line

Initial phenotypic characterisation of the CENP-C conditional KO cell line has been described elsewhere (Hori et al., 2008a; Kwon et al., 2007). Figure 11A shows a representative growth curve of WT cells versus CENP-C knockouts, as judged by counting viable cells using a trypan blue exclusion assay. The rate of growth of CENP-C knockouts matches that of WT DT40 cells (Cl18). Doxycycline treatment affects proliferation ~36 to 48 hours after treatment in the inducible cell line, whilst WT cells remain unperturbed. Consistent with (Kwon et al., 2007), cells eventually progress towards apoptosis; however, the graph plateaus at a slightly later time point when compared with the reported study (72 hours compared to 60 hours). As cells continue to proliferate normally after 36 hours of doxycycline treatment, cells were subjected to a 12-13 hour mitotic block using nocodazole at 0, 24 and 36 hours following the initiation of doxycycline treatment. Following this, chromosomes were isolated (Figure 11B). It should be noted that cells are still maintained in doxycycline during the nocodazole treatment. Therefore the time points shown in Figure 11B indicate the initial period of cell growth in the presence of doxycycline. Unless otherwise indicated this format will be used to refer to cell culture conditions prior to harvest throughout the report.

The Coomassie stained gel clearly depicts highly concentrated banding patterns associated with histones (~17 kDa and ~34 kDa). Other non-histone proteins are predominantly found in the upper portion of the gel (Gassmann et al., 2005; Morrison et al., 2002). The isolated chromosomes were subjected to Western blot analysis with antibodies against CENP-C, Topo II, INCENP and ATP-synthase (Figure 11C). Total lysate samples from asynchronous cell populations are also depicted.

CENP-C levels were much higher in the conditional KO cell line but this was expected as it is expressed from an exogenous promoter. CENP-C is depleted from chromosomes 24 hours following doxycycline addition (+ 12-13 hours nocodazole; thus 36-37 hours in total), while Topo II and INCENP signals remain unchanged across the chromosome isolation samples, indicating that their abundance on chromosomes is unaffected by the loss of CENP-C. Mitochondrial proteins are common contaminants in chromosomal preparations, but ATP-synthase (which localises to the inner mitochondrial membrane) is only detected in very small amounts on chromosome samples, even after a long exposure of the blot. This indicates that under these conditions isolated chromosomes were pure enough for proteomics analysis.

Based on these findings, I chose to isolate mitotic chromosomes from the CENP-C inducible KO cell lines after an initial 36 hour treatment with doxycycline. The total protein recovered from chromosome isolations is shown in Figure 11D, with each repeat consisting of 3 pooled chromosomal preparations. Characteristic chromosomal protein patterns are clearly visible in repeat 1 (silver stained gel) and repeat 2 (Gel code blue stained gel). For ease of handling, chromosome pellets were concentrated and re-solubilised in small volumes of sample buffer. To release the protein from the DNA pellet multiple boiling and sonication steps were required (see Materials and Methods section 2.10.1). Samples shown in Figure 11D are 2.5% of the total volume of supernatant 1 (S1), supernatant 2 (S2) and pellet (P) fractions. Most of the proteins were released in fractions S1 and S2 which were, for this reason, combined for final mass spectrometry analysis.

Figure 11. Chromosome isolation from CENP-C KO cell lines A. Representative growth curve of WT (Cl18) and CENP-C KO cell lines in the presence or absence of doxycycline. Doxycycline was added at time 0 and living cells counted after trypan blue staining **B.** Commassie stained gel of chromosomes isolated from CENP-C KO cell lines at the indicated time points after doxycycline treatment with an additional 12-13 hour mitotic block (+Noc) **C.** Immunoblots of asynchronous total lysate samples from WT and CENP-C KO cell lines ($5x10^5$ cells per well) and the corresponding chromosome isolation samples in (B). Antibodies against CENP-C show a significant depletion in doxycycline treated cells. Topo II and INCENP detection is unaffected and ATP-synthase is present in low amounts in chromosome preparations. **D.** Silver stained (repeat 1) or gel code blue stained (repeat 2) gels of isolated chromosomes used for mass spectrometry analysis. Each repeat consists of 3 separate pooled chromosome preparations (individual isolations are described in Figure 10B). To release the protein from the DNA pellet, sonication steps were required. 2.5% of the total volume of supernatant 1 (S1), supernatant 2 (S2) and DNA pellet (P) are shown. Large proportions of proteins are released in fractions S1 and S2, which were combined for the final analysis.

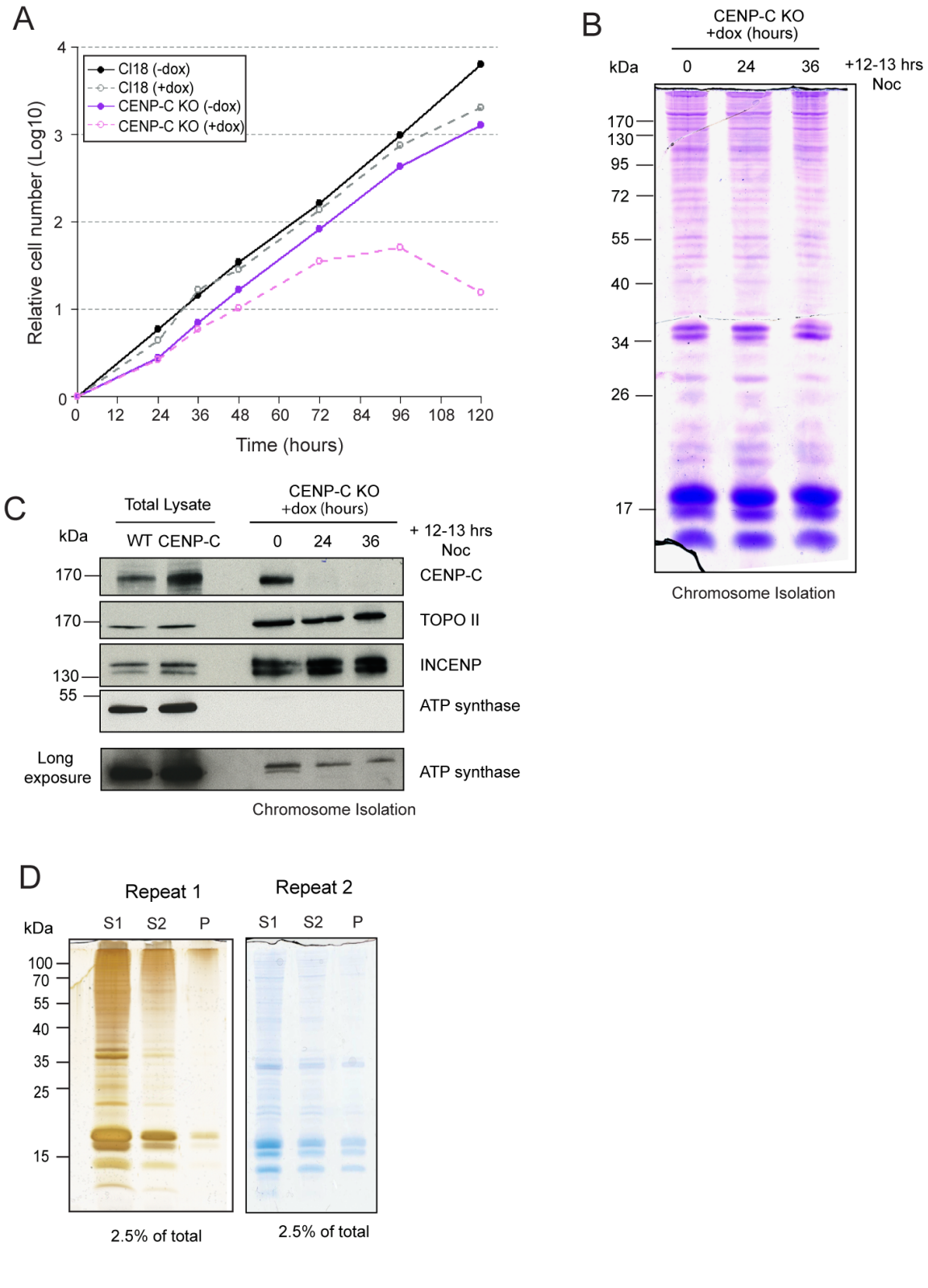
A
Relative cell number (Log10)
Time (hours)
CI18 (-dox)
CI18 (+dox)
CENP-C KO (-dox)
CENP-C KO (+dox)
B
CENP-C KO
+dox (hours)
kDa
0
24
36
+12-13 hrs
Noc
Chromosome Isolation
C
Total Lysate
CENP-C KO
+dox (hours)
WT CENP-C
+ 12-13 hrs
Noc
CENP-C
TOPO II
INCENP
ATP synthase
Long
exposure
Chromosome Isolation
D
Repeat 1
Repeat 2
S1
S2
P
2.5% of total
2.5% of total

3.2.2.2 CENP-T and CENP-W conditional KO cell lines

A recent attempt to identify the complete composition of inner kinetochore CCAN components revealed CENP-W, a small histone fold domain-containing protein that could be reciprocally pulled down as a close interacting partner of CENP-T (Hori et al., 2008a). This association has now been expanded with the description of a CENP-T/W/S/X containing heterotetramer forming a structure that is able to make direct contacts with DNA (Foltz and Stukenberg, 2012; Nishino et al., 2012). The Fukagawa laboratory have generated tetracycline-regulated DT40 conditional KO cell lines for CENP-T and CENP-W and characterised many of the direct consequences of removing this subcomplex from kinetochores (Hori et al., 2008a). In accordance with their studies, we found that the steady state of proliferation in the CENP-T KO cell line was slowed in comparison to WT cells (Cl18) (Figure 12A). While addition of doxycycline had no effect on WT cell growth, the conditional KO cell line showed inhibition of proliferation 48 hours after the onset of treatment. In the original study this plateau occurred at 36 hours and cells had died by 96 hours (Hori et al., 2008a). I found that progression into cell death was a more gradual process, with a population of unstained cells (viable) still seen in the trypan blue assay 3.5 days after doxycycline addition. One explanation could be that CENP-T is inefficiently depleted under the conditions I am using. Although this cell line should be fully depleted of CENP-T 24 hours after tetracycline treatment as detected by Western blot analysis (Hori et al., 2008a), I found that residual amounts of the protein were still visible 72 hours later and therefore this was a partial depletion (Figure 12C).

I next wanted to clarify how much of the remaining CENP-T might be associated with chromosomes. A Coomassie stained gel (InstantBlue) of chromosomal proteins isolated from WT cells and doxycycline treated CENP-T knockouts (0, 30, 36 and 42 hours) is depicted in Figure 12B. Chromosomal banding patterns were similar between the different conditions and the corresponding Western blots of these isolated samples are shown in Figure 12D. Relative protein levels of CENP-T measured using Licor Odyssey

imaging are shown as a percentage along the bottom panel. This method measures abundance based on the signals from fluorescent dye-labelled secondary antibodies. In comparison to the untreated control, CENP-T signals were gradually reduced during extended periods of doxycycline treatment, reaching a minimum of 44% at the 42 hour time point and is therefore a partial depletion. In contrast, Topo II and INCENP levels did not drastically change over the same period. When comparing total lysate samples in the asynchronous population, protein levels of CENP-T are increased in the inducible KOs in comparison to WT cells. This is not the case in the nocodazole blocked (12-13 hours) mitotic fractions, which display equal amounts of signal in the two populations. This suggests that although no longer expressed from the endogenous promoter, CENP-T levels in the KO are tightly regulated in mitosis. The amount of anti-Topo II, anti-INCENP and anti-Histone H3 detection in asynchronous versus mitotic populations is the same across WT and conditional KO cell lines.

Although the depletion of CENP-T was not complete, I chose to go ahead with SILAC experiments after 30 hours of doxycycline treatment. At this time point the mitotic index was >80% and chromosomes could be consistently isolated at high yields. The hypothesis was that even a partial loss might still confer some detectable compositional changes within the kinetochore. Two repeats of mass spectrometry analysis were performed, with each sample containing multiple chromosome preparations. Repeat 1 is comprised of material from 3 isolation procedures, while repeat 2 contains 4 separate preparations (Figure 12E). Western blot analysis of WT cells (heavy) and CENP-T depleted populations (light) used in individual SILAC experiments are shown. Relative to an anti-Histone H3 loading control (bottom panel), CENP-T levels (top panel) are clearly reduced in the tetracycline-repressive total lysate samples (Figure 12E).

Figure 12. Optimal conditions for chromosomal isolation from CENP-T KO cell lines. A. Representative growth curve of WT and CENP-T KO cell lines in the presence or absence of doxycycline. Doxycycline was added at time 0 and living cells counted after trypan blue staining. **B.** An Instant Blue stained gel of chromosomes isolated from WT or CENP-T KO cell lines at the indicated times after doxycycline treatment (+12-13 hours nocodazole treatment). **C.** Immunoblots of total lysate samples from WT and CENP-T KO cell lines at the indicated time points after doxycycline treatment ($5x10^5$ cells per well). **D.** Immunoblots corresponding to the chromosome isolation gel in (B) along with asynchronous and mitotically arrested (nocodazole block 12-13 hours) total lysate samples from WT and CENP-T tetracycline-repressive cell lines ($5x10^5$ cells per well). Quantitative Licor Odyssey analysis of immunoblot signals shows that CENP-T is not effectively depleted in the KO cell line (relative fluorescence intensity shown as total percentage). Isolated chromosomes used for detection of INCENP, Topo II and histone H3 is also depicted. **E.** Western blot analysis of cell populations used for chromosome isolation samples subjected to mass spectrometry analysis. Each repeat pools 3 (repeat 1) or 4 (repeat 2) individual chromosome preparations. Anti-CENP-T was used to ensure that in total lysate samples signals were depleted from the tetracycline-repressive cell line. A total of $5x10^5$ cells were loaded per well with anti-Histone H3 signals acting as a loading control. Signal detection was achieved by chemiluminescence reactions in repeat 1 or Licor Odyssey imaging (secondary antibodies conjugated to a fluorescent dye) in the second repeat.

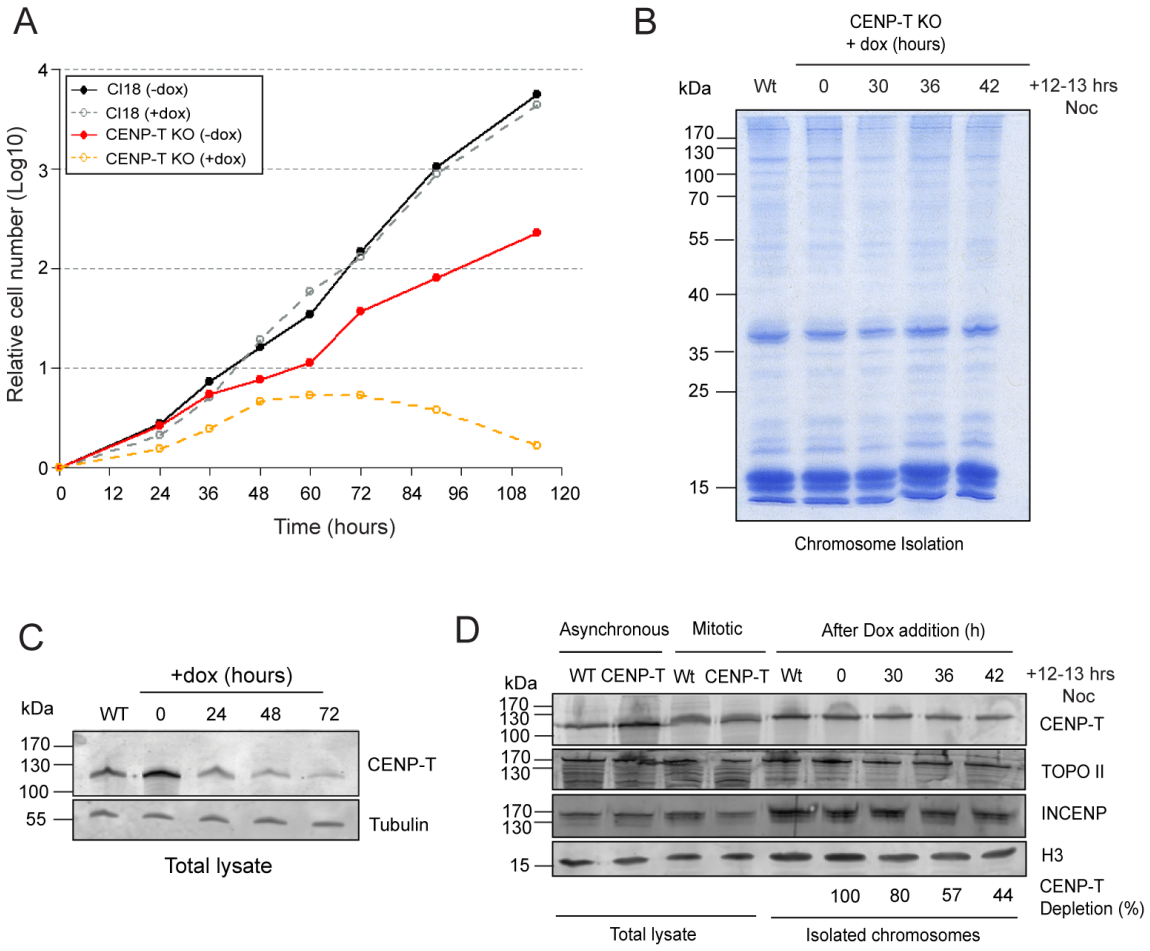
A
Relative cell number (Log10)
Time (hours)
CI18 (-dox)
CI18 (+dox)
CENP-T KO (-dox)
CENP-T KO (+dox)
B
CENP-T KO
+ dox (hours)
kDa
Wt
0
30
36
42
+12-13 hrs
Noc
Chromosome Isolation
C
+dox (hours)
WT
0
24
48
72
CENP-T
Tubulin
Total lysate
D
Asynchronous
Mitotic
After Dox addition (h)
WT CENP-T
Wt
CENP-T
TOPO II
INCENP
H3
CENP-T
Depletion (%)
100
80
57
44
Total lysate
Isolated chromosomes
E
Repeat 1
Repeat 2
Xs Prep 1
Xs Prep 2
Xs Prep 3
Xs Prep 4
WT
CENP-T
Total Lysate

In the hope of achieving a more complete knockdown of the CENP-T/W complex, I also performed the same characterisation on CENP-W conditional KO cell lines. As published previously, KO cell lines grow with kinetics similar to the WT (Cl18), but stop proliferating 36 hours after doxycycline treatment (Figure 13A). Chromosomes from mitotically blocked (+12-13 hours nocodazole) CENP-W conditional KO cells can be successfully isolated after 0, 30 and 36 hour doxycycline treatments. The total protein banding pattern visualised by Coomassie staining (InstantBlue) is comparable with the WT control (Figure 13B). I was unable to get the CENP-W antibody (Fukagawa laboratory) to work, but based on the principle that their localisation to kinetochores is interdependent (Hori et al., 2008a) and that they form a stoichiometric one-to-one subcomplex (Nishino et al., 2012) I used anti-CENP-T antibodies as an alternative measure of depletion. Western blot analysis showed a dramatic reduction in CENP-T levels on chromosomes after 30 hours in doxycycline (top panel Figure 13C). Licor Odyssey values are shown as a percentage and normalised to anti-Histone H3 signals. After 30 hours of doxycycline treatment 25% of total levels seen in the untreated samples (0 hours) are observed, and this is reduced further to 14% at 36 hours. Topo II and INCENP signals remained relatively constant across all chromosome isolation conditions. Immunoblots of asynchonous and mitotic cell populations in WT and inducible KO cell lines show that levels of INCENP, Topo II and histone H3 do not change, but CENP-T levels are slightly reduced in the nocodazole arrested mitotic samples.

As the levels of CENP-T on chromosomes are significantly reduced 30 hours after doxycycline treatment, I have chosen these conditions for subsequent SILAC experiments. Immunoblotting with anti-CENP-T and anti-Histone H3 of whole cell extracts used for chromosome isolations is shown in Figure 13D. Both repeat 1 and repeat 2 consist of three separate chromosome isolation procedures. CENP-T levels are consistently reduced in the conditional KO cell lines when compared with the WT control.

Figure 13. Chromosome isolation from CENP-W KO cells. A. Representative growth curve of WT and CENP-W KO cell lines in the presence or absence of doxycycline. Doxycycline was added at time 0. **B.** Instant Blue stained gel of chromosomes isolated from WT or CENP-W KO cell lines at the indicated times after doxycycline treatment and mitotically blocked for an additional 12-13 hours with nocodazole. **C.** Immunoblots corresponding to the chromosome isolation gel in (B) along with asynchronous and mitotically arrested (nocodazole treated 12-13 hours) total lysate samples from WT and CENP-W KO cell lines ($5x10^5$ cells per well). Due to an inability to get the CENP-W antibody to work, CENP-T was used to measure the extent of depletion of the complex. Licor Odyssey analysis of immunoblots indicated that CENP-T depletion, after normalisation to histone H3, was significantly reduced after doxycycline treatment (shown as total percentage). Immunoblots of chromosome samples using anti-INCENP, anti-Topo II and anti-Histone H3 antibodies are also shown. **D.** Western blot analysis of total lysate samples from WT cells and tetracycline-repressed cell populations used for individual SILAC experiments. Two repeats were analysed by mass spectrometry with each pooling 3 individual chromosome preparations. For the same reason as described above, anti-CENP-T was used as an indicator to predict CENP-W depletion in total lysate samples from doxycycline treated CENP-W KO cells and WT controls. A total of $5x10^5$ cells were loaded per well and Histone H3 was used as a loading control.

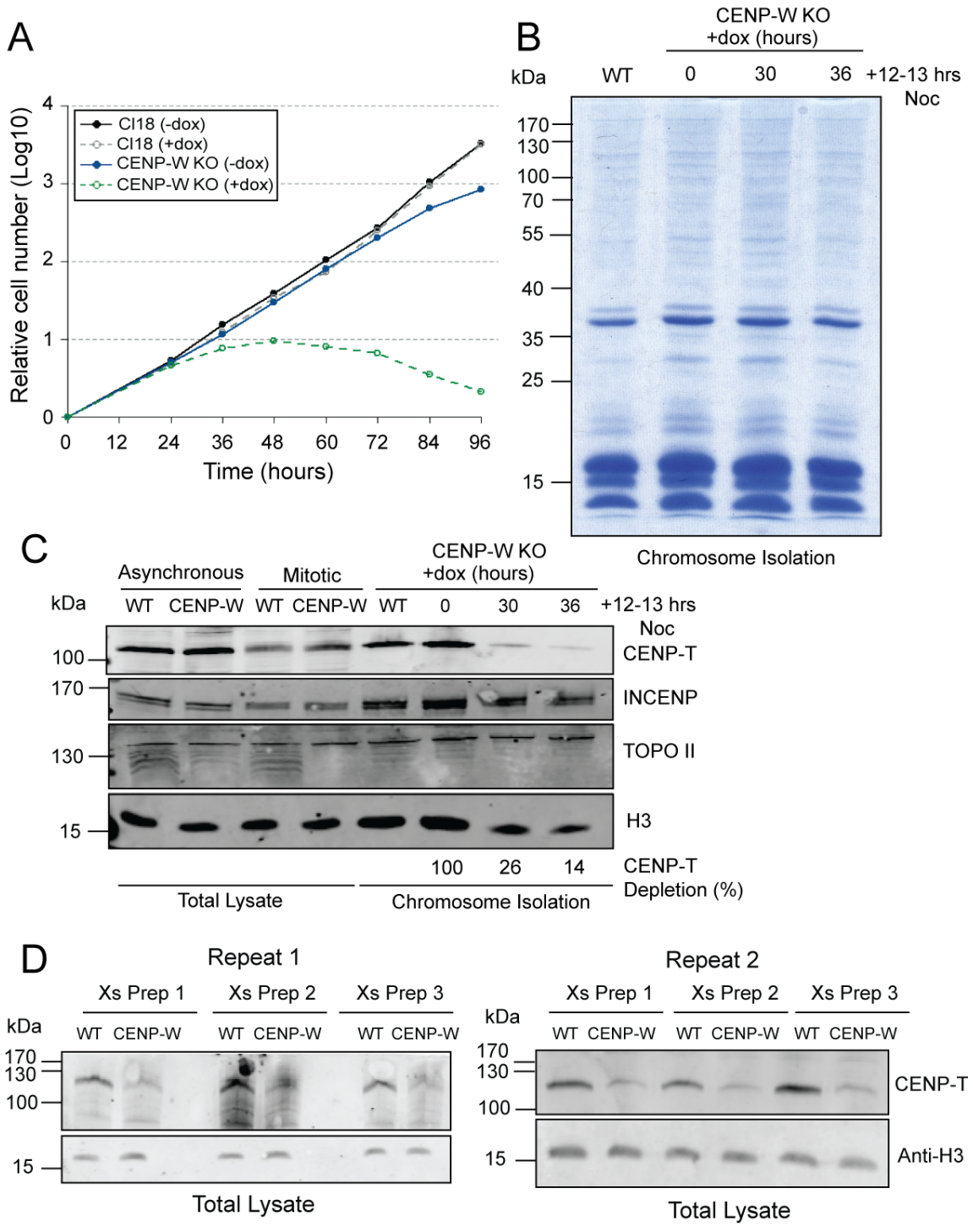
A
Relative cell number (Log10)
Time (hours)
Cl18 (-dox)
Cl18 (+dox)
CENP-W KO (-dox)
CENP-W KO (+dox)
B
CENP-W KO
+dox (hours)
kDa
WT
0
30
36
+12-13 hrs
Noc
Chromosome Isolation
C
Asynchronous
Mitotic
CENP-W KO
+dox (hours)
WT CENP-W WT CENP-W WT 0 30 36 +12-13 hrs
Noc
CENP-T
INCENP
TOPO II
H3
100 26 14
CENP-T
Depletion (%)
Total Lysate
Chromosome Isolation
D
Repeat 1
Repeat 2
Xs Prep 1
Xs Prep 2
Xs Prep 3
WT CENP-W
CENP-T
Anti-H3
Total Lysate

3.2.2.3 Ndc80 conditional KO cell line

Using DT40 tetracycline-repressible cell lines, it has already been shown that suppressing Ndc80 expression results in a prometaphase block, abnormal spindle formation and chromosome hypercondensation (Hori et al., 2003). Consistent with the published characterisation of this cell line we found that growth rates, counted using the trypan blue exclusion assay, are directly comparable with WT DT40 cells (Figure 14A). Upon addition of doxycycline at 0 hours, cell proliferation is perturbed in the knockouts after ~12 hours and is followed by rapid cell death.

Chromosome isolations were carried out 0, 3, 6 and 12 hours after doxycycline treatments. Total protein staining of chromosomes from the indicated conditions showed comparable staining patterns (Figure 14B). Immunoblots of these samples are depicted in Figure 14C. The top two panels highlight equal levels of INCENP and Topo II across all chromosome isolation conditions; while ATP-synthase, a common mitochondrial contaminant, is absent. Comparison of whole cell extracts from asynchronous versus mitotic conditions shows no difference in the signals of INCENP and ATP-synthase. However, Topo II detection is relatively weak and it is possible that it may have been degraded in these samples. The two bottom panels depict immunoblots using histone H3 and Ndc80 antibodies. Greater quantities of the chromosome isolation samples were loaded to fully distinguish the extent of Ndc80 depletion between the various doxycycline treatments (x2.5 the volume loaded for the top three panels). Depletion represented as a total percentage of Ndc80 levels according to Licor quantitation is shown along the bottom panel. After 12 hours of doxycycline treatment (+ 12-13 hour mitotic block) Ndc80 levels were reduced to 15% of normal levels.

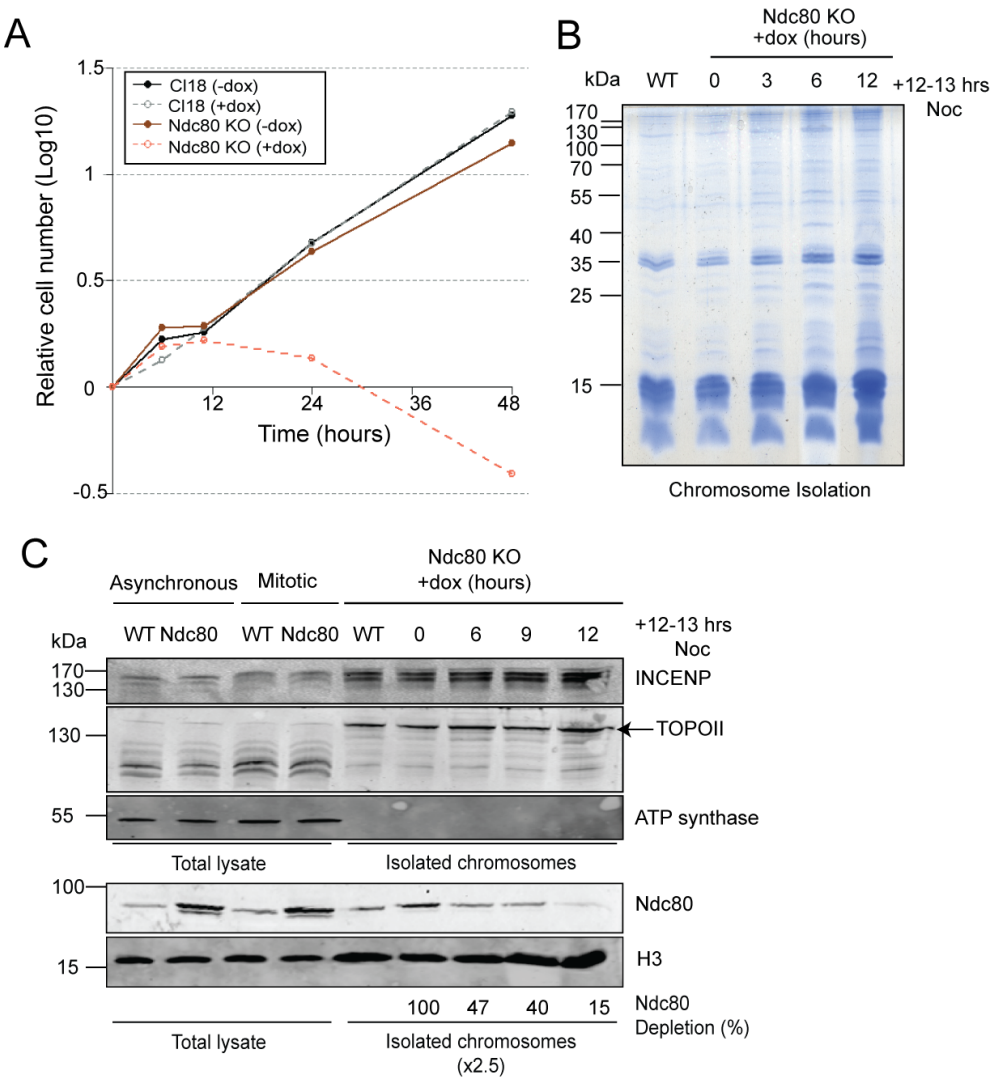

Figure 14. Optimal conditions for chromosomal isolation from Ndc80 KO cell lines. A. Representative growth curves of WT and Ndc80 KO cell lines in the presence or absence of doxycycline. Doxycycline was added at time 0. **B.** Coomassie stained gel (InstantBlue) of chromosomes isolated from WT or Ndc80 KO cell lines at the indicated times after doxycycline treatment and blocked for an additional period of 12-13 hours in nocodazole. **C.** Immunoblots corresponding to the chromosome isolation gel in (B) along with asynchronous and mitotically arrested (nocodazole 12-13 hours) total lysate samples from WT and Ndc80 KO cell lines ($5x10^5$ cells per well). The top three panels indicate blots for INCENP, Topo II and ATP-synthase. The two bottom panels use anti-Ndc80 and anti-Histone H3 antibodies. Greater quantities of the isolated chromosomes were loaded to fully distinguish the extent of Ndc80 depletion between the various doxycycline treatments (x2.5 the volume loaded for the top three panels). The extent of Ndc80 depletion indicated is the total percentage of Ndc80 levels according to relative fluorescence signals as quantified using Li-Cor Odyssey software.

As cells stop proliferating within a very short time window (~12 hours after doxycycline addition), I also wanted to check the number of cells progressing into apoptosis. The apoptotic assay used employs a fluorescent dye bound to annexin V – a protein that recognises phosphatidylserine flipped to the outer membrane during cell death. Flow cytometry analysis was used to quantify cells displaying either high or low levels of fluorescence. High fluorescence levels are indicative of apoptosis and will shift cells from the left to the right hand side of the plot (Figure 15A). Basal levels of apoptosis ranged from 15-20% in untreated cells, but autofluorescence was not accounted for in these cell populations. As unstained controls were not measured (these would account for autofluorescence) and used to normalise the apoptotic measurements, it is more important to pay attention to the general trend of apoptotic progression, rather than the absolute percentages.

Figure 15A depicts representative images of flow cytometry counts from WT and Ndc80 KO cell lines. In WT cells, addition of nocodazole (mitotic block) had no dramatic affect on the apoptotic index (ranging from ~15-20%). On the other hand, addition of nocodazole to the tetracycline-repressive Ndc80 cell lines results in a doubling of cell death compared to the untreated population (~15% to 33%). No further increase was observed if preceded by doxycycline addition for 3, 6 and 9 hours. However, a further increase in apoptotic rates was observed at 18 and 24 hour time points (~54% and 68%, respectively). Figure 15B shows the results from two separate repeats and it is clear that a substantial increase in the apoptotic index of mitotically arrested cells is seen with >18 hours of doxycycline treatment.

Although the Nocodazole treatment alone increased apoptotic index, the chromosome isolation procedure requires cells to be blocked in mitosis. As Ndc80 is sufficiently depleted after 12 hours of doxycycline treatment, and this additional treatment does not lead to further cell death, I chose these conditions for further analysis. Figure 15C depicts immunoblots from all the SILAC chromosome isolations. Two experimental repeats combining 3 chromosome preparations each are shown, and were separately

analysed by mass spectrometry. The levels of Ndc80 were dramatically reduced in whole cell extracts from doxycycline treated conditional KO cell lines in comparison to the WT population (Figure 15C).

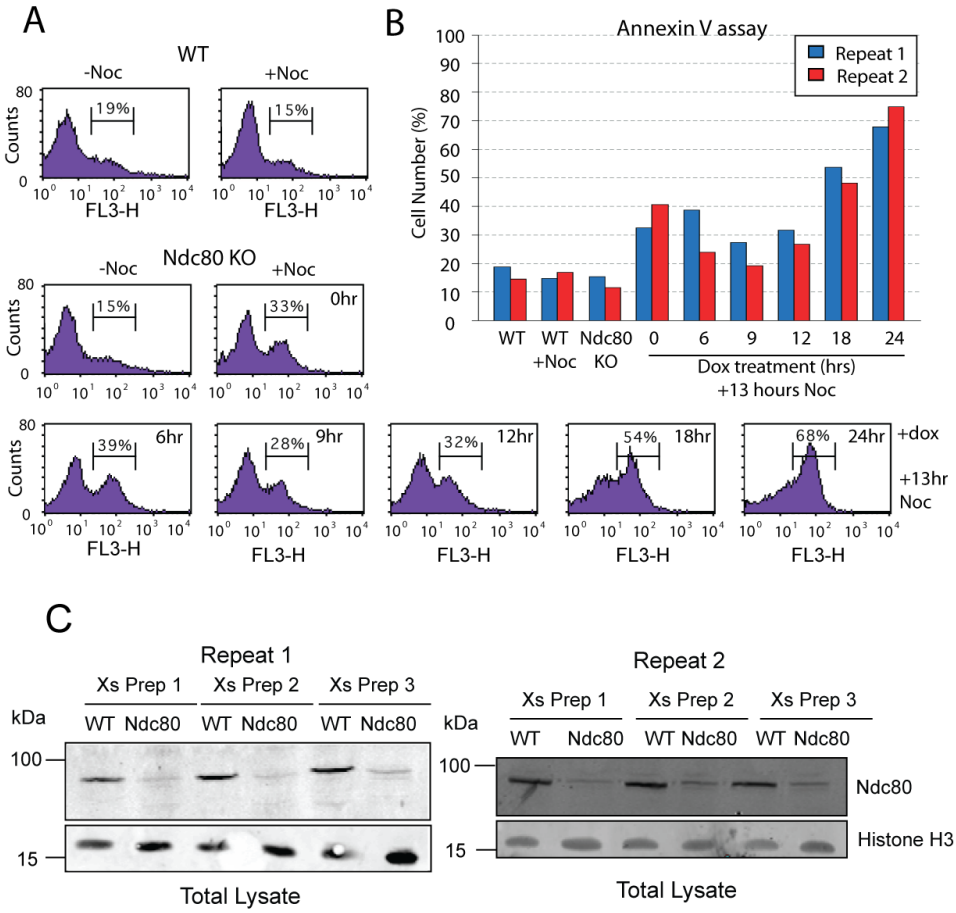

Figure 15. Ndc80 depleted cells progress into apoptosis. A. FACs analysis measuring the total population of apoptotic cells. Ndc80 KO cells were treated with doxycycline for different time periods (0, 6, 9, 12, 18, 24 hours) followed by a block in mitosis (13 hour nocodazole treatment) and compared against WT cells. The mitotic arrest applies to all conditions unless otherwise indicated. Fluorescence intensity of the PE-Annexin V signal (a marker for apoptotic cells) is shown on the x-axis and cell count is plotted on the y- axis. The percentage of cells displaying high Annexin-V signals is shown. **B.** Barplot of apoptotic cell count as a percentage in two independent experiments. **C.** Western blot analysis of SILAC cell populations used for chromosome isolations. Each repeat was analysed by mass spectrometry separately and 3 individual chromosome preparations were pooled. Immunoblots were analysed by Licor Odyssey software using antibodies against Ndc80 and histone H3.

3.2.3 SILAC: Normalisation and reproducibility of biological repeats

3.2.3.1 Data normalisation

Using the tetracycline-repressible cell lines and chromosome isolation conditions described above, SILAC-based quantitative proteomics was performed to compare the relative abundance of individual proteins in each sample. Briefly, protein extracts were digested with trypsin and the complex peptide mixture fractionated using SCX procedures and analysed by mass spectrometry on a LTQ Velos with online Reverse Phase (RP)-LC. The resulting raw data was subjected to Maxquant analysis, which is able to identify and compare heavy and light peptide pair intensities, and convert these into SILAC ratios (Cox and Mann, 2008; Cox et al., 2011). The final protein ratios are calculated by taking the median from all SILAC values, each originating from a particular heavy/light peptide pair that maps onto the protein sequence. Using ≥1 unique peptide (i.e. a stretch of amino acids whose sequence can only be matched with a specific protein) as a basis for quantitation, between 1226 and 2568 proteins were identified across experiments (Figure 16; N number). The distribution of H/L SILAC ratios on a $\log_2$ scale is depicted as boxplots in Figure 16 and includes duplicate experiments from CENP-C, CENP-T, CENP-W and Ndc80 conditional KO cell lines (light) compared with WT controls (heavy). The original SILAC ratio outputs from Maxquant analysis, or 'unnormalised' datasets (left), are compared with values normalised to histone H4 ratios (right). The rationale is that histone H4 is a highly abundant chromatin protein that can be used to account for unequal mixing of cells in the early stages of the SILAC experiment. In addition, unlike histone H3, there appear to be no known sequence variants of histone H4 (Kamakaka and Biggins, 2005).

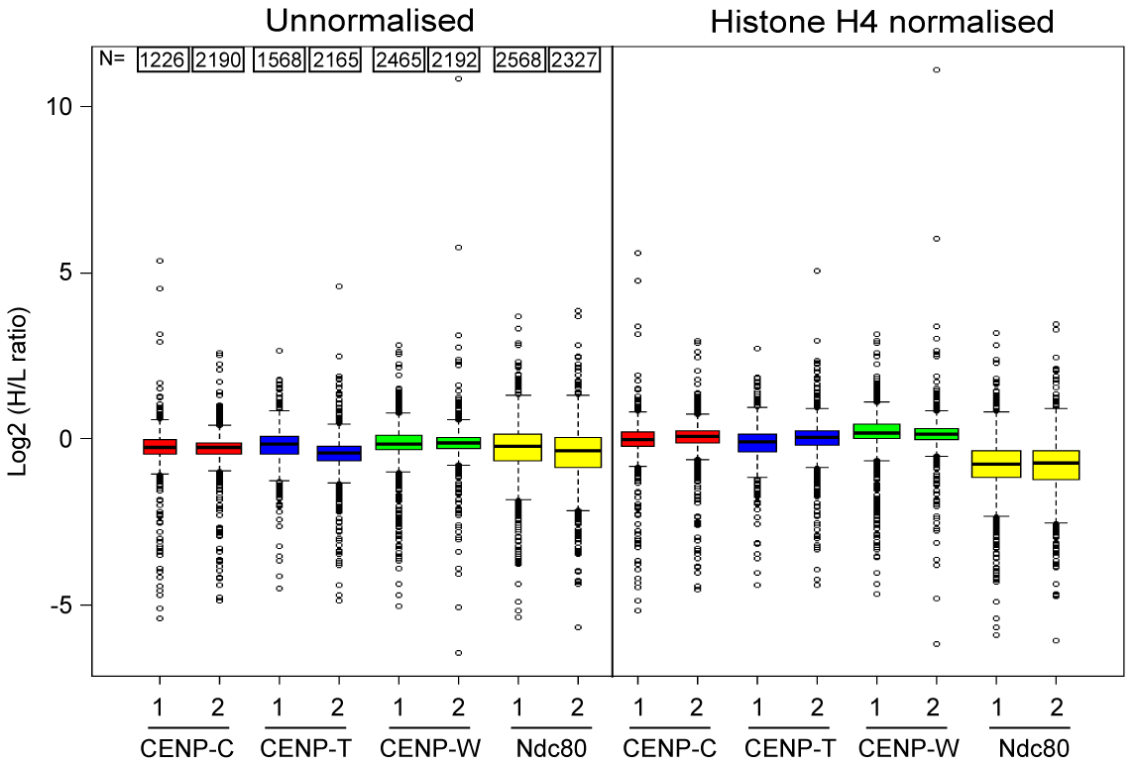

Figure 16. Normalisation of SILAC ratios to histone H4. Box and whisker plots are used to depict the spread of $\log_2$ H/L ratios in individual experiments. The median ratio is shown as a central black line surrounded by a box representing the interquartile range containing the median +/- 25% of the data. Whiskers extend a maximum of 2 standard deviations from the median; outliers are depicted with circles. The width of each box is proportional to the number of proteins identified with a H/L SILAC ratio in each experiment (also indicated by N). Repeats are labelled 1 and 2 and CENP-C, CENP-T, CENP-W and Ndc80 KO datasets are coloured red, green, blue and yellow respectively. The distribution of protein ratios is shown **(A)** Before normalisation and **(B)** after normalisation to histone H4. After normalisation the population median is close to 0 for all experiments apart from Ndc80 KO SILAC datasets.

As centromeres represent a discrete and relatively small locus on chromosomes I would expect most chromosomal bound proteins to be unaffected by depletion of integral kinetochore components. Indeed, in the unnormalised H/L ratios, the population median (black line within the box) and the upper and lower quantiles (box including 50% of the data) were very close to 0 across all experiments. Histone H4 normalisation promotes only small shifts in the distributions of CENP-C, CENP-T and CENP-W KO experiments, with a large proportion of the ratios still centred around 0. In contrast,

histone H4 normalisation of the Ndc80 KO data sets leads to a shift towards more proteins displaying negative H/L SILAC ratios (median and quantile distributions move downwards on the boxplot). This population of proteins would represent candidates that are abnormally recruited onto chromosomes after removal of the Ndc80 containing complexes.

Ndc80 KO cell lines cease proliferation much faster upon doxycycline addition than the other cell lines examined, creating a short time window for chromosome isolation prior to cell death. I also found that, even in the absence of doxycycline, a mitotic block alone results in higher levels of apoptosis (see previous section). It is possible that changes in chromosome properties in unhealthy Ndc80 KO cells might cause more contaminants to bind chromosomes when compared directly with WT DT40 cells. Alternatively, the Ndc80-depleted chromosomes could be associating with apoptotic bodies.

It is also possible that the level of histone H4 in the Ndc80 KO cells could itself be reduced on chromosomes, making it an unsuitable protein for normalisation. However, I do not believe this to be the case for two reasons. First, if I take the unnormalised ratios for the kinetochore sub-group, most proteins have a tendency to depend on Ndc80 for their localisation onto chromosomes (i.e. they have a shift towards positive H/L ratios and are therefore depleted from chromosomes). For example, this shift includes CENP-A and other CCAN components. This would contradict published literature showing that CENP-A, CENP-C and CENP-H centromere localisation is unaffected in doxycycline treated Ndc80 and Nuf2 conditional KO cell lines (Hori et al., 2003). Once normalised to histone H4 this shift is no longer observed and inner kinetochore proteins are more evenly spread about a $\log_2$ ratio of 0 (i.e. no change in abundance on chromosomes). Second, normalising to other abundant chromosomal proteins such as SMC2/SMC4 (condensin complex) or KIF4 would have the same affect as normalising to histone H4 on H/L SILAC ratio distribution. This indicates that infact chromosomes from WT and doxycycline treated cells were probably not mixed in an exact 1:1 ratio. Based on this reasoning, all SILAC datasets were normalised to histone H4.

3.2.3.2 Reproducibility between replicate experiments

To visualise CENP-C, CENP-T, CENP-W and Ndc80 SILAC data set distributions in an alternative manner and assess the correlation between biological replicates (e.g. reproducibility), $\log_2$ H/L ratios from duplicate experiments were plotted against one another (Figures 17A-D). All proteins included in this analysis must have been quantitatively identified in the two individual experiments and represented by at least 1 unique heavy/light peptide pair. Red circles depict proteins that have previously been implicated in kinetochore structure, with the number of proteins represented in this group indicated by n (red). The Pearson correlation co-efficient was used to measure correlations of overall protein profiles between biological replicates. According to the Pearson correlation coefficient, SILAC ratios for kinetochore proteins exhibit a strong positive linear dependency ($r>0.8$) between duplicate experiments. This holds true across all KO cell conditions and demonstrates sufficient accuracy and reproducibility of the methodology in terms of kinetochore protein identification.

The total number of proteins quantified with H/L ratios and represented in both repeats includes both the kinetochore subgroup and all other proteins (n number; bottom right). A clear shift towards proteins displaying a negative H/L ratio is observed in the Ndc80 KO cell lines (Figure 17D). Importantly, this feature is reproducible across the two repeats, but is not seen in the other cell lines, meaning it is a specific physiological state of Ndc80 KO cells. When considering all H/L ratios, the read-outs for linear correlation were dramatically affected by the large number of proteins showing small differential changes in abundance, and therefore centred around 0. This lack in the spread of H/L SILAC ratios about 0 resulted in small r values (<0.8), which suggest poor correlation between replicate datasets. However, as the depletion of kinetochore components only affects the abundance ratio of that particular subgroup of proteins, Pearson coefficients based on the whole chromosomal proteome were not good readouts of correlation/accuracy between replicates.

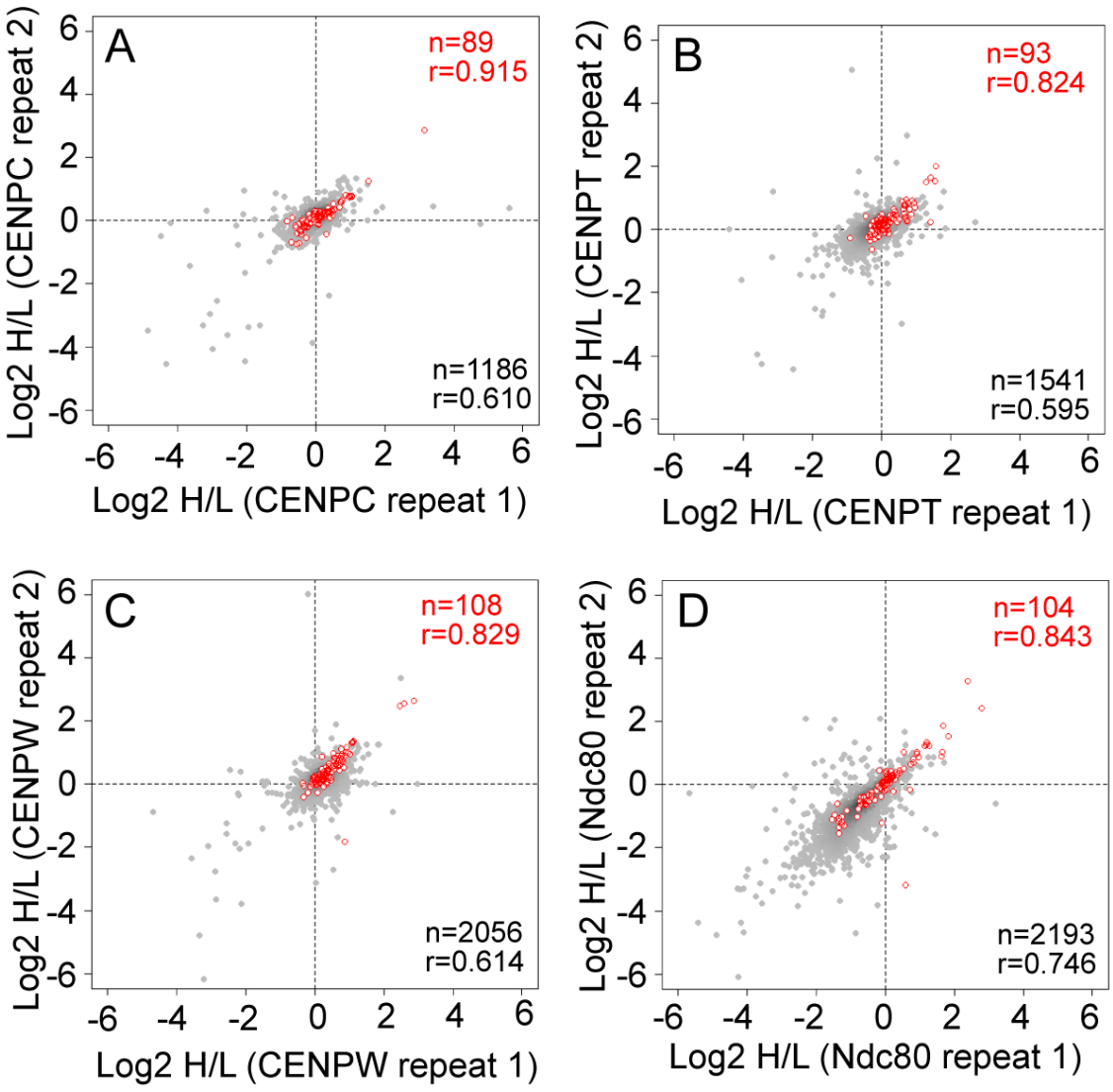

Figure 17. Correlation between replicate experiments. Scatter plots depicting $\log_2$ H/L ratios of biological duplicates (repeat 1: x axis, repeat 2: y axis) for **(A)** CENP-C **(B)** CENP-T **(C)** CENP-W and **(D)** Ndc80 KO SILAC experiments. A minimum of 1 unique H/L count was used for quantitation. Red circles indicate proteins that have been classified as kinetochore proteins, while grey points represent all other proteins. The Pearson correlation co-efficient (r) and protein number (n) for the kinetochore subgroup (red) and all data points (grey and red points) are shown.

3.2.3.3 Using 1 unique peptide for quantitation

In quantitative proteomics experiments it is often advised to use a minimum of 3 H/L ratio events as a cut-off for reliable protein quantitation (Cox and Mann, 2008). This is important, as this curtails the effect of outliers on the median value. For example, with 3 data points a single extreme value will have no effect on the median. In contrast to this, I have chosen to use 1 unique peptide pair for quantitation. The justification for this is presented in Figure 18 using the Ndc80 KO data sets. Correlation plots of the two individual repeats with $\log_2$ H/L ratio values are shown with increasing thresholds of H/L peptide pairs required for quantitation (1, 2 and 3 ratio counts). Kinetochore proteins are displayed as red circles. Although linear correlation of H/L protein ratios between repeats becomes stronger (Pearson correlation (r) is closer to 1) as the number of ratio counts is increased, this is accompanied by a concomitant reduction in the number of quantifiable members in the kinetochore subgroup (n). Each additional H/L count increment in the cut-off resulted in a ~10% drop in the number of kinetochore proteins identified. I therefore opted to retain as much information as possible and use an additional readout of accuracy to highlight those H/L ratios that should be interpreted with greater caution.

An additional measure of accuracy is to highlight proteins that have H/L SILAC ratios that significantly differ between the two replicates and are therefore not reproducible. Histogram plots of the fold difference between replicates 1 and 2 across all cell conditions are shown (Figures 19A-D) (fold difference= ($\log_2$ H/L repeat 2)-($\log_2$ H/L repeat 1)). Those showing large differences in fold change between replicates will deviate from 0, while those sharing similar values will be clustered around this central point.

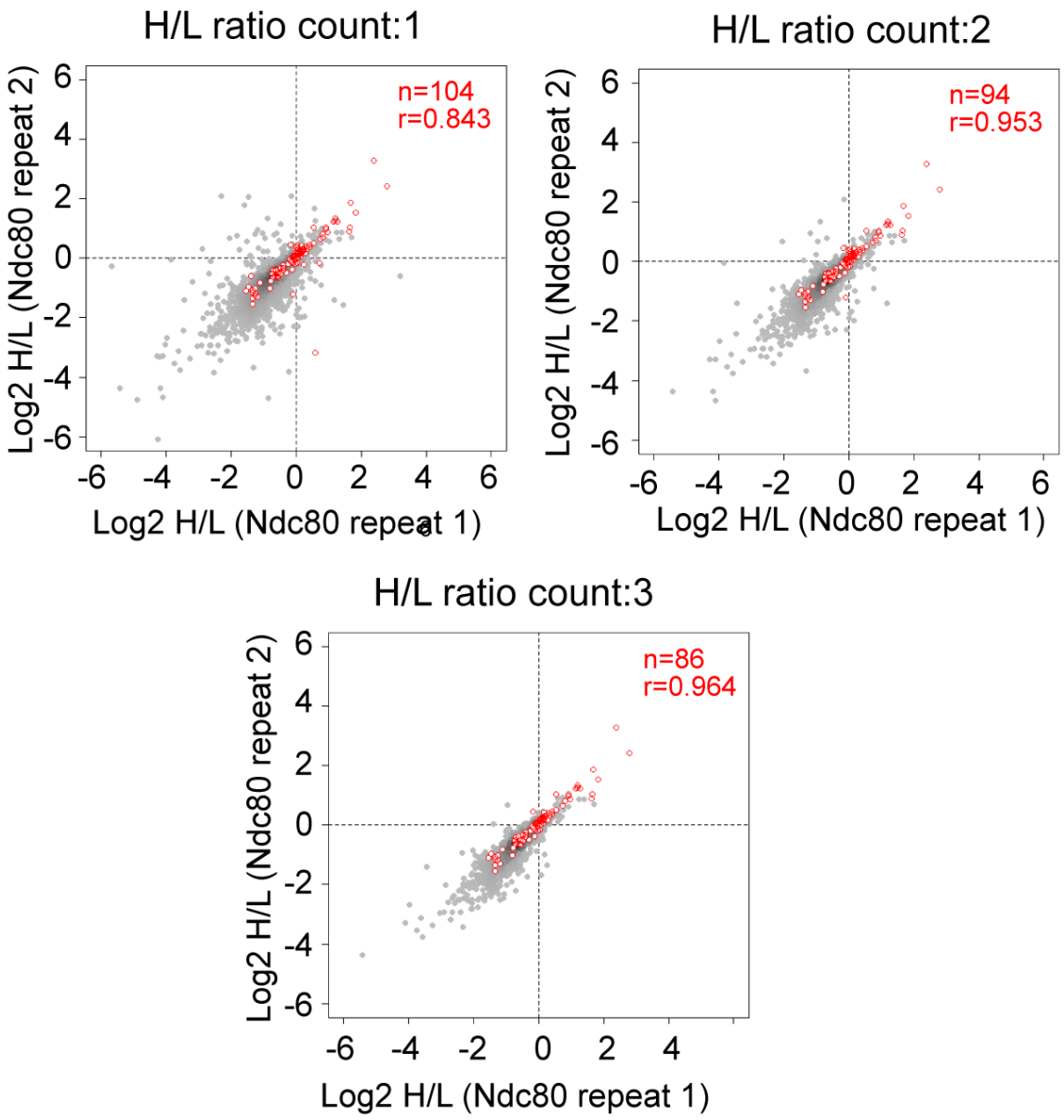

Figure 18. Justification for using 1 unique peptide for quantitation. Scatter plots depicting $\log_2$ H/L ratios of biological duplicates (repeat 1: x axis, repeat 2: y axis) for the Ndc80 KO data set using >1, 2 or 3 H/L ratio counts as a threshold for quantitation. The Pearson correlation coefficient (r) and protein number (n) for the kinetochore subgroup (red) is shown.

A simple way to define proteins whose SILAC ratios significantly deviate between replicate experiments is to use the median absolute deviation (MAD) (Hampel, 1974). In this case the median of the dataset is the central tendency indicator and MAD is a measure of scale. This method is more resistant to the presence of outliers than the mean and standard deviation. The MAD was calculated using the mad( ) function in R (www.r-project.org). Using a cut-off of 2.5 MADs below and above the median, I could define a threshold criterion for rejection (Figures 19A-D; blue dashed lines). This roughly equates to a 1.5-fold change between replicates. This cut-off is important as only mild variations in chromosomal abundance are observed for many of the kinetochore proteins (< 1.5 fold-change).

The location of known kinetochore proteins in respect to the fold difference is depicted as a rug plot along the top of the graph. Only a small number of kinetochore constituents lie outside of the 2.5 MAD range and most are very close to the outlier threshold. Only APC5, CENP-F and Ska3 SILAC ratios quantitated in CENP-T, CENP-W and Ndc80 experiments, respectively, deviate significantly between replicates. All other kinetochore proteins found within the outlier region lie very close to the 2.5 MAD boundaries.

This method allows quantitative values for more kinetochore proteins to be considered for further interpretation. Using the Ndc80 KO experiments as an example, 6 kinetochore proteins lie outside of the 2.5 MAD range (Figure 19). If 3 H/L ratio counts are used for quantitation, 18 kinetochore proteins are excluded from further analysis (Figure 18). I have chosen not to remove the ‘outliers’ as such, but will consider these during subsequent interpretations of the data sets. This will be particularly important in the later chapters for filtering out contaminants, as these are likely to vary more greatly in their ability to bind chromosomes.

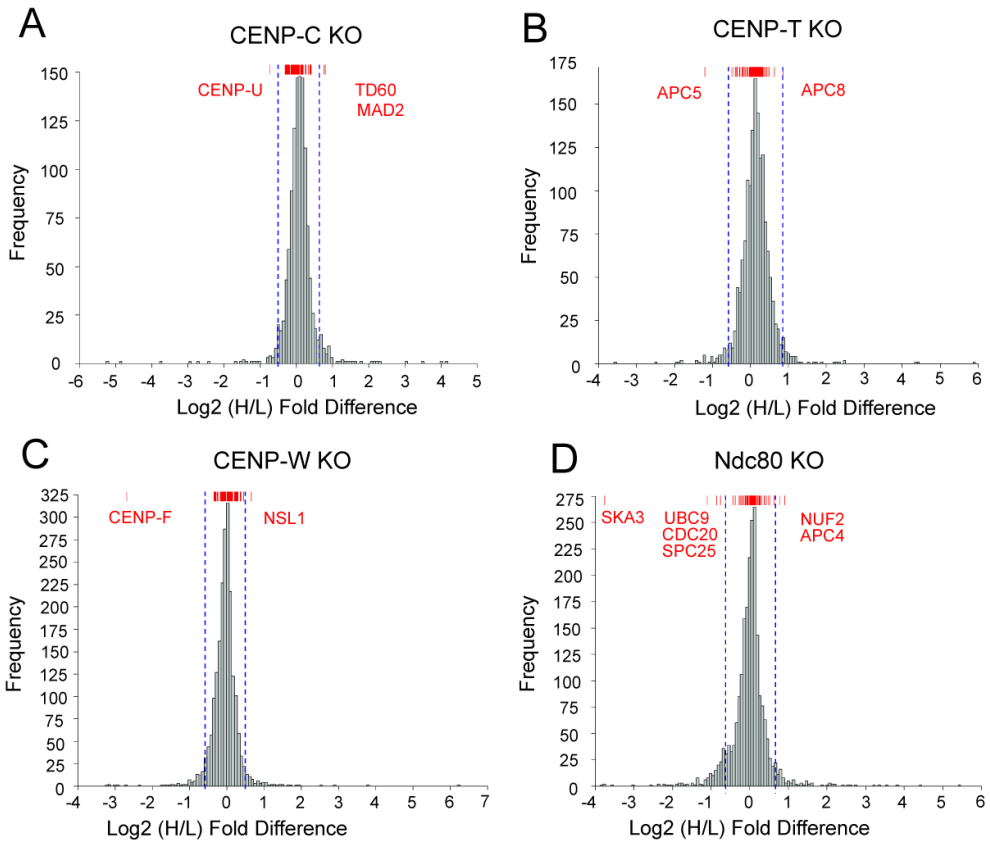

Figure 19. Identification of potential outliers. Histogram plots depicting the $\log_2$ H/L fold difference between ratios for the same protein across two biological replicates in **(A)** CENP-C **(B)** CENP-T **(C)** CENP-W and **(D)** Ndc80 KO experiments. When H/L SILAC protein ratios are similar between replicates, these will have a small fold difference. Those that are varied will display a large negative or positive value. Blue dashed lines indicate the median +/- 2.5 MAD threshold. Values lying outside of this range could be considered outliers. Along the top of each graph a rug plot (red) marks the location of known kinetochore proteins within the histogram. Kinetochore proteins are mostly situated within the 2.5 MAD boundaries and therefore do not differ significantly between replicate experiments. Those kinetochore proteins that lie outside this threshold are labelled in red.

3.2.4 Dependencies of known kinetochore proteins

3.2.4.1 Fold change differences in kinetochore proteins

Mass spectrometry analysis of isolated chromosomes is consistently able to identify and quantify the relative abundance of many known kinetochore proteins (Ohta et al., 2010). A simple approach to assess changes in the levels of these chromosomally-bound proteins is to define a fold change cut-off (e.g. >1.5 or 2-fold), where proteins displaying SILAC ratios larger than this will be classified as differentially abundant (Ting et al., 2009). Barplots in Figure 20 depict H/L ratios for centromeric proteins grouped and colour-coded into previously reported functional subcomplexes. Here, I have chosen >1.5-fold change as a cut-off for differential abundance as only mild changes, even for known kinetochore proteins, are often observed. Protein ratios that exceed this measure fall over the blue and red lines on the plots and represent a significant decrease or increase in protein amounts, respectively. Bars marked with '1' were only quantified in one out of two repeats, while all other values represent the mean $\log_2$ H/L ratio. Labelling with 'v' (variable) signifies ratios where the fold change between biological duplicates show less correlative power based on the principles described in the previous section. Caution is advised in drawing conclusions from single experiments and 'v' marked ratios.

Although CENP-C is clearly depleted from chromosomes under CENP-C KO conditions only modest changes are observed in the abundance of other kinetochore subcomplexes. For example, the HP1 complex, CPC, Nup107-160 complex, Ska components, RZZ and Dynein-Dynactin all show only slight deviations about 0, indicating a 1-to-1 abundance ratio. Most CCAN components are only slightly depleted from chromosomes, apart from the CENP-T/W/S/X complex which lies very close to the 1.5 fold-change boundary. Members of the outer kinetochore are however affected, with the Ndc80 complex, Mis12 components and KNL-1 all showing fold changes >1.5. Interestingly, there is no significant decrease in Mis18 complex levels, in particular KNL2 (Mis18bp1), which

has been reported elsewhere to localise *in vitro* on metaphase chromosomes in a CENP-C dependent manner (Moree et al., 2011). Two proteins, CENP-V and Sgo1, are abnormally recruited onto chromosomes in the absence of CENP-C. Both have been shown to be important for CPC targeting to centromeres (Tadeu et al., 2008; Tsukahara et al., 2010). However, CPC levels do not appear increased as a result of this recruitment.

As described recently, it is clear from both the CENP-T and CENP-W conditional KO datasets that the CENP-T/W/S/X components form a highly inter-dependent complex (Hori et al., 2008a; Nishino et al., 2012). This loss is more extensive in the CENP-W KO cell lines, and is consistent with Western blot analysis in section 3.2.2.2. A more complete depletion, as seen with the CENP-W KO, promotes more pronounced losses of certain sub-groups; namely CCAN components, Mis12, Ndc80, Ska and RZZ complexes (except Zwint which is not yet annotated in the chicken genome). However, out of all the CCAN components, CENP-C and CENP-U are the only proteins that do not drift towards the >1.5-fold threshold. This would support the role of CENP-C as an independent linker to the outer kinetochore (Gascoigne et al., 2011; Hori et al., 2008a; Milks et al., 2009; Przewloka et al., 2011; Screpanti et al., 2011). Similarly CENP-A, which is an upstream marker of kinetochore assembly, remains unchanged (Gascoigne and Cheeseman, 2010). Interestingly, when CENP-T is partially lost from chromosomes CENP-O complex members (apart from CENP-U) behave differently from the other CCAN components, suggesting that its association with kinetochores has a slightly different dependency. This is not seen in the CENP-W KO data sets (more complete loss of CENP-T/W), and is lost from chromosomes to the same extent as CENP-H/I/K and CENP-L/M/N containing complexes.

The APC/C activating co-factor Cdc20, which promotes progression from metaphase to anaphase (Musacchio and Salmon, 2007), does not appear to form a stable complex with other chromosomal-associated APC/C subunits when CENP-W gene expression is suppressed. Other checkpoint signalling components, including Mad1 and Mad2, also

decrease in abundance in response to partial or complete loss of CENP-T/CENP-W. Taken together, this suggests that Mad1 and Mad2 (or a subpopulation thereof) behave differently from other spindle checkpoint constituents in relation to their CENP-T/W dependency for chromosomal association.

Absence of the Ndc80 complex has no impact on the abundance ratios of inner kinetochore components forming the CCAN. However, in accordance with the CENP-T and CENP-W datasets Mis12/KNL-1, the RZZ complex, Mad1-Mad2 and CENP-E are all reduced below the >1.5-fold change cut-off. Interestingly, there appears to be a graded effect, with a greater loss of the Ndc80 complex associated with a more pronounced reduction in these downstream factors. The CENP-C KO data set, despite a significant amount of KMN loss, does not show the same extent of depletion for the RZZ complex, Mad1-Mad2 and CENP-E, suggesting that Ndc80 levels have not yet fallen below critical threshold. Certainly, the Ndc80 complex has been linked in published work to the localisation of CENP-E and Mad1-Mad2 (Hori et al., 2003; Liu et al., 2007; Martin-Lluesma et al., 2002). There is also evidence that Ndc80 binds Zwint (Lin et al., 2006), which is in turn required for RZZ and consequently Mad1-Mad2 recruitment (Kops et al., 2005; Wang et al., 2004).

Asymmetry in KMN chromosomal abundance is also observed, with CENP-C depletion showing a slight preference for loss of Mis12/KNL-1, while a greater loss of the Ndc80 complex is associated with CENP-T/CENP-W. This pattern of dependency has been described in human cells depleted of CENP-C or CENP-T by siRNA (Gascoigne et al., 2011). Taken together, we observe that subunits within known kinetochore subcomplexes generally behave in a like manner in terms of their dependencies on inner and outer kinetochore components.

Figure 20. Members of the same kinetochore subcomplex show similar dependency patterns. Barplots of mean $\log_2$ H/L ratios from CENP-C, CENP-T, CENP-W and Ndc80 experiments. All proteins listed on the left hand side have previously been identified as kinetochore proteins or proteins closely associated with kinetochore-fibre assembly. Groupings have been made based on the current literature on the formation of defined subcomplexes and are colour coded. Blue and red lines represent a cut-off of 1.5-fold change of decreasing or increasing abundance, respectively. The bars labelled '1' were only identified in one replicate. 'v' labelled entries highlight proteins that have a fold difference of >2.5 MAD between the two replicates. 'NA' values depict missing data. Note that CENP-U in the CENP-C KO cell line is no longer considered an outlier (i.e. not labelled 'v' as in Figure 19A). Entry Q2Z1W2 (CENP-U) only had quantifiable H/L ratios in the CENP-C KO experiments. For consistency, an alternative Uniprot entry (F1NUU9) assigned to CENP-U, that had H/L SILAC values associated with at least one biological replicate across all KO experiments was used instead.

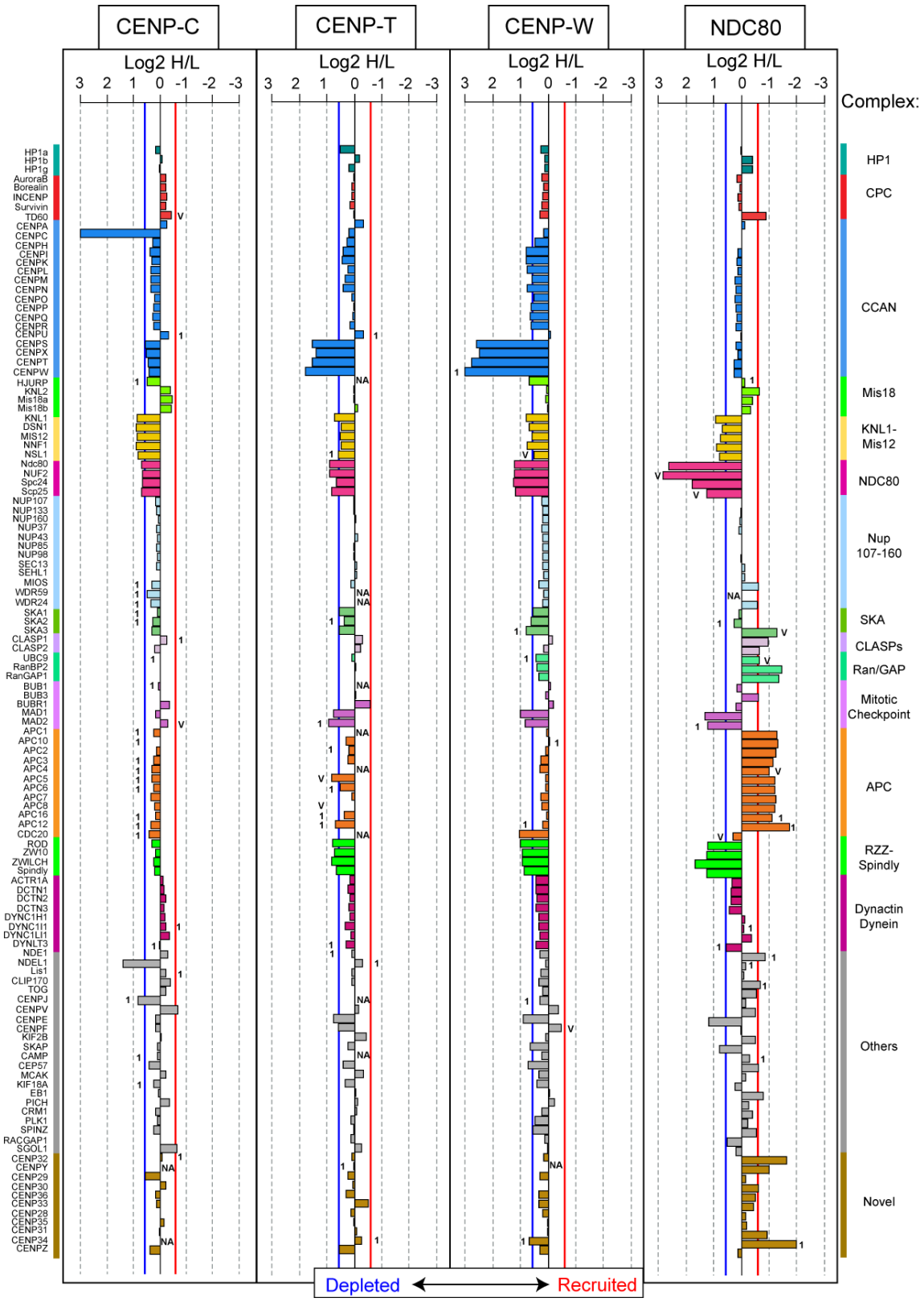
CENP-C
CENP-T
CENP-W
NDC80
Log2 H/L
3 2 1 0 -1 -2 -3
Complex:
HP1a
HP1b
HP1g
AuroraB
Borealin
INCENP
Survivin
TD60
CENPA
CENPC
CENPH
CENPI
CENPK
CENPL
CENPM
CENPN
CENPO
CENPP
CENPQ
CENPR
CENPU
CENPS
CENPX
CENPT
CENPW
HJURP
KNL2
Mis18a
Mis18b
KNL1
DSN1
MIS12
NNF1
NSL1
Ndc80
NUF2
Spc24
Scp25
NUP107
NUP133
NUP160
NUP37
NUP43
NUP85
NUP98
SEC13
SEHL1
MIOS
WDR59
WDR24
SKA1
SKA2
SKA3
CLASP1
CLASP2
UBC9
RanBP2
RanGAP1
BUB1
BUB3
BUBR1
MAD1
MAD2
APC1
APC10
APC2
APC3
APC4
APC5
APC6
APC7
APC8
APC16
APC12
CDC20
ROD
ZW10
ZWILCH
Spindly
ACTR1A
DCTN1
DCTN2
DCTN3
DYNC1H1
DYNC1I1
DYNC1LI1
DYNLT3
NDE1
NDEL1
Lis1
CLIP170
TOG
CENPJ
CENPV
CENPE
CENPF
KIF2B
SKAP
CAMP
CEP57
MCAK
KIF18A
EB1
PICH
CRM1
PLK1
SPINZ
RACGAP1
SGOL1
CENP32
CENPY
CENP29
CENP30
CENP36
CENP33
CENP28
CENP35
CENP31
CENP34
CENPZ
HP1
CPC
CCAN
Mis18
KNL1-
Mis12
NDC80
Nup
107-160
SKA
CLASPs
Ran/GAP
Mitotic
Checkpoint
APC
RZZ-
Spindly
Dynactin
Dynein
Others
Novel
Depleted
Recruited

Strikingly, several known kinetochore subcomplexes are co-ordinately recruited onto chromosomes in the absence of the Ndc80 complex. These include the CLASP1/2, RanBP2/RanGAP1 and APC/C complexes. It is also possible to see dramatic changes in the abundance ratios of a subgroup of 'novel' kinetochore proteins. CENP-Y, CENP-Z and CENP-28 to 36 were identified in a single collaborative study between the Earnshaw and Rapsillber labs (see section 4.1) (Ohta et al., 2010). The localisation of these proteins to centromeric regions was confirmed through GFP-tagged fusion protein expression combined with immunofluorescence. However, additional functional characterisation was only reported for CENP-32. Here, CENP-31, -32, -34 and CENP-Y display the most extreme fold changes and are increased on chromosomes.

As described earlier, the abundance of many proteins on chromosomes is increased in the Ndc80 KO cell line. In Figures 21 A-D $\log_2$ H/L ratios for individual proteins and across replicate experiments are plotted against one another for the KO SILAC data sets, with known kinetochore proteins depicted by red circles. Using a 1.5-fold change cut-off (red lines) 1182 proteins in the Ndc80 KO experiments were classified as abnormally recruited onto chromosomes in both replicates when compared with WT cells (Figure 21D). In contrast, only 25, 62 and 19 proteins were identified with the same criterion in the CENP-C, CENP-T and CENP-W tetracycline-repressive cell lines, respectively (Figure 21A-C).

The pie chart in Figure 21E depicts the breakdown of classifications associated with the 1182 proteins that are recruited onto chromosomes in the absence of Ndc80. A large proportion (33%) is considered 'non-chromosomal' as the proteins have been shown to primarily localise to other sub-cellular compartments (e.g. mitochondria, cell membrane) (Ohta et al., 2010). This could represent cellular stress or a physiological state of Ndc80 KO cells, rather than a direct consequence of Ndc80 complex loss. The recruitment of membrane proteins and components usually associated with interphase nuclei could be explained by the co-purification of apoptotic bodies. Therefore, any protein that appears to be enriched on chromosomes within this data set should be interpreted with caution.

Some known chromosomal proteins (red; 19%) are also enriched on chromosomes in the Ndc80 KO data sets. These include transcription factors, histone modifiers and DNA replication/repair proteins. Centromeric proteins within this region make-up only 2% of the whole protein population. Complexes that have been shown to load in late mitosis/G1 phase of the cell cycle are enriched in Ndc80 KO cells (Figure 21E; barplot). Examples would include origin recognition complex (ORC) and minichromosome maintenance (MCM) components that bind to replication origins and are involved in 'licencing' DNA replication to ensure that DNA is only synthesised once during the cell cycle (Blow and Dutta, 2005). Quantitative live cell imaging of fluorescently tagged MCM components has shown that this complex is loaded onto chromosomes cumulatively throughout G1 and removed by the act of replication in S phase (Kuipers et al., 2011). The cohesin complex is required for sister chromatid tethering and associates with chromosomes in late G1 in S.*cerevisiae* or telophase in vertebrate cells (Rudra and Skibbens, 2013). In addition, regulatory proteins responsible for G1/S progression (CDK6 and CDK2) and the transition through mitosis (CDK1, cyclin-B2 and cyclin-B3) (Malumbres and Barbacid, 2009) are up- and down-regulated, respectively. Other chromosomal complexes, such as condensin I/II and SMC5/6 components are not enriched on Ndc80 KO chromosomes (Figure 21E; barplot). This suggests that Ndc80 chromosomes may have been contaminated with apoptotic bodies originating from cells in the G1 phase of the cell cycle. Another explanation could be that in the absence of a functional SAC (both Mad1 and Mad2 are significantly depleted from chromosomes), APC/C is no longer inhibited, therefore biochemically the cells could be transitioning from a mitotic to a G1 state without segregating their chromosomes.

Figure 21. Prolonged Ndc80 depletion leads to the global recruitment of proteins onto chromosomes. Scatter plots depicting $\log_2$ H/L ratios of biological duplicates (repeat 1: x axis, repeat 2: y axis) for **(A)** CENP-C **(B)** CENP-T **(C)** CENP-W and **(D)** Ndc80 KO SILAC experiments. A minimum of 1 unique peptide (1 ratio H/L count) was used for quantitation. Red circles indicate proteins that have been classified as kinetochore proteins, while grey points represent all other proteins. Red lines define a 1.5-fold change cut-off. Proteins within the lower left hand quadrant are abnormally recruited onto chromosomes in both repeats (n= number of proteins identified within this threshold). **E.** In comparison to the other data sets, Ndc80 KO experiments display a wider spread of data, with many more proteins displaying negative $\log_2$ H/L ratios. Proteins falling beyond the 1.5-fold cut off for increasing levels on chromosomes in this data set are classified into functional groups. Entries were mapped to the IPI data set generated by (Ohta et al., 2010). Any entry that remained unclassified was subjected to BLAST searches to identify the function of the human homolog. Note that one Uniprot identifier turned out to be a second entry for the kinetochore protein RanBP2. This is not represented by a red point on the scatterplot, but is included in the centromere subgroup in the piechart. On the right hand side a barplot showing the mean $\log_2$ H/L ratios of known chromosomal complexes from the Ndc80 SILAC experiments is depicted. Blue and red lines represent a cut-off of 1.5-fold change of decreasing or increasing abundance, respectively. The bars labelled '*' were only identified in one replicate. 'NA' values depict missing data.

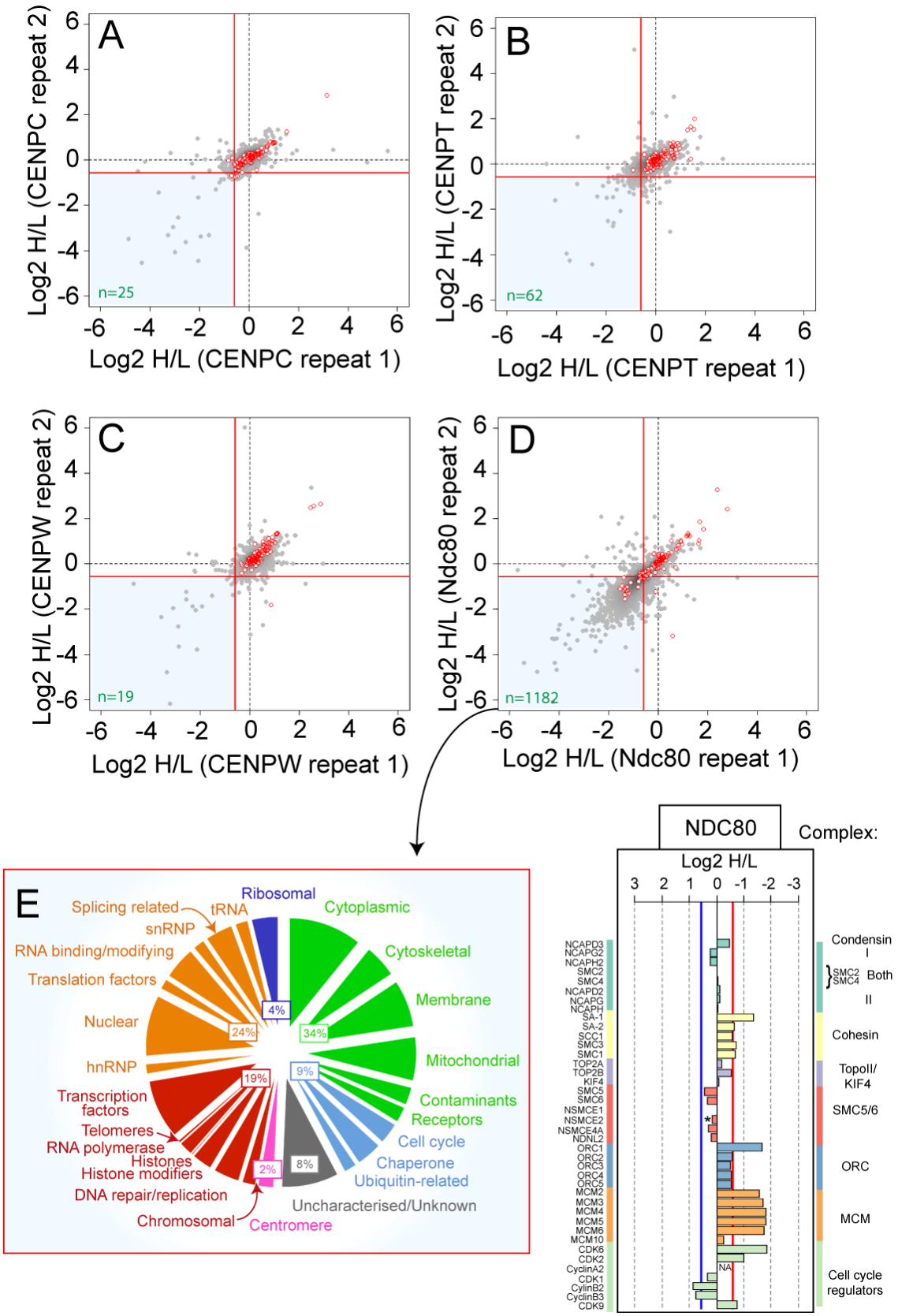
A
Log2 H/L (CENPC repeat 2)
Log2 H/L (CENPC repeat 1)
n=25
B
Log2 H/L (CENPT repeat 2)
Log2 H/L (CENPT repeat 1)
n=62
C
Log2 H/L (CENPW repeat 2)
Log2 H/L (CENPW repeat 1)
n=19
D
Log2 H/L (Ndc80 repeat 2)
Log2 H/L (Ndc80 repeat 1)
n=1182
E
Ribosomal
Cytoplasmic
Cytoskeletal
Membrane
Mitochondrial
Contaminants
Receptors
Cell cycle
Chaperone
Ubiquitin-related
Uncharacterised/Unknown
Centromere
Chromosomal
DNA repair/replication
Histone modifiers
Histones
RNA polymerase
Telomeres
Transcription factors
hnRNP
Nuclear
Translation factors
RNA binding/modifying
snRNP
tRNA
Splicing related
4%
34%
9%
8%
2%
19%
24%
NDC80
Complex:
Log2 H/L
NCAPD3
NCAPG2
NCAPH2
SMC2
SMC4
NCAPD2
NCAPG
NCAPH
SA-1
SA-2
SCC1
SMC3
SMC1
TOP2A
TOP2B
KIF4
SMC5
SMC6
NSMCE1
NSMCE2
NSMCE4A
NDNL2
ORC1
ORC2
ORC3
ORC4
ORC5
MCM2
MCM3
MCM4
MCM5
MCM6
MCM10
CDK6
CDK2
CyclinA2
CDK1
CyclinB2
CyclinB3
CDK9
NA
Condensin I
SMC2
SMC4
Both
II
Cohesin
TopoII/ KIF4
SMC5/6
ORC
MCM
Cell cycle regulators

3.2.4.2 Kinetochore assembly pathways using Significance B scores

Although the fold change cut-off can be used to define differential abundance, it does not take into account the statistical variance in detection (i.e. those proteins that are low in abundance and close to the limits of detection will show more variability in their measurements when compared with highly abundant proteins). As an alternative measure of true differential abundance, Perseus derived Significance B scores can be used to highlight kinetochore proteins that significantly deviate from the main distribution, whilst taking into account intensity-weighted variation (Cox and Mann, 2008).

Scatter plots depicting total intensity versus the $\log_2$ H/L ratios are depicted in Figures 22A-D. Each grey dot represents the mean $\log_{10}$-intensity and mean $\log_2$-H/L ratio values for a single protein identified across the 2 repeats. Red circles depict proteins identified in both biological repeats that are classified within the kinetochore subgroup. Filled red points indicate kinetochore proteins that only have a H/L SILAC value in one experiment. The distribution of all protein ratios demonstrates that the majority of proteins remains unchanged in response to the depletion of core inner kinetochore components CENP-C, CENP-T and CENP-W (Figure 22A-C) and centre at a 1:1 ratio (i.e. 0). The spread of data for Ndc80-depleted chromosomes is slightly larger and, as described previously, shows a skew towards negative data points (accumulation on chromosomes). Kinetochore protein distributions are depicted as a rug plot along the bottom of the graphs. These also show a larger spread of H/L ratios within the Ndc80 silenced background in contrast to the other conditional KO datasets.

Figure 22. Kinetochore dependencies using Significance B scores. Scatterplots show **A.** CENP-C, **B.** CENP-T, **C.** CENP-W and **D.** Ndc80 KO experiments. For each plot the mean $\log_2$ H/L ratios of all chromosomal proteins and their mean $\log_{10}$ summed peak intensities are shown. Red circles represent known kinetochore proteins identified in both replicate experiments. Red points are known kinetochore proteins that were only quantified in one out of the two replicates. Labelled kinetochore proteins are coloured according to Significance B scores (orange<0.01, 0.01>blue<0.05). Some of the non-kinetochore proteins that are significantly depleted or increased on chromosomes in the tet-repressive kinetochore KO cell lines are also labelled. **E.** Venn diagram showing the overlap between kinetochore proteins classified as significant across all KO conditions. Labelled kinetochore proteins are colour coded as described above.

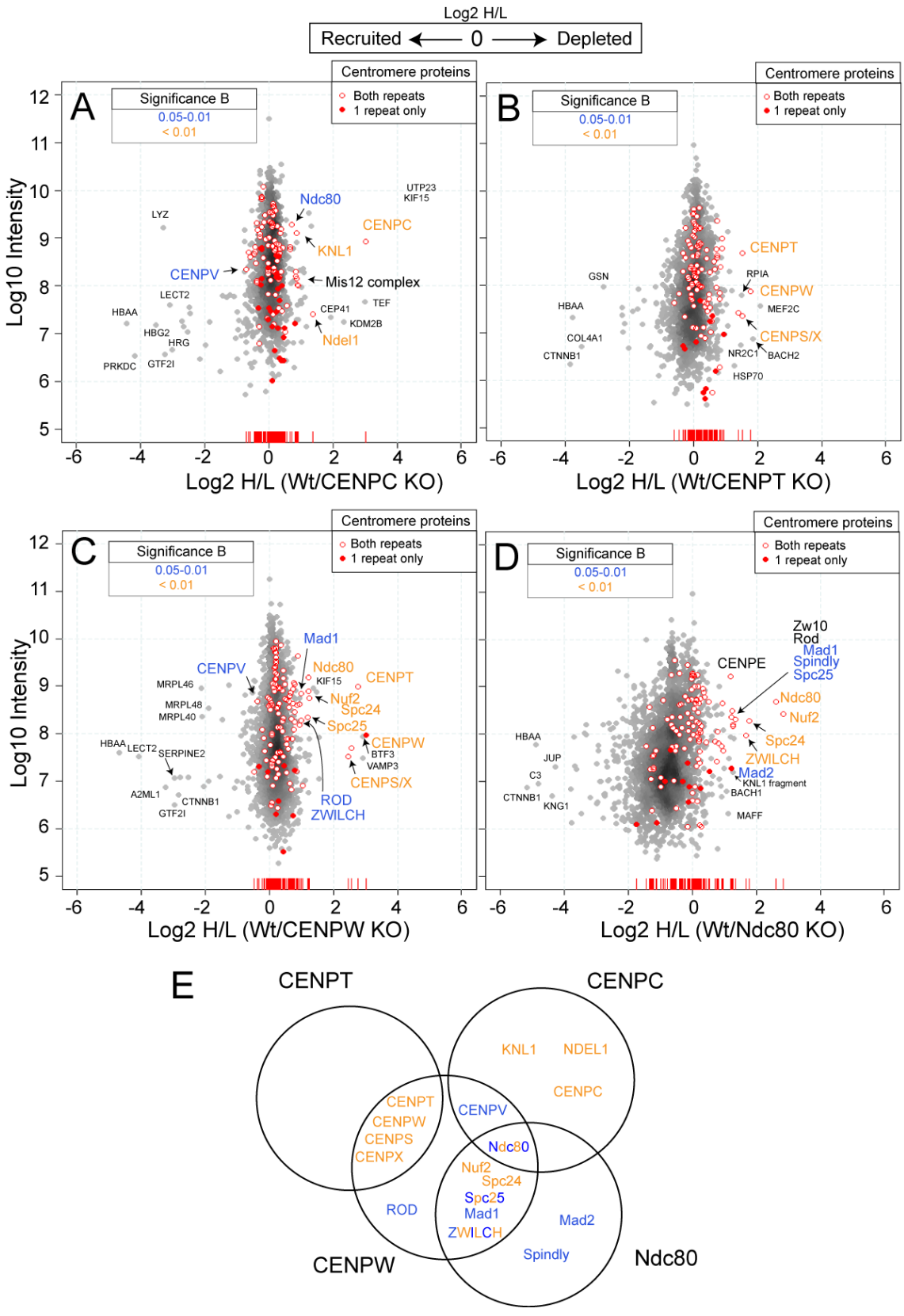
Log2 H/L
Recruited
0
Depleted
A
Centromere proteins
Both repeats
1 repeat only
Significance B
0.05-0.01
< 0.01
Log10 Intensity
Log2 H/L (Wt/CENPC KO)
Ndc80
CENPC
KNL1
CENPV
Mis12 complex
Ndel1
B
Log2 H/L (Wt/CENPT KO)
CENPT
CENPW
CENPS/X
C
Log2 H/L (Wt/CENPW KO)
Mad1
CENPV
Ndc80
CENPT
Nuf2
Spc24
Spc25
CENPW
CENPS/X
ROD
ZWILCH
D
Log2 H/L (Wt/Ndc80 KO)
Zw10
Rod
Mad1
Spindly
Spc25
CENPE
Ndc80
Nuf2
Spc24
ZWILCH
Mad2
E
CENPT
CENPC
CENPW
KNL1
NDEL1
CENPV
Ndc80
Nuf2
Spc24
Spc25
Mad1
ZWILCH
ROD
Mad2
Spindly

The intensity-weighted significance B statistic was used at *p* value thresholds of 0.01-0.05 or <0.01, with kinetochore proteins found within these constraints labelled blue or orange, respectively. In addition, some of the non-kinetochore proteins that are significantly depleted or increased on chromosomes in the tet-repressive kinetochore KO cell lines are also labelled (This will be discussed further in results chapter 2). In Figure 22A, CENP-C gene suppression leads to a significant increase in H/L SILAC ratios for outer kinetochore components KNL-1, Ndc80 and Nde1. This suggests that the levels of these proteins are significantly decreased on chromosomes. Mis12 complex components are also detected, but do not show significant deviations in their protein abundance. CENP-V is the only centromeric protein that is significantly recruited onto chromosomes upon CENP-C loss, with a calculated *p* value cut-off between 0.05 and 0.01.

As expected, the CENP-T/W/S/X complex is significantly reduced in the CENP-T or CENP-W-depleted chromosomes in comparison to WT DT40 chromosomes (Figures 22B and C). A more complete loss of this subcomplex results in significant differences in protein abundance ratios of additional centromeric factors. Dependency on the Ndc80 complex is seen for outer kinetochore components including Mad1 and RZZ complex components: Rod and ZWILCH. Similarly to CENP-C KO conditions, a significant increase in CENP-V protein abundance was observed.

When comparing doxycycline treated NDC80 conditional knockouts with WT cells the Ndc80 complex, Mad1, Mad2, Spindly and Rod are significantly depleted from chromosomes, having *p* values <0.05 (Figure 22D). Therefore, the localisation of these components onto chromosomes is dependent on Ndc80. No centromeric proteins were found to significantly increase on chromosomes. The significance B score takes into account the distribution of the whole protein population. A skew towards negative H/L SILAC data points in the Ndc80 KO experiments could mask kinetochore subgroup members (with negative H/L values; increase on chromosomes) that would have been deemed significant if the whole population had been centred around 0.

The Venn diagram in Figure 22E depicts the overlapping dependencies of proteins that have been categorised as possessing significantly differing abundance ratios amongst the various conditions. It is clear that only a relatively small number of kinetochore proteins are significantly affected by depletion of core kinetochore components using the rigorous Significance B calculations. CENP-T/W/S/X subcomplex abundance on chromosomes is not influenced by CENP-C or Ndc80 loss. Similarly, CENP-C, KNL-1 and NDEL1 are only significantly lost from chromosomes upon suppression of CENP-C gene expression. Other groups, such as the Ndc80 complex, are significantly depleted from chromosomes in multiple kinetochore KO conditions.

3.2.4.3 Hierarchical cluster analysis of known kinetochore proteins

It is clear from the fold-change threshold and Significance B scores described above that only a small number of kinetochore proteins are significantly different in chromosomes isolated from each KO. However, many more proteins display smaller changes in their SILAC ratios. Despite being small, these differences in SILAC ratios often co-vary within known kinetochore subcomplexes. For this reason, co-varying patterns of enrichment and depletion over multiple experiments may suggest a functional link. Hierarchical clustering acts as an unbiased method to do this and is visualised as a heatmap (Figure 23). For this analysis, I have chosen to exclude those kinetochore proteins that have missing values in >50% of the data sets (must see SILAC ratios in at least 4 out of the 8 individual experiments); grey regions within the heatmap depict missing data values.

This analysis reveals that many closely associated subcomplexes are hierarchically clustered using this analysis; this is exemplified by the Mis18 complex, core CPC subunits and KNL-1-Mis12. Although not found directly adjacent to each other, Spc24/25 and Nuf2/Ndc80 heterodimers are confined within a region of the heatmap that shows dependency for all KO cell lines (Blue region; bottom). RZZ components, CENP-E and Mad1 are also located within this region.

Most CCAN subunits cluster together, however, CENP-H and CENP-U remain independent from their respective known subcomplexes (CENP-H and CENP-O complex; please refer to the introduction). This could implicate these proteins, or a sub population thereof, in alternative roles at kinetochores. CENP-T/W/S/X and CENP-C are also grouped away from the rest of the inner kinetochore proteins, but this may be a consequence of scaling issues (i.e. proteins directly targeted in the tetracycline-conditional KO system will show extreme SILAC ratios in comparison to the rest of the population).

Other core complexes also show variations in their inter-dependencies. The Nup107-160 complex is another example. Negligible changes in abundance across conditions are observed for most nucleoporins. WDR24 and Mio, which are not members of the complex but interact with Seh1, pair together yet are distinct from the rest of the complex. This suggests that they might have an independent role on chromosomes. A similar scatter of functional components is also seen with mitotic checkpoint proteins. We find that Mad1 displays the greatest dependency for its localisation onto chromosomes and is found adjacent to CENP-E and RZZ components. All members of the APC/C group together on the heatmap, apart from Cdc20; a coactivator of the APC/C, which is found adjacent to Mad2. BubR1 is located next to Bub1, but Bub3 does not behave the same as any of these components. It has been proposed that these proteins form a complex on unattached kinetochores and help to maintain the “anaphase wait” signal (Foley and Kapoor, 2013). My data suggests that they may colocalise with one another, but are unlikely to form a physical complex on the chromosome.

Figure 23. Members of the same kinetochore subcomplex cluster together in heatmap analysis. The $\log_2$ H/L SILAC ratios from CENP-C, CENP-T, CENP-W and Ndc80 experiments were used for cluster analysis. The repeats for each condition were considered separately and labelled 1 or 2. Values not determined in a given experiment are shown in grey and were not used to create the row or column dendrograms. Proteins that did not display a SILAC ratio for at least half of the experiments (4 out of 8; any combination) were not considered. The merging of clusters into larger clusters (agglomeration) was performed using the Ward method (Key, 2012). The colour key is shown on the right with a density plot of all H/L values. Those proteins with a high SILAC ratio are depleted from chromosomes and depicted in blue. Alternatively, the colour red indicates a negative $\log_2$ H/L ratio, signifying an increase in recruitment. A value of 0, as shown in white, signifies no change in abundance. Row groupings based on the localisation to sub-compartments of the kinetochore are found on the left of the heatmap: inner centromere, inner plate, outer plate and novel kinetochore. The novel kinetochore group is formed from those proteins identified in (Ohta et al., 2010). Known complexes are colour coded as in Figure 20 and tend to cluster together.

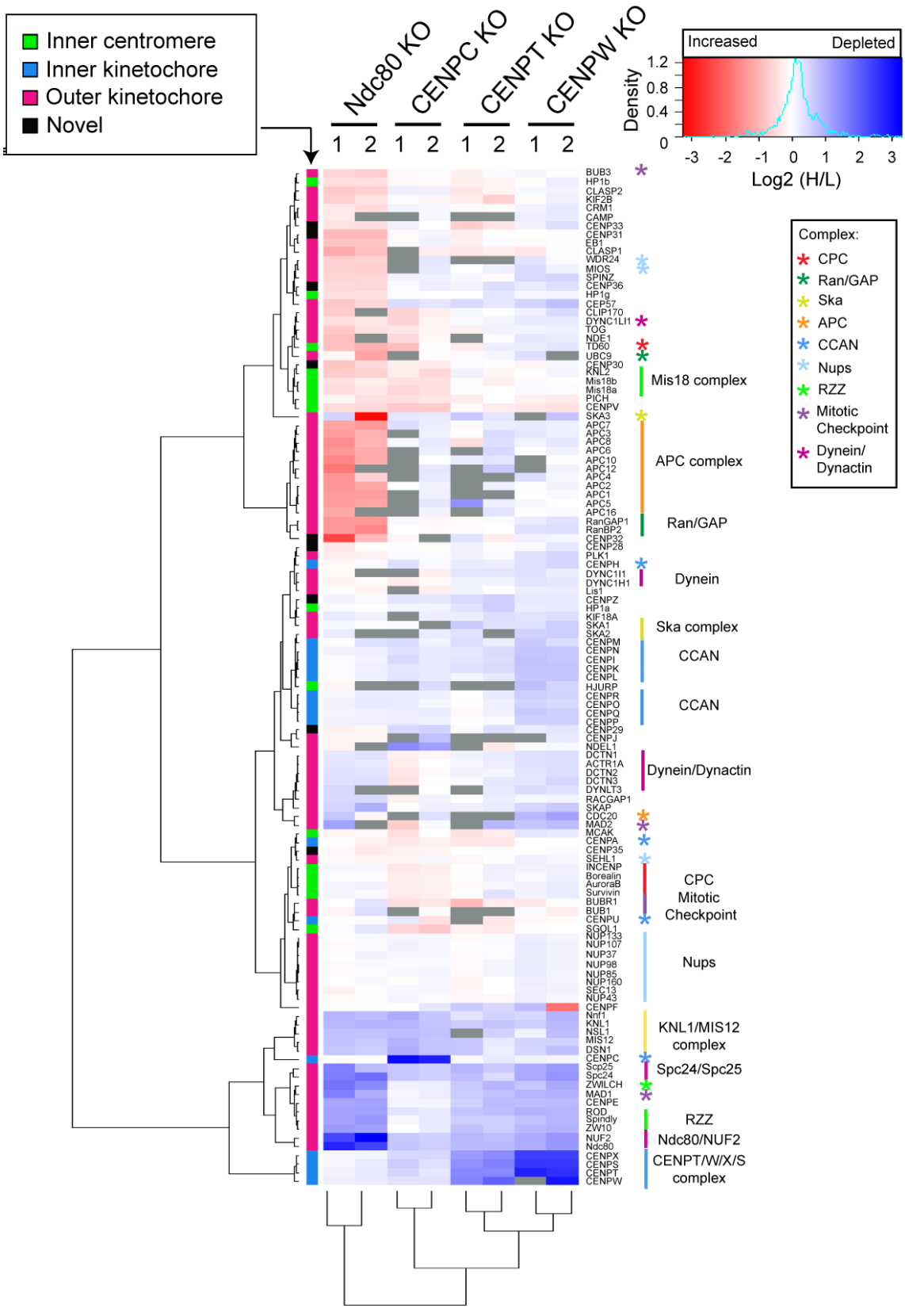
Inner centromere
Inner kinetochore
Outer kinetochore
Novel
Ndc80 KO
CENPC KO
CENPT KO
CENPW KO
1 2 1 2 1 2 1 2
Increased
Depleted
Density
1.2
0.8
0.4
0
-3 -2 -1 0 1 2 3
Log2 (H/L)
Complex:
CPC
Ran/GAP
Ska
APC
CCAN
Nups
RZZ
Mitotic Checkpoint
Dynein/ Dynactin
BUB3
HP1b
CLASP2
KIF2B
CRM1
CAMP
CENP33
CENP31
EB1
CLASP1
WDR24
MIOS
SPINZ
CENP36
HP1g
CEP57
CLIP170
DYNC1LI1
TOG
NDE1
TD60
UBC9
CENP30
KNL2
Mis18b
Mis18a
PICH
CENPV
Mis18 complex
SKA3
APC7
APC3
APC8
APC6
APC10
APC12
APC4
APC2
APC1
APC5
APC16
APC complex
RanGAP1
RanBP2
CENP32
CENP28
Ran/GAP
PLK1
CENPH
DYNC1I1
DYNC1H1
Lis1
Dynein
CENPZ
HP1a
KIF18A
SKA1
SKA2
Ska complex
CENPM
CENPN
CENPI
CENPK
CENPL
CCAN
HJURP
CENPR
CENPO
CENPQ
CENPP
CENP29
CENPJ
CCAN
NDEL1
DCTN1
ACTR1A
DCTN2
DCTN3
DYNLT3
Dynein/Dynactin
RACGAP1
SKAP
CDC20
MAD2
MCAK
CENPA
CENP35
SEHL1
INCENP
Borealin
AuroraB
Survivin
BUBR1
BUB1
CENPU
CPC
Mitotic Checkpoint
SGOL1
NUP133
NUP107
NUP37
NUP98
NUP85
NUP160
SEC13
NUP43
Nups
CENPF
Nnf1
KNL1
NSL1
MIS12
DSN1
KNL1/MIS12 complex
CENPC
Scp25
Spc24
Spc24/Spc25
ZWILCH
MAD1
CENPE
ROD
Spindly
ZW10
RZZ
NUF2
Ndc80
Ndc80/NUF2
CENPX
CENPS
CENPT
CENPW
CENPT/W/X/S complex

This type of analysis can also be used to predict the functions of novel proteins that have been shown to localise to kinetochores. For example, Ohta et al (2010) implicated CENP-27, one of several novel kinetochore proteins identified in that study, as a functional component of the APC/C by hierarchical clustering (Ohta et al., 2010). This finding was confirmed by other groups and CENP-27 is now termed APC16 (Hutchins et al., 2010). In our results, we too find that APC16 does indeed cluster with the other subunits of the complex.

The other novel CENPs from the previous study were included in the heatmap analysis (indicated by black row groups along the left hand side of the heatmap). To describe a few, I found that CENP-33 and CENP-31 lie close to proteins implicated in K-fibre maintenance or attachment such as CLASP1/2, KIF2B, CRM1, CAMP and EB1, suggesting that they might also localise to the outer kinetochore. Although CENP-32 was expected to cluster within this region based on previous observations (Ohta et al., 2010), in this analysis it shares abundance ratios characteristic of RanBP2/RanGAP1 or APC/C complexes. CENP-30 displays behaviour similar to inner centromere proteins (green row groupings): Mis18 complex, PICH and CENP-V. CENP-35 H/L SILAC ratios, on the other hand, do not dramatically deviate from the 1:1 ratio and clusters close to CENP-A and CPC components.

Hierarchical clustering allows an unbiased interpretation of proteins that might be behaving similarly in terms of their kinetochore dependencies and we find that many known complexes do group together on the heatmap. It is also possible to identify proteins that have been shown to form functional constituents of core subcomplexes, but display distinct patterns of behaviour. This suggests that these might have additional independent functions on chromosomes.

3.3 Discussion

The approach described here utilises chromosome isolation techniques and mass spectrometry to compare the abundance of proteins on chromosomes isolated from several different cell populations: WT cells and a range of kinetochore KO backgrounds. Analysis of the data reveals that members of known kinetochore subcomplexes do in general behave in a similar manner in terms of their dependencies. Second, by depleting proteins from both inner and outer compartments, structural hierarchies within the kinetochore can be established. Third, this analysis reveals proteins that have been previously associated with core complexes, but may have alternative roles on chromosomes based on their differing patterns of assembly/inter-dependencies.

3.3.1 Experimental design

Here, I use DT40 conditional KO cell lines, in which the expression of a target kinetochore protein can be turned off within minutes of doxycycline treatment. I was unable to directly compare 'ON' with 'OFF' conditions, as many of these cell lines displayed reduced rates of proliferation when grown in dialyzed serum and were therefore not amenable to metabolic labelling with heavy amino acids. Instead WT DT40 cells (Cl18), which are not sensitive to SILAC growth conditions, were directly compared with doxycycline treated tetracycline-repressive cells ('OFF') cultured in normal medium. It is likely that the tetracycline-repressable KO cell lines require low molecular mass growth factors, which are excluded from dialysed serum. This may well be due to transcriptional changes induced by expression of the tetracycline trans-activator (tTA). We assume this difference in signalling sensitivity is not reflected by cell-type specific changes in the chromosomal proteome. As an alternative, dialysed serum with a low molecular-mass cut-off, or small amounts of undialysed serum, could be used to promote growth in KO cell lines (Mann, 2006). This would allow for a quantitative comparison of chromosome-bound proteins in the presence or absence of a specific kinetochore component within the same clone.

Another important caveat to keep in mind is that in the tetracycline-conditional KO systems we are not measuring the immediate effects of depletion. This is particularly true for members of the inner kinetochore. Mitotic chromosomes from CENP-C, CENP-T and CENP-W cell lines were collected between 2 and 3 days after doxycycline addition, as only then had significant levels of the polypeptide fallen sufficiently. During this time, cells can pass through multiple cell cycles. Thus, SILAC quantitation could reflect various secondary effects associated with extended periods of partial loss. To overcome this drawback, systems that deplete polypeptides within minutes by targeting at the protein level have recently been employed to study kinetochore function (Holland et al., 2012; Nishimura et al., 2009). I will directly address this problem in Results Chapter 3.

In Ndc80 conditional KO cells, the protein is depleted within a very short time frame and cells stop proliferating between 6-12 hours after doxycycline addition. The general spread of data behaves differently from all other KO cell lines tested and is characterised by a large number of proteins recruited onto chromosomes (displaying negative SILAC ratios). This trend is reproducible; however, it is unclear whether this is a secondary effect associated with a physiological state of the cell, or a direct result of removing Ndc80 containing complexes from kinetochores. The recruitment of non-histone proteins: membrane receptors, histone modifiers, cytoplasmic proteins, chromosomal proteins and transcription factors, could reflect an increase in chromosome surface area during the hypotonic treatment and lysis of cells during the isolation procedure. A similar result has been seen with increased levels of chromosomal periphery proteins upon depletion of the chromokinesin, KIF4 (Samejima et al., 2012). KIF4 functions with condensin to laterally compact chromosome arms during mitosis (Samejima et al., 2012). In contrast, the Ndc80 complex localises to centromeric regions and centrosomes in DT40 cells and is therefore unlikely to directly impact on chromosome morphology (Hori et al., 2003).

A more likely explanation is that this could reflect cells that are unhealthy/closer to cell death. For example, chromosome isolates could be contaminated with apoptotic bodies. It became evident that chromosomal proteins specifically associated with the G1 phase of the cell cycle were enriched on chromosomes from Ndc80 KO cell lines (For example, MCM complex, ORC complex and cohesin). This could suggest that contaminating proteins reflect the cell cycle phase from which apoptosis was initiated. Although live cell imaging showed that most Ndc80 KO cells block in prometaphase and then progress into apoptosis, the Fukagawa lab also observed an increase in cells displaying aneuploidy (Hori et al., 2003). This indicates that some cells can escape the mitotic arrest- it is suggested that this population of cells has a small amount of Ndc80 remaining and this allows it to release from the mitotic block. An accumulation in G1 phase was not observed by measuring DNA content via FACs analysis (Hori et al., 2003), so it is unclear whether these cells subsequently block in G1 and then die. To confirm this a TUNEL assay could be used to assess the cell cycle stage in which cell death occurred. Labelled nucleotides (e.g. Br-dUTP) are added to the 5' ends of DNA fragments and fluorescent antibodies combined with FACs analysis can be used to assess the DNA content of apoptotic populations (Darzynkiewicz et al., 2008).

An alternative explanation could also be that in the absence of a functional SAC, APC/C activity is no longer perturbed and a population of cells may have had time to transition from mitotis into a G1 biochemical state without chromosome segregation events taking place. Certainly, Cyclin-B and CDK1 are reduced on Ndc80 chromosomes suggesting that this might be the case. A shorter doxycycline treatment (< 12 hours) may be required in future experiments. Alternatively dual treatment with an apoptotic inhibitor, such as ZVAD-FMK, could prevent apoptotic entry and at the same time allow for maximum depletion of Ndc80 containing complexes.

3.3.2 Kinetochore dependencies

My results agree with recent publications that the CENP-T/W/S/X complex forms a highly inter-dependent protein assembly (Hori et al., 2008a; Nishino et al., 2012). Inadvertently the CENP-T KO cell line represents a partial depletion of the complex (~2-3 fold reduction). In contrast, the CENP-W conditional KO system shows a more complete loss (~4-6 fold-change). This difference is reflected in the levels of other CCAN components at kinetochores. A more complete loss of CENP-T/W/S/X results in a ~1.5 fold-change reduction in the levels of most CCAN components, apart from CENP-A, CENP-C and CENP-U. CENP-A levels are unaffected across all KO conditions, supporting its role as the most upstream marker in kinetochore assembly (Cheeseman and Desai, 2008). Our data is also in accordance with immunofluorescence experiments showing that the localisation of CENP-C to centromeres in both DT40 chicken and human cells is independent of CENP-T/W and vice versa (Gascoigne et al., 2011; Hori et al., 2008a).

CENP-U is thought to form an integral component of the CENP-O complex (Eskat et al., 2012; Hori et al., 2008b). As with the CENP-W KO cell line, the CENP-T partial KO shows that the levels of CENP-O complex components, apart from CENP-U, behave in a similar manner in terms of their dependencies. This deviation in inter-dependencies suggests that CENP-U could function outside of the CENP-O complex. CENP-U certainly has some interesting properties, such as its ability to dimerise at ectopic chromatin sites (Eskat et al., 2012), form a ternary complex with CENP-Q/PLK1 (Kang et al., 2011) and interact with Ndc80 and microtubules (Hua et al., 2011), but whether these represent populations that are functionally separate from the whole CENP-O complex is still unclear. Our data would argue that CENP-U localisation at kinetochores is partially independent of CENP-Q or Ndc80, as these components are both reduced in the CENP-W KO cell line while CENP-U levels remain unchanged.

Kinetochores lacking CENP-C and CENP-T/W show reduced levels of KMN recruitment, but Ndc80 loss has no reciprocal effect on the levels of CCAN components. The KMN is therefore downstream of constituents of the inner kinetochore. Interestingly, single depletions of CENP-C or CENP-T/W lead to a partial, rather than complete, loss of KMN components (1.5-2 fold change), indicative of multiple branch points for recruitment. Recent findings have focused on the direct interactions linking CENP-C and CENP-T with Mis12 and Ndc80 complexes, respectively (Bock et al., 2012; Gascoigne et al., 2011; Hori et al., 2008a; Malvezzi et al., 2013; Nishino et al., 2013; Przewloka et al., 2011; Schleiffer et al., 2012; Screpanti et al., 2011). Tethering of both of these inner kinetochore proteins to LacO arrays is required for stoichiometric recruitment of core KMN components. When tethered individually, the Ndc80 sub-unit is detected at higher levels on ectopic kinetochores nucleated via CENP-T, while Dsn1 recruitment (Mis12 complex) is increased when analysing CENP-C-LacI tethering alone (Gascoigne et al., 2011). My data are consistent with this, as in the CENP-C KO Mis12 complex levels are affected more than Ndc80 complex levels. Just the reverse is true in the CENP-T and CENP-W conditional knockouts.

If CENP-C and the CENP-T/W/S/X complex are the two main platforms linking the inner and outer kinetochore, depletion of both of these proteins should produce a severe kinetochore null phenotype. In human cells, double depletion of CENP-C and CENP-T by siRNA leads to a complete loss of Ndc80, Dsn1 (Mis12 complex), and KNL-1 from kinetochores by immunofluorescence (Gascoigne et al., 2011). Double-conditional DT40 KO cells of CENP-C and CENP-W have been generated by the Fukagawa lab (Hori et al., 2008a) and are available to use for SILAC proteomics experiments. Isolating chromosomes from this cell line would reveal whether CENP-C and CENP-T/W/S/X are the sole contributors to outer kinetochore assembly. We would hypothesise that an additive effect associated with KMN recruitment would be seen with this cell line when compared with the CENP-W and CENP-C single knockouts.

Even though Mis12 is thought to act as a 'hub' within the KMN (Petrovic et al., 2010), Ndc80 depletion can reduce the levels of Mis12 and KNL-1 at kinetochores, indicating that there is a feedback mechanism in KMN assembly. The levels of CENP-E, Mad1-Mad2, Spindly and the RZZ complex are all reduced on chromosomes lacking CENP-T/W and Ndc80. Interestingly, the extent of loss of these proteins correlates with the amount of Ndc80 complex remaining on chromosomes (i.e. greater reduction in Ndc80 complex components leads to a more pronounced loss). This is supported by yeast-two hybrid experiments that show an interaction between Ndc80 and Zwint1, which is in turn required for RZZ recruitment (Lin et al., 2006). In other studies, Mad1 and Mad2 have also been placed downstream of RZZ complex components (Buffin et al., 2005; Kops et al., 2005; Varma et al., 2013). CENP-C KO cells do not display the same dependency relationships, indicating that in those chromosomes Ndc80 levels may not have reached a critical threshold for disassembly of this pathway. However, a recent study has shown that Ndc80 is not required to recruit the RZZ complex to kinetochores in human cells treated with nocodazole, but instead KNL-1 plays a more dominant role (Varma et al., 2013). KNL1 is also the proposed key scaffolding protein for RZZ in C. *elegans* (Gassmann et al., 2008; Varma et al., 2013). Our SILAC experiments argue against this as KNL1 is depleted to similar levels across CENP-C, CENP-T, CENP-W and Ndc80 experiments, but RZZ levels remain unaffected in the CENP-C conditional KO cell line. Therefore, KNL-1 cannot be the sole contributor to RZZ recruitment in DT40 cells.

It is possible that a reduction in the levels of CENP-E, Mad1-Mad2, Spindly and the RZZ complex could represent secondary effects associated with partial loss of the CENP-T/W -Ndc80 pathway over multiple cell cycles. In future experiments I would use the AID system to test this hypothesis (Nishimura et al., 2009). The AID system can be used to deplete proteins at the protein level within a very short time period (within 1-2 hours)(Holland et al., 2012; Nishimura et al., 2009). As described in results chapter 3, an AID-CENP-T cell line has been generated and I would use this system, along with the established SILAC proteomics of isolated chromosomes, to test RZZ, Mad1/2 and

CENP-E dependencies within the context of a single mitosis. With this data set, I would be able to assess the immediate consequences of CENP-T depletion on the composition of the kinetochore.

Loss of the RZZ complex and Spindly does not appear to have a dramatic effect on Dynein-Dynactin levels on isolated chromosomes, even though this connection at kinetochores has been shown in both *C. elegans* and human cells (Chan et al., 2009; Gassmann et al., 2008; Gassmann et al., 2010). The localisation of dynein at kinetochores is required for the formation of lateral microtubule attachments, which in turn increases the probability of forming end-on attachments (Stukenberg and Foltz, 2010). This relationship may be masked by a second population of Dynein-Dynactin as other factors including Lis1, NDE1 and NDEL1 have been implicated in the kinetochore targeting of this complex (Bader and Vaughan, 2010).

APC/C core components are dramatically increased on chromosomes isolated from Ndc80 KO cell lines. This was not seen in conditional knockouts of inner kinetochore components and may reflect a secondary effect associated with changes in cell physiology. If this is a specific downstream effect of removing the Ndc80 complex, it is unclear how loss of outer kinetochore proteins would facilitate additional docking sites for APC/C. Interestingly, Cdc20 does not behave co-ordinately with the other sub-units. Instead, cluster analysis reveals that Cdc20 behaves in a similar manner to Mad2. In support of this link a recent study has shown that Mad2 and the APC/C compete for the same binding site on Cdc20 (Izawa and Pines, 2012).

Although KNL-1 has been shown to act as a scaffold for the recruitment of Bub1-Bub3 and possibly BubR1 to kinetochores (London et al., 2012; Rischitor et al., 2007; Shepperd et al., 2012; Yamagishi et al., 2012), those proteins are not significantly depleted from chromosomes lacking KMN components. This suggests a KNL-1 independent route for their recruitment. This sub-group also separates using cluster analysis, with only BubR1 and Bub1 showing similar dependencies. This could reflect a

further functional diversification within the complex. Importantly, when Mad1 and Mad2 are removed from kinetochores (CENP-T/W and Ndc80 KO cells) BubR1 and Bub1 abundance levels remain relatively unchanged.

A dependency map based on the findings described in this chapter are summarised in Figure 24. To confirm these pathways of assembly, quantitative western blot analysis (Licor) on isolated chicken chromosomes could be performed to verify dramatic increases or decreases in protein levels. As a follow up experiment I would also want to verify these findings by quantitating kinetochore signals of different proteins by immunofluorescence in the conditional knockout DT40 cell lines.

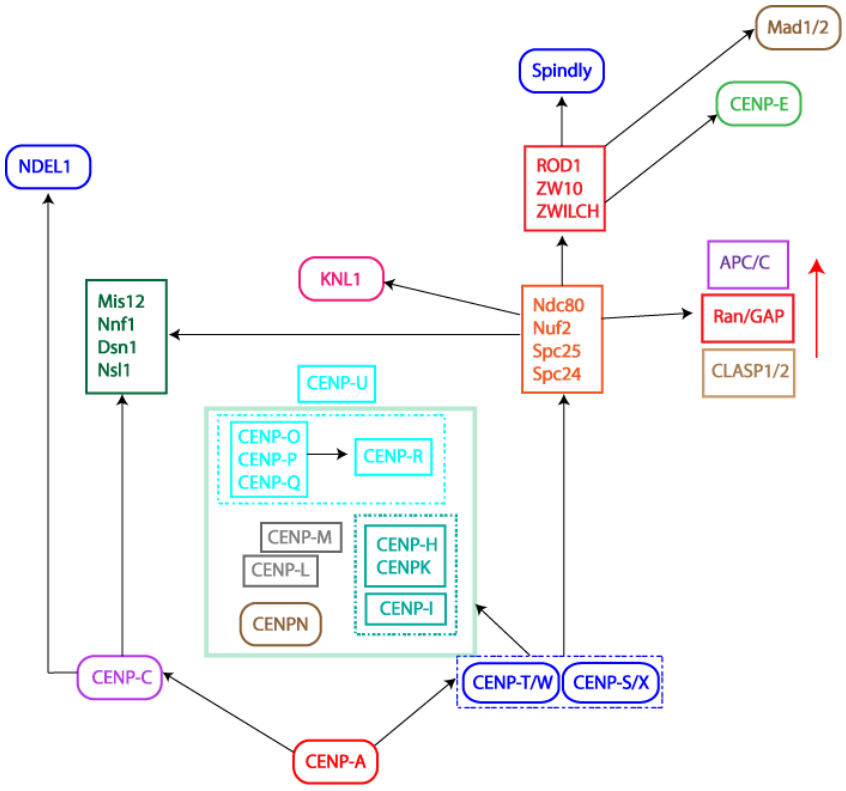

Figure 24. A summary of kinetochore dependency networks identified in this study. The assembly network of key inner and outer kinetochore components. Arrows indicate assembly pathways within the sub-structure of the kinetochore. Arrows may represent partial or complete dependency. The APC/C, RanBP2/RanGAP1 and CLASP1/2 are protein complexes that are recruited onto chromosomes in the absence of Ndc80.

3.3.3 Concluding remarks

Removal of any of the single kinetochore proteins tested did not completely abolish assembly of the kinetochore. Instead chromosomes from each KO cell line exhibit reproducible changes (usually depletion) of a characteristic set of kinetochore protein complexes. I believe these changes reflect interconnectivity between different assembly pathways. This would argue against a linear map of assembly for any given kinetochore protein. In summary, this type of analysis allows us to integrate data sets and draw conclusions on the dependency networks defining the kinetochore as an organic unit, rather than examining relationships for each part in isolation. The data presented here will be particularly important in aiding the interpretation of intricate molecular mechanisms underlying a functionally impaired kinetochore.

4 Results Chapter 2: Identifying novel kinetochore components

4.1 Introduction

Based on the extensive number of established kinetochore proteins (>100) described in the literature, it would be reasonable to assume that our understanding of the full composition of this macromolecular complex is reaching close to completion. Certainly, researchers within the field have resorted to a diverse range of biological systems, technical procedures and computational analysis in an attempt to single out additional factors that might otherwise have been missed using classical affinity-purification based techniques (Akiyoshi et al., 2009; Gassmann et al., 2005; Kittler et al., 2007; Ohta et al., 2010).

The development of innovative isolation methods has significantly aided expansion of the list of kinetochore proteins. For example, proteomic analysis of the chromosomal scaffold; an insoluble protein network that remains after histones and DNA have been removed from isolated chromosomes using high salt buffers, identified CENP-V (Gassmann et al., 2005). This protein was later shown to be important for defining the boundaries of pericentromeric regions and for the recruitment of the CPC, an important regulator of chromosome dynamics (Tadeu et al., 2008). Bod1, which has also recently been shown to function within kinetochores, was originally co-fractionated with >250 polypeptides that bind mitotic chromosomes assembled *in vitro* using *Xenopus* egg extracts (Porter et al., 2007). Finally, isolation of yeast minichromosomes harbouring the LacO array as a means for purification combined with quantitative SILAC based comparisons, has revealed Fin1 to be a novel PP1 recruiter at centromeres (Akiyoshi et al., 2009).

High-throughput data generation, large-scale analysis and combinatorial comparisons of distinct data sets has proven invaluable in the identification of novel mitotic regulators, including a subset of new kinetochore proteins. In human cell lines, RNAi-mediated depletion followed by automated phenotypic profiling has been used to cluster genes that display similar defects (Kittler et al., 2007; Neumann et al., 2010). In one study, Laser scanning flow cytometry was used to efficiently establish parameters based on the DNA content of individual cells (Kittler et al., 2007). In that stand-alone study many potential mitosis and cytokinesis genes were identified. When clustered with cell viability and localization results, however, the kinetochore localized Ska complex was predicted and verified to contain a third member, Ska3 (Theis et al., 2009). Similar predictive powers successfully singled out APC16, a novel subunit that binds in close proximity to the arc region within the APC complex (Hutchins et al., 2010). Information from RNAi phenotypic screens was used to narrow the list of candidate proteins. When combined with large-scale localization and protein interaction results this enabled construction of relationship networks with strong functional insights. APC16 was also predicted to be a functional component of the APC/C complex based on cluster analysis with known kinetochore proteins. This was performed with SILAC data sets focused on defining the chromosomal proteome in chicken DT40 cells (Ohta et al., 2010).

It is important to note that published data sets have the potential for further bioinformatics analysis by other groups. A recent example saw publicly available co-expression or interaction network data (PPI; protein-protein interactions) compared against a pre-defined set of ‘core’ kinetochore candidates, with the rationale being that functional complexes are likely to share the same expression profile. This resulted in the discovery of novel kinetochore protein TRIP13 through its high-ranking classification in co-expression data analysis (Tipton et al., 2012).

A more recent report suggests that the kinetochore is much more complex than previously anticipated, with as many as 97 additional components yet to be discovered (Ohta et al., 2010). As well as optimising conditions for the isolation of whole mitotic

chromosomes, (Ohta et al., 2010) also placed a particular emphasis on integrative analysis, this time tailored towards defining all chromosomal associated proteins. Isolated chicken mitotic chromosomes contain >4000 polypeptides, many of which were proposed to act as 'hitchhikers'; proteins that bind to negatively charged chromosomes following nuclear envelope breakdown (NEB), but do not play a functional role during mitosis. To uncover 'true' chromosomal proteins SILAC was first employed to quantitatively compare the amounts of individual proteins in mitotic chromosomes within the context of several different classifiers. Details of all classifiers can be found in Figure 25A; however, Classifier V is of particular relevance as my studies are based on the experimental setup used for that experiment. This classifier compares the proteome of mitotic chromosomes isolated from WT and Ska3 KO cell lines. Ska3 is an important protein for K-MT attachments (Lan and Cleveland, 2010; Ohta et al., 2010).

Classifiers, when considered individually, cannot be used to define a clear boundary between chromosomal and cytoplasmic contaminants (i.e hitchhikers) (Ohta et al., 2010). However, a machine-learning approach called random forest analysis was able to integrate all these data sets and detect relationships between components. In highly simplified terms this is a probabilistic algorithmic method that uses decision trees generated using pre-defined training sets, in this case known 'chromosomal' and 'non-chromosomal' proteins. Each node of the decision tree is formed by a data value cut-off chosen from one of the classifiers selected at random (e.g. does a protein have a SILAC ratio less than or greater than 4 in classifier V). If a protein tends to behave more like a chromosomal protein, based on its SILAC values, more of the decision trees will vote 'positive' rather than 'negative' for its predicted chromosomal function. The protein will therefore have a random forest score closer to 1. A line can be drawn to separate the two training sets based on their random forest scores (Figure 25B). Any protein that falls to the right of the line is found within the 'True' or positive chromosomal region, while those to the left are more likely to be contaminating proteins/ 'hitchhikers'. This not only enables background proteins that do not share similar characteristics with *bona fide* chromosomal proteins to be filtered out of further analysis, but also acts as a platform,

along with heat map analysis, as a means to predict functional behaviour. Importantly, 13 previously uncharacterized proteins when tagged with GFP were shown to be present at kinetochores, and as described above, many more are predicted to come to light.

By comparing the datasets described in results Chapter 1 individually and as a whole and using the definitive 'true/positive' chromosome list as a means to filter out false positives, I have developed a list of potential kinetochore candidates worthy of further study.

Figure 25. Multi-classifier combinatorial proteomics (MCCP). A. Schematic representation of the workflow of events for the generation and integrative analysis of several distinct classifiers. Classifiers can take many forms and represent any data sets that can be scored and sorted on a numerical basis. Classifier I sorts proteins according to their total copy number within chromosomes (Abundance). Classifiers II-V use SILAC as a means to rank individual proteins based on H/L ratios under various conditions. For instance, Classifier II measures protein enrichment in chromosomes relative to cytoplasm under normal conditions (wild type cells). The ability of heavy isotope-labelled proteins to hop onto crudely isolated chromosomes following a short incubation was an indicator of exchangeability (Classifier III). Classifier IV and V measure protein dependencies in the context of SMC2 (sub-unit of Condensin) and Ska3 (kinetochore protein) KO cell lines. Finally, a bioinformatics based classifier scores proteins in accordance with the number of chromosomal and non-chromosomal domains that they are predicted to possess. Adapted from (Lan and Cleveland, 2010). **B.** The two training sets used for random forest analysis can be separated into 'True/positive' or 'False/negative' chromosomal regions on the plot. Panel B taken from (Ohta et al., 2010).

A

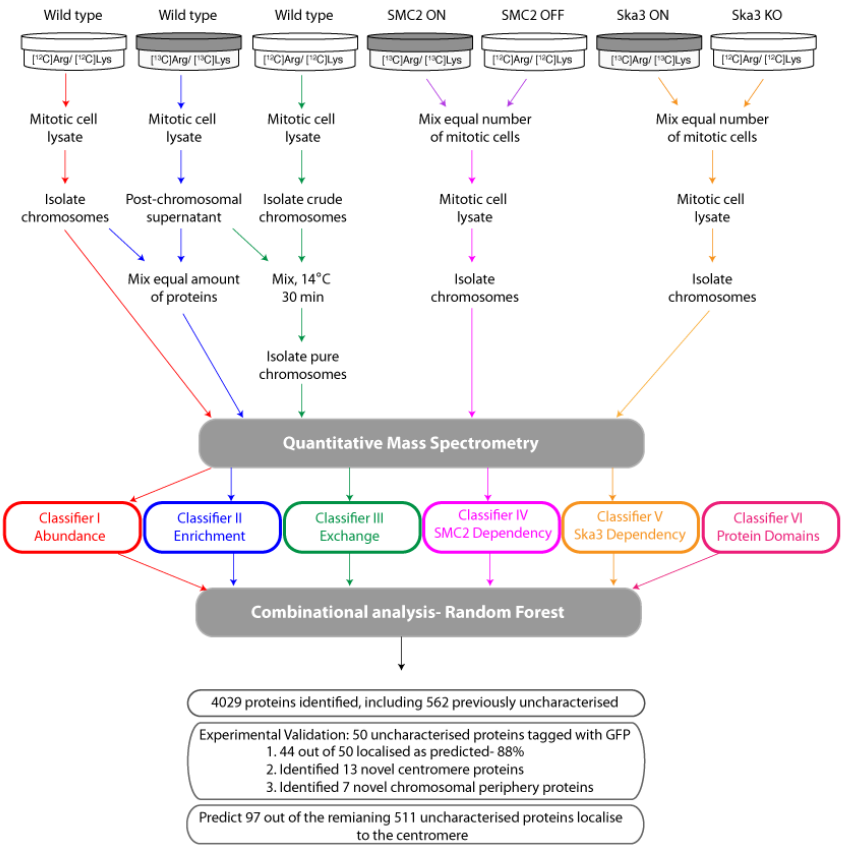
Wild type
Wild type
Wild type
SMC2 ON
SMC2 OFF
Ska3 ON
Ska3 KO
[12C]Arg/ [12C]Lys
[13C]Arg/ [13C]Lys
[13C]Arg/ [12C]Lys
Mitotic cell lysate
Mix equal number of mitotic cells
Isolate chromosomes
Post-chromosomal supernatant
Isolate crude chromosomes
Mix equal amount of proteins
Mix, 14°C 30 min
Isolate pure chromosomes
Quantitative Mass Spectrometry
Classifier I Abundance
Classifier II Enrichment
Classifier III Exchange
Classifier IV SMC2 Dependency
Classifier V Ska3 Dependency
Classifier VI Protein Domains
Combinational analysis- Random Forest
4029 proteins identified, including 562 previously uncharacterised
Experimental Validation: 50 uncharacterised proteins tagged with GFP
1. 44 out of 50 localised as predicted- 88%
2. Identified 13 novel centromere proteins
3. Identified 7 novel chromosomal periphery proteins
Predict 97 out of the remiaining 511 uncharacterised proteins localise to the centromere

B

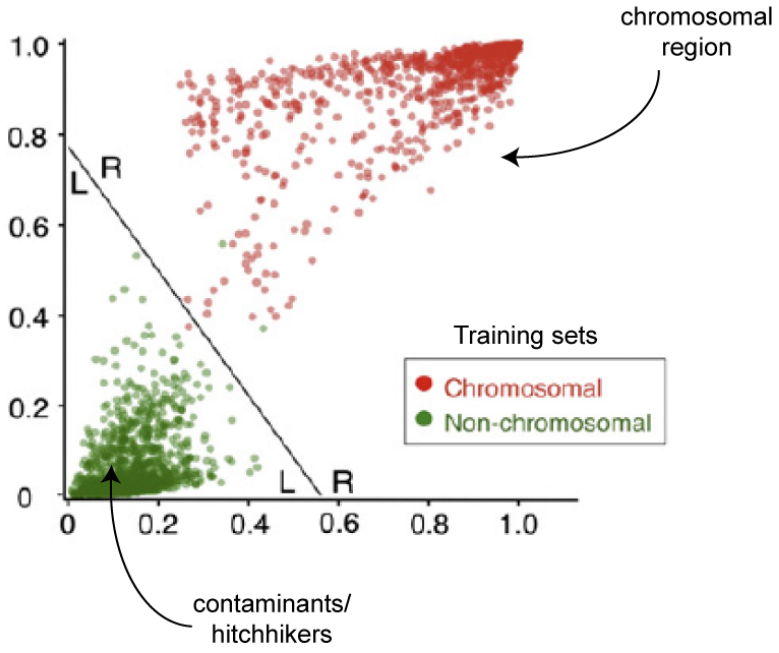
chromosomal region
1.0
0.8
0.6
0.4
0.2
0
L
R
L
R
0
0.2
0.4
0.6
0.8
1.0
Training sets
Chromosomal
Non-chromosomal
contaminants/ hitchhikers

4.2 Results

4.2.1 Identification of novel chromosomal proteins

As described in the introduction, different classifiers can be integrated together using combinatorial analysis and a random forest score assigned to individual proteins (Ohta et al., 2010). By plotting random forest scores for (Classifiers I-V) and (Classifiers I-VI) against one another, a clear boundary between known chromosomal and non-chromosomal proteins could be drawn (Figure 25B). To further validate this boundary human homologs of 50 previously uncharacterized proteins were tagged with GFP, expressed in human U2OS cells and their localization determined using fluorescence microscopy. Overall, 30 of the 34 predicted chromosomal and 2 of the 16 predicted non-chromosomal proteins localised on mitotic chromatin (Ohta et al., 2010). I cloned 32 of these constructs and these are listed in Table 9 along with their predicted behaviours (True =chromosomal, False =Non chromosomal) and verified localizations. The localization of nine of these cloned proteins could not be determined due to low transfection efficiencies (data not shown).

Several predicted chromosomal GFP-tagged proteins discovered in (Ohta et al., 2010) have not been fully characterised in regards to their localisation throughout the cell cycle. Figure 26 shows the dynamic localization of human DEAD box polypeptide 27 (DDX27), re-named cPERP-F as it was found to distribute along the chromosome periphery (Ohta et al., 2010). This perichromosomal layer is not well studied in comparison to other domains, but has been shown to consist of a large number of nucleolar and ribosomal proteins, which could provide a protective coat during mitosis (Van Hooser et al., 2005).

Protein name in chicken	Predicted True/False	Ensembl Gene ID of Human homolog	Localisation	new name
FLJ11184	T	ENSG00000198498	Chromosome	-
MSTP101	T	ENSG00000170234	Chromosome	-
Unknown kinase	T	ENSG00000204256	Chromosome	-
chromodomain helicase-DNA-binding protein 4	T	ENSG00000111642	Chromosome	-
Uncharacterized protein C5orf24	T	ENSG00000181904	Chromosome	-
C9orf32	T	ENSG00000148335	unlocalized	-
Uncharacterized protein FLJ43968	T	ENSG00000157741	unlocalized	-
Uncharacterized protein C2orf29	T	ENSG00000158435	unlocalized	-
C22orf28	T	ENSG00000100220	n/a	-
breast cancer metastasis-suppressor 1-like	T	ENSG00000100916	n/a	-
C15orf44 homolog	T	ENSG00000138614	n/a	-
Uncharacterized protein FLJ30717	T	ENSG00000147679	n/a	-
Uncharacterized protein FLJ20309	T	ENSG00000114933	n/a	-
Protein DDX26B	T	ENSG00000165359	n/a	-
YTH domain-containing protein 1	T	ENSG00000083896	n/a	-
Ras association domain family 2	F	ENSG00000101265	Centromere	CENP-34
C12orf23 homolog	F	ENSG00000151135	Chromosome	-
C16orf63 homolog	F	ENSG00000133393	unlocalized	-
CXorf56	F	ENSG00000018610	unlocalized	-
CG1218-PA (LOC646058)	F	ENSG00000056050	unlocalized	-
LOC418765 UPF0430	F	ENSG00000134884	unlocalized	-
Uncharacterised protein C4orf14	F	ENSG00000084092	unlocalized	-
TBC1 domain family, member 15	F	ENSG00000121749	unlocalized	-
KH domain-containing	F	ENSG00000121774	unlocalized	-
VAC14 homolog	F	ENSG00000103043	unlocalized	-
Uncharacterized protein C10orf119	F	ENSG00000197771	unlocalized	-
Neighbor of COX4	F	ENSG00000131148	unlocalized	-
Uncharacterized protein FLJ90500	F	ENSG00000119777	unlocalized	-
kelch domain containing 4	F	ENSG00000104731	unlocalized	-
Ankyrin repeat domain-containing protein 28	F	ENSG00000206560	unlocalized	-
Leucine-rich repeat-containing protein 28	F	ENSG00000108829	unlocalized	-
WD repeat protein 61	F	ENSG00000140395	n/a	-

Table 9. List of cloned previously uncharacterised GFP-tagged proteins found in our original chromosomal dataset. Listed are the predictive outcomes of integrative random forest analysis (True-chromosomal, False-Non-chromosomal) and the corresponding localizations for a number of proteins identified in chromosome preparations. Many do not localize to the chromosomes (unlocalised). Others display general chromosomal localizations, while CENP-34 represents a novel centromere protein.

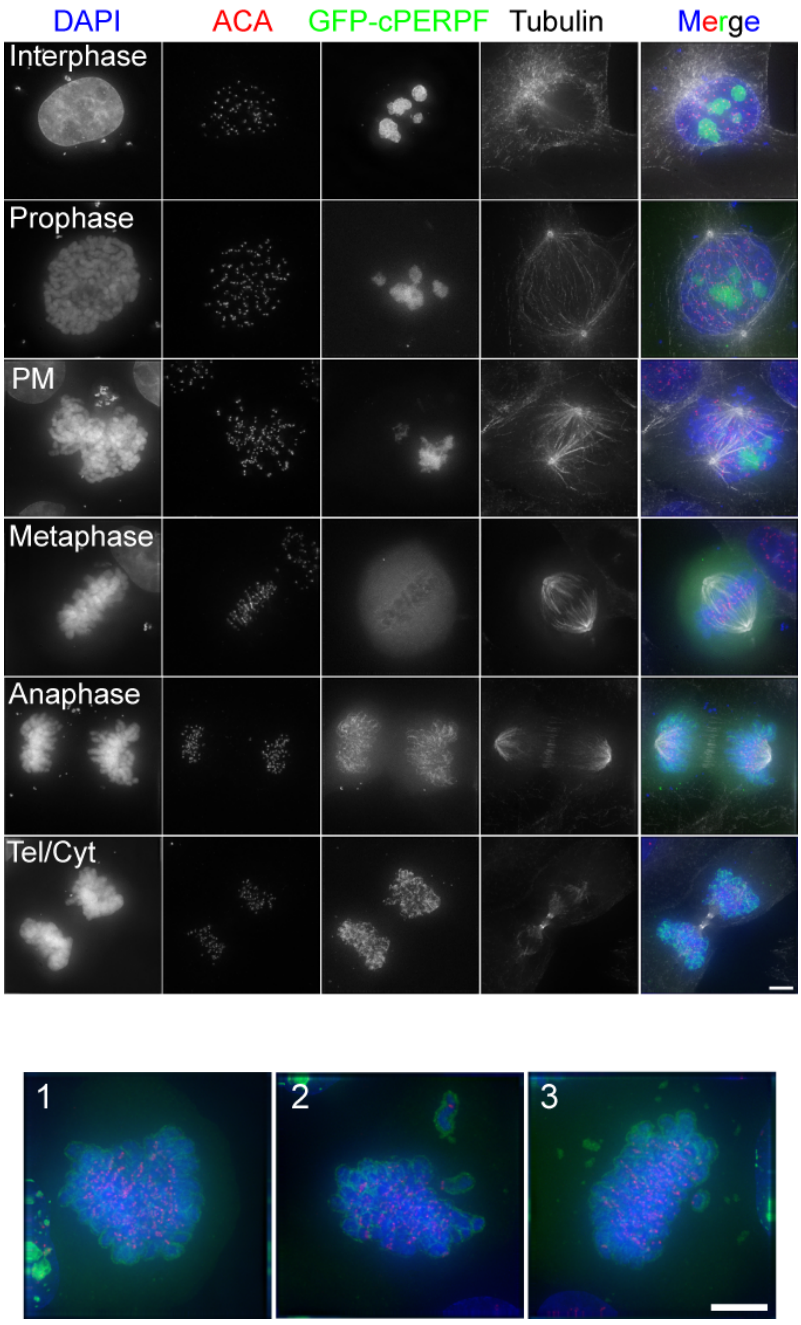

Figure 26. Characterisation of novel periphery proteins. The localisation of transiently expressed GFP-cPERP-F in different phases of mitosis. U2OS cells were fixed 24 hours after transfection and stained using antibodies against ACA and tubulin. DAPI was used to stain the DNA. Cells in interphase, prophase, prometaphase, metaphase, anaphase and telophase are shown. Images 1-3 depict GFP-cPERP-F (green), ACA (red) and DNA (blue) only. Scale bar: 5 μm.

Through transient transfections and fixed cell analysis GFP-cPERP-F was found to localise to nucleoli in interphase (Figure 26). Redistribution of cPERP-F correlates with the breakdown of nucleoli as depicted in prophase and prometaphase images. It should be noted that although nucleoli classically breakdown upon exiting prophase, U2OS cells frequently delay this event. Image number 1 and 2 depict early and later prometaphase cells, respectively. Here, nucleoli have dis-assembled and cPERP-F is clearly localized on the periphery of all chromosomes. In metaphase, varying amounts of peripheral localisation are seen depending on the cell, with low levels depicted in Figure 26 and higher signals seen in image 3. Importantly, cPERP-F does not appear to co-localize with ACA staining, a marker of centromeric regions. The peripheral distribution of GFP-tagged cPERP-F was more easily identifiable in anaphase cells and on de-condensing chromosomes in telophase.

4.2.2 Removing contaminants using the chromosomal proteome

We would hypothesise that any novel kinetochore protein might also reside in this 'chromosomal prediction' region depicted in Figure 25B. This would help us to identify contaminating proteins that bind to chromosomes, but play no functional roles during mitosis so that these can be removed from further consideration. Figure 27A depicts 562 proteins present in the whole chromosomal proteome that were termed 'uncharacterised' in relation to their function in (Ohta et al., 2010). The line in Figure 27A separates those entries that are predicted to be chromosomal (right) from those that are predicted to be 'hitchhikers' (left). Out of these 562 proteins, 526 were mapped successfully to the new UniProt datasets (the IPI database was used in the original study). These included 247 chromosomal and 279 non-chromosomal predictions (Figure 27B). I decided that these proteins must be identified in both biological replicates and quantified with >=1 unique peptide pair to be considered for further analysis. In addition, the above criterion had to hold true in at least 4 out of 5 SILAC KO datasets (CENP-C, CENP-T, CENP-W, Ndc80 and Ska3 KO SILAC datasets).

Figure 27. Identification of potential kinetochore candidates using the 'true chromosomal' proteome. Random forest analysis of classifiers can successfully separate two training sets of known chromosomal and non-chromosomal proteins (Ohta et al., 2010). **A.** Scatterplot of uncharacterised proteins predicted to lie within the chromosomal or non-chromosomal regions of the graph. **B.** Schematic representation of the analytical workflow used to select potential kinetochore proteins from a list of 562 uncharacterised chicken proteins reported by (Ohta et al., 2010). 526 of these proteins successfully mapped to uniprot identifiers, of which 247 were predicted to be chromosomal based on MCCP (Ohta et al., 2010). For further inclusion, proteins must have been quantitated by at least 1 unique peptide, be represented in both biological repeats and ≥4 out of 5 distinct SILAC experiments. Further statistical analysis in the form of significance B scores (p value<0.05) and hierarchical cluster analysis resulted in a total of 15 potential kinetochore candidates.

A

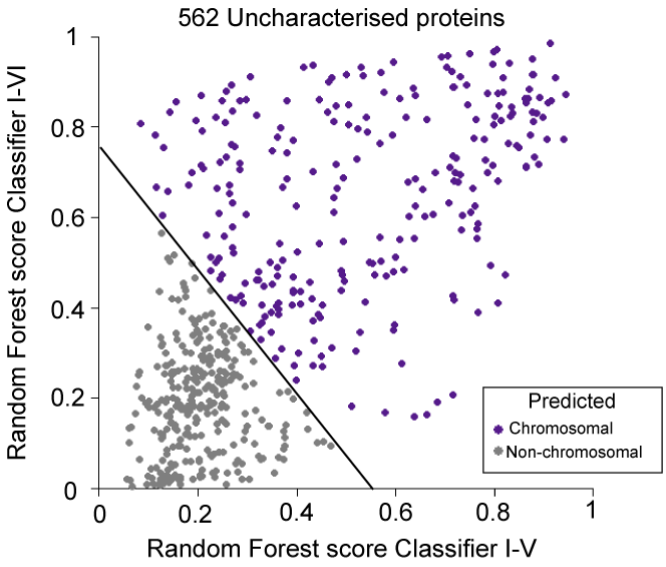
562 Uncharacterised proteins
Random Forest score Classifier I-VI
Random Forest score Classifier I-V
0
0.2
0.4
0.6
0.8
1
Predicted
Chromosomal
Non-chromosomal

B

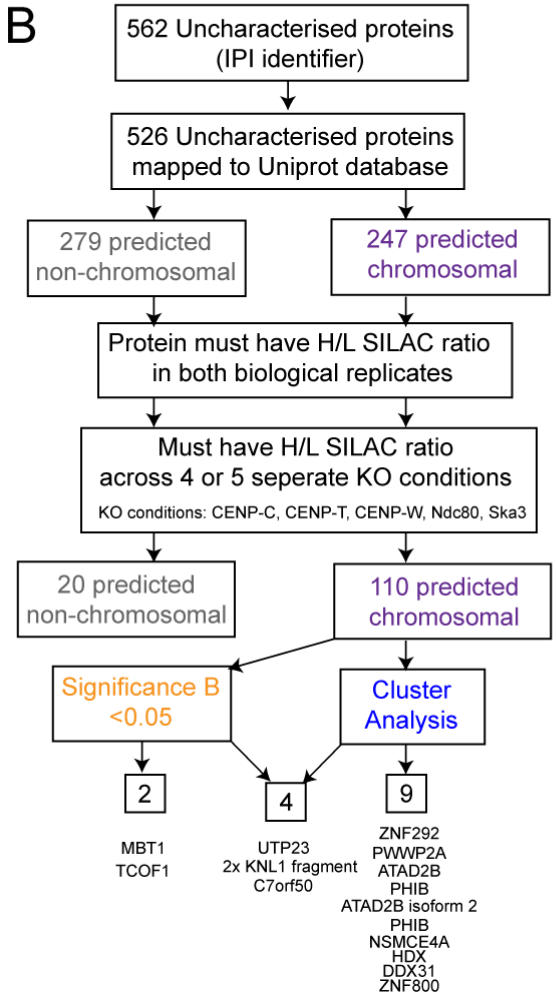
562 Uncharacterised proteins (IPI identifier)
526 Uncharacterised proteins mapped to Uniprot database
279 predicted non-chromosomal
247 predicted chromosomal
Protein must have H/L SILAC ratio in both biological replicates
Must have H/L SILAC ratio across 4 or 5 seperate KO conditions
KO conditions: CENP-C, CENP-T, CENP-W, Ndc80, Ska3
20 predicted non-chromosomal
110 predicted chromosomal
Significance B <0.05
Cluster Analysis
2
4
9
MBT1
TCOF1
UTP23
2x KNL1 fragment
C7orf50
ZNF292
PWWP2A
ATAD2B
PHIB
ATAD2B isoform 2
PHIB
NSMCE4A
HDX
DDX31
ZNF800

Ska3 dependency SILAC ratios have previously been published (Ohta et al., 2010). This entire analytical workflow is depicted in Figure 27B. Interestingly, using this filtering system, 110 chromosomal (44.5%) and only 20 non-chromosomal proteins (7.2%) remained. Thus likely contaminants were less frequently identified across these samples. This may be because my chromosome isolation procedure yields a different population of hitchhikers/contaminants from that of Dr. Ohta.

From here it was important to try and select proteins from the list of 110 predicted chromosomal proteins that were more likely to function as part of the kinetochore complex. We hypothesise that proteins that are significantly increased or reduced on chromosomes based on their dependency for known kinetochore proteins would be good candidates for cloning and centromere localisation studies. As described in section 3.2.4.2, Significance B scores (p values <0.05) can be calculated using Perseus (Cox and Mann, 2008) and aims to identify proteins that show significantly differential H/L abundance ratios (i.e. those proteins whose levels are significantly increased or decreased on chromosomes when compared with the main distribution of chromosomally bound proteins).

I found that six of the targets associated with dramatic increases or decreases in abundance ratios assessed using the Significance B value successfully mapped onto this inclusion list of 110 proteins (Table 10). MBT1 and TCOF1 have a Significant B SILAC score with a p value<0.05 in CENPC and Ndc80 conditional KO experiments, respectively (Table 10; red arrows). Overall these proteins show behaviour across experiments more consistent with abnormal recruitment onto chromosomes when core kinetochore proteins are depleted.

The 4 remaining proteins; UTP23, 2 unknown entries and C7orf50, were generally depleted from chromosomes across KO SILAC conditions (i.e. Log_2 H/L SILAC ratio >0). The 2 unknown entries were shown through BLAST searches to be KNL-1 fragments and thus act as a positive control for this type of analysis. In spite of KNL1

fragment identification using Significance B scores as a threshold, the two candidates were only classified as significant in a single kinetochore KO condition (Table 10; blue arrows), suggesting that this type of analysis is very stringent. UTP23 was the only candidate that was significantly depleted from more than one KO experiment (CENP-C and CENP-W). This would suggest that UTP23 localisation onto chromosomes is extremely dependent on both CENP-C and CENP-W kinetochore proteins.

Analysing the data using the Significance B value of Perseus is probably not the best strategy to identify novel kinetochore proteins. This is because many of the known kinetochore components (e.g. CCAN, MIS12 complex) do not display SILAC ratios that significantly deviate from the rest of the population. For this reason, it would be more informative to find proteins that display similar dependency patterns. The SILAC ratios from the chromosome inclusion list (110 entries in total) were combined and clustered with known kinetochore proteins using heatmap analysis (Figure 28). In terms of identifying new 'core' kinetochore proteins there were two regions of interest. Panel A displays proteins that are mildly depleted from chromosomes. Interestingly, this group contains 9 out of the 16 CCAN components. Seven proteins from the inclusion list fall within this section of the diagram and are labelled with the gene name associated with the human homolog (marked with a (*)). Panel B includes the KMN, CENP-T/W/S/X, CENP-C and RZZ complexes. Six uncharacterised proteins are clustered in this area. Interestingly, 4 of these candidates overlap with proteins that were also identified when using the Significance B score (p value<0.05) as a filter. This would include C7orf50, UTP23 and the 2 KNL1 fragments.

Chicken Uniprot	Ensembl Gene ID of Human homolog	Name	Significance B (p value <0.05)			
			CENP-C	CENP-T	CENP-W	Ndc80
E1BU97	ENSG00000198945	MBT1, Lethal (3) malignant brain tumor-like protein 3	⇑ **-1.3175**	0.3255	-0.3185	-0.5238
F1NRG3	ENSG0000070814	TCOF1, Treacher Collins syndrome protein	-0.43996	-0.8123	-0.56296	⇑**-2.2799**
F1NLP4	ENSG00000146540	Uncharacterised protein C7orf50	⇓**1.1202**	0.6980	0.8169	-0.16396
E1BZI2	ENSG00000147679	UTP23, rRNA-processing protein UTP23 homolog	⇓ **0.709**	0.6402	⇓ **0.9532**	0.0015
E1C0P5	ENSG00000259494	KNL1 fragment	0.8635	0.5814	0.7783	⇓**1.2783**
F1NPJ7	ENSG00000161405	KNL1 fragment	⇓**0.8556**	0.6947	0.8173	0.9246

Table 10. List of potential kinetochore candidates. Proteins that are significantly depleted (blue arrows) or enriched (red arrows) on chromosomes isolated from a specific kinetochore KO cell line (CENP-C, CENP-T, CENP-W or Ndc80 conditional KO cell lines). The H/L SILAC ratios for each protein are listed. *p* values <0.05 were calculated using Perseus Significance B score. Those proteins that were not significantly depleted or enriched according to Significance B calculations are depicted in black font.

It should also be noted that the novel centromeric proteins identified previously (CENP-28-to-33, -35, -36 and CENP-Z) although predicted to be chromosomal and included in this filtering workflow, were not identified as potential kinetochore candidates. However, CENP-28, -29, -31, -35 and -36 have already been observed to function in complexes that modify or bind histones and are therefore implicated to function in chromatin rather than act as core structural components of the kinetochore (Ohta et al., 2010). Similarly, none of the new chromosomal periphery proteins (cPERPs A-D) behave like 'core' kinetochore proteins.

The positive candidates identified through Significance B statistical analysis and/or hierarchical clustering are summarised in Table 11 (KNL-1 fragments are not included). Some of these proteins have, to some extent, been functionally characterised or possess predicted roles falling into the transcriptional regulation or ribosome biogenesis categories. Although it has a role in ribosome formation, UTP23 is of particular interest as it has previously been pulled down in budding yeast with minichromosome bound kinetochores (Akiyoshi et al., 2010). As yet, kinetochore localisation of UTP23 has not been established. We also found AAA- (ATPases associated with diverse cellular activities) ATPase superfamily member ATAD2B. This is important as a more extensively studied member of this family, p97/VCP (Cdc48), has been shown in mitosis to co-ordinate chromosome biorientation and condensation events (Vaz et al., 2013). To verify these predictions, localisation studies must first be performed.

Figure 28. Heatmap analysis of kinetochore proteins and 'true chromosomal' candidate proteins. The $\log_2$ H/L SILAC ratios from CENP-C, CENP-T, CENP-W and Ndc80 experiments were used for cluster analysis. The repeats for each condition were considered separately and labelled 1 or 2. NA values are shown in grey and were not used to create the row or column dendrograms. Those proteins that did not display a SILAC ratio for at least half of the experiments (4 out of 8; any combination) were not considered. Merging of clusters into larger clusters (agglomeration) was performed using the Ward method (Key, 2012). The colour key is shown on the right with a density plot of all H/L values. Those proteins with a high SILAC ratio are depleted from chromosomes and are depicted by the colour blue. Alternatively, the colour red represents an increase in recruitment. A value of 0, as shown in white, depicts proteins that do not change in abundance. Row groupings highlighting the location of 'Kinetochore' and 'True chromosomal' subgroups are shown. Panel A and B highlight areas of interest on the heatmap and red stars (*) label potential novel kinetochore proteins worth further study.

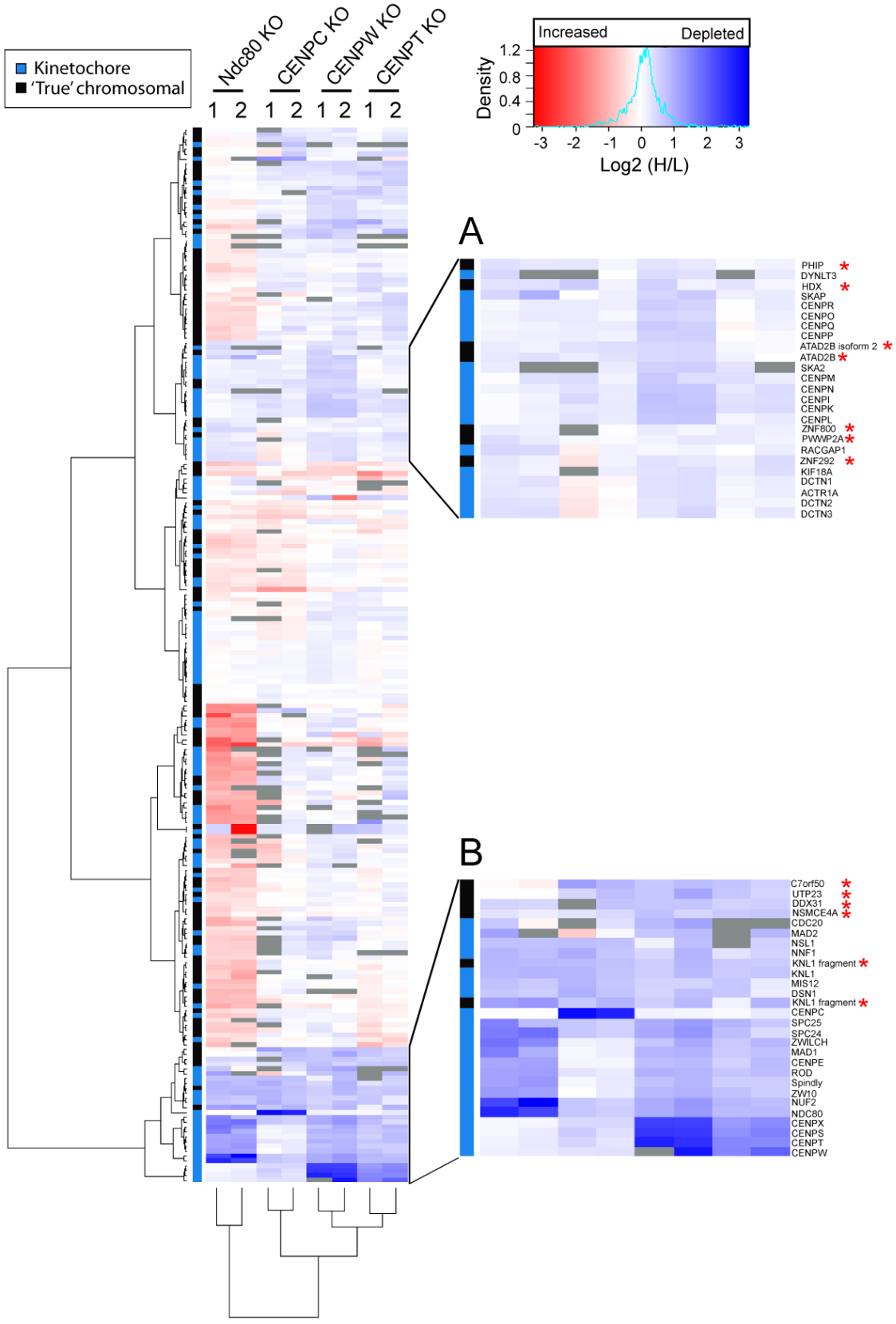
Kinetochore
'True' chromosomal
Ndc80 KO
CENPC KO
CENPW KO
CENPT KO
1 2 1 2 1 2 1 2
Increased
Depleted
Density
1.2
0.8
0.4
0
-3 -2 -1 0 1 2 3
Log2 (H/L)
A
PHIP *
DYNLT3
HDX *
SKAP
CENPR
CENPO
CENPQ
CENPP
ATAD2B isoform 2 *
ATAD2B *
SKA2
CENPM
CENPN
CENPI
CENPK
CENPL
ZNF800 *
PWWP2A *
RACGAP1
ZNF292 *
KIF18A
DCTN1
ACTR1A
DCTN2
DCTN3
B
C7orf50 *
UTP23 *
DDX31 *
NSMCE4A *
CDC20
MAD2
NSL1
NNF1
KNL1 fragment *
KNL1
MIS12
DSN1
KNL1 fragment *
CENPC
SPC25
SPC24
ZWILCH
MAD1
CENPE
ROD
Spindly
ZW10
NUF2
NDC80
CENPX
CENPS
CENPT
CENPW

Chicken Uniprot	Ensembl Gene ID of Human homolog	Human Gene Name	Human Name	Comments
E1BU97	ENSG00000198945	Lethal (3) malignant brain tumor-like protein 3	MBT1/ L3MBTL3	Putative Polycomb group (PcG) protein
F1P1N8	ENSG00000188994	Zinc finger protein 292	ZNF292	May be involved in transcriptional regulation
F1NRG3	ENSG00000070814	Treacher Collins syndrome protein	TCOF1	May be involved in nucleolar-cytoplasmic transport and ribosome biogenesis
E1BWL2	ENSG00000170234	PWWP domain-containing protein 2A	PWWP2A	NA
F1NUZ7	ENSG00000119778	(Isoform 1) ATPase family AAA domain-containing protein 2B	ATAD2B	Binds acetylated lysine residues in histone H1.4, H2A, H2B, H3 and H4
F1NXP9	ENSG00000146247	Pleckstrin homology domain-interacting protein variant 1	PHIP	Stimulates cell proliferation through regulation of cyclin transcription
F1NUE7	ENSG00000119778	(Isoform 2) ATPase family AAA domain-containing protein 2B	ATAD2B	Binds acetylated lysine residues in histone H1.4, H2A, H2B, H3 and H4
F1NV66	ENSG00000107672	Non-structural maintenance of chromosomes element 4 homolog A	NSMCE4A	SMC5-SMC6 complex component
E1BZI2	ENSG00000147679	rRNA-processing protein UTP23 homolog	UTP23	Involved in rRNA-processing and ribosome biogenesis
Q5ZKW8	ENSG00000165259	Highly divergent homeobox	HDX	NA
F1NLP4	ENSG00000146540	Uncharacterised protein C7orf50	C7orf50	NA
F1NM06	ENSG00000125485	DEAD box protein 31	DDX31	Probable ATP-dependent RNA helicase
E1BWK9	ENSG00000048405	Zinc finger protein 800	ZNF800	May be involved in transcriptional regulation

Table 11. List of potential kinetochore candidates. All proteins listed are defined as being 'true chromosomal' proteins when using integrative random forest analysis (Ohta et al., 2010). They must also show significant differences in their total abundance on chromosomes in different kinetochore KO conditions or behave like core kinetochore proteins upon cluster analysis.

4.2.3 C7orf50 localises to chromosomes

The first uncharacterised protein I chose to investigate for cloning and localisation studies was C7orf50. The human homolog is 194 amino acids long and was tagged via its N-terminus to GFP. To verify its localisation during mitosis HeLa-Kyoto cells were transfected with the construct and fixed 72 hours later. I found that exogenous protein expression was very high 1-2 days after transfection, this was slightly reduced by 3 days and this was therefore chosen as the time point to image cells. Clear signals for the GFP-fusion can be seen in interphase where the protein localises to nucleoli (Figure 29A) and in punctate regions consistently seen on chromosomes progressing through telophase/cytokinesis. In the other mitotic phases it is possible to see some chromosomal signal, but the high background levels mask the extent of this distribution (Figure 29B). The pattern observed appears to be typical of proteins associated with the perichromosomal layer. However, it is possible that kinetochore localisation might be disguised by over-expression.

In order to look more clearly at the distribution of C7orf50 on chromosomes, transient transfection, followed by cytospin and pre-extraction procedures were performed. Figure 29C depicts the chromosomal localisation of GFP-tagged CENP-Z and C7orf50 using this protocol. It is clear that CENP-Z is capable of localising on either side of the primary constriction (as indicated by the white arrows). This is in accordance with its known kinetochore localisation (Ohta et al., 2010). On the other hand, no discernible chromosomal signal is seen at the same regions for C7orf50, indicating that it does not localise to centromeres. Chromosomal signals are also no longer observed, suggesting that C7orf50 might be weakly associating with the perichromosomal layer or that this protein domain is not maintained during the protocol.

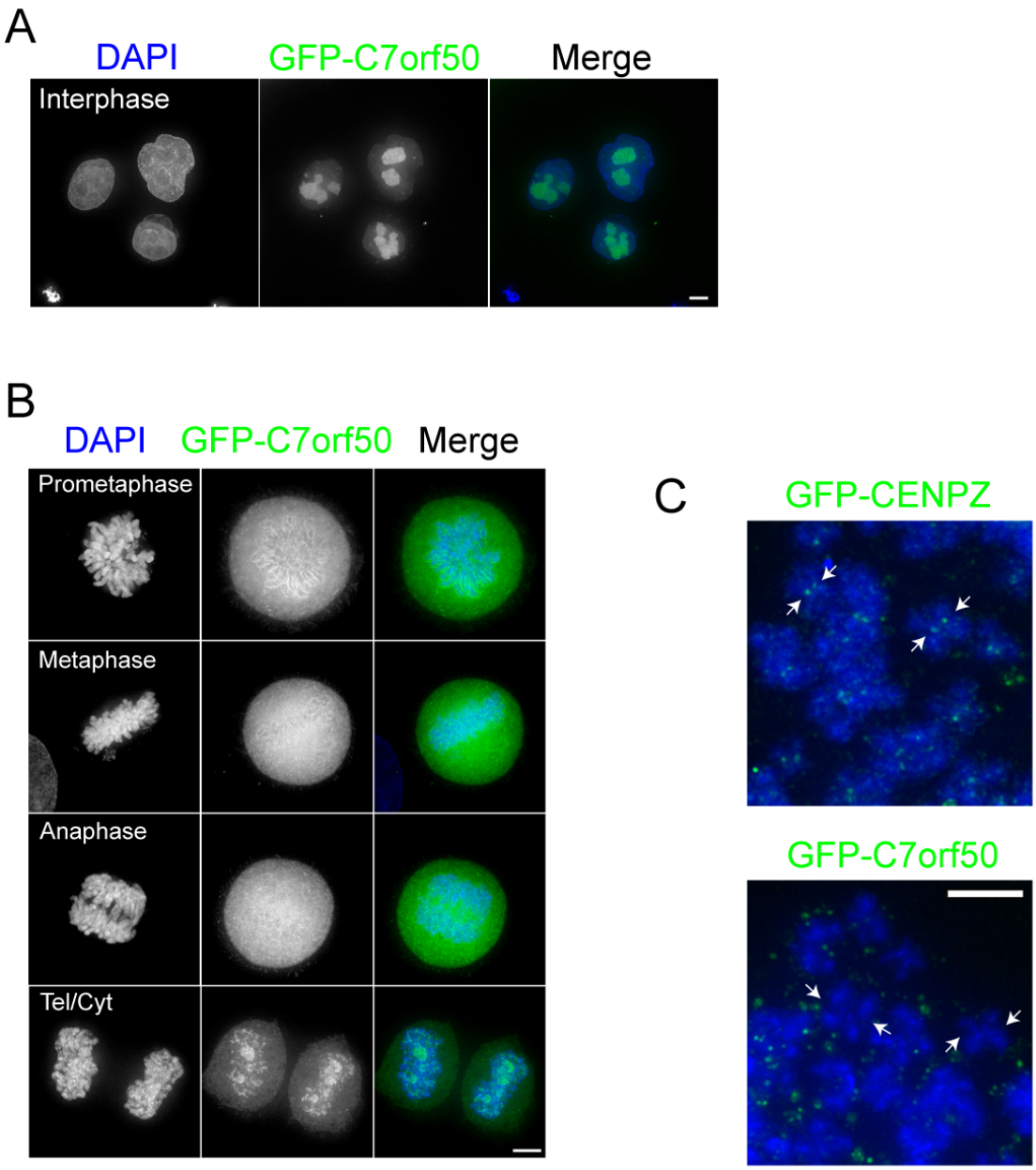

Figure 29. Localisation of C7orf50. The localization of transiently expressed GFP-C7orf50 in **A.** interphase and **B.** Mitosis. HeLa-Kyoto cells were pre-extracted with 0.02% Triton-X and fixed 72 hours after transfection. DAPI was used to stain the DNA. **B.** Cells in prophase, prometaphase, metaphase, anaphase and telophase are shown. **C.** HeLa Kyoto cells were transiently transfected with the indicated GFP-fusion protein and cultured for ~36 hours before a 3 hour mitotic block with nocodazole. Hypotonic swelling and cytospin procedures were followed by pre-extraction (0.1% Triton-X), fixation and staining with DAPI to visualise chromosome spreads. Scale bar: 5 μm.

4.3 Discussion

SILAC was used to quantitatively compare the proteome of WT chromosomes against those missing individual integral kinetochore components. In this chapter, these data sets were analysed to try and identify novel kinetochore candidates.

A list of uncharacterised proteins that had previously been predicted to be chromosomal based on integrative data analysis (Ohta et al., 2010) was used as a first step to filter out functionally unknown proteins that were unlikely to be novel kinetochore components. A total of 110 uncharacterised proteins mapped on to the kinetochore KO SILAC datasets based on the criteria described in Figure 27B. From here, it was hypothesised that proteins with an extreme $\log_2$ SILAC ratio (i.e. greater deviation from 0; p value<0.05) would directly reflect dependency for chromosomal association on a known integral kinetochore component. Cluster analysis was also used to highlight those candidates that share similar dependency patterns with known kinetochore subcomplexes and therefore might be functionally linked. Using these two methods, a list of 13 candidates was generated.

Due to lack of time, only one attempt was made to validate the list of uncharacterised proteins. In these experiments candidate protein, C7orf50, did not appear to localise to centromeric regions, but did weakly distribute along the chromosomal periphery when expressed in human cells. However, even chromosomal peripheral localisation of GFP-tagged C7orf50 was no longer detected on chromosomes from metaphase spreads. Therefore, the exact localisation of this protein in mitosis is still under debate. In the future I would plan to tag C7orf50 via its C-terminal to ensure that the N-terminal tag did not account for the varied localisation of the protein. I would also be eager to generate an antibody against chicken C7orf50 to check localisation via immunofluorescence in DT40 cells. As C7orf50 chromosomal recruitment is highly dependent on CENP-C according to Significance B statistical analysis (Table 10), it

would be interesting to see if C7orf50 signals decrease upon doxycycline addition in the CENP-C conditional KO cell line.

In regards to some of the other candidate proteins, PWWP2A could be implicated at centromeric regions as PWWP domain containing proteins have been identified as H3K36me3 interactors (Vermeulen et al., 2010). This mark is enriched at human centromeres by CHIP (as well as being associated with transcribed genes) (Bergmann et al., 2011). Several Zinc finger-containing proteins, including CENP-Z (Ohta et al., 2010), CAMP (Itoh et al., 2011), ZNF330 (Bolivar et al., 1999) and ZNF397 (Bailey et al., 2008) do localise to centromeres/kinetochores. Thus, ZNF800 and ZNF292 identified in this study are reasonable targets for further analysis. More recently, the RWD domain has been described as a platform for core kinetochore assembly in both yeast (Schmitzberger and Harrison, 2012) and vertebrate cells (Nishino et al., 2013). This could therefore be an additional feature to consider when ranking candidate proteins for characterisation studies. In any case, the localisation of the other 12 targets was not confirmed in this study.

As validation for this type of analysis other candidates have already been shown to localise or function at centromeric regions. Although originally classified as being uncharacterised, NSMCE4A is a known member of the SMC5/6 complex (De Piccoli et al., 2009). Other components of this complex follow the same pattern and are depleted from chromosomes (data not shown). In budding yeast this complex has recently been implicated in regulating recombination and sumolyation events at centromeres and therefore could be an interesting candidate for further study (Yong-Gonzales et al., 2012). Another example is TCOF1 that has been described as a centrosome and kinetochore associated protein in dissociated cortical progenitor cells progressing through mitosis (Sakai et al., 2012). The same study also showed co-localisation between TCOF1 (Treacle) and CENP-E in prometaphase/metaphase HeLa cells.

It should be noted that this strategy did not take into account those proteins that have already been associated with a specific function. Examples of categories would include ribosomal, DNA repair, DNA replication, histone modifiers and membrane proteins. This is important as a protein could take part in a number of secondary functions and have different localisation patterns depending on the cellular context. A good example is KIF15. KIF15 is a motor protein that is targeted to mitotic spindles by TPX2 and the two proteins are proposed to function together to push centrosomes apart during bipolar spindle assembly by bridging anti-parallel microtubules in the mid-zone (Tanenbaum et al., 2009). Interestingly, KIF15 binding to the mitotic spindle is dependent on the presence of K-fibres, as interference in their formation leads to a loss of spindle localisation (Sturgill and Ohi, 2013). In the same study it was also reported that in detergent extracted cells KIF15 staining co-localised with signals from the outer kinetochore protein, Hec1. In our studies KIF15 is significantly depleted from chromosomes (Significance B score; p value<0.05) in CENP-C and CENP-W KO SILAC experiments and would support findings for KIF15 kinetochore localisation. Proteins that are already functionally characterised, but whose levels are reduced or enriched on chromosomes depleted of integral kinetochore proteins should still be considered for further analysis.

In the future I would also like to carry out localisation studies at various time points in the cell cycle to assess if/when a candidate protein localises to centromeric regions. This is important as many proteins are only transiently associated with the kinetochore complex at specific stages of mitosis and could act as a clue towards their function. For example, the spindle checkpoint proteins Mad1 and Mad2 localise to unattached kinetochores, but their levels are dramatically reduced upon microtubule attachment (Howell et al., 2004; Shah et al., 2004). I would also like to perform siRNA depletion studies of candidate proteins using live-cell imaging with a stable HeLa cell line expressing mcherry-Histone H2B and GFP-tubulin. I would use this as a tool to study defects in mitotic progression and spindle morphology. Finally, affinity purification experiments and proteomics analysis could be used to identify interesting interacting

proteins of candidates. I would perform these experiments by pulling-down streptavidin binding protein (SBP)-tagged candidates from mitotically blocked HeLa cells using streptavidin coated magnetic beads. The hope would be to identify subcomplex interactors within the kinetochore.

5 Results Chapter 3: AID system and CENP-T function

5.1 Introduction

To fully understand a protein's function it is important to be able to study its behaviour *in vivo*. Whereas in the past many functional characterisations were carried out using overexpression studies, in recent years the development of systems that can reduce the expression or conditionally inactivate a particular gene of interest is common practice in many labs. This has been achieved predominantly by eliminating mRNA production or destroying transcribed mRNAs using RNAi and gene targeting (Elbashir et al., 2001; Gossen and Bujard, 1992; Sauer and Henderson, 1988). Although these techniques are very powerful, methods allowing direct inactivation or depletion at the protein level are being developed. These tackle some of the disadvantages associated with technologies that target mRNA; mainly the time taken for depletion and the level, specificity and reversibility of target protein depletion.

5.1.1 Pitfalls of common gene silencing technologies

Endogenous genes can be deleted or disrupted by exploiting various recombination pathways (Hall et al., 2009). This has been applied to many mammalian systems, including human cells and the creation of KO mice (Doyle et al., 2012; Rago et al., 2007; Smithies et al., 1985; Topaloglu et al., 2005). Of course, for proteins that are required for cell viability constitutive application of these approaches is not applicable. Instead, conditional techniques whereby the expression of a gene can be turned off within hours, for example by the addition of tetracycline/doxycycline (tetracycline ON/OFF system), can be used to study the development of a lethal phenotype (Banaszynski and Wandless, 2006). In particular, this conditional KO approach has been readily applied in DT40 chicken cells where homologous recombination is high in comparison to other vertebrate cell lines (Okada et al., 2006b; Winding and Berchtold, 2001).

Much more commonly, siRNA have been used to target particular mRNAs directly. Small double strand (ds)-RNA molecules help target the RNA-induced silencing complex (RISC) to complimentary mRNA segments and direct their cleavage, thereby reducing the pool of transcripts for protein translation (Huppi et al., 2005; Medema, 2004). With simple design tools, cost-effective commercial siRNA synthesis and ease of transfection into cell lines, this technique has become a widely accepted step for initial readouts of target protein function (Medema, 2004).

However, these silencing techniques suffer from the fact that the speed of depletion is dependent on the stability of the pre-existing protein. Long-lived polypeptides that are degraded slowly can induce various secondary effects as their levels gradually fall below a critical threshold. This can allow enough time for compensatory signalling pathways to be activated, masking or confusing the direct consequences of protein depletion (Medema, 2004). Therefore, interpreting loss of function phenotypes can be very difficult. This especially holds true for proteins that have many different roles, for example in highly dynamic settings such as mitosis. In these instances the particular dominant phenotype may hide other more subtle, but also important phenotypes.

The extent of silencing is also a very important factor to consider when studying function. In many instances a reduced pool of the target, as long as it is above a critical level, will still be able to perform its main roles. A good example is CENP-A, where siRNA studies have shown that even at 10% of its original levels the recruitment of additional kinetochore components and overall kinetochore structure is normal (Liu et al., 2006). This caveat is particularly relevant for siRNA, which can show great variability between oligos for the same protein, and from cell to cell, and could lead to confusing gradients in the severity of a phenotype.

Specificity is also a problem for RNA-based knockdown experiments as it is possible that other unrelated transcripts may also be targeted for cleavage, leading to off-target

effects. Hence, interesting results must be backed up by several siRNAs or complementation with a non-targeted cDNA whose RNA product is "immune" to degradation by the siRNA (Medema, 2004). Finally, gene inactivation and siRNA treatments are not readily reversible as siRNAs are not easily washed out of cells.

5.1.2 Methods for direct depletion at the protein level

To overcome the limitations described above, systems that target the proteins themselves more directly are now being developed. First, small molecules that can permeate the cell membrane have been employed to rapidly mis-localise proteins to cellular compartments where they cannot function. 'Anchor away' or 'knocksideways' methodologies are two such examples that exploit the defined FKBP12-rapamycin-mTOR binding pathway (Geda et al., 2008; Haruki et al., 2008; Robinson et al., 2010). This system takes the specific protein domains involved in this interaction (FKBP and FRB) and fuses them onto two independent proteins: the target protein, and a factor that has a defined subcellular localisation, such as the mitochondrial outer membrane. In the presence of rapamycin such fusion proteins can be rapidly, and reversibly re-routed to a specific compartment unrelated to its function.

In some situations it might be more advantageous to completely remove a protein from the cell. This can be achieved through the direct manipulation of ubiquitin-ligase degradation systems in which a target protein is made to be a direct substrate for degradation by fusing to it a short amino acid sequence known as a degron. There are many different types of peptide sequences associated with ubiquitin dependent degradation (Ravid and Hochstrasser, 2008), however one successful application has been in yeast genetics using a temperature shift-inducible 'N-degron' system, whereby the stability of a given protein is determined by the nature of its N-terminal residues (Dohmen et al., 1994; Kanemaki et al., 2003).

Other studies use the core components of the degradation machinery for artificial tethering or fusion of target proteins (Banaszynski and Wandless, 2006). For example, variable F-box containing adaptors of a multi-subunit E3 ligase can be engineered to contain additional domains that promote interactions with a protein of interest, thereby reducing proximity and facilitating ubiquitination (Su et al., 2003; Zhou et al., 2000).

The auxin-inducible degron (AID) system takes aspects from all of these technologies (Nishimura et al., 2009). First, a specific 'degron' sequence is fused to the target. Concomitantly, an adaptor is exogenously expressed to create a link between the protein of interest and the core ubiquitin ligase machinery. Lastly, a small molecule (auxins, a group of plant hormones) brings the two together inducing binding, ubiquitination and ultimate degradation (Nishimura et al., 2009). This creates a very specific, rapid and reversible method for reducing protein levels. The molecular principles are described below.

5.1.3 Proteosomal degradation and AID technology

Proteosomal degradation is initiated by many different types of E3 ligases. Amongst these, Cullin-Ring Ligases (CRLs) are required for modulating proteins involved in a diverse array of cellular pathways (Petroski and Deshaies, 2005). The various multi-subunit E3 ubiquitin ligases are defined by their incorporation of a specific substrate recognition protein. The SCF (Skp1-Cullin1-Fbox protein) complex is one of the most well-characterised E3 ligases in mammalian systems (Cardozo and Pagano, 2004). The catalytic core of this ligase is formed from Cullin-1 (Cul-1), S-phase kinase-associated protein 1 (Skp1) and the RING finger domain containing protein Rbx1 (RING box 1). Cul-1 acts as a rigid molecular scaffold linking and organising the additional subunits. The Cul-1 C-terminal end is able to bind Rbx1, which in turn is required to recruit a specific E2 ubiquitin-conjugating enzyme. The N-terminal domains of Cul-1 associates with Skp-1, an adaptor for interchangeable F-box proteins that directly recognise and specify the substrate (Cardozo and Pagano, 2004) (Figure 30; left).

The variability of F-box motif-containing proteins ensures that a wide range of polypeptides are targeted for poly-ubiquitination and subsequent degradation in response to a wide range of specific signals. In plants, an SCF complex containing transport inhibitor response 1 (TIR1; an auxin signalling F-Box protein (AFB)) can promote the degradation of Auxin/Indole-3-Acetic Acid (Aux/IAA) transcriptional repressors that regulate gene expression during plant development. Importantly targets are recognised only in the presence of auxin (Dharmasiri et al., 2005; Kepinski and Leyser, 2005; Tan et al., 2007). These targets must contain an AID motif that binds to a pocket on TIR1 only when that pocket is also occupied by a bound auxin molecule. As a result, the hormone can mediate substrate-TIR1-SCF interactions, thereby inducing their polyubiquitination and successive re-routing to the proteasome for degradation (Figure 30; right).

In eukaryotes the core SCF components are highly conserved, but TIR1 and AID-substrate orthologs do not exist in animal cells (Nishimura et al., 2009). This feature makes this pathway highly amenable for the examination of molecular processes in animal cells. As long as TIR1 is exogenously expressed and the desired candidate is fused to an AID module, addition of auxin can potentially induce rapid proteasome-dependent degradation of the AID-tagged protein. Moreover, when performed in a cell line in which the endogenous counterpart is removed, this allows rapid functional characterisation of the consequences of rapid loss of the protein target.

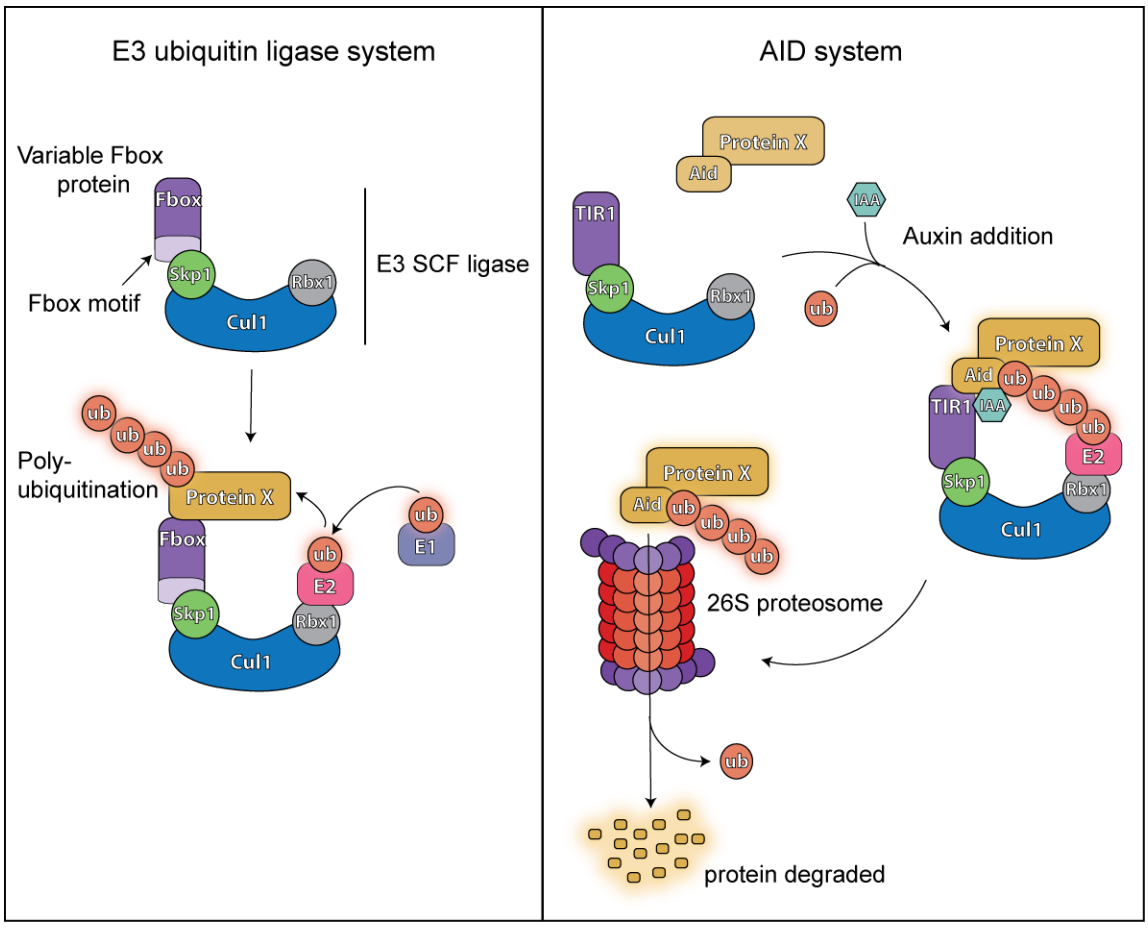

Figure 30. The SCF complex and the AID system. A. The SCF E3 ubiquitin ligase consists of 4 units: Rbx1, Cul-1, Skp1 and F-box containing proteins (FBPs). Cul-1 acts as a bridge forming contacts with Rbx1 and Skp1 at its C and N terminus, respectively. Rbx1 is able to bind E2 ubiquitin-conjugating enzymes primed with ubiquitin previously transferred from an E1 ubiquitin-activating enzyme, while Skp1 directly interacts with the F-box motif of various FBPs. Substrate recognition by FBPs is through protein domains found C-terminal to the Skp1 binding site and includes WD-40 repeats, Leucine-rich repeats (LRR), calponin-homology (CH), Traf-domain like (TDL), zinc-finger domains and many more (Cardozo and Pagano, 2004). This variability ensures tight regulation, so that target proteins are only polyubiquitinated once bought into close proximity with the SCF machinery. **B.** A schematic representation of the auxin-induced degradation system applied in eukaryotes. Auxin hormone (such as IAA) binding to the ectopically expressed TIR1 receptor promotes contacts with target proteins fused to the AID sequence. The SCF-TIR1 E3 ligase can then polyubiquitinate the AID tag, promoting degradation of the substrate by the 26S proteasome.

To date this technique has been employed in yeast (Kanke et al., 2011; Morawska and Ulrich, 2013; Nishimura et al., 2009; Watase et al., 2012), chicken DT40 systems (Nishimura et al., 2009; Nishino et al., 2013) and human cells (Holland et al., 2012;

Nishimura et al., 2009). The original studies were optimised in *S. cerevisiae* and showed that GFP containing a nuclear localisation signal (NLS) and fused via either its N or C terminus with an AID tag (IAA17 of *Arabidopsis thaliana*) could be depleted within 30 minutes of auxin treatment (Nishimura et al., 2009). The method thus allows the freedom to choose which end of the target protein might be more suitable for tagging in terms of maintaining protein functionality. Using this method, proteins localising in chromatin (histone H2B and CENP-A; constituents of nucleosomes) (Holland et al., 2012) and on chromosome-bound macro-molecular complexes (kinetochores (Holland et al., 2012; Nishimura et al., 2009; Nishino et al., 2013) and telomeres (Holland et al., 2012)) can be removed.

For the AID-tagged version of a protein to become functionally essential the endogenous form of the corresponding protein must first be removed. As described in section 3.2, KO backgrounds can be efficiently generated in chicken DT40 cells allowing them to be rapidly combined with this methodology. This has been validated with the kinetochore protein CENP-H, where direct comparison with the tetracycline-repressible cell line (transcriptional repression) highlighted the initial effects of rapid protein depletion: immediate inhibition of proliferation and accumulation in G2/M phase of the cell cycle (Nishimura et al., 2009). Here, I use the auxin-induced degradation system to rapidly deplete the integral kinetochore protein, CENP-T. This was achieved by stably introducing AID-tagged-CENP-T and the TIR1 receptor into a tetracycline-regulated conditional KO background. Although a similar cell line has been generated by direct integration into the endogenous CENP-T gene locus (tetracycline-responsive transgene no longer required) (Nishino et al., 2013), full functional characterisation has not yet been described.

5.2 Results

5.2.1 Generation of the AID-tagged CENP-T cell line

It has previously been shown in CENP-T conditional KO cell lines that suppression of CENP-T transcription leads to mitotic arrest and hypercondensed chromosomes (Hori et al., 2008a). Into this KO cell line I stably incorporated the OsTIR1 receptor and full length CENP-T N-terminally fused to an AID tag (IAA17) (Nishimura et al., 2009) (Figure 31A; Dr Kumiko Samejima cloned this AID plasmid). All together 13 antibiotic resistant colonies were identified, of which 7 successfully expressed the AID construct. In these clones the ability to degrade the degron-tagged CENP-T was assessed by Western blot analysis (Figure 31B). In untreated cells (-/-) two bands were detected using anti-CENP-T antibodies. The lower molecular weight band corresponds to CENP-T expressed from the tetracycline-conditional promoter (**). The upper band is the degron-tagged version of the protein (*). Addition of doxycycline for 72 hours (+/-) eliminates the lower band. Interestingly, the AID-CENP-T protein is concomitantly upregulated in many of the clones. Importantly, these cells continue to proliferate, indicating that AID-CENP-T is functional. Treatment of these cells with auxin for 1 hour (+/+) reduces the upper band. This suggests that the TIR1 protein is expressed and successfully incorporated into the endogenous SCF complex. The efficiency of the auxin depletion is represented as a barplot in Figure 31C using Licor Odyssey imaging to quantitate the bands observed during Western blot analysis. Endogenous levels of CENP-T were measured for WT cells and ideally I wanted the AID-CENP-T fusion to be expressed to a similar extent upon doxycycline addition (-/+). Clones 2, 5 and 6 fit most closely to this criterion. Although all 3 clones displayed reduced levels of the degron-fused CENP-T after treatment with auxin (+/+) I chose clone 6 for further characterisation as it showed the most complete loss of the tagged protein.

Figure 31. Generation of the AID-CENP-T cell line. A. A schematic of CENP-T KO cell line creation and introduction of the AID system. To generate the original CENP-T KO mutant antibiotic resistance cassettes were sequentially targeted to the endogenous CENP-T gene locus via homologous recombination (Histidinol (HisD) and Blastocydine (BS)) (Hori et al., 2008a). A transgene expressing the CENP-T cDNA under the control of a tet-repressible promoter was stably introduced. Tetracycline operator (tetO) repeats in the promoter region provide binding sites for the tetracycline transactivator (tTA). In the presence of doxycycline tTA is mislocalised and cDNA expression is inhibited. Plasmids encoding OsTIR1 and full length CENP-T N-terminally fused with the AID tag were transfected into the KO cell line. The vector consists of a cytomegalovirus (CMV) promoter, the two cDNAs separated by a T2A polypeptide coding sequence and a SV40 polyadenylation sequence. A single polyadenylated mRNA encoding the two proteins is transcribed. This makes the two proteins simultaneously using the T2A for translational processing. **B.** Western blot analysis of whole cell extracts from WT cells and isolated AID-CENP-T clones. A total of $5x10^5$ cells were loaded per well. Cultures were left untreated (-/-), treated with doxycycline for 72 hours (+/-) or left in doxycycline and given auxin for an additional 1 hour (+/+). Blots were probed with anti-CENP-T antibodies to determine the levels of the protein originating from the CENP-T KO background (**) and the AID-tagged construct (*). An antibody against tubulin was used as a loading control. **C.** A histogram showing the relative fluorescence intensities of Western blot bands depicted in (B) quantitated using Licor Odyssey imaging. Values show the CENP-T levels normalised to tubulin signals. WT grey bars represent the endogenous levels of CENP-T, while grey bars from the individual clones depict protein levels originating from the tetracycline-regulated transgene. Blue bars signify the levels of degron-tagged CENP-T.

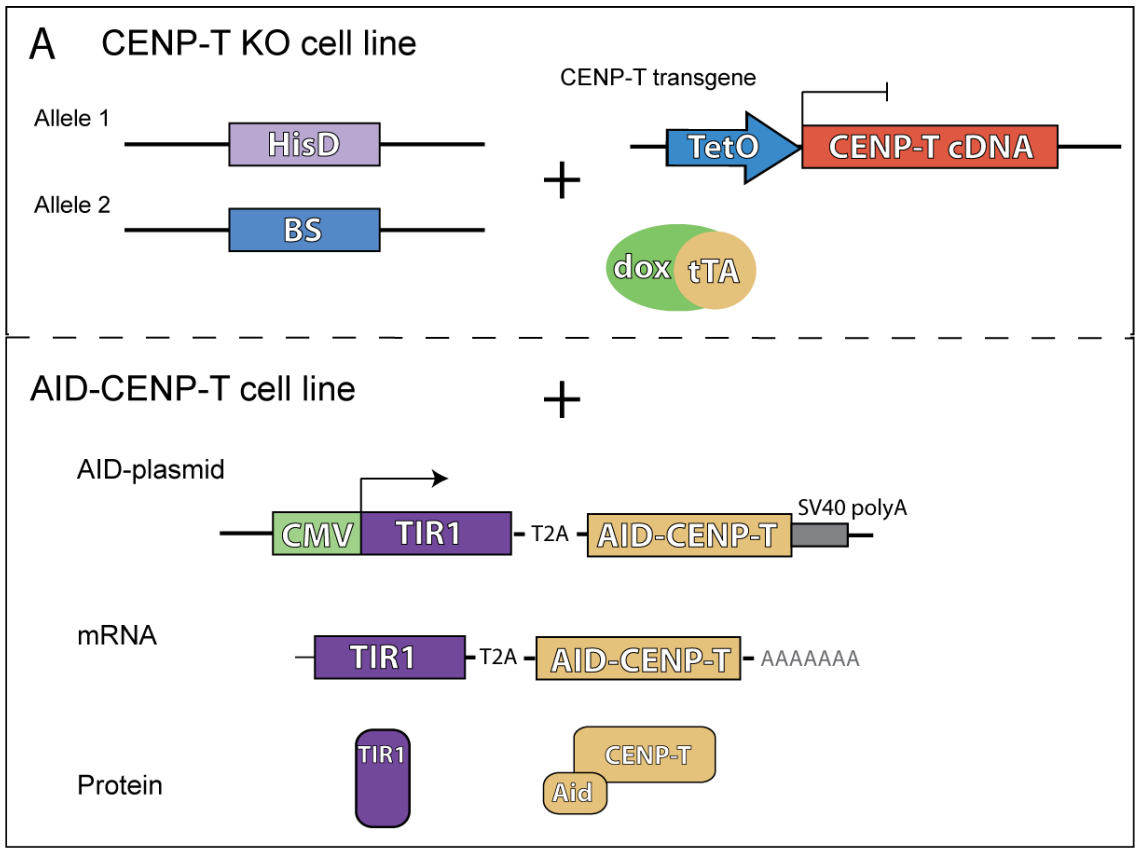
A
CENP-T KO cell line
CENP-T transgene
Allele 1
HisD
TetO
CENP-T cDNA
Allele 2
BS
dox
tTA
AID-CENP-T cell line
AID-plasmid
CMV
TIR1
T2A
AID-CENP-T
SV40 polyA
mRNA
TIR1
T2A
AID-CENP-T
AAAAAAA
Protein
TIR1
CENP-T
Aid

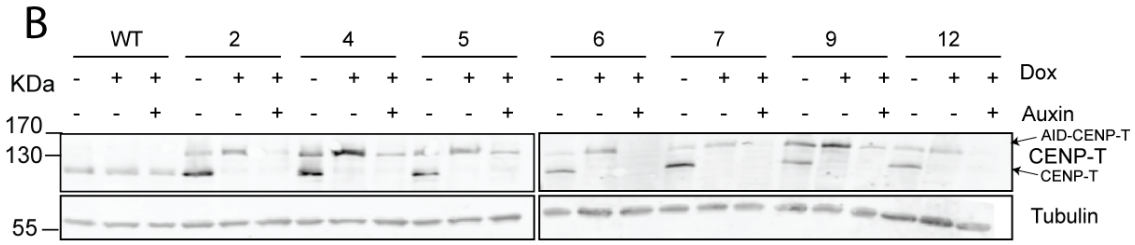
B
WT
2
4
5
6
7
9
12
KDa
Dox
Auxin
170
130
55
AID-CENP-T
CENP-T
CENP-T
Tubulin

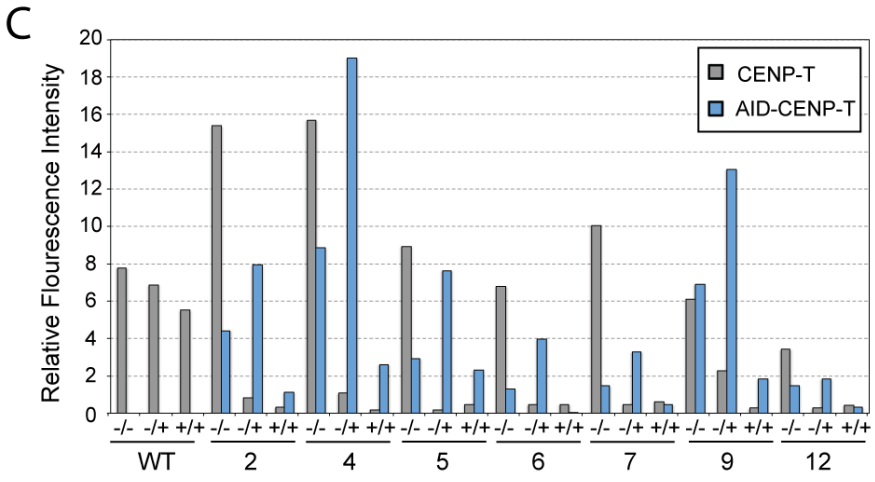
C
Relative Flourescence Intensity
CENP-T
AID-CENP-T
-/- -/+ +/+
WT
2
4
5
6
7
9
12

5.2.2 AID-CENP-T is functional and rapidly/reversibly degraded

Where it has been tested the AID system produces protein depletion within minutes, rather than hours (Holland et al., 2012; Nishimura et al., 2009). To assess the length of time needed for complete depletion of degron-tagged CENP-T in Clone 6 (from now on referred to as the AID-CENP-T cell line) cells were subjected to sequential treatments with doxycycline and auxin and whole cell extracts analysed by Western blot. After 24 hours of doxycycline treatment tetracycline-regulated CENP-T signals were no longer detected (**), while the upper band demonstrates upregulation of AID-CENP-T (*) (Figure 32A). The levels of the AID-CENP-T fusion protein remain the same after 2 and 3 days of doxycycline treatment and are comparable with WT CENP-T protein levels. Strikingly, rapid loss of this fusion protein was seen within minutes of auxin addition and no visible signal was observed after 1 hour. This information is summarised quantitatively in Figure 32B using Licor Odyssey imaging to measure signals from individual Western blot bands. As expected, this is significantly different to the original tetracycline conditional KO cell line (Figure 32A; right panels) where residual levels of CENP-T were observed even after 72 hours of doxycycline treatment. Even though they use the same system it is still unclear why doxycycline addition after 24 hours in the AID-CENP-T cell line leads to a significant reduction in the levels of tetracycline-regulated CENP-T, while residual levels are still present in the CENP-T KO cell line after 72 hours. One explanation could be that the CENP-T KO cell line is no longer derived from a single clone and there might be a subpopulation that is less sensitive to doxycycline treatment.

To establish how rapid loss of CENP-T affects cell proliferation I compared the growth rates of WT DT40 cells, CENP-T KO mutants and the AID-CENP-T cell line using a trypan blue exclusion assay (Figure 32C). Cells were grown with and without doxycycline for 96 hours, at which point auxin was added to all cultures. In the presence of doxycycline the conditional KO cell line stops proliferating after 48-72 hours. The same doxycycline treatment had no affect on AID-CENP-T cell growth. However if

auxin was added at 96 hours, inhibition of proliferation was immediate. In controls, AID-CENP-T cells cultured in the absence of doxycycline and subsequently treated with auxin did not display growth defects. Taken together, these experiments reveal that degron-tagged CENP-T is able to functionally replace the tetracycline-regulated version of the protein. Although the overall rate of cell growth was slightly reduced in the KO and its AID-CENP-T subline when compared to the WT cells, neither doxycycline nor auxin treatment impacts negatively on cell proliferation in the WT cells at this concentration (125uM auxin, 0.5ug/ml Doxycycline).

An advantageous feature of the AID system is that the target protein can be rapidly recovered by removing the auxin. To test the ability of the AID-CENP-T fusion to re-accumulate at the protein level cells maintained in doxycycline for 72 hours were treated with auxin for 1 hour to deplete the AID-CENP-T fusion. Cells were subsequently washed and grown in media without auxin to see how long it took for AID-CENP-T protein levels to return. The upper band of the Western blot corresponds to the AID-CENP-T fusion protein (*). This band is clearly absent from WT and CENP-T KO cell lines (Figure 32D). Antibodies against CENP-T demonstrate that levels of AID-CENP-T begin to recover 30 minutes after withdrawal of the hormone. After 3 hours, signals for the degron-tagged protein are comparable with those seen for doxycycline treated cells (i.e. before auxin addition). Thus, CENP-T removal in this cell line is rapid and reversible.

Figure 32. Comparing DT40 cell lines depleted of CENP-T at the mRNA or protein levels. **A.** Immunoblot detection of endogenous CENP-T (WT cells), exogenously expressed CENP-T in the tetracycline-regulated KO cell line (**), or AID-tagged CENP-T (*). Doxycycline was added at time 0 and cells harvested every 24 hours for 3 days. AID-CENP-T cell lines were further treated with auxin and cell lysates taken 15 minutes, 30 minutes and 1 hour after addition. $5x10^5$ cells were loaded per well and anti-tubulin blots used as a loading control. **B.** Histogram corresponding to the signal intensity of immunoblot bands in (A, top panel). Relative fluorescence intensities measured by Licor Odyssey imaging were normalised to tubulin signals. **C.** Growth curves of WT, CENP-T KO and the AID-CENP-T cell lines in the presence or absence of doxycycline. Doxycycline was introduced at time 0 and viable cells counted every 24 hours using trypan blue staining. At 96 hours, auxin was added to all cell populations and cells counted as described above. CENP-T KO cells gradually stop proliferating after doxycycline treatment, while auxin addition only affects the growth of AID-CENP-T cells maintained in doxycycline. **D.** Same as in (A) but followed by additional wash steps to remove the auxin. Cell lysates were taken 30 minutes, 1, 3, 9 and 12 hours after the wash step. $2.5x10^5$ cells were loaded per well.

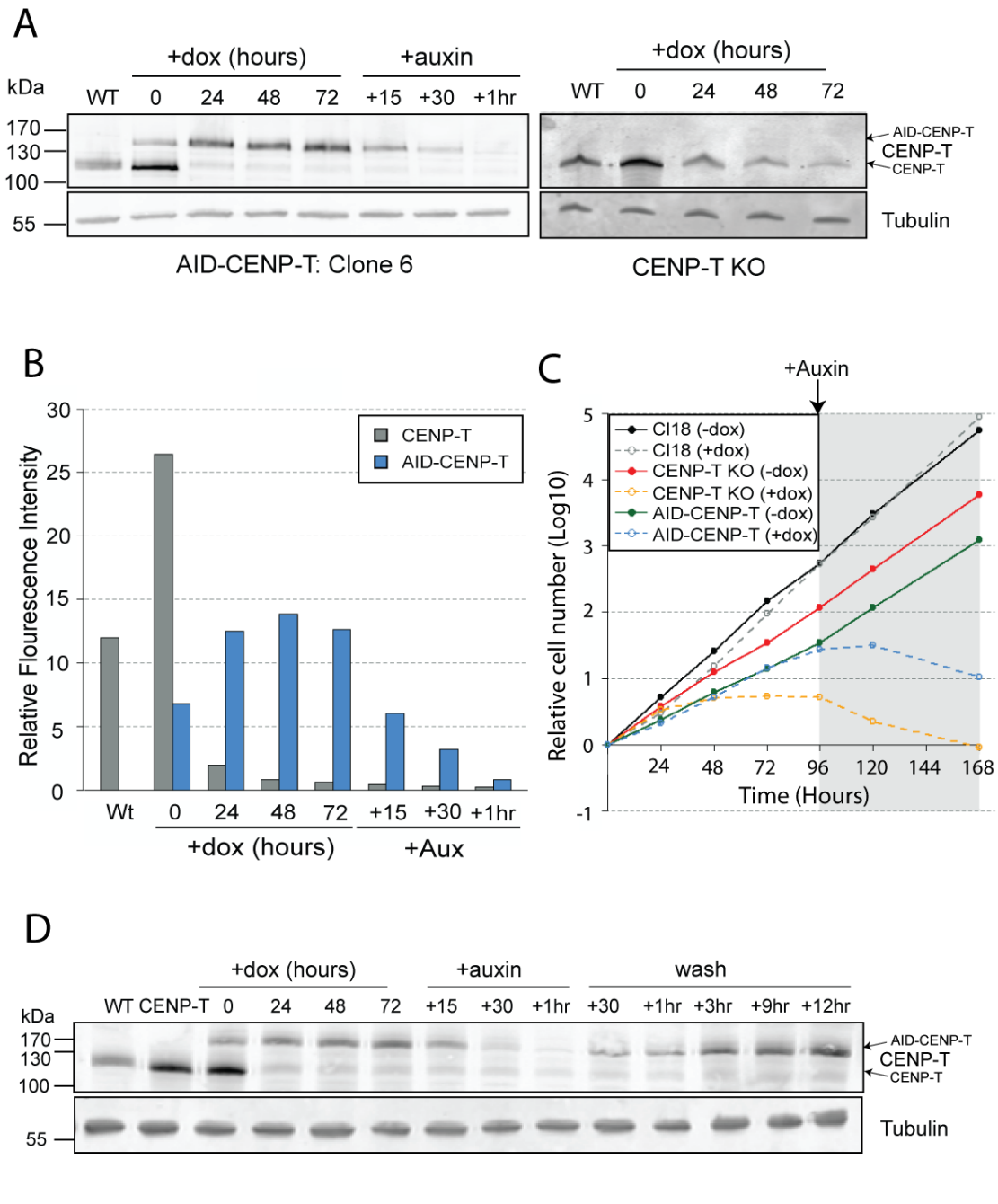
A
+dox (hours)
+auxin
kDa
WT 0 24 48 72 +15 +30 +1hr
170
130
100
55
AID-CENP-T
CENP-T
CENP-T
Tubulin
AID-CENP-T: Clone 6
+dox (hours)
WT 0 24 48 72
CENP-T KO
B
Relative Flourescence Intensity
CENP-T
AID-CENP-T
Wt 0 24 48 72 +15 +30 +1hr
+dox (hours)
+Aux
C
+Auxin
Relative cell number (Log10)
CI18 (-dox)
CI18 (+dox)
CENP-T KO (-dox)
CENP-T KO (+dox)
AID-CENP-T (-dox)
AID-CENP-T (+dox)
Time (Hours)
D
+dox (hours)
+auxin
wash
WT CENP-T 0 24 48 72 +15 +30 +1hr +30 +1hr +3hr +9hr +12hr
kDa
170
130
100
55
AID-CENP-T
CENP-T
CENP-T
Tubulin

5.2.3 AID-CENP-T is rapidly depleted from mitotic kinetochores

I next wanted to determine whether AID-tagged CENP-T localised correctly to kinetochores. AID-CENP-T cells were maintained in doxycycline, thus according to Western blot analysis any kinetochore signals of CENP-T are likely to be attributable to the AID-fusion protein. To confirm this, signal distribution was examined by immunofluorescence and kinetochores were identified by transient transfection with GFP-CENP-A. Similar to WT and CENP-T KO populations, I found distinct CENP-T signals co-localising with kinetochores in untreated and mock-treated (+EtOH) mitotic cells (Figure 33). However, this punctate pattern was abolished when cells were cultured for 1 hour in auxin, even though GFP-CENP-A signals were still clearly visible. An imageJ macro based on CraQcode v1.06 (Bodor et al., 2012) and adjusted by Nuno Martins (Earnshaw lab) was used to quantify CENP-T signals at kinetochores. Signal intensities of each protein (% ± standard deviation) were measured using the mean signal intensity per centromere relative to an adjacent local background. Centromeres were detected using the GFP-CENP-A signal. The localisation of CENP-T signals at kinetochores in prometaphase auxin treated cells was reduced to 16-20% when compared with ethanol treated cells. This indicates that a population of the AID-CENP-T signal has not yet been degraded and may require a longer treatment with auxin before a more complete depletion is achieved. Therefore, the AID-CENP-T fusion cannot only localise to kinetochores, but its incorporation into the macromolecular complex does not affect its ability to be speedily degraded by the ubiquitin ligase system.

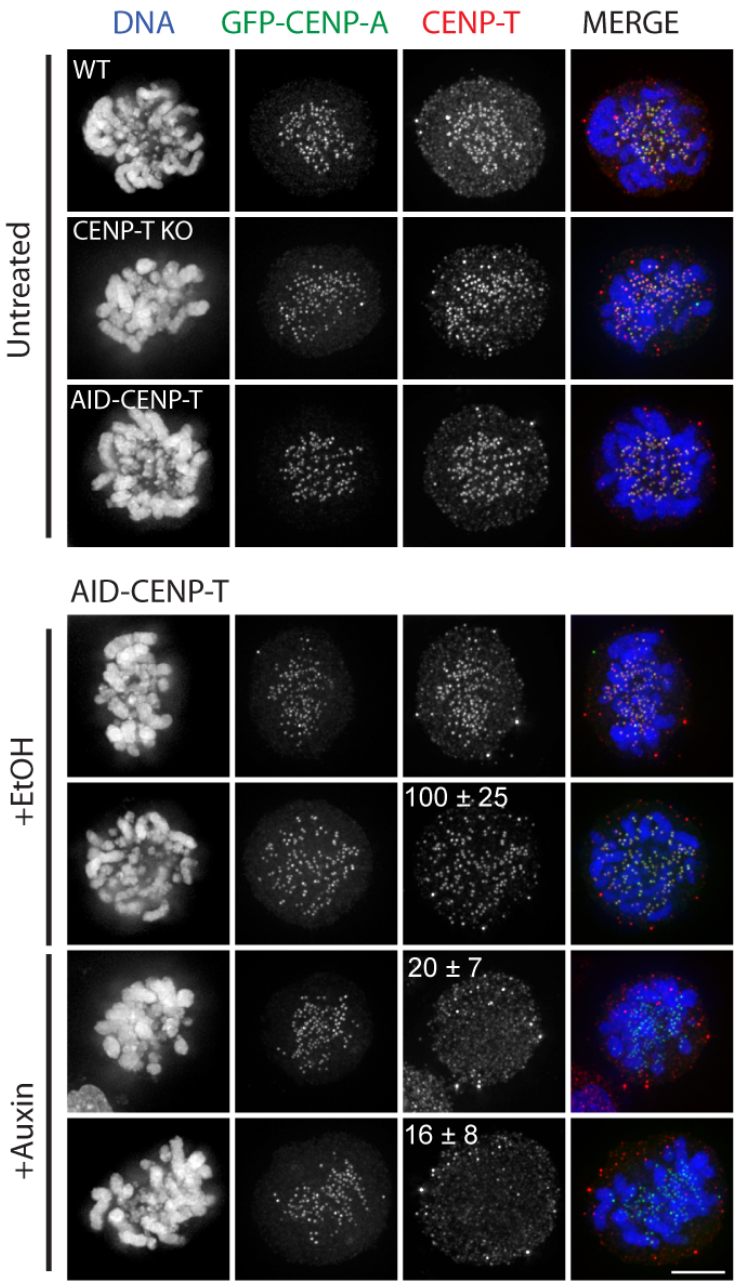

Figure 33. CENP-T is absent from kinetochores after treatment with auxin. GFP-CENP-A was introduced into WT, CENP-T KO or AID-CENP-T cell lines. ~40 hours after transfection cells were either left untreated or cultured with ethanol (+EtOH) or auxin (+Auxin) for 1 hour (AID cells were maintained in doxycycline at all times). Attachment to polylysine coated coverslips was followed by fixation and staining using antibodies against CENP-T. DAPI depicts DNA staining. Signal intensities of each protein (% ± standard deviation) were measured using the mean signal intensity per centromere relative to an adjacent local background. Centromeres were detected using the GFP-CENP-A signal. Scale bar: 5 μm.

5.2.4 CENP-T is required for centromeric localisation of CENP-O, CENP-H and Ndc80 complexes

Above I demonstrate that CENP-T can be rapidly depleted from kinetochores using the AID system. Importantly, this system allows CENP-T dependent assembly networks within the kinetochore to be defined within the first cell cycle after protein depletion.

It has been shown that many CCAN components and outer kinetochore proteins are dependent on CENP-T for their localisation to centromeres (Gascoigne et al., 2011; Hori et al., 2008a; Nishino et al., 2013). To ask whether these proteins require CENP-T for their maintenance at kinetochores, cells maintained in doxycycline were subjected to an additional 6 hour treatment with ethanol or the auxin hormone. Antibodies against GgCENP-O, GgCENP-H and GgNdc80 were used to verify co-localisation with transiently transfected GFP-CENP-A (Figures 34A, C and B, respectively). Although a punctate distribution co-localising with GFP-CENP-A could be seen to different extents with all chicken antibodies listed above, there was also a significant amount of background signal. Maximum intensity projections of all stacks taken from the top to the bottom of the cell often masked kinetochore co-localisation due to the high background. Therefore, for display purposes images are represented by maximum projections of 10 stacks (0.2 μm distance between stacks; i.e. a 2 μm section through a cell). It should be noted that quantitation analysis was performed with all stacks.

In chicken DT40 cells, immunofluorescence studies have shown that CENP-O complex components are depleted from kinetochores absent of CENP-T signals (Hori et al., 2008a). Here, in the mock treated cell populations (+EtOH) kinetochore signals are detected for CENP-O, but upon auxin treatment this distribution is visibly reduced. In prometaphase cells, CENP-O loss ranges from ~37-52% of normal levels, while in metaphase cells ~39% of the protein remains. This is similar to CENP-O abundance levels on chromosomes in CENP-W KO cells, which was only reduced by ~1.5 fold in SILAC experiments (~66% of normal wild type levels; section 3.2.4). As CENP-O is not

reduced to the same extent as CENP-T, these experiments would suggest that an additional pathway is required for its maintenance at kinetochores.

In AID-CENP-T depleted cells (+Auxin) Ndc80 signals are also reduced, although it is possible to observe residual staining at some GFP-CENP-A loci (Figure 34B). The levels of Ndc80 range from 61-86% of normal levels in auxin treated cells. This suggests that the Ndc80 complex relies on additional factors for its maintenance at kinetochores. This is consistent with studies that have also used AID dependent depletion of CENP-T to look at Ndc80 assembly networks. There, it was suggested that Mis12 components form a parallel targeting pathway (Nishino et al., 2013). In the CENP-W KO cell line, SILAC proteomics analysis showed that Ndc80 complex components are reduced by just over 2-fold (equivalent to 50% of normal levels). Mis12 complex components are also partly reduced in this experiment and could account for the more complete loss of the Ndc80 complex.

Quantitative immunofluorescence analysis suggested that CENP-H signals at kinetochores were greatly increased in auxin treated cells when compared with the mock treated (+EtOH) control cells (143-188%). Increased CENP-H signal intensity was not observed at GFP-CENP-A loci in magnified regions of cell sections (Figure 34C). In addition, SILAC proteomics analysis of CENP-W KO cells found that CENP-H is partially depleted (>1.5 fold change) from chromosomes absent of CENP-T (section 3.2.4). One possibility is that protein depletion of CENP-T within a single cell cycle acts to recruit CENP-H to kinetochores. However, it is more likely that background signals associated with CENP-H antibody staining affected the quantitative analysis of centromeric signals.

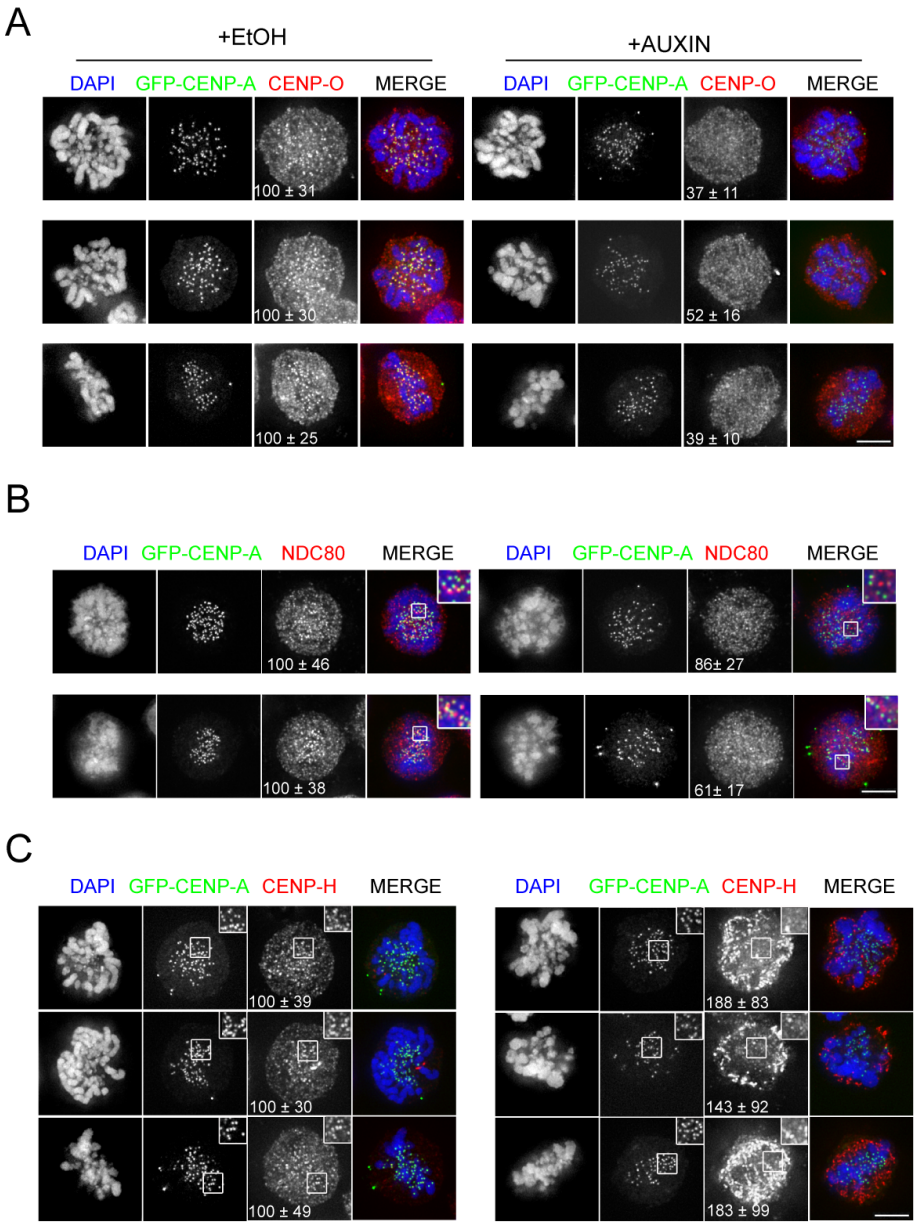

Figure 34. Inner and outer kinetochore components are dependent on CENP-T for their localisation to kinetochores. AID-CENP-T cells maintained in doxycycline and expressing transiently transfected GFP-CENPA (~40 hours) were treated with ethanol (+EtOH) or auxin (+Auxin) for 6 hours before fixation and immunofluorescence analysis. Mitotic cells were probed with **A.** anti-GgCENP-O **B.** anti-GgNdc80 and **C.** anti-GgCENP-H antibodies. Signals were detected with Alexa Fluor 594 conjugated secondary antibodies (red). DNA was counterstained with DAPI (blue). Signal intensities of each protein (% ± standard deviation) were measured using the mean signal intensity per centromere relative to an adjacent local background. Centromeres were detected using the GFP-CENP-A signal. Scale bar: 5 μm.

5.2.5 Rapid loss of CENP-T results in prometaphase arrest and cell death

Phenotypes associated with conditional KO of CENP-T have included mitotic arrests and the development of hypercondensed chromosomes (Hori et al., 2008a). However, these phenotypes develop in the context of gradual depletion over several cell cycles. The AID system provides an opportunity to study the consequences of CENP-T depletion within a single cell cycle. Asynchronous populations of AID-CENP-T cells (maintained in doxycycline to suppress expression of the untagged cDNA) were treated with auxin for 6, 9, 12 and 24 hours (Figure 35). When compared with ethanol treated controls a clear accumulation of cells in mitosis was observed. This was characterised by a prometaphase arrest that displayed varying phenotypic severities. In the magnified images in Figure 35, a subgroup of chromosomes can be seen localising to one side of the cell and by 24 hours this cluster became hypercondensed in appearance.

To examine the development of this mitotic phenotype, DNA and immunofluorescence staining of microtubules were used (Figure 36A). As aforementioned, in the presence of auxin most cells block in mitosis. This is extremely penetrant, with 70-80% of cells displaying a mitotic arrest after 12 hours of auxin treatment (Figure 36B). These mitotically arrested cells exhibit high rates of aberrant prometaphases. Two predominant phenotypes were observed (Figure 36A). Phenotype 1: cells could be seen with a large cluster of chromosomes residing on one side of the cell and an ill-defined bipolar spindle on the other. Smaller, individual chromosomes were often found in the vicinity of the bipolar spindle. Phenotype 2: cells displayed hypercondensed clumps of chromosomes with a highly abnormal spindle morphology. In some instances these spindles appear monopolar in appearance, however without centrosomal staining we were unable to confirm these observations.

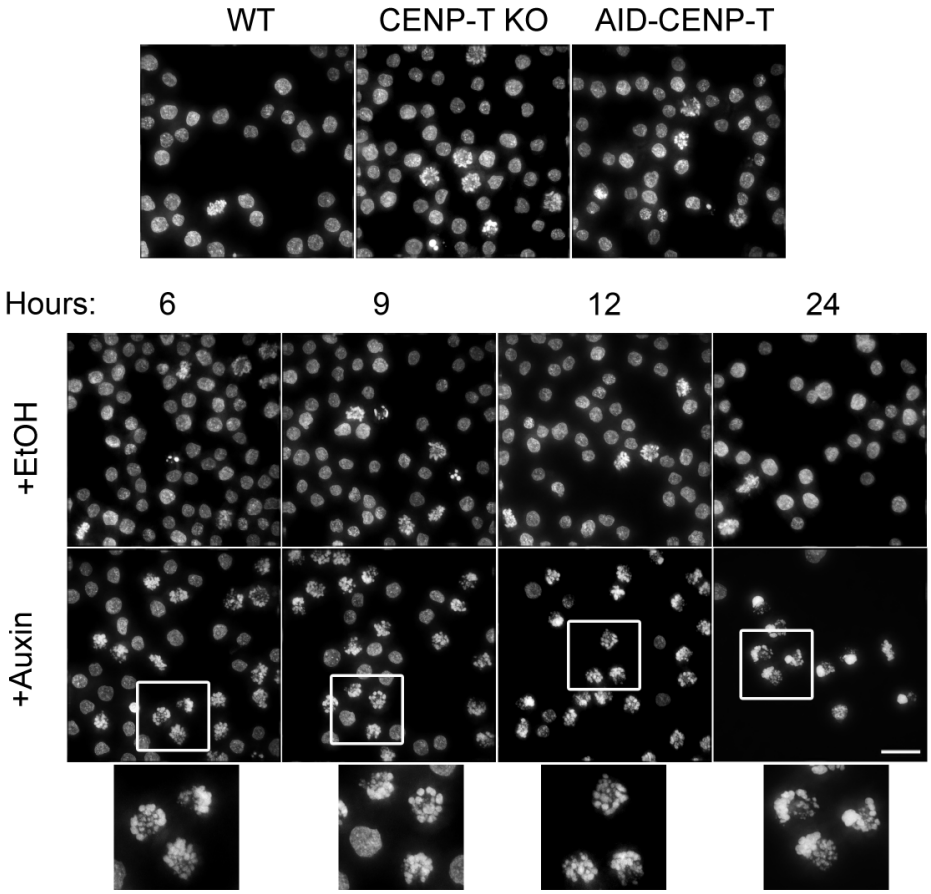

Figure 35. Rapid CENP-T depletion at the protein level leads to a mitotic arrest. The top panel depicts untreated WT, CENP-T KO and AID-CENP-T cell lines. AID-CENP-T cells maintained in doxycycline were treated with ethanol (+EtOH) or auxin (+Auxin) for the indicated times. The inset shows a zoomed in view of auxin treated cells as defined by the white squares. Images were taken with a 60x objective. Scale bar: 20 μm.

The relative distribution of AID-CENP-T cells in the various mitotic phases are shown as percentages in Figure 36B (right) together with the percentages of the two dominant phenotypes. We observed that CENP-T knockouts and AID-CENP-T cell lines, even in the absence of auxin, have a higher number of cells in prometaphase in comparison to WT DT40s. An increased background level of cells displaying multipolar spindles was also identified (data not shown). This could explain the slower rates of growth observed in both of these cell populations (refer to Figure 32C).

Figure 36. Cell cycle phenotype associated with rapid depletion of CENP-T. A. DT40 AID-CENP-T cells maintained in doxycycline were treated with ethanol (+EtOH) or auxin (+Auxin) for 3, 6, 9 and 24 hours. After the indicated time period, cells were processed for immunofluorescence and stained with DAPI (DNA; Blue) and anti-tubulin (mitotic spindle; Red). WT, CENP-T KO and untreated AID-CENP-T cells were fixed and stained in the same way. The top panel shows representative cell cycle images of prometaphase, metaphase, anaphase and cytokinesis. Typical prometaphase phenotypes associated with untreated (-drugs), ethanol treated (+EtOH) and auxin treated (+Auxin) cells are also shown. Phenotype 1 is characterised by chromosomes and a bipolar spindle that are pushed to one side of the cell, while phenotype 2 depicts chromosomes that have a severe hypercondensed appearance. Scale bar: 5 μm. **B.** Cell count of experiment illustrated in (A). Left graph reports the mean percentage +/- Standard Error (SE) of mitotic vs interphase cell number (2 repeats; N=~500). Right graph depicts the cell counts associated with mitotic phenotypes. The means as a percentage +/- SE are depicted for two repeats (N=~100). Ethanol treated cells are not shown **C.** Representative flow cytometry analysis measuring the total population of apoptotic cells. Fluorescence intensity of the PE-Annexin V signal, a marker for apoptotic cells, is shown on the x-axis and cell count is displayed on the y-axis. The percentage of cells represented in the right peak showing high Annexin-V signal intensity is normalised to unstained controls. A graph displaying the mean percentage +/- SE of apoptotic cells from 3 repeats is shown.

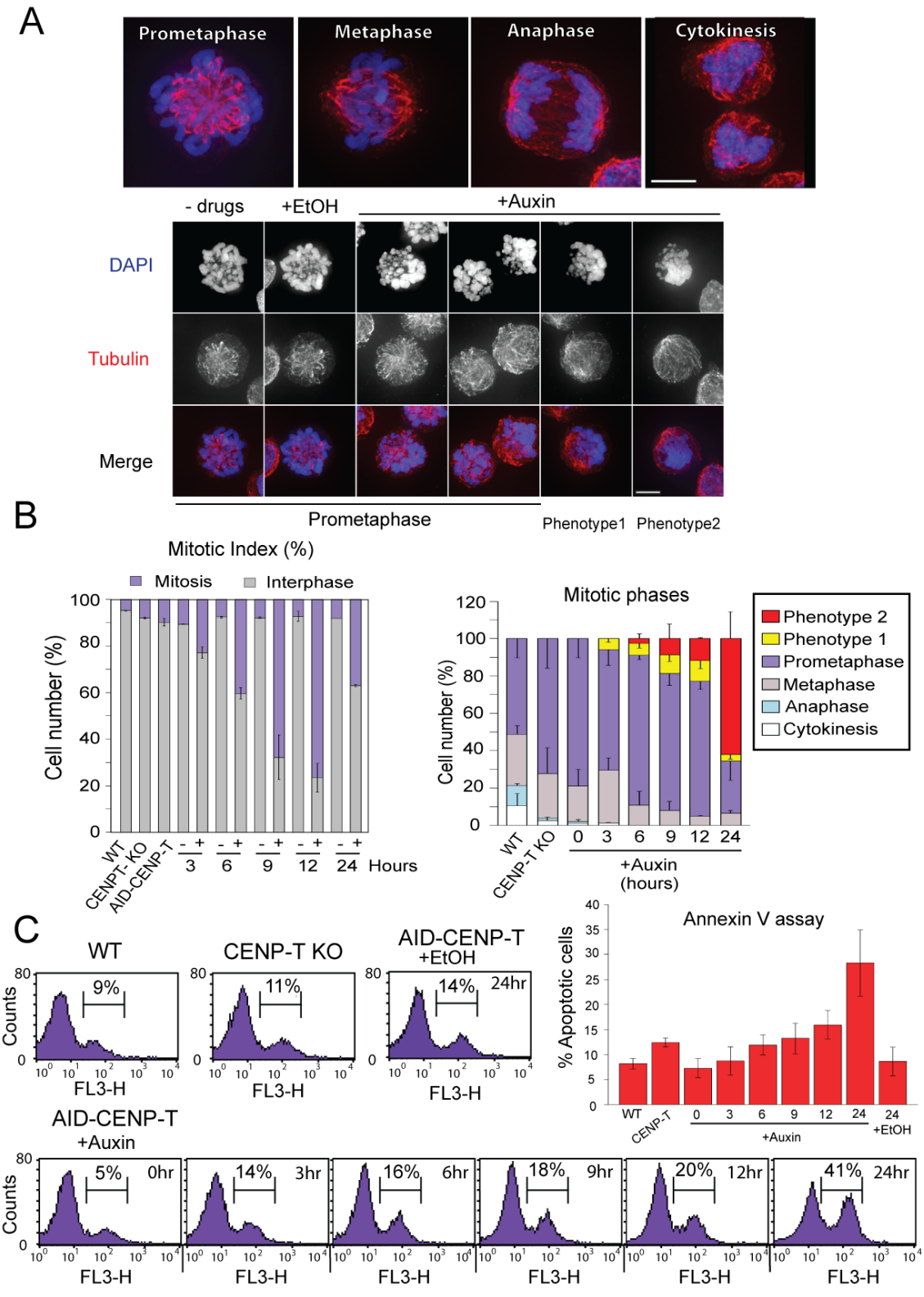
A
Prometaphase
Metaphase
Anaphase
Cytokinesis
- drugs
+EtOH
+Auxin
DAPI
Tubulin
Merge
Prometaphase
Phenotype1
Phenotype2
B
Mitotic Index (%)
Mitosis
Interphase
Cell number (%)
WT
CENPT- KO
AID-CENP-T
Hours
Mitotic phases
Phenotype 2
Phenotype 1
Prometaphase
Metaphase
Anaphase
Cytokinesis
+Auxin
(hours)
C
WT
CENP-T KO
AID-CENP-T
+EtOH
Counts
FL3-H
9%
11%
14%
24hr
Annexin V assay
% Apoptotic cells
+EtOH
AID-CENP-T
+Auxin
5%
0hr
14%
3hr
16%
6hr
18%
9hr
20%
12hr
41%
24hr

In the presence of auxin the percentage of cells blocked specifically in prometaphase was increased, with no cells representing anaphase or cytokinesis counted past the 6 hour treatment point. It should be noted that this prometaphase population did not display 'normal' chromosome distributions, but was too similar to the untreated counterpart to be scored as a discrete phenotype. The percentage of cells categorised as phenotype 1 or phenotype 2 gradually increased with prolonged auxin treatment. At 24 hours this included >60% of cells, with the highest proportion formed from phenotype 2. This progression suggests that cells are unable to align chromosomes on the metaphase plate and instead arrest in prometaphase for prolonged periods, eventually leading to irreversible chromatin condensation events.

If the mitotic block following CENP-T depletion is irreversible we would expect to eventually observe high rates of cell death. However, the apoptotic index could not be accurately determined in the microscope as cells in this state freely detach from the coverslip. I did find increased incidence of interphase cells 24 hours after auxin treatment when compared with the 12 hour time point. One explanation for this could be that the previously mitotic populations had progressed into cell death and therefore been released. To overcome this technical hurdle, an alternative assay was employed. This utilises the ability of Annexin V to strongly associate with phosphatidylserine which becomes externalised on the cell membrane during cell death/apoptosis. Flow cytometry analysis was used to detect those cells bound by fluorescent conjugates of Annexin V (Figure 36C). Cell populations positive for this mark gradually increased upon extended periods of exposure to auxin (% values). Maximum levels were seen at 24 hours with >30% of cells displaying an apoptotic phenotype. Importantly, this increase was not seen with ethanol treatment alone (ethanol is the vehicle for auxin: +EtOH; 24 hours).

I conclude that rapid depletion of CENP-T eventually leads to cell death.

5.2.6 Absence of CENP-T results in MT attachment defects

Above I show that the assembly of specific kinetochore proteins is disrupted upon CENP-T depletion and that cells subjected to this treatment do not progress past a prometaphase arrest. The most likely explanation for this is that unaligned chromosomes may not be able to form a robust metaphase plate because of defects in microtubule attachments. To examine this further, cells were transfected with GFP-CENP-A and spindle microtubules visualised by immunofluorescence. In WT and CENP-T ON tetracycline-repressive conditional KO cell lines (-doxycycline), prometaphase and metaphase-aligned chromosomes with bipolar attachments were readily observed (Figure 37; arrow heads). Similarly, AID-CENP-T cell lines treated with ethanol (+EtOH) (maintained in doxycycline) display many chromosomes in a bioriented state. However, in CENP-T depleted AID-CENP-T cells (+Auxin) there appeared to be a reduction in the number of GFP-CENP-A signals making contacts with spindle microtubules. Although chromosomal bi-orientation was infrequently observed, some apparent end-on attachments were still visible, as indicated by the arrowheads. As described earlier, in more severe prometaphase phenotypes bipolar spindles could form, but these frequently occupied an off-centre location and did not display the 'robust' morphology associated with metaphase cells. Smaller individual chromosomes remained in close proximity to these abnormal spindles, while larger clusters tended to distribute to the opposite side of the cell. The nature of K-MT interactions for these smaller distinct chromosomes was not entirely clear from these experiments, as they were quite often found in dense regions of tubulin staining. However, we did observe GFP-CENP-A signals orientated in a way that could suggest lateral interactions with spindle microtubules (Figure 37; stars).

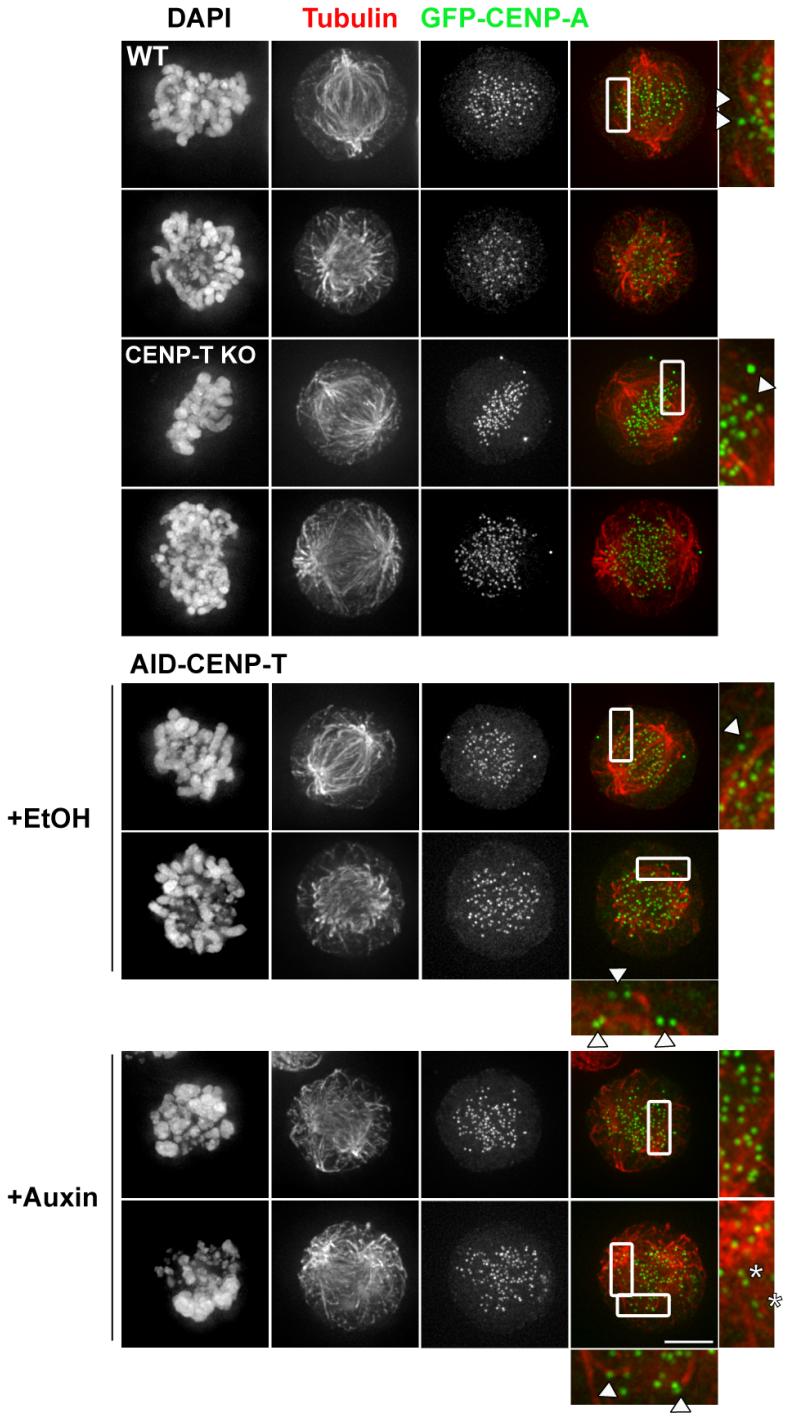

Figure 37. CENP-T loss leads to microtubule attachment defects. GFP-CENP-A was introduced into WT, CENP-T KO or AID-CENP-T cell lines. ~40 hours after transfection cells were either left untreated or cultured with ethanol (+EtOH) or auxin (+Auxin) for 6.5 hours (AID-CENP-T cells must be maintained in doxycycline at all times). Attachment to polylysine coated coverslips was followed by fixation and staining using antibodies against tubulin. DAPI depicts DNA staining. Scale bar: 5 μm.

Correlation Light Electron Microscopy (CLEM) was employed to further study K-MT interactions in these phenotypes at the ultrastructural level. In CLEM, light microscopy images can be used as a reference for the identification of a cell of interest, which can then be processed for electron microscopy. Samples were prepared on gridded coverslips where co-ordinates can be used to determine the exact location of a cell. In prometaphase/metaphase and/or displaying the auxin induced phenotype. WT cells and AID-CENP-T cells treated with auxin for 6.5 hours were fixed and counterstained with DAPI. After light microscopy imaging, ribbons of 85 nm longitudinal sections were collected on formvar coated copper grids. In Figure 38A a representative electron micrograph of WT DT40 cells displaying bioriented K-MT attachments is shown. In these control cells we observed electron dense structures corresponding to the inner and outer plates of the kinetochore (white arrows) and microtubules orientated towards these regions (black arrows). Similar structures were not found in CENP-T deficient cells (Figure 38B and C). Instead, we observed microtubules that passed close to the surface of chromosomes. Although kinetochore plates were not obvious, this is consistent with our conclusion that some CENP-T depleted kinetochore remnants may be able to participate in lateral interactions with microtubules.

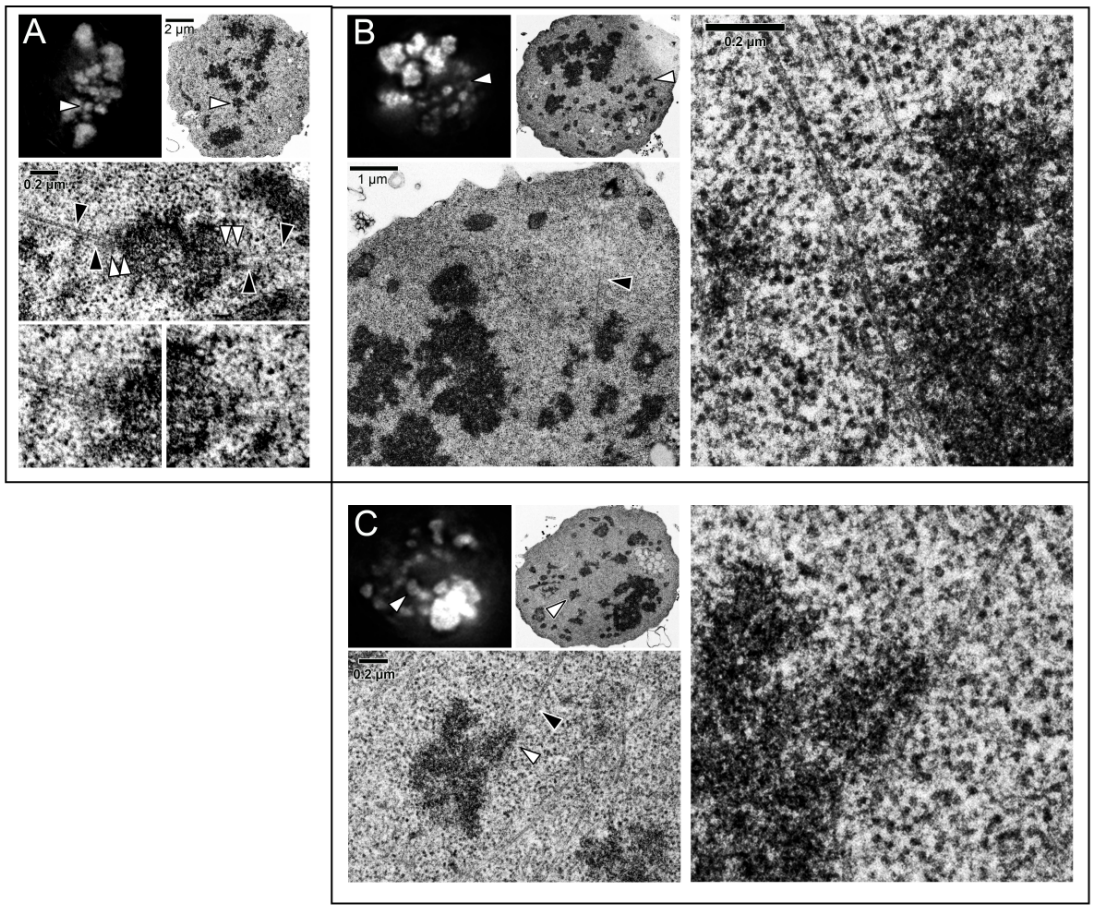

Figure 38. CLEM of AID-CENP-T depleted cells. A. Light microscopy image (DAPI; left) of a WT metaphase cell subsequently processed for thin-section transmission electron microscopy (TEM; right). White arrows depict a metaphase aligned chromosome, with lower panels displaying magnified electron micrographs of the chromosome of interest. In these images white arrows highlight inner and outer kinetochore plates, while black arrows signify microtubules. **B.** Mild and **C.** Severe phenotypes associated with rapid CENP-T depletion. AID-CENP-T cells were treated with auxin for 6.5 hours before immediate processing for electron microscopy. Cells analysed by light microscopy (DAPI; left) and TEM (right) are depicted. White arrows mark the chromosome of interest. Magnified EM images show sites of potential K-MT lateral interactions. Black arrows depict microtubules, while white arrows show interactions with chromosomes. Scale bar as indicated. CLEM processing and imaging was performed by myself and Dr Daniel Booth.

5.3 Discussion

5.3.1 The AID system for rapid protein loss of CENP-T

In this study I have performed preliminary characterisation of a CENP-T auxin-degron allele in DT40 cells. As has been shown previously for other kinetochore proteins (Holland et al., 2012; Nishimura et al., 2009), the fact that CENP-T is a core component of a macromolecular complex does not affect its ability to be degraded from kinetochores during mitosis. Importantly, this depletion is fast, yet reversible, and the AID-tagged protein can functionally replace the endogenous counterpart.

5.3.1.1 Characterisation of the AID-CENP-T cell line

Loss of function cell lines using a tetracycline-regulated promoter to repress CENP-T at the level of transcription arrest in mitosis, with a 48 hour tetracycline treatment capable of promoting a block in G2/M in 57% of cells (Hori et al., 2008a). In contrast, we find that >70% of cells halt in mitosis after only 12 hours using the AID system. Our data demonstrate a progression from prometaphase arrest into phenotypes characterised by hypercondensed chromosomes displaced from abnormal spindles. Similar observations were also reported through live cell imaging of CENP-W conditional KO cells and Ndc80 tet-repressive cells (Hori et al., 2008a; Hori et al., 2003). Here I elaborate on this finding and have used fixed cells to describe two intermediate phenotypes preceding cell death. First, I observed cells displaying an ill-defined bipolar spindle with large chromosomal clusters positioned at the opposite side of the cell. Second, I observed hypercondensed clumps of chromosomes with highly abnormal spindles. Interestingly, cell counts at various time points suggest that phenotype 2 follows on from phenotype 1, as it accumulates during more prolonged auxin treatments.

This was a terminal phenotype as no anaphase cells were seen after 3 hours of auxin treatment and cell death increased after arresting in mitosis. In Ndc80 KO cell lines,

shortly after entering mitosis an abnormal spindle is formed with similar phenotypic properties as described above, followed by a ~400 minute prometaphase arrest and subsequent cell death (Hori et al., 2003). This phenotype is not a feature of all essential kinetochore proteins as CENP-H (Fukagawa et al., 2001), CENP-I (Nishihashi et al., 2002) and CENP-C (Kwon et al., 2007) can progress to the next cell cycle after a mitotic delay. This would functionally link CENP-T with Ndc80 and is corroborated by recent publications that show direct interactions between CENP-T and Ndc80 complex components (Bock et al., 2012; Gascoigne and Cheeseman, 2013; Gascoigne et al., 2011; Malvezzi et al., 2013; Nishino et al., 2013; Schleiffer et al., 2012). We aimed to confirm this progression using in vivo time-lapse imaging, however several attempts to make stable AID cells expressing mcherry-H2B and GFP-tubulin were unsuccessful. Conditions have now been set up to visualise AID cells after transient transfection of those two constructs.

I used immunofluorescence and electron microscopy techniques to try and ascertain whether kinetochores could still form end-on attachments following rapid depletion of CENP-T. Although chromosome bi-orientation was dramatically inhibited, some end-on, and possibly lateral K-MT attachments were still observed. Interestingly, in those cells that maintained some form of bipolar spindle a population of small individual chromosomes was seen in the vicinity of this structure; whereas larger, condensed chromatin clusters were not. Chicken DT40 cells possess 10 pairs of macro-chromosomes, 28 pairs of micro-chromosomes and Z/X sex chromosomes (Masabanda et al., 2004; Shang et al., 2010). It is possible that residual levels of KMN components (Ndc80 described above) could initially support the movement of micro-chromosomes, while unstable attachments are not robust enough to cope with the pulling-forces generated during the transport of larger chromosomes. If this threshold value holds true, this particular phenotype could act as a read-out of kinetochores that have partially lost their ability to form load-bearing attachments.

In the future the stability of K-MT attachments will be examined using a cold shock assay. In comparison to non-K-MTs, K-MTs are less sensitive to cooling at 4°C and remain stable during short cold treatments (Rieder, 1981). Transiently expressing GFP-CENP-A and staining for anti-tubulin would allow quantification of kinetochores with cold-stable microtubule fibres. Another method to assess stable chromosome bi-orientation is to measure interkinetochore distances, as disrupting these connections reduces the tension across sister kinetochores and negatively affects centromere stretching (Waters et al., 1996). Those chromosomes that cannot successfully align will have smaller interkinetochore distances.

Attempts to analyse auxin treated cells at the ultrastructural level were not conclusive. It was readily possible to find bi-orientated chromosomes and structures that resemble kinetochores in unperturbed cell populations. But it became very difficult to interpret attachments in auxin-treated AID cells. Previous EM images have shown that loss of CENP-T effectively removes blocks of electron dense material forming the outer plate (Hori et al., 2008a). For this reason we found it was very difficult to identify chromosomal sub-structures that might or might not be kinetochores. On some occasions we observed chromosomes that could possibly have been taking part in lateral interactions with microtubules, but again the exact site of centromeric regions was unclear. To overcome this problem in the future I would like to perform CLEM on cells expressing GFP-CENP-A. CENP-A localisation is not affected by loss of CENP-T and therefore acts as a perfect mark to pinpoint the exact location of kinetochore assemblies.

5.3.1.2 Dependency pathways downstream of CENP-T using the AID system

The Fukagawa laboratory (Nishino et al., 2013) has used this methodology to study kinetochore interaction pathways linking CENP-T with outer MT-binding complexes. They showed that upon auxin-induced CENP-T degradation, considerable levels of Ndc80 could still be detected at regions of kinetochore assembly (~43% of normal Ndc80 levels after 1 hour of auxin treatment), and residual Ndc80 signals at the outer

kinetochore were maintained by Mis12 subunits (Nishino et al., 2013). We also observed significant amounts of Ndc80 localising within close proximity to CENP-A. In this case, Ndc80 levels were reduced to 61-86% of its original levels in AID-CENP-T cells treated with auxin for 6 hours. In my immunofluorescence images high background levels using the Ndc80 antibody could account for the discrepancies in overall Ndc80 levels between the two experiments. In any case, both studies indicate that only a subpopulation of the Ndc80 complex is acutely dependent on CENP-T depletion. Even though a significant amount of Ndc80 is still present at kinetochores, cells still block in prometaphase. This could suggest that minor changes in Ndc80 complex levels have major implications on microtubule end-coupled attachments and the congression of chromosomes to the metaphase plate.

Due to difficulties with the CENP-H antibody staining it is still unclear as to whether it is depleted, increased or unchanged on chromosomes absent of CENP-T. However, the inner kinetochore protein CENP-O did appear reduced at centromeric regions. In DT40 cells, CENP-O has been shown to form a tight inter-dependent subcomplex with CENP-P, CENP-Q, CENP-R and CENP-U (Hori et al., 2008b) and we would hypothesise that these components are lost from the kinetochore to the same extent (40-50%). Although other inner kinetochore protein localisations in the AID-CENP-T system will need to be examined, these findings currently support a model where outer kinetochore components can be recruited in the absence/reduced levels of many constituents of the inner plate. A similar result has been shown using ectopic kinetochores built on LacO arrays, where KMN interacting fragments of CENP-C and CENP-T could co-ordinately direct chromosome segregation. This could bypass the requirement for CENP-A nucleosomes and other CCAN components (Gascoigne et al., 2011). Therefore, the AID system can be used to analyse the immediate consequences of protein depletion on kinetochore architecture; highlighting components that are absolutely dependent on the degraded protein for their association with kinetochores, or those that are recruited through multiple branch points.

To generate more reliable quantitative measurements of how acute depletion of CENP-T affects kinetochore protein amounts, SILAC experiments could be performed. Preliminary results indicate that AID-CENP-T is significantly depleted from chromosomes isolated from mitotic cells after 2 hours of auxin treatment (Figure 39A). The aim would be to compare SILAC results from AID-CENP-T and CENP-W KO experiments (Figure 39B). By examining the effects of rapid depletion of CENP-T from mitotic cells, we would be able to rule out dependencies caused by loss of the CENP-T complex over multiple cell cycles. This would reveal proteins that are acutely dependent on CENP-T for their abundance on mitotic chromosomes.

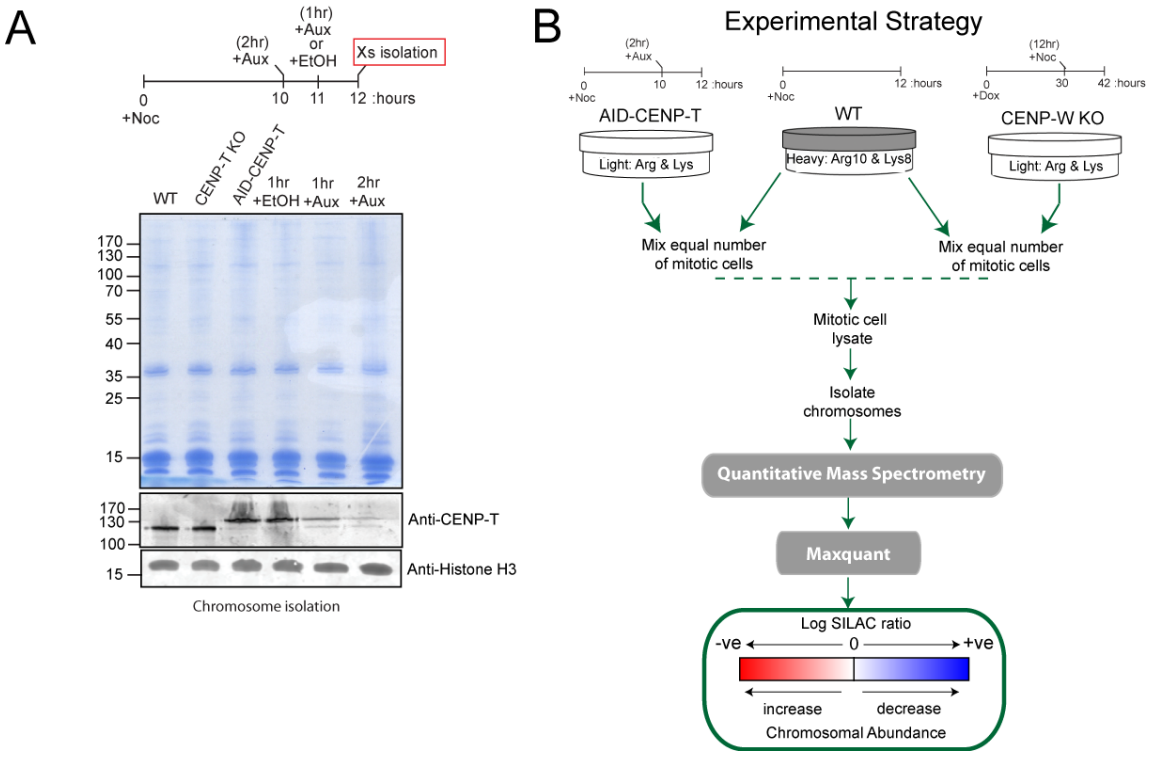

Figure 39. SILAC proteomics combined with the AID-CENP-T system. A. Schematic representation of indicated lengths of nocodazole and auxin treatments before chromosome isolation procedures. Commassie stained gels corresponding to the chromosome isolation samples from WT, CENP-T KO and AID-CENP-T cell lines. Chromosomes isolated from the AID-CENP-T cell line after ethanol (EtOH) or auxin treatment for the indicated time periods are also shown. Corresponding immunoblots of chromosome samples using anti-CENP-T and anti-Histone H3 antibodies are depicted. **B.** Schematic diagram of the SILAC/proteomics experimental strategy. WT cells are grown in heavy SILAC medium, while the AID-CENP-T cells are cultured in the presence of light amino acids. AID-CENP-T cells are maintained in doxycycline to 'turn off' the expression of the inducible transgene and ensure that AID-tagged CENP-T becomes the dominant form of the protein. Both cell types are blocked in mitosis with nocodazole for 12 hours. 10 hours into the nocodazole block auxin is added to the AID-CENP-T cell line to promote the degradation of the AID-tagged protein. Similarly, the CENP-W KO cell line is cultured in the presence of light amino acids. Doxycycline (+Dox) is added for 30 hours to 'turn off' the expression of the inducible transgene and ensure that the previously synthesised target protein has been degraded. This is followed by a mitotic block in nocodazole for 12 hours (+doxycycline for a total of 42 hours). The strategy for chromosome isolations and mass spectrometry analysis are described in section 3.2.1.

5.3.2 Temporal examination of Kinetochore assembly

As described in section 1.4.2, unravelling kinetochore dependency pathways is not straightforward as kinetochores are formed from highly intricate, inter-connected assembly networks. Although kinetochores are functional during cell division and we must also consider interactions between their constituents at other times in the cell cycle. The auxin-inducible degradation system can now be used to take into account this additional layer of complexity. As long as cells can be synchronised at a specific cell cycle stage then quick and efficient degradation of a protein of interest can resolve its associated kinetochore dependencies in a temporal manner. So far, I have attempted to isolate G1 cells using elutriation procedures and late G2 cells with R03306 treatment (Cdk1 inhibitor); however, further optimization is required. A double thymidine block and nocodazole treatment could also be employed to increase S-phase and mitotic cell populations, respectively.

It is possible to compare kinetochore assembly pathways in each of these phases using antibodies against various kinetochore components in immunofluorescence studies (-/+ auxin). Alternatively, SILAC combined with mass spectrometry could be used. In the previous results sections I have shown that many known kinetochore proteins, when isolated with whole chromosomes, can be identified and quantified using SILAC methods. As long as this holds true for isolated DT40 nuclei then this would provide a way to directly compare kinetochore proteomes in the presence or absence of CENP-T in different cell cycle stages. The activity of SCF-TIR1 in G1, S, G2 and mitosis has already been confirmed in human cells (Holland et al., 2012). As the AID system is readily reversible, it would also be interesting to see how re-introducing CENP-T (by washing out the auxin) would impact on kinetochore assembly. However, this would only work efficiently if CENP-T mRNA is present and the translational machinery is active.

In terms of kinetochore interactions during mitosis there is now a notion of architectural 'fluidity', where shifting configurations could help to deal with the pressures of changing spindle forces during mitosis. This property has been examined recently in a number of reports investigating CENP-T interactions (Bock et al., 2012; Gascoigne and Cheeseman, 2013; Gascoigne et al., 2011; Malvezzi et al., 2013; Nishino et al., 2013; Schleiffer et al., 2012). In yeast, Cnn1 (CENP-T homolog) and the Mtw1 complex (Mis12 components) bind Ndc80 subunits in a mutually exclusive manner (Bock et al., 2012; Malvezzi et al., 2013; Schleiffer et al., 2012). However, this interaction is only thought to come into play during anaphase when Mps1/Cdk1 activity is low and CENP-T is in an unphosphorylated state (Bock et al., 2012; Malvezzi et al., 2013; Schleiffer et al., 2012). This situation is different in vertebrate cell lines as CENP-T phosphorylation by Cdk1 enhances the CENP-T-Ndc80 interaction and functions side-by-side with MIS12-Ndc80 pathways (Gascoigne and Cheeseman, 2013; Gascoigne et al., 2011; Nishino et al., 2013). In both cases phosphorylation/dephosphorylation events modulate specific kinetochore configurations. In theory, the relative contributions of CENP-T interactions could be assessed in different mitotic stages using the AID system. For example, in budding yeast we might expect that depletion of CENP-T is only detrimental upon anaphase onset. The exact steps to achieve adequately enriched mitotic stages in DT40 cells are still unclear.

5.3.3 Concluding remarks

In summary, the AID system is a valuable tool for the analysis of protein function. The use of such rapid/inducible degradation pathways gives researchers, for the first time, the opportunity to tease apart the relative contributions of target proteins during highly dynamic processes. One clear example is mitosis, where cells progress through multiple consecutive phases before two daughter cells are created. Here, we have applied this methodology to study CENP-T, an essential kinetochore protein required for successful mitotic progression. In asynchronous cell populations degron-tagged CENP-T is rapidly lost from centromeric regions, leading to prometaphase arrest and eventual cell death.

With this AID-CENP-T cell line now in place we hope it will be possible to elucidate how CENP-T loss impacts on kinetochore assembly pathways during different cell cycle stages and at different phases of mitosis.

6 Conclusions/final perspectives

Over 100 proteins have been shown to be important in kinetochore architecture and function. Rather than trying to define the complete composition of this macro-molecular complex, many of the publications in recent years have begun to focus on delineating the exact inter-dependencies, assembly pathways and functional contributions of individual sub-groups, and how these are implicated in the diverse roles of the kinetochore.

The first part of this thesis has focused on global effects of perturbing the assembly pathways defining mitotic kinetochores (prometaphase). Our data confirmed that known kinetochore sub-complexes, in general, behave in an inter-dependent fashion in regards to their localisation onto chromosomes. One key assembly pathway that was revealed links both CENP-C and CENP-T/W to the recruitment of the KMN, which in turn may be required for CENP-E, Mad1-Mad2 and RZZ complex kinetochore localisation. However, it became clear that the removal of a single component, even those forming the inner plate, did not lead to a complete depletion of all members of this pathway, indicating that multiple parallel interaction networks exist. Future challenges are geared towards using the different types of quantitative analysis to fully interpret these large proteomics data sets. Integrating SILAC values in the form of principle component analysis (PCA) (Borner et al., 2012) and machine learning techniques (random forest) (Ohta et al., 2010) has already been applied to define the functional proteome of coated vesicles and chicken chromosomes, respectively. It will be interesting to see if either of these methods can be used to distinguish kinetochore components/sub-complexes from other chromosomally bound proteins.

One of the pitfalls of this study is that the DT40 tetracycline-regulated conditional KO systems work by preventing gene expression. As a result depletion at the protein level is dependent on the stability of the target protein. The development of the AID system for the rapid depletion of kinetochore proteins, exemplified here with CENP-T, provides an approach to studying kinetochore dependencies in a temporal manner in different stages

of the cell cycle. By applying the same proteomics methods we can analyse the immediate consequences of CENP-T depletion (within 1 hour) on kinetochore architecture; highlighting components that are absolutely dependent, or those that are recruited through multiple pathways. Ultimately, I would hope to directly compare the assembly pathways initiated by the CENP-T/W/S/X complex in the context of the tet-repressive systems (CENP-T KO and CENP-W KO) and the AID cell line.

In summary, the proteomics approach described here provides a unique opportunity to study the structural contributions of individual kinetochore proteins in the context of the whole chromosomal proteome.

7 References

Akiyoshi, B., Nelson, C.R., Ranish, J.A., and Biggins, S. (2009). Quantitative proteomic analysis of purified yeast kinetochores identifies a PP1 regulatory subunit. Genes Dev *23*, 2887-2899.

Akiyoshi, B., Sarangapani, K.K., Powers, A.F., Nelson, C.R., Reichow, S.L., Arellano-Santoyo, H., Gonen, T., Ranish, J.A., Asbury, C.L., and Biggins, S. (2010). Tension directly stabilizes reconstituted kinetochore-microtubule attachments. Nature *468*, 576-579.

Allshire, R.C., and Karpen, G.H. (2008). Epigenetic regulation of centromeric chromatin: old dogs, new tricks? Nat Rev Genet *9*, 923-937.

Alonso, A., Fritz, B., Hasson, D., Abrusan, G., Cheung, F., Yoda, K., Radlwimmer, B., Ladurner, A.G., and Warburton, P.E. (2007). Co-localization of CENP-C and CENP-H to discontinuous domains of CENP-A chromatin at human neocentromeres. Genome Biol *8*, R148.

Alushin, G.M., Ramey, V.H., Pasqualato, S., Ball, D.A., Grigorieff, N., Musacchio, A., and Nogales, E. (2010). The Ndc80 kinetochore complex forms oligomeric arrays along microtubules. Nature *467*, 805-810.

Amano, M., Suzuki, A., Hori, T., Backer, C., Okawa, K., Cheeseman, I.M., and Fukagawa, T. (2009). The CENP-S complex is essential for the stable assembly of outer kinetochore structure. J Cell Biol *186*, 173-182.

Amaro, A.C., Samora, C.P., Holtackers, R., Wang, E., Kingston, I.J., Alonso, M., Lampson, M., McAinsh, A.D., and Meraldi, P. (2010). Molecular control of kinetochore-microtubule dynamics and chromosome oscillations. Nat Cell Biol *12*, 319-329.

Andersen, J.S., Wilkinson, C.J., Mayor, T., Mortensen, P., Nigg, E.A., and Mann, M. (2003). Proteomic characterization of the human centrosome by protein correlation profiling. Nature *426*, 570-574.

Asbury, C.L., Tien, J.F., and Davis, T.N. (2011). Kinetochores' gripping feat: conformational wave or biased diffusion? Trends Cell Biol *21*, 38-46.

Bader, J.R., and Vaughan, K.T. (2010). Dynein at the kinetochore: Timing, Interactions and Functions. Semin Cell Dev Biol *21*, 269-275.

Bailey, S.L., Chang, S.C., Griffiths, B., Graham, A.N., Saffery, R., Earle, E., Choo, K.H., and Kalitsis, P. (2008). ZNF397, a new class of interphase to early prophase-

specific, SCAN-zinc-finger, mammalian centromere protein. Chromosoma *117*, 367-380.

Banaszynski, L.A., and Wandless, T.J. (2006). Conditional control of protein function. Chem Biol *13*, 11-21.

Bergmann, J.H., Martins, N.M., Larionov, V., Masumoto, H., and Earnshaw, W.C. (2012). HACking the centromere chromatin code: insights from human artificial chromosomes. Chromosome Res *20*, 505-519.

Bergmann, J.H., Rodriguez, M.G., Martins, N.M., Kimura, H., Kelly, D.A., Masumoto, H., Larionov, V., Jansen, L.E., and Earnshaw, W.C. (2011). Epigenetic engineering shows H3K4me2 is required for HJURP targeting and CENP-A assembly on a synthetic human kinetochore. EMBO J *30*, 328-340.

Blow, J.J., and Dutta, A. (2005). Preventing re-replication of chromosomal DNA. Nat Rev Mol Cell Biol *6*, 476-486.

Bock, L.J., Pagliuca, C., Kobayashi, N., Grove, R.A., Oku, Y., Shrestha, K., Alfieri, C., Golfieri, C., Oldani, A., Dal Maschio, M*., et al.* (2012). Cnn1 inhibits the interactions between the KMN complexes of the yeast kinetochore. Nat Cell Biol *14*, 614-624.

Bodor, D.L., Rodriguez, M.G., Moreno, N., and Jansen, L.E. (2012). Analysis of protein turnover by quantitative SNAP-based pulse-chase imaging. Curr Protoc Cell Biol *Chapter 8*, Unit8 8.

Bolanos-Garcia, V.M., Lischetti, T., Matak-Vinkovic, D., Cota, E., Simpson, P.J., Chirgadze, D.Y., Spring, D.R., Robinson, C.V., Nilsson, J., and Blundell, T.L. (2011). Structure of a Blinkin-BUBR1 complex reveals an interaction crucial for kinetochore-mitotic checkpoint regulation via an unanticipated binding Site. Structure *19*, 1691-1700.

Bolivar, J., Diaz, I., Iglesias, C., and Valdivia, M.M. (1999). Molecular cloning of a zinc finger autoantigen transiently associated with interphase nucleolus and mitotic centromeres and midbodies. Orthologous proteins with nine CXXC motifs highly conserved from nematodes to humans. J Biol Chem *274*, 36456-36464.

Booth, D.G., Cheeseman, L.P., Prior, I.A., and Royle, S.J. (2013). Methods in Cell Biology, Vol Volume 115 (Academic Press).

Borner, G.H., Antrobus, R., Hirst, J., Bhumbra, G.S., Kozik, P., Jackson, L.P., Sahlender, D.A., and Robinson, M.S. (2012). Multivariate proteomic profiling identifies novel accessory proteins of coated vesicles. J Cell Biol *197*, 141-160.

Buchwitz, B.J., Ahmad, K., Moore, L.L., Roth, M.B., and Henikoff, S. (1999). A histone-H3-like protein in C. elegans. Nature *401*, 547-548.

Buffin, E., Lefebvre, C., Huang, J., Gagou, M.E., and Karess, R.E. (2005). Recruitment of Mad2 to the kinetochore requires the Rod/Zw10 complex. Curr Biol *15*, 856-861.

Caldas, G.V., and Deluca, J.G. (2013). KNL1: bringing order to the kinetochore. Chromosoma.

Cardozo, T., and Pagano, M. (2004). The SCF ubiquitin ligase: insights into a molecular machine. Nat Rev Mol Cell Biol *5*, 739-751.

Carlton, J.G., Caballe, A., Agromayor, M., Kloc, M., and Martin-Serrano, J. (2012). ESCRT-III governs the Aurora B-mediated abscission checkpoint through CHMP4C. Science *336*, 220-225.

Carmena, M., Wheelock, M., Funabiki, H., and Earnshaw, W.C. (2012). The chromosomal passenger complex (CPC): from easy rider to the godfather of mitosis. Nat Rev Mol Cell Biol *13*, 789-803.

Carroll, C.W., Milks, K.J., and Straight, A.F. (2010). Dual recognition of CENP-A nucleosomes is required for centromere assembly. J Cell Biol *189*, 1143-1155.

Carroll, C.W., Silva, M.C., Godek, K.M., Jansen, L.E., and Straight, A.F. (2009). Centromere assembly requires the direct recognition of CENP-A nucleosomes by CENP-N. Nat Cell Biol *11*, 896-902.

Chan, Y.W., Fava, L.L., Uldschmid, A., Schmitz, M.H., Gerlich, D.W., Nigg, E.A., and Santamaria, A. (2009). Mitotic control of kinetochore-associated dynein and spindle orientation by human Spindly. J Cell Biol *185*, 859-874.

Cheeseman, I.M., Chappie, J.S., Wilson-Kubalek, E.M., and Desai, A. (2006). The conserved KMN network constitutes the core microtubule-binding site of the kinetochore. Cell *127*, 983-997.

Cheeseman, I.M., and Desai, A. (2008). Molecular architecture of the kinetochore-microtubule interface. Nat Rev Mol Cell Biol *9*, 33-46.

Cheeseman, I.M., Hori, T., Fukagawa, T., and Desai, A. (2008). KNL1 and the CENP-H/I/K complex coordinately direct kinetochore assembly in vertebrates. Mol Biol Cell *19*, 587-594.

Chen, R.H. (2002). BubR1 is essential for kinetochore localization of other spindle checkpoint proteins and its phosphorylation requires Mad1. J Cell Biol *158*, 487-496.

Ciferri, C., Pasqualato, S., Screpanti, E., Varetti, G., Santaguida, S., Dos Reis, G., Maiolica, A., Polka, J., De Luca, J.G., De Wulf, P.*, et al.* (2008). Implications for kinetochore-microtubule attachment from the structure of an engineered Ndc80 complex. Cell *133*, 427-439.

Coffman, V.C., Wu, P., Parthun, M.R., and Wu, J.Q. (2011). CENP-A exceeds microtubule attachment sites in centromere clusters of both budding and fission yeast. J Cell Biol *195*, 563-572.

Comings, D.E., and Okada, T.A. (1971). Fine structure of kinetochore in Indian muntjac. Exp Cell Res *67*, 97-110.

Cox, J., and Mann, M. (2008). MaxQuant enables high peptide identification rates, individualized p.p.b.-range mass accuracies and proteome-wide protein quantification. Nat Biotechnol *26*, 1367-1372.

Cox, J., Neuhauser, N., Michalski, A., Scheltema, R.A., Olsen, J.V., and Mann, M. (2011). Andromeda: a peptide search engine integrated into the MaxQuant environment. J Proteome Res *10*, 1794-1805.

Cronshaw, J.M., Krutchinsky, A.N., Zhang, W., Chait, B.T., and Matunis, M.J. (2002). Proteomic analysis of the mammalian nuclear pore complex. J Cell Biol *158*, 915-927.

Darzynkiewicz, Z., Galkowski, D., and Zhao, H. (2008). Analysis of apoptosis by cytometry using TUNEL assay. Methods *44*, 250-254.

Daum, J.R., Wren, J.D., Daniel, J.J., Sivakumar, S., McAvoy, J.N., Potapova, T.A., and Gorbsky, G.J. (2009). Ska3 is required for spindle checkpoint silencing and the maintenance of chromosome cohesion in mitosis. Curr Biol *19*, 1467-1472.

De Piccoli, G., Torres-Rosell, J., and Aragon, L. (2009). The unnamed complex: what do we know about Smc5-Smc6? Chromosome Res *17*, 251-263.

De Rop, V., Padeganeh, A., and Maddox, P.S. (2012). CENP-A: the key player behind centromere identity, propagation, and kinetochore assembly. Chromosoma *121*, 527-538.

De Wulf, P., McAinsh, A.D., and Sorger, P.K. (2003). Hierarchical assembly of the budding yeast kinetochore from multiple subcomplexes. Genes Dev *17*, 2902-2921.

Dejardin, J., and Kingston, R.E. (2009). Purification of proteins associated with specific genomic Loci. Cell *136*, 175-186.

Desai, A., Rybina, S., Muller-Reichert, T., Shevchenko, A., Shevchenko, A., Hyman, A., and Oegema, K. (2003). KNL-1 directs assembly of the microtubule-binding interface of the kinetochore in C. elegans. Genes Dev *17*, 2421-2435.

Dharmasiri, N., Dharmasiri, S., and Estelle, M. (2005). The F-box protein TIR1 is an auxin receptor. Nature *435*, 441-445.

Dohmen, R.J., Wu, P., and Varshavsky, A. (1994). Heat-inducible degron: a method for constructing temperature-sensitive mutants. Science *263*, 1273-1276.

Dong, Y., Vanden Beldt, K.J., Meng, X., Khodjakov, A., and McEwen, B.F. (2007). The outer plate in vertebrate kinetochores is a flexible network with multiple microtubule interactions. Nat Cell Biol *9*, 516-522.

Doyle, A., McGarry, M.P., Lee, N.A., and Lee, J.J. (2012). The construction of transgenic and gene knockout/knockin mouse models of human disease. Transgenic Res *21*, 327-349.

Earnshaw, W.C., and Rothfield, N. (1985). Identification of a family of human centromere proteins using autoimmune sera from patients with scleroderma. Chromosoma *91*, 313-321.

Elbashir, S.M., Harborth, J., Lendeckel, W., Yalcin, A., Weber, K., and Tuschl, T. (2001). Duplexes of 21-nucleotide RNAs mediate RNA interference in cultured mammalian cells. Nature *411*, 494-498.

Erhardt, S., Mellone, B.G., Betts, C.M., Zhang, W., Karpen, G.H., and Straight, A.F. (2008). Genome-wide analysis reveals a cell cycle-dependent mechanism controlling centromere propagation. J Cell Biol *183*, 805-818.

Eskat, A., Deng, W., Hofmeister, A., Rudolphi, S., Emmerth, S., Hellwig, D., Ulbricht, T., Doring, V., Bancroft, J.M., McAinsh, A.D.*, et al.* (2012). Step-wise assembly, maturation and dynamic behavior of the human CENP-P/O/R/Q/U kinetochore sub-complex. PLoS One *7*, e44717.

Evans, T., Rosenthal, E.T., Youngblom, J., Distel, D., and Hunt, T. (1983). Cyclin: a protein specified by maternal mRNA in sea urchin eggs that is destroyed at each cleavage division. Cell *33*, 389-396.

Foley, E.A., and Kapoor, T.M. (2013). Microtubule attachment and spindle assembly checkpoint signalling at the kinetochore. Nat Rev Mol Cell Biol *14*, 25-37.

Foltz, D.R., Jansen, L.E., Black, B.E., Bailey, A.O., Yates, J.R., 3rd, and Cleveland, D.W. (2006). The human CENP-A centromeric nucleosome-associated complex. Nat Cell Biol *8*, 458-469.

Foltz, D.R., and Stukenberg, P.T. (2012). A new histone at the centromere? Cell *148*, 394-396.

Fukagawa, T., Mikami, Y., Nishihashi, A., Regnier, V., Haraguchi, T., Hiraoka, Y., Sugata, N., Todokoro, K., Brown, W., and Ikemura, T. (2001). CENP-H, a constitutive centromere component, is required for centromere targeting of CENP-C in vertebrate cells. EMBO J *20*, 4603-4617.

Gaitanos, T.N., Santamaria, A., Jeyaprakash, A.A., Wang, B., Conti, E., and Nigg, E.A. (2009). Stable kinetochore-microtubule interactions depend on the Ska complex and its new component Ska3/C13Orf3. EMBO J *28*, 1442-1452.

Ganem, N.J., and Compton, D.A. (2006). Functional roles of poleward microtubule flux during mitosis. Cell Cycle *5*, 481-485.

Gascoigne, K.E., and Cheeseman, I.M. (2010). Kinetochore assembly: if you build it, they will come. Curr Opin Cell Biol.

Gascoigne, K.E., and Cheeseman, I.M. (2013). CDK-dependent phosphorylation and nuclear exclusion coordinately control kinetochore assembly state. J Cell Biol *201*, 23-32.

Gascoigne, K.E., Takeuchi, K., Suzuki, A., Hori, T., Fukagawa, T., and Cheeseman, I.M. (2011). Induced ectopic kinetochore assembly bypasses the requirement for CENP-A nucleosomes. Cell *145*, 410-422.

Gassmann, R., Essex, A., Hu, J.S., Maddox, P.S., Motegi, F., Sugimoto, A., O'Rourke, S.M., Bowerman, B., McLeod, I., Yates, J.R., 3rd*, et al.* (2008). A new mechanism controlling kinetochore-microtubule interactions revealed by comparison of two dynein-targeting components: SPDL-1 and the Rod/Zwilch/Zw10 complex. Genes Dev *22*, 2385-2399.

Gassmann, R., Henzing, A.J., and Earnshaw, W.C. (2005). Novel components of human mitotic chromosomes identified by proteomic analysis of the chromosome scaffold fraction. Chromosoma *113*, 385-397.

Gassmann, R., Holland, A.J., Varma, D., Wan, X., Civril, F., Cleveland, D.W., Oegema, K., Salmon, E.D., and Desai, A. (2010). Removal of Spindly from microtubule-attached kinetochores controls spindle checkpoint silencing in human cells. Genes Dev *24*, 957-971.

Geda, P., Patury, S., Ma, J., Bharucha, N., Dobry, C.J., Lawson, S.K., Gestwicki, J.E., and Kumar, A. (2008). A small molecule-directed approach to control protein localization and function. Yeast *25*, 577-594.

Glotzer, M., Murray, A.W., and Kirschner, M.W. (1991). Cyclin is degraded by the ubiquitin pathway. Nature *349*, 132-138.

Gonczy, P., Echeverri, C., Oegema, K., Coulson, A., Jones, S.J., Copley, R.R., Duperon, J., Oegema, J., Brehm, M., Cassin, E.*, et al.* (2000). Functional genomic analysis of cell division in C. elegans using RNAi of genes on chromosome III. Nature *408*, 331-336.

Gonen, S., Akiyoshi, B., Iadanza, M.G., Shi, D., Duggan, N., Biggins, S., and Gonen, T. (2012). The structure of purified kinetochores reveals multiple microtubule-attachment sites. Nat Struct Mol Biol *19*, 925-929.

Gordon, D.J., Resio, B., and Pellman, D. (2012). Causes and consequences of aneuploidy in cancer. Nat Rev Genet *13*, 189-203.

Gossen, M., and Bujard, H. (1992). Tight control of gene expression in mammalian cells by tetracycline-responsive promoters. Proc Natl Acad Sci U S A *89*, 5547-5551.

Guse, A., Carroll, C.W., Moree, B., Fuller, C.J., and Straight, A.F. (2011). In vitro centromere and kinetochore assembly on defined chromatin templates. Nature *477*, 354-358.

Hadwiger, J.A., Wittenberg, C., Mendenhall, M.D., and Reed, S.I. (1989). The Saccharomyces cerevisiae CKS1 gene, a homolog of the Schizosaccharomyces pombe suc1+ gene, encodes a subunit of the Cdc28 protein kinase complex. Mol Cell Biol *9*, 2034-2041.

Hall, B., Limaye, A., and Kulkarni, A.B. (2009). Overview: generation of gene knockout mice. Curr Protoc Cell Biol *Chapter 19*, Unit 19 12 19 12 11-17.

Hampel, F.R. (1974). The influence curve and its role in robust estimation. Journal of the American Statistical Association *69*, 383-393.

Hanisch, A., Sillje, H.H., and Nigg, E.A. (2006). Timely anaphase onset requires a novel spindle and kinetochore complex comprising Ska1 and Ska2. EMBO J *25*, 5504-5515.

Haruki, H., Nishikawa, J., and Laemmli, U.K. (2008). The anchor-away technique: rapid, conditional establishment of yeast mutant phenotypes. Mol Cell *31*, 925-932.

Hellwig, D., Emmerth, S., Ulbricht, T., Doring, V., Hoischen, C., Martin, R., Samora, C.P., McAinsh, A.D., Carroll, C.W., Straight, A.F.*, et al.* (2011). Dynamics of CENP-N kinetochore binding during the cell cycle. J Cell Sci *124*, 3871-3883.

Hemmerich, P., Weidtkamp-Peters, S., Hoischen, C., Schmiedeberg, L., Erliandri, I., and Diekmann, S. (2008). Dynamics of inner kinetochore assembly and maintenance in living cells. J Cell Biol *180*, 1101-1114.

Henikoff, S., Ahmad, K., Platero, J.S., and van Steensel, B. (2000). Heterochromatic deposition of centromeric histone H3-like proteins. Proc Natl Acad Sci U S A *97*, 716-721.

Hershko, A., Ganoth, D., Pehrson, J., Palazzo, R.E., and Cohen, L.H. (1991). Methylated ubiquitin inhibits cyclin degradation in clam embryo extracts. J Biol Chem *266*, 16376-16379.

Heun, P., Erhardt, S., Blower, M.D., Weiss, S., Skora, A.D., and Karpen, G.H. (2006). Mislocalization of the Drosophila centromere-specific histone CID promotes formation of functional ectopic kinetochores. Dev Cell *10*, 303-315.

Hinshaw, S.M., and Harrison, S.C. (2013). An Iml3-Chl4 heterodimer links the core centromere to factors required for accurate chromosome segregation. Cell Rep *5*, 29-36.

Holland, A.J., Fachinetti, D., Han, J.S., and Cleveland, D.W. (2012). Inducible, reversible system for the rapid and complete degradation of proteins in mammalian cells. Proc Natl Acad Sci U S A *109*, E3350-3357.

Hori, T., Amano, M., Suzuki, A., Backer, C.B., Welburn, J.P., Dong, Y., McEwen, B.F., Shang, W.H., Suzuki, E., Okawa, K.*, et al.* (2008a). CCAN makes multiple contacts with centromeric DNA to provide distinct pathways to the outer kinetochore. Cell *135*, 1039-1052.

Hori, T., Haraguchi, T., Hiraoka, Y., Kimura, H., and Fukagawa, T. (2003). Dynamic behavior of Nuf2-Hec1 complex that localizes to the centrosome and centromere and is essential for mitotic progression in vertebrate cells. J Cell Sci *116*, 3347-3362.

Hori, T., Okada, M., Maenaka, K., and Fukagawa, T. (2008b). CENP-O class proteins form a stable complex and are required for proper kinetochore function. Mol Biol Cell *19*, 843-854.

Hori, T., Shang, W.H., Takeuchi, K., and Fukagawa, T. (2013). The CCAN recruits CENP-A to the centromere and forms the structural core for kinetochore assembly. J Cell Biol *200*, 45-60.

Hornung, P., Maier, M., Alushin, G.M., Lander, G.C., Nogales, E., and Westermann, S. (2011). Molecular architecture and connectivity of the budding yeast Mtw1 kinetochore complex. J Mol Biol *405*, 548-559.

Howell, B.J., McEwen, B.F., Canman, J.C., Hoffman, D.B., Farrar, E.M., Rieder, C.L., and Salmon, E.D. (2001). Cytoplasmic dynein/dynactin drives kinetochore protein transport to the spindle poles and has a role in mitotic spindle checkpoint inactivation. J Cell Biol *155*, 1159-1172.

Howell, B.J., Moree, B., Farrar, E.M., Stewart, S., Fang, G., and Salmon, E.D. (2004). Spindle checkpoint protein dynamics at kinetochores in living cells. Curr Biol *14*, 953-964.

Hua, S., Wang, Z., Jiang, K., Huang, Y., Ward, T., Zhao, L., Dou, Z., and Yao, X. (2011). CENP-U cooperates with Hec1 to orchestrate kinetochore-microtubule attachment. J Biol Chem *286*, 1627-1638.

Huppi, K., Martin, S.E., and Caplen, N.J. (2005). Defining and assaying RNAi in mammalian cells. Mol Cell *17*, 1-10.

Hutchins, J.R., Toyoda, Y., Hegemann, B., Poser, I., Heriche, J.K., Sykora, M.M., Augsburg, M., Hudecz, O., Buschhorn, B.A., Bulkescher, J*., et al.* (2010). Systematic analysis of human protein complexes identifies chromosome segregation proteins. Science *328*, 593-599.

Ishihama, Y., Rappsilber, J., and Mann, M. (2006). Modular stop and go extraction tips with stacked disks for parallel and multidimensional Peptide fractionation in proteomics. J Proteome Res *5*, 988-994.

Itoh, G., Kanno, S., Uchida, K.S., Chiba, S., Sugino, S., Watanabe, K., Mizuno, K., Yasui, A., Hirota, T., and Tanaka, K. (2011). CAMP (C13orf8, ZNF828) is a novel regulator of kinetochore-microtubule attachment. EMBO J *30*, 130-144.

Izawa, D., and Pines, J. (2012). Mad2 and the APC/C compete for the same site on Cdc20 to ensure proper chromosome segregation. J Cell Biol *199*, 27-37.

Izuta, H., Ikeno, M., Suzuki, N., Tomonaga, T., Nozaki, N., Obuse, C., Kisu, Y., Goshima, N., Nomura, F., Nomura, N*., et al.* (2006). Comprehensive analysis of the ICEN (Interphase Centromere Complex) components enriched in the CENP-A chromatin of human cells. Genes Cells *11*, 673-684.

Jeyaprakash, A.A., Santamaria, A., Jayachandran, U., Chan, Y.W., Benda, C., Nigg, E.A., and Conti, E. (2012). Structural and functional organization of the Ska complex, a key component of the kinetochore-microtubule interface. Mol Cell *46*, 274-286.

Joglekar, A.P., Bloom, K., and Salmon, E.D. (2009). In vivo protein architecture of the eukaryotic kinetochore with nanometer scale accuracy. Curr Biol *19*, 694-699.

Joglekar, A.P., Bouck, D., Finley, K., Liu, X., Wan, Y., Berman, J., He, X., Salmon, E.D., and Bloom, K.S. (2008). Molecular architecture of the kinetochore-microtubule attachment site is conserved between point and regional centromeres. J Cell Biol *181*, 587-594.

Joglekar, A.P., Bouck, D.C., Molk, J.N., Bloom, K.S., and Salmon, E.D. (2006). Molecular architecture of a kinetochore-microtubule attachment site. Nat Cell Biol *8*, 581-585.

Johnston, K., Joglekar, A., Hori, T., Suzuki, A., Fukagawa, T., and Salmon, E.D. (2010). Vertebrate kinetochore protein architecture: protein copy number. J Cell Biol *189*, 937-943.

Jokelainen, P.T. (1967). The ultrastructure and spatial organization of the metaphase kinetochore in mitotic rat cells. J Ultrastruct Res *19*, 19-44.

Kamakaka, R.T., and Biggins, S. (2005). Histone variants: deviants? Genes Dev *19*, 295-310.

Kanemaki, M., Sanchez-Diaz, A., Gambus, A., and Labib, K. (2003). Functional proteomic identification of DNA replication proteins by induced proteolysis in vivo. Nature *423*, 720-724.

Kang, Y.H., Park, C.H., Kim, T.S., Soung, N.K., Bang, J.K., Kim, B.Y., Park, J.E., and Lee, K.S. (2011). Mammalian polo-like kinase 1-dependent regulation of the PBIP1-CENP-Q complex at kinetochores. J Biol Chem *286*, 19744-19757.

Kanke, M., Nishimura, K., Kanemaki, M., Kakimoto, T., Takahashi, T.S., Nakagawa, T., and Masukata, H. (2011). Auxin-inducible protein depletion system in fission yeast. BMC Cell Biol *12*, 8.

Kapoor, T.M., Lampson, M.A., Hergert, P., Cameron, L., Cimini, D., Salmon, E.D., McEwen, B.F., and Khodjakov, A. (2006). Chromosomes can congress to the metaphase plate before biorientation. Science *311*, 388-391.

Kepinski, S., and Leyser, O. (2005). The Arabidopsis F-box protein TIR1 is an auxin receptor. Nature *435*, 446-451.

Key, M. (2012). A tutorial in displaying mass spectrometry-based proteomic data using heat maps. BMC Bioinformatics *13 Suppl 16*, S10.

Kittler, R., Pelletier, L., Heninger, A.K., Slabicki, M., Theis, M., Miroslaw, L., Poser, I., Lawo, S., Grabner, H., Kozak, K.*, et al.* (2007). Genome-scale RNAi profiling of cell division in human tissue culture cells. Nat Cell Biol *9*, 1401-1412.

Kiyomitsu, T., Murakami, H., and Yanagida, M. (2011). Protein interaction domain mapping of human kinetochore protein Blinkin reveals a consensus motif for binding of spindle assembly checkpoint proteins Bub1 and BubR1. Mol Cell Biol *31*, 998-1011.

Kops, G.J., Kim, Y., Weaver, B.A., Mao, Y., McLeod, I., Yates, J.R., 3rd, Tagaya, M., and Cleveland, D.W. (2005). ZW10 links mitotic checkpoint signaling to the structural kinetochore. J Cell Biol *169*, 49-60.

Krenn, V., Wehenkel, A., Li, X., Santaguida, S., and Musacchio, A. (2012). Structural analysis reveals features of the spindle checkpoint kinase Bub1-kinetochore subunit Knl1 interaction. J Cell Biol *196*, 451-467.

Kuipers, M.A., Stasevich, T.J., Sasaki, T., Wilson, K.A., Hazelwood, K.L., McNally, J.G., Davidson, M.W., and Gilbert, D.M. (2011). Highly stable loading of Mcm proteins onto chromatin in living cells requires replication to unload. J Cell Biol *192*, 29-41.

Kwon, M.S., Hori, T., Okada, M., and Fukagawa, T. (2007). CENP-C is involved in chromosome segregation, mitotic checkpoint function, and kinetochore assembly. Mol Biol Cell *18*, 2155-2168.

Laemmli, U.K., Cheng, S.M., Adolph, K.W., Paulson, J.R., Brown, J.A., and Baumbach, W.R. (1978). Metaphase chromosome structure: the role of nonhistone proteins. Cold Spring Harb Symp Quant Biol *42 Pt 1*, 351-360.

Lan, W., and Cleveland, D.W. (2010). Multiclassifier proteomics to define complexes yields new chromosomal proteins. Dev Cell *19*, 356-359.

Lawrimore, J., Bloom, K.S., and Salmon, E.D. (2011). Point centromeres contain more than a single centromere-specific Cse4 (CENP-A) nucleosome. J Cell Biol *195*, 573-582.

Lewis, C.D., and Laemmli, U.K. (1982). Higher order metaphase chromosome structure: evidence for metalloprotein interactions. Cell *29*, 171-181.

Lin, Y.T., Chen, Y., Wu, G., and Lee, W.H. (2006). Hec1 sequentially recruits Zwint-1 and ZW10 to kinetochores for faithful chromosome segregation and spindle checkpoint control. Oncogene *25*, 6901-6914.

Liu, D., Ding, X., Du, J., Cai, X., Huang, Y., Ward, T., Shaw, A., Yang, Y., Hu, R., Jin, C.*, et al.* (2007). Human NUF2 interacts with centromere-associated protein E and is essential for a stable spindle microtubule-kinetochore attachment. J Biol Chem *282*, 21415-21424.

Liu, D., Vader, G., Vromans, M.J., Lampson, M.A., and Lens, S.M. (2009). Sensing chromosome bi-orientation by spatial separation of aurora B kinase from kinetochore substrates. Science *323*, 1350-1353.

Liu, D., Vleugel, M., Backer, C.B., Hori, T., Fukagawa, T., Cheeseman, I.M., and Lampson, M.A. (2010). Regulated targeting of protein phosphatase 1 to the outer kinetochore by KNL1 opposes Aurora B kinase. J Cell Biol *188*, 809-820.

Liu, S.T., Rattner, J.B., Jablonski, S.A., and Yen, T.J. (2006). Mapping the assembly pathways that specify formation of the trilaminar kinetochore plates in human cells. J Cell Biol *175*, 41-53.

Lohka, M.J., Hayes, M.K., and Maller, J.L. (1988). Purification of maturation-promoting factor, an intracellular regulator of early mitotic events. Proc Natl Acad Sci U S A *85*, 3009-3013.

London, N., and Biggins, S. (2014). Mad1 kinetochore recruitment by Mps1-mediated phosphorylation of Bub1 signals the spindle checkpoint. Genes Dev *28*, 140-152.

London, N., Ceto, S., Ranish, J.A., and Biggins, S. (2012). Phosphoregulation of Spc105 by Mps1 and PP1 regulates Bub1 localization to kinetochores. Curr Biol *22*, 900-906.

Maiato, H., DeLuca, J., Salmon, E.D., and Earnshaw, W.C. (2004). The dynamic kinetochore-microtubule interface. J Cell Sci *117*, 5461-5477.

Malumbres, M., and Barbacid, M. (2009). Cell cycle, CDKs and cancer: a changing paradigm. Nat Rev Cancer *9*, 153-166.

Malvezzi, F., Litos, G., Schleiffer, A., Heuck, A., Mechtler, K., Clausen, T., and Westermann, S. (2013). A structural basis for kinetochore recruitment of the Ndc80 complex via two distinct centromere receptors. EMBO J *32*, 409-423.

Mann, M. (2006). Functional and quantitative proteomics using SILAC. Nat Rev Mol Cell Biol *7*, 952-958.

Mao, Y., Abrieu, A., and Cleveland, D.W. (2003). Activating and silencing the mitotic checkpoint through CENP-E-dependent activation/inactivation of BubR1. Cell *114*, 87-98.

Martin-Lluesma, S., Stucke, V.M., and Nigg, E.A. (2002). Role of Hec1 in spindle checkpoint signaling and kinetochore recruitment of Mad1/Mad2. Science *297*, 2267-2270.

Masabanda, J.S., Burt, D.W., O'Brien, P.C., Vignal, A., Fillon, V., Walsh, P.S., Cox, H., Tempest, H.G., Smith, J., Habermann, F.*, et al.* (2004). Molecular cytogenetic definition of the chicken genome: the first complete avian karyotype. Genetics *166*, 1367-1373.

Maskell, D.P., Hu, X.W., and Singleton, M.R. (2010). Molecular architecture and assembly of the yeast kinetochore MIND complex. J Cell Biol *190*, 823-834.

McAinsh, A.D., Meraldi, P., Draviam, V.M., Toso, A., and Sorger, P.K. (2006). The human kinetochore proteins Nnf1R and Mcm21R are required for accurate chromosome segregation. EMBO J *25*, 4033-4049.

McAinsh, A.D., Tytell, J.D., and Sorger, P.K. (2003). Structure, function, and regulation of budding yeast kinetochores. Annu Rev Cell Dev Biol *19*, 519-539.

McClelland, S.E., Borusu, S., Amaro, A.C., Winter, J.R., Belwal, M., McAinsh, A.D., and Meraldi, P. (2007). The CENP-A NAC/CAD kinetochore complex controls chromosome congression and spindle bipolarity. EMBO J *26*, 5033-5047.

McIntosh, J.R., O'Toole, E., Zhudenkov, K., Morphew, M., Schwartz, C., Ataullakhanov, F.I., and Grishchuk, E.L. (2013). Conserved and divergent features of kinetochores and spindle microtubule ends from five species. J Cell Biol *200*, 459-474.

Medema, R.H. (2004). Optimizing RNA interference for application in mammalian cells. Biochem J *380*, 593-603.

Meluh, P.B., Yang, P., Glowczewski, L., Koshland, D., and Smith, M.M. (1998). Cse4p is a component of the core centromere of Saccharomyces cerevisiae. Cell *94*, 607-613.

Milks, K.J., Moree, B., and Straight, A.F. (2009). Dissection of CENP-C-directed centromere and kinetochore assembly. Mol Biol Cell *20*, 4246-4255.

Minoshima, Y., Hori, T., Okada, M., Kimura, H., Haraguchi, T., Hiraoka, Y., Bao, Y.C., Kawashima, T., Kitamura, T., and Fukagawa, T. (2005). The constitutive centromere component CENP-50 is required for recovery from spindle damage. Mol Cell Biol *25*, 10315-10328.

Morawska, M., and Ulrich, H.D. (2013). An expanded tool kit for the auxin-inducible degron system in budding yeast. Yeast.

Moree, B., Meyer, C.B., Fuller, C.J., and Straight, A.F. (2011). CENP-C recruits M18BP1 to centromeres to promote CENP-A chromatin assembly. J Cell Biol *194*, 855-871.

Morrison, C., Henzing, A.J., Jensen, O.N., Osheroff, N., Dodson, H., Kandels-Lewis, S.E., Adams, R.R., and Earnshaw, W.C. (2002). Proteomic analysis of human metaphase chromosomes reveals topoisomerase II alpha as an Aurora B substrate. Nucleic Acids Res *30*, 5318-5327.

Moyle, M.W., Kim, T., Hattersley, N., Espeut, J., Cheerambathur, D.K., Oegema, K., and Desai, A. (2014). A Bub1-Mad1 interaction targets the Mad1-Mad2 complex to unattached kinetochores to initiate the spindle checkpoint. J Cell Biol *204*, 647-657.

Musacchio, A., and Salmon, E.D. (2007). The spindle-assembly checkpoint in space and time. Nat Rev Mol Cell Biol *8*, 379-393.

Nash, R., Tokiwa, G., Anand, S., Erickson, K., and Futcher, A.B. (1988). The WHI1+ gene of Saccharomyces cerevisiae tethers cell division to cell size and is a cyclin homolog. EMBO J *7*, 4335-4346.

Nasmyth, K., Peters, J.M., and Uhlmann, F. (2000). Splitting the chromosome: cutting the ties that bind sister chromatids. Science *288*, 1379-1385.

Neumann, B., Walter, T., Heriche, J.K., Bulkescher, J., Erfle, H., Conrad, C., Rogers, P., Poser, I., Held, M., Liebel, U.*, et al.* (2010). Phenotypic profiling of the human genome by time-lapse microscopy reveals cell division genes. Nature *464*, 721-727.

Nishihashi, A., Haraguchi, T., Hiraoka, Y., Ikemura, T., Regnier, V., Dodson, H., Earnshaw, W.C., and Fukagawa, T. (2002). CENP-I is essential for centromere function in vertebrate cells. Dev Cell *2*, 463-476.

Nishimura, K., Fukagawa, T., Takisawa, H., Kakimoto, T., and Kanemaki, M. (2009). An auxin-based degron system for the rapid depletion of proteins in nonplant cells. Nat Methods *6*, 917-922.

Nishino, T., Rago, F., Hori, T., Tomii, K., Cheeseman, I.M., and Fukagawa, T. (2013). CENP-T provides a structural platform for outer kinetochore assembly. EMBO J *32*, 424-436.

Nishino, T., Takeuchi, K., Gascoigne, K.E., Suzuki, A., Hori, T., Oyama, T., Morikawa, K., Cheeseman, I.M., and Fukagawa, T. (2012). CENP-T-W-S-X forms a unique centromeric chromatin structure with a histone-like fold. Cell *148*, 487-501.

Norbury, C., and Nurse, P. (1992). Animal cell cycles and their control. Annu Rev Biochem *61*, 441-470.

Obuse, C., Yang, H., Nozaki, N., Goto, S., Okazaki, T., and Yoda, K. (2004). Proteomics analysis of the centromere complex from HeLa interphase cells: UV-damaged DNA binding protein 1 (DDB-1) is a component of the CEN-complex, while BMI-1 is transiently co-localized with the centromeric region in interphase. Genes Cells *9*, 105-120.

Ohta, S., Bukowski-Wills, J.C., Sanchez-Pulido, L., Alves Fde, L., Wood, L., Chen, Z.A., Platani, M., Fischer, L., Hudson, D.F., Ponting, C.P.*, et al.* (2010). The protein composition of mitotic chromosomes determined using multiclassifier combinatorial proteomics. Cell *142*, 810-821.

Ohta, S., Wood, L., Bukowski-Wills, J.C., Rappsilber, J., and Earnshaw, W.C. (2011). Building mitotic chromosomes. Curr Opin Cell Biol *23*, 114-121.

Okada, M., Cheeseman, I.M., Hori, T., Okawa, K., McLeod, I.X., Yates, J.R., 3rd, Desai, A., and Fukagawa, T. (2006a). The CENP-H-I complex is required for the efficient incorporation of newly synthesized CENP-A into centromeres. Nat Cell Biol *8*, 446-457.

Okada, M., Hori, T., and Fukagawa, T. (2006b). The DT40 system as a tool for analyzing kinetochore assembly. Subcell Biochem *40*, 91-106.

Ong, S.E., Blagoev, B., Kratchmarova, I., Kristensen, D.B., Steen, H., Pandey, A., and Mann, M. (2002). Stable isotope labeling by amino acids in cell culture, SILAC, as a simple and accurate approach to expression proteomics. Mol Cell Proteomics *1*, 376-386.

Ong, S.E., and Mann, M. (2006). A practical recipe for stable isotope labeling by amino acids in cell culture (SILAC). Nat Protoc *1*, 2650-2660.

Painter, R.B., and Young, B.R. (1980). Radiosensitivity in ataxia-telangiectasia: a new explanation. Proc Natl Acad Sci U S A *77*, 7315-7317.

Peters, J.M. (2002). The anaphase-promoting complex: proteolysis in mitosis and beyond. Mol Cell *9*, 931-943.

Petroski, M.D., and Deshaies, R.J. (2005). Function and regulation of cullin-RING ubiquitin ligases. Nat Rev Mol Cell Biol *6*, 9-20.

Petrovic, A., Pasqualato, S., Dube, P., Krenn, V., Santaguida, S., Cittaro, D., Monzani, S., Massimiliano, L., Keller, J., Tarricone, A.*, et al.* (2010). The MIS12 complex is a protein interaction hub for outer kinetochore assembly. J Cell Biol *190*, 835-852.

Porter, I.M., McClelland, S.E., Khoudoli, G.A., Hunter, C.J., Andersen, J.S., McAinsh, A.D., Blow, J.J., and Swedlow, J.R. (2007). Bod1, a novel kinetochore protein required for chromosome biorientation. J Cell Biol *179*, 187-197.

Prendergast, L., van Vuuren, C., Kaczmarczyk, A., Doering, V., Hellwig, D., Quinn, N., Hoischen, C., Diekmann, S., and Sullivan, K.F. (2011). Premitotic assembly of human CENPs -T and -W switches centromeric chromatin to a mitotic state. PLoS Biol *9*, e1001082.

Przewloka, M.R., Venkei, Z., Bolanos-Garcia, V.M., Debski, J., Dadlez, M., and Glover, D.M. (2011). CENP-C is a structural platform for kinetochore assembly. Curr Biol *21*, 399-405.

Przewloka, M.R., Zhang, W., Costa, P., Archambault, V., D'Avino, P.P., Lilley, K.S., Laue, E.D., McAinsh, A.D., and Glover, D.M. (2007). Molecular analysis of core kinetochore composition and assembly in Drosophila melanogaster. PLoS One *2*, e478.

Raaijmakers, J.A., Tanenbaum, M.E., Maia, A.F., and Medema, R.H. (2009). RAMA1 is a novel kinetochore protein involved in kinetochore-microtubule attachment. J Cell Sci *122*, 2436-2445.

Rago, C., Vogelstein, B., and Bunz, F. (2007). Genetic knockouts and knockins in human somatic cells. Nat Protoc *2*, 2734-2746.

Rappsilber, J., Ishihama, Y., and Mann, M. (2003). Stop and go extraction tips for matrix-assisted laser desorption/ionization, nanoelectrospray, and LC/MS sample pretreatment in proteomics. Anal Chem *75*, 663-670.

Ravid, T., and Hochstrasser, M. (2008). Diversity of degradation signals in the ubiquitin-proteasome system. Nat Rev Mol Cell Biol *9*, 679-690.

Ribeiro, S.A., Gatlin, J.C., Dong, Y., Joglekar, A., Cameron, L., Hudson, D.F., Farr, C.J., McEwen, B.F., Salmon, E.D., Earnshaw, W.C., *et al.* (2009). Condensin regulates the stiffness of vertebrate centromeres. Mol Biol Cell *20*, 2371-2380.

Ribeiro, S.A., Vagnarelli, P., Dong, Y., Hori, T., McEwen, B.F., Fukagawa, T., Flors, C., and Earnshaw, W.C. (2010). A super-resolution map of the vertebrate kinetochore. Proc Natl Acad Sci U S A *107*, 10484-10489.

Rieder, C.L. (1981). The structure of the cold-stable kinetochore fiber in metaphase PtK1 cells. Chromosoma *84*, 145-158.

Rieder, C.L., Cole, R.W., Khodjakov, A., and Sluder, G. (1995). The checkpoint delaying anaphase in response to chromosome monoorientation is mediated by an inhibitory signal produced by unattached kinetochores. J Cell Biol *130*, 941-948.

Ris, H., and Witt, P.L. (1981). Structure of the mammalian kinetochore. Chromosoma *82*, 153-170.

Rischitor, P.E., May, K.M., and Hardwick, K.G. (2007). Bub1 is a fission yeast kinetochore scaffold protein, and is sufficient to recruit other spindle checkpoint proteins to ectopic sites on chromosomes. PLoS One *2*, e1342.

Robinson, M.S., Sahlender, D.A., and Foster, S.D. (2010). Rapid inactivation of proteins by rapamycin-induced rerouting to mitochondria. Dev Cell *18*, 324-331.

Rout, M.P., Aitchison, J.D., Suprapto, A., Hjertaas, K., Zhao, Y., and Chait, B.T. (2000). The yeast nuclear pore complex: composition, architecture, and transport mechanism. J Cell Biol *148*, 635-651.

Roy, B., Varshney, N., Yadav, V., and Sanyal, K. (2013). The process of kinetochore assembly in yeasts. FEMS Microbiol Lett *338*, 107-117.

Rudra, S., and Skibbens, R.V. (2013). Cohesin codes - interpreting chromatin architecture and the many facets of cohesin function. J Cell Sci *126*, 31-41.

Saitoh, H., Tomkiel, J., Cooke, C.A., Ratrie, H., 3rd, Maurer, M., Rothfield, N.F., and Earnshaw, W.C. (1992). CENP-C, an autoantigen in scleroderma, is a component of the human inner kinetochore plate. Cell *70*, 115-125.

Sakai, D., Dixon, J., Dixon, M.J., and Trainor, P.A. (2012). Mammalian neurogenesis requires Treacle-Plk1 for precise control of spindle orientation, mitotic progression, and maintenance of neural progenitor cells. PLoS Genet *8*, e1002566.

Salmon, E.D. (1989). Cytokinesis in animal cells. Curr Opin Cell Biol *1*, 541-547.

Salmon, E.D., and Wolniak, S.M. (1990). Role of microtubules in stimulating cytokinesis in animal cells. Ann N Y Acad Sci *582*, 88-98.

Samejima, K., Samejima, I., Vagnarelli, P., Ogawa, H., Vargiu, G., Kelly, D.A., de Lima Alves, F., Kerr, A., Green, L.C., Hudson, D.F.*, et al.* (2012). Mitotic chromosomes are compacted laterally by KIF4 and condensin and axially by topoisomerase IIalpha. J Cell Biol *199*, 755-770.

Santaguida, S., and Musacchio, A. (2009). The life and miracles of kinetochores. EMBO J *28*, 2511-2531.

Sauer, B., and Henderson, N. (1988). Site-specific DNA recombination in mammalian cells by the Cre recombinase of bacteriophage P1. Proc Natl Acad Sci U S A *85*, 5166-5170.

Schevchenko, A., Tomas, H., Havlis, J., Olsen, J.V., and Mann, M. (2006). In-gel digestion for mass spectrometric characterization of proteins and proteomes. Nat Protocols *1*, 1754-2189.

Schittenhelm, R.B., Heeger, S., Althoff, F., Walter, A., Heidmann, S., Mechtler, K., and Lehner, C.F. (2007). Spatial organization of a ubiquitous eukaryotic kinetochore protein network in Drosophila chromosomes. Chromosoma *116*, 385-402.

Schleiffer, A., Maier, M., Litos, G., Lampert, F., Hornung, P., Mechtler, K., and Westermann, S. (2012). CENP-T proteins are conserved centromere receptors of the Ndc80 complex. Nat Cell Biol *14*, 604-613.

Schmidt, J.C., Arthanari, H., Boeszoermenyi, A., Dashkevich, N.M., Wilson-Kubalek, E.M., Monnier, N., Markus, M., Oberer, M., Milligan, R.A., Bathe, M.*, et al.* (2012). The kinetochore-bound Ska1 complex tracks depolymerizing microtubules and binds to curved protofilaments. Dev Cell *23*, 968-980.

Schmidt, J.C., and Cheeseman, I.M. (2011). Chromosome segregation: keeping kinetochores in the loop. Curr Biol *21*, R110-112.

Schmitzberger, F., and Harrison, S.C. (2012). RWD domain: a recurring module in kinetochore architecture shown by a Ctf19-Mcm21 complex structure. EMBO Rep *13*, 216-222.

Scholey, J.M., Brust-Mascher, I., and Mogilner, A. (2003). Cell division. Nature *422*, 746-752.

Screpanti, E., De Antoni, A., Alushin, G.M., Petrovic, A., Melis, T., Nogales, E., and Musacchio, A. (2011). Direct binding of Cenp-C to the Mis12 complex joins the inner and outer kinetochore. Curr Biol *21*, 391-398.

Shah, J.V., Botvinick, E., Bonday, Z., Furnari, F., Berns, M., and Cleveland, D.W. (2004). Dynamics of centromere and kinetochore proteins; implications for checkpoint signaling and silencing. Curr Biol *14*, 942-952.

Shang, W.H., Hori, T., Toyoda, A., Kato, J., Popendorf, K., Sakakibara, Y., Fujiyama, A., and Fukagawa, T. (2010). Chickens possess centromeres with both extended tandem repeats and short non-tandem-repetitive sequences. Genome Res *20*, 1219-1228.

Shepperd, L.A., Meadows, J.C., Sochaj, A.M., Lancaster, T.C., Zou, J., Buttrick, G.J., Rappsilber, J., Hardwick, K.G., and Millar, J.B. (2012). Phosphodependent recruitment of Bub1 and Bub3 to Spc7/KNL1 by Mph1 kinase maintains the spindle checkpoint. Curr Biol *22*, 891-899.

Skop, A.R., Liu, H., Yates, J., 3rd, Meyer, B.J., and Heald, R. (2004). Dissection of the mammalian midbody proteome reveals conserved cytokinesis mechanisms. Science *305*, 61-66.

Sluder, G. (1979). Role of spindle microtubules in the control of cell cycle timing. J Cell Biol *80*, 674-691.

Sluder, G. (1989). Centrosomes and the cell cycle. J Cell Sci Suppl *12*, 253-275.

Smithies, O., Gregg, R.G., Boggs, S.S., Koralewski, M.A., and Kucherlapati, R.S. (1985). Insertion of DNA sequences into the human chromosomal beta-globin locus by homologous recombination. Nature *317*, 230-234.

Steen, H., and Mann, M. (2004). The ABC's (and XYZ's) of peptide sequencing. Nat Rev Mol Cell Biol *5*, 699-711.

Stukenberg, P.T., and Foltz, D.R. (2010). Kinetochores: orchestrating the chromosomal minuet. Curr Biol *20*, R522-525.

Sturgill, E.G., and Ohi, R. (2013). Kinesin-12 differentially affects spindle assembly depending on its microtubule substrate. Curr Biol *23*, 1280-1290.

Su, Y., Ishikawa, S., Kojima, M., and Liu, B. (2003). Eradication of pathogenic beta-catenin by Skp1/Cullin/F box ubiquitination machinery. Proc Natl Acad Sci U S A *100*, 12729-12734.

Suzuki, A., Hori, T., Nishino, T., Usukura, J., Miyagi, A., Morikawa, K., and Fukagawa, T. (2011). Spindle microtubules generate tension-dependent changes in the distribution of inner kinetochore proteins. J Cell Biol *193*, 125-140.

Swedlow, J.R., Sedat, J.W., and Agard, D.A. (1997). Deconvolution in optical microscopy. In Deconvolution of Images and Spectra, 284–309.

Tadeu, A.M., Ribeiro, S., Johnston, J., Goldberg, I., Gerloff, D., and Earnshaw, W.C. (2008). CENP-V is required for centromere organization, chromosome alignment and cytokinesis. EMBO J *27*, 2510-2522.

Takahashi, K., Chen, E.S., and Yanagida, M. (2000). Requirement of Mis6 centromere connector for localizing a CENP-A-like protein in fission yeast. Science *288*, 2215-2219.

Takeuchi, K., and Fukagawa, T. (2012). Molecular architecture of vertebrate kinetochores. Exp Cell Res *318*, 1367-1374.

Tan, X., Calderon-Villalobos, L.I., Sharon, M., Zheng, C., Robinson, C.V., Estelle, M., and Zheng, N. (2007). Mechanism of auxin perception by the TIR1 ubiquitin ligase. Nature *446*, 640-645.

Tanaka, K. (2013). Regulatory mechanisms of kinetochore-microtubule interaction in mitosis. Cell Mol Life Sci *70*, 559-579.

Tanaka, K., Chang, H.L., Kagami, A., and Watanabe, Y. (2009). CENP-C functions as a scaffold for effectors with essential kinetochore functions in mitosis and meiosis. Dev Cell *17*, 334-343.

Tanaka, T.U., Rachidi, N., Janke, C., Pereira, G., Galova, M., Schiebel, E., Stark, M.J., and Nasmyth, K. (2002). Evidence that the Ipl1-Sli15 (Aurora kinase-INCENP) complex promotes chromosome bi-orientation by altering kinetochore-spindle pole connections. Cell *108*, 317-329.

Tanenbaum, M.E., Macurek, L., Janssen, A., Geers, E.F., Alvarez-Fernandez, M., and Medema, R.H. (2009). Kif15 cooperates with eg5 to promote bipolar spindle assembly. Curr Biol *19*, 1703-1711.

Theis, M., Slabicki, M., Junqueira, M., Paszkowski-Rogacz, M., Sontheimer, J., Kittler, R., Heninger, A.K., Glatter, T., Kruusmaa, K., Poser, I.*, et al.* (2009). Comparative profiling identifies C13orf3 as a component of the Ska complex required for mammalian cell division. EMBO J *28*, 1453-1465.

Ting, L., Cowley, M.J., Hoon, S.L., Guilhaus, M., Raftery, M.J., and Cavicchioli, R. (2009). Normalization and statistical analysis of quantitative proteomics data generated by metabolic labeling. Mol Cell Proteomics *8*, 2227-2242.

Tipton, A.R., Wang, K., Oladimeji, P., Sufi, S., Gu, Z., and Liu, S.T. (2012). Identification of novel mitosis regulators through data mining with human centromere/kinetochore proteins as group queries. BMC Cell Biol *13*, 15.

Tooley, J.G., Miller, S.A., and Stukenberg, P.T. (2011). The Ndc80 complex uses a tripartite attachment point to couple microtubule depolymerization to chromosome movement. Mol Biol Cell *22*, 1217-1226.

Topaloglu, O., Hurley, P.J., Yildirim, O., Civin, C.I., and Bunz, F. (2005). Improved methods for the generation of human gene knockout and knockin cell lines. Nucleic Acids Res *33*, e158.

Toso, A., Winter, J.R., Garrod, A.J., Amaro, A.C., Meraldi, P., and McAinsh, A.D. (2009). Kinetochore-generated pushing forces separate centrosomes during bipolar spindle assembly. J Cell Biol *184*, 365-372.

Trazzi, S., Perini, G., Bernardoni, R., Zoli, M., Reese, J.C., Musacchio, A., and Della Valle, G. (2009). The C-terminal domain of CENP-C displays multiple and critical functions for mammalian centromere formation. PLoS One *4*, e5832.

Tsukahara, T., Tanno, Y., and Watanabe, Y. (2010). Phosphorylation of the CPC by Cdk1 promotes chromosome bi-orientation. Nature *467*, 719-723.

Van Hooser, A.A., Yuh, P., and Heald, R. (2005). The perichromosomal layer. Chromosoma *114*, 377-388.

Varma, D., and Salmon, E.D. (2012). The KMN protein network--chief conductors of the kinetochore orchestra. J Cell Sci *125*, 5927-5936.

Varma, D., Wan, X., Cheerambathur, D., Gassmann, R., Suzuki, A., Lawrimore, J., Desai, A., and Salmon, E.D. (2013). Spindle assembly checkpoint proteins are positioned close to core microtubule attachment sites at kinetochores. J Cell Biol *202*, 735-746.

Vaz, B., Halder, S., and Ramadan, K. (2013). Role of p97/VCP (Cdc48) in genome stability. Front Genet *4*, 60.

Vermeulen, M., Eberl, H.C., Matarese, F., Marks, H., Denissov, S., Butter, F., Lee, K.K., Olsen, J.V., Hyman, A.A., Stunnenberg, H.G.*, et al.* (2010). Quantitative interaction proteomics and genome-wide profiling of epigenetic histone marks and their readers. Cell *142*, 967-980.

Wallace, W., Schaefer, L.H., and Swedlow, J.R. (2001). A workingperson's guide to deconvolution in light microscopy. Biotechniques *31*, 1076-1078, 1080, 1082 passim.

Wan, X., O'Quinn, R.P., Pierce, H.L., Joglekar, A.P., Gall, W.E., DeLuca, J.G., Carroll, C.W., Liu, S.T., Yen, T.J., McEwen, B.F.*, et al.* (2009). Protein architecture of the human kinetochore microtubule attachment site. Cell *137*, 672-684.

Wang, H., Hu, X., Ding, X., Dou, Z., Yang, Z., Shaw, A.W., Teng, M., Cleveland, D.W., Goldberg, M.L., Niu, L.*, et al.* (2004). Human Zwint-1 specifies localization of Zeste White 10 to kinetochores and is essential for mitotic checkpoint signaling. J Biol Chem *279*, 54590-54598.

Warburton, P.E., Cooke, C.A., Bourassa, S., Vafa, O., Sullivan, B.A., Stetten, G., Gimelli, G., Warburton, D., Tyler-Smith, C., Sullivan, K.F.*, et al.* (1997). Immunolocalization of CENP-A suggests a distinct nucleosome structure at the inner kinetochore plate of active centromeres. Curr Biol *7*, 901-904.

Watase, G., Takisawa, H., and Kanemaki, M.T. (2012). Mcm10 plays a role in functioning of the eukaryotic replicative DNA helicase, Cdc45-Mcm-GINS. Curr Biol *22*, 343-349.

Waters, J.C., Skibbens, R.V., and Salmon, E.D. (1996). Oscillating mitotic newt lung cell kinetochores are, on average, under tension and rarely push. J Cell Sci *109 (Pt 12)*, 2823-2831.

Wei, R.R., Al-Bassam, J., and Harrison, S.C. (2007). The Ndc80/HEC1 complex is a contact point for kinetochore-microtubule attachment. Nat Struct Mol Biol *14*, 54-59.

Weinert, T.A., and Hartwell, L.H. (1988). The RAD9 gene controls the cell cycle response to DNA damage in Saccharomyces cerevisiae. Science *241*, 317-322.

Welburn, J.P., and Cheeseman, I.M. (2008). Toward a molecular structure of the eukaryotic kinetochore. Dev Cell *15*, 645-655.

Welburn, J.P., Grishchuk, E.L., Backer, C.B., Wilson-Kubalek, E.M., Yates, J.R., 3rd, and Cheeseman, I.M. (2009). The human kinetochore Ska1 complex facilitates microtubule depolymerization-coupled motility. Dev Cell *16*, 374-385.

Westermann, S., Cheeseman, I.M., Anderson, S., Yates, J.R., 3rd, Drubin, D.G., and Barnes, G. (2003). Architecture of the budding yeast kinetochore reveals a conserved molecular core. J Cell Biol *163*, 215-222.

Westermann, S., Drubin, D.G., and Barnes, G. (2007). Structures and functions of yeast kinetochore complexes. Annu Rev Biochem *76*, 563-591.

Westhorpe, F.G., and Straight, A.F. (2013). Functions of the centromere and kinetochore in chromosome segregation. Curr Opin Cell Biol *25*, 334-340.

Willard, H.F. (1990). Centromeres of mammalian chromosomes. Trends Genet *6*, 410-416.

Winding, P., and Berchtold, M.W. (2001). The chicken B cell line DT40: a novel tool for gene disruption experiments. J Immunol Methods *249*, 1-16.

Wojcik, E., Basto, R., Serr, M., Scaerou, F., Karess, R., and Hays, T. (2001). Kinetochore dynein: its dynamics and role in the transport of the Rough deal checkpoint protein. Nat Cell Biol *3*, 1001-1007.

Yamagishi, Y., Yang, C.H., Tanno, Y., and Watanabe, Y. (2012). MPS1/Mph1 phosphorylates the kinetochore protein KNL1/Spc7 to recruit SAC components. Nat Cell Biol *14*, 746-752.

Yong-Gonzales, V., Hang, L.E., Castellucci, F., Branzei, D., and Zhao, X. (2012). The Smc5-Smc6 complex regulates recombination at centromeric regions and affects kinetochore protein sumoylation during normal growth. PLoS One *7*, e51540.

Zhang, G., Kelstrup, C.D., Hu, X.W., Kaas Hansen, M.J., Singleton, M.R., Olsen, J.V., and Nilsson, J. (2012). The Ndc80 internal loop is required for recruitment of the Ska complex to establish end-on microtubule attachment to kinetochores. J Cell Sci *125*, 3243-3253.

Zhou, P., Bogacki, R., McReynolds, L., and Howley, P.M. (2000). Harnessing the ubiquitination machinery to target the degradation of specific cellular proteins. Mol Cell *6*, 751-756.